ISBN 978-90-6266-422-1

USES No. 103
LPP Contributions Series No. 45

Author contact: j.frieling1@uu.nl or joost.frieling@gmail.com

Cover:
Copyright © 2016 J. Frieling. All rights reserved. No part of this publication may be reproduced in any form, by print or photo print, microfilm or any other means, without written permission by the author.

Printed in the Netherlands by WPS, Zutphen.

Climate, Carbon Cycling and Marine Ecology during the Paleocene-Eocene Thermal Maximum

Klimaat, koolstofkringloop en marine ecologie tijdens het Paleoceen – Eoceen Thermisch Maximum

(met samenvatting in het Nederlands)

PROEFSCHRIFT

ter verkrijging van de graad van doctor aan de Universiteit Utrecht op gezag van de rector magnificus, prof. dr. G.J. van der Zwaan, ingevolge het besluit van het college voor promoties in het openbaar te verdedigen op

woensdag 11 mei 2016 des middags te 2.30 uur

door

Joost Frieling,

geboren 21 augustus 1987 te Nijmegen

Promotoren:

Prof. dr. A. Sluijs
Prof. dr. G.-J. Reichart

This thesis was accomplished with financial support from the European Research Council

Members of the dissertation committee:

Prof. dr. ir. Jaap S. Sinninghe Damsté
Royal NIOZ & Utrecht University, the Netherlands

Prof. dr. Jörg Pross
Ruprecht-Karls-Universität Heidelberg, Germany

Prof. dr. Lucas J. Lourens
Utrecht University, the Netherlands

Prof. dr. Gerald R. Dickens
William Marsh Rice University, Houston, United States of America

Prof. dr. Caroline Slomp
Utrecht University, the Netherlands

Contents

9 **Chapter 1**
Introduction, outstanding issues and synopsis

21 **Chapter 2**
Paleocene - Eocene warming and biotic response in the epicontinental West Siberian Sea

Joost Frieling, Alina I. Iakovleva, Gert-Jan Reichart, Galina N. Aleksandrova, Zinaida N. Gnibidenko, Stefan Schouten, and Appy Sluijs

Geology 42, 767-770 (2014)

45 **Chapter 3**
Extreme warmth and plankton regime shift in the tropics during the Palaeocene – Eocene Thermal Maximum

Joost Frieling, Holger Gebhardt, Matthew Huber, Olabisi A. Adekeye, Samuel O. Akande, Gert-Jan Reichart, Jack J. Middelburg, Stefan Schouten and Appy Sluijs

Submitted

71 **Chapter 4**
A smoking gun for methane hydrate release during the Paleocene-Eocene Thermal Maximum

Joost Frieling, Francien Peterse, Daniel Lunt, Steven M. Bohaty, Jaap S. Sinninghe Damsté, Gert-Jan Reichart and Appy Sluijs

To be submitted

99 **Chapter 5**
Tropical Atlantic Climate and Ecosystem Regime Shifts during The Paleocene-Eocene Thermal Maximum

Joost Frieling, Gert-Jan Reichart, Jack J. Middelburg, Ursula Röhl, Thomas Westerhold, Steve M. Bohaty, and Appy Sluijs

To be submitted

115 **Chapter 6**
Thermogenic methane release as a cause for the long duration of the Paleocene-Eocene Thermal Maximum

Joost Frieling, Henrik H. Svensen, Sverre Planke, Margot J. Cramwinckel, Haavard Selnes and Appy Sluijs

Submitted

137 **Chapter 7**
Ecological preferences of Paleocene – Eocene dinoflagellates
Joost Frieling and Appy Sluijs

To be submitted

169 **References**

195 **Summary in Dutch (Samenvatting in het Nederlands)**

203 **Acknowledgments (Dankwoord)**

205 **Curriculum vitae**

1

Introduction and Synopsis

1.1 CO_2 through geological time

From the year 1850 to the present, CO_2 concentrations have risen from 280 parts per million (ppm) to 400 ppm. Ice core data shows that this is the first time that CO_2 concentrations has risen above ~300 parts per million (ppm) since at least 800,000 years (800 kyr). The present day CO_2 concentration is similar to that of the middle Pliocene, about 4 million years ago (Ma), based on proxy data from sediments (Martínez-Botí et al., 2015; Zachos et al., 2008) Figure 1). Since CO_2 is a strong greenhouse gas, higher concentrations will lead to higher temperatures, as observed during the Pliocene. Furthermore, part of the CO_2 added to the atmosphere is taken up by the oceans and, if added rapidly, leads to ocean acidification (e.g. Honisch et al., 2012). Although climates were warmer during the Pliocene, there is ample evidence that pCO_2 was even higher (>1000 ppm) during much of the last 65 million years (Myr). Especially the Paleocene (66-56 Ma) and Eocene (56-34 Ma) were most likely marked by high CO_2 concentrations and much warmer climates.

This period is therefore suitable for studying climate in a high CO_2 world and, as such, may provide crucial information regarding climate change of the coming centuries if the rise in CO_2 concentrations persists. Although the background conditions, notably continental geography, differ markedly, the interval from 60 to 50 Ma is of particular interest.

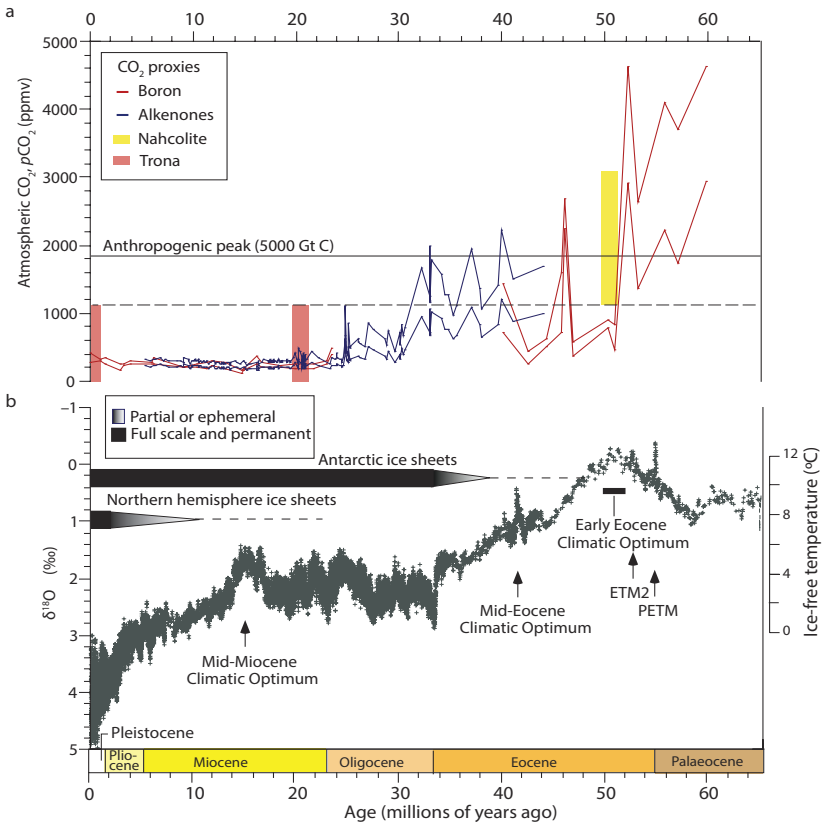

Figure 1. *Deep ocean temperature and CO_2 evolution over the last 65 Ma, redrawn from Zachos et al. (2008).*

1.2 Characteristics of Paleocene-Eocene climate

Much of the late Paleocene and Eocene are characterized by extreme greenhouse climates (IPCC, 2014; Zachos et al., 2008). There is no convincing evidence for permanent ice on land or in the sea at the poles. In contrast, temperate to subtropical climates characterized mid to high latitude regions (Bijl et al., 2009; Hollis et al., 2012; Pross et al., 2012; Sluijs et al., 2008b). In the absence of large ice sheets, stable oxygen isotope ($\delta^{18}O$) records from benthic foraminifera provide insight in deep ocean temperatures (Zachos et al., 2008). From ~60 to 50 million years ago (Ma) deep ocean temperature increased gradually by ~8 °C, to a maximum of 15 °C during the Early Eocene Climate Optimum (EECO) (Figure 1). In contrast to the present day, most of the deep water formation took place in the Southern Ocean (Thomas et al., 2003) and therefore these deep water temperatures likely track high southern latitude (winter) temperatures. As the poles were essentially ice-free during these periods, and sea floor spreading rates were higher than at present, sea level was much (70m) higher (e.g., Kominz et al., 2008; Muller et al., 2008) so that large portions of the continental shelves were flooded (Figure 2).

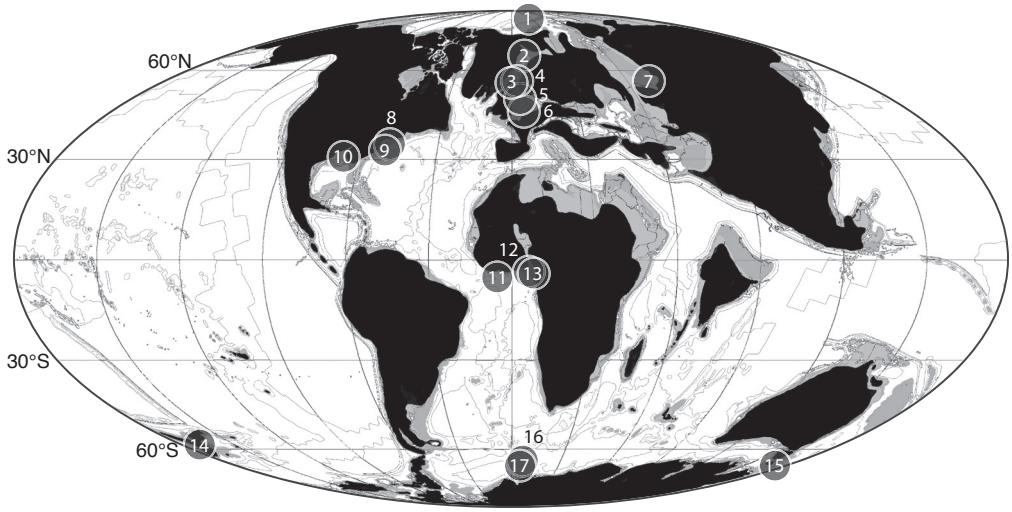

Figure 2. *Paleogeographic reconstruction modified from (Markwick, 2007) at 55 Ma, localities from which data was used or generated. Grey shading represents flooded continental shelf area.* ***1.*** *Arctic Coring Expedition (ACEX), (Sluijs et al., 2009, 2008b, 2006).* ***2.*** *Spitsbergen (Harding et al., 2011).* ***3.*** *Ocean Drilling Program (ODP) Site 642E, (Abdelmalak et al., 2016).* ***4.*** *Wildcat 6607/12-1 Norwegian Sea, Chapter 7.* ***5.*** *22A04/1 North Sea (Eldrett et al., 2014).* ***6.*** *Woensdrecht borehole, North Sea (Sluijs et al., 2008a).* ***7.*** *Well 10 borehole, West Siberian Sea, Chapter 2 & 6.* ***8.*** *Wilson Lake, New Jersey (Sluijs et al., 2007b; Zachos et al., 2006).****9.*** *Bass River, New Jersey(Sluijs et al., 2007b).* ***10.*** *Harrell core, Gulf of Mexico (Sluijs et al., 2014)* ***11.*** *ODP Site 959D, Chapter 4, 5 & 6.* ***12.*** *Sagamu Quarry, Nigeria, Chapter 3 & 6.* ***13****. Ilaro borehole 10 A & B, Nigeria, Chapter 3 & 6.* ***14.*** *Tawanui, New Zealand(Crouch and Brinkhuis, 2005).* ***15.*** *International Ocean Drilling Program (IODP) Site 1172, South Tasman Plateau (Sluijs et al., 2011).* ***16.*** *ODP Site 689, Maud Rise,(Zachos et al., 2007).* ***17.*** *ODP Site 690, Maud Rise(Kelly, 2002; Thomas et al., 2002).*

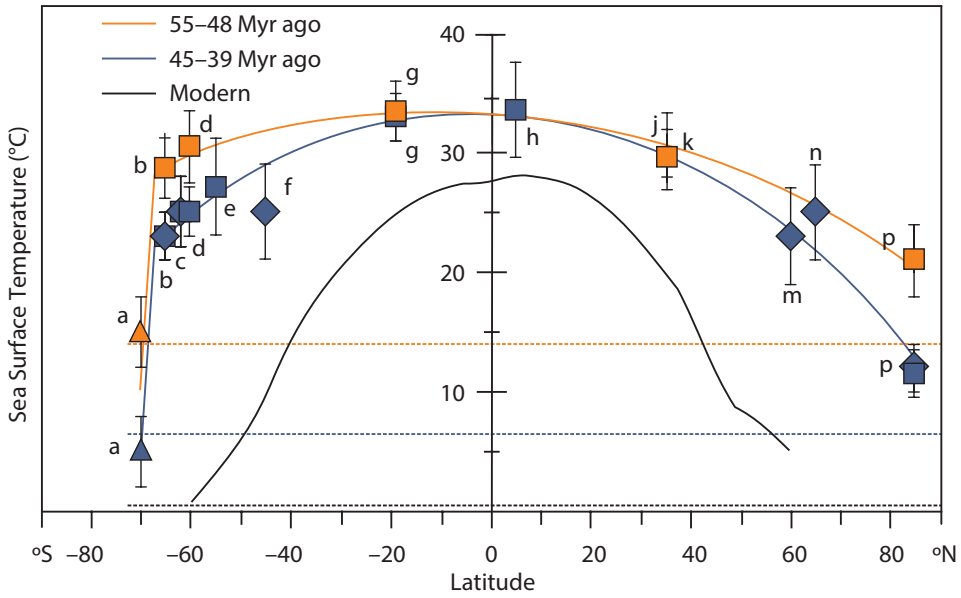

Figure 3. *Surface temperature gradients across latitude, modified from (Bijl et al., 2009).*

The warmest interval in the last 66 Myr, the Early Eocene (56 to 50 Ma) was marked by the presence of (sub-) tropical biota, e.g. palms, mangrove forests and crocodilians, at many mid and high latitude locations (Crouch and Visscher, 2003; Markwick, 2007; Pross et al., 2012). Importantly, these biota are evidence of a crucial feature of greenhouse climates; mid and high latitudes typically experienced amplified effects of warming (e.g. Huber and Caballero, 2011; Figure 3). Tropical regions may not have been much (perhaps 5 °C) warmer then today during much of the interval (Pearson et al., 2007), while high latitude regions were perhaps temporally up to 30 °C warmer then at present (e.g., Sluijs et al., 2011). This implies that the equator to pole temperature gradient was much shallower than today (e.g. Bijl et al., 2009), Figure 3). Although recent climate model simulations correctly reflect mid-latitude temperature reconstructions during the Early Eocene (Huber and Caballero, 2011), they struggle to reproduce the extreme warmth at high latitudes.

1.3 'Hyperthermal' events

The interval from 56 to 50 Ma is further characterized by several transient (10-100 kyr scale) perturbations of the carbon cycle, which are somewhat analogous to anthropogenic carbon input (e.g., Zeebe and Zachos, 2013). These short warming events, that are superimposed on a ~7 Myr period of gradual warming are affectionately called 'hyperthermal events' (Thomas and Zachos, 2000). Essentially, hyperthermal events mark phases of rapid (10^3 – 10^4 years) warming, at least widespread but likely global, associated with a drop in the stable carbon isotopic composition of the global exogenic carbon pool and ocean acidification(Cramer et al., 2003; Galeotti et al., 2010; Lourens et al., 2005; McInerney and Wing, 2011; Nicolo et al., 2007; Sluijs et al., 2007a). These characteristics provide strong evidence that these warming events are related to rapid anomalous carbon input from a reservoir outside the global exogenic carbon cycle (Dickens et al., 1997, 1995).

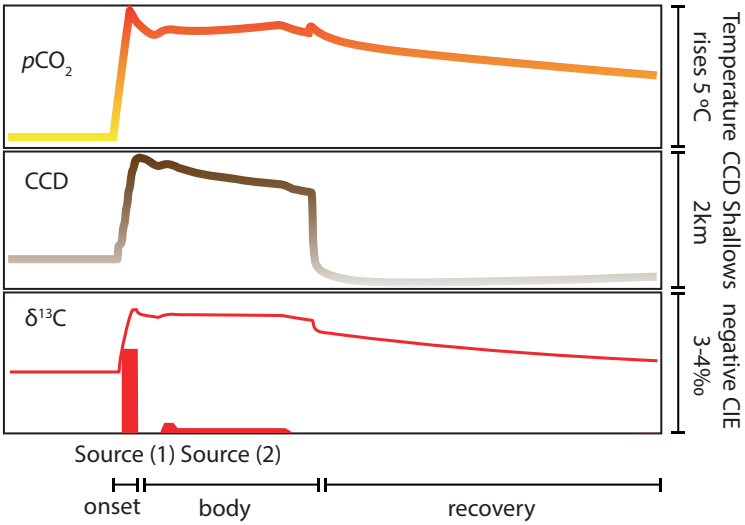

Figure 4. *Schematic view of stable carbon isotope, temperature and carbon sources during the PETM, modified from (Zeebe et al., 2009).*

1.4 The Paleocene Eocene Thermal Maximum

The Paleocene – Eocene Thermal Maximum (PETM, ~56 Ma) is the hyperthermal with the largest magnitude of global warming (+4 °C; Dunkley Jones et al., 2013) and negative carbon isotope excursion (CIE; >3‰, e.g., Sluijs and Dickens, 2012). In addition, it stands out relative to other hyperthermals in both duration and shape of the CIE (Cramer et al., 2003; Stap et al., 2010). The onset of the CIE takes several millennia (e.g. Zeebe et al., 2014) followed by the "body", representing a stable period of ~70 kyr and a recovery to background values that lasts ~100 kyr (Murphy et al., 2010; Röhl et al., 2007) (Figure 4). Ample evidence for associated environmental perturbations have been recorded. As global temperatures increased, the hydrological cycle accelerated (Handley et al., 2012; Pagani et al., 2006b; Schmitz and Pujalte, 2007; Sluijs et al., 2014) and oceans experienced lower oxygen concentrations (Dickson et al., 2012), both in bottom and surface waters (e.g. Palike et al., 2014; Sluijs et al., 2014). The large rapid carbon input caused ocean acidification and as a result the carbonate compensation depth (CCD) shallowed in the Pacific (Colosimo et al., 2006) but notably in the Atlantic (Zachos et al., 2005). This means that deep ocean records suffer from carbonate dissolution during the PETM.

2. Outstanding questions

2.1 Carbon source(s)

Since the discovery of the PETM (Kennett and Stott, 1991; Thomas, 1990), many high-resolution sedimentary records have been generated (e.g. McInerney and Wing, 2011). This has resolved patterns in environmental parameters, including temperature, anoxia, stable carbon isotope changes, water column stratification and migrations of flora and fauna (e.g., McInerney and Wing, 2011; Sluijs et al., 2014, 2007a). The shear amount of publications focusing on the PETM may give the impression that a large part of the causes and effects have been resolved.

However, although much is indeed known about the effects of carbon input and warming during the PETM, many outstanding issues remain regarding the cause. For example, despite at least 6 independent hypotheses (DeConto et al., 2012; Dickens et al., 1995; Higgins and Schrag, 2006; Morgan et al., 2004; Nisbet et al., 2009; Svensen et al., 2004) it remains uncertain where the injected ^{13}C-depleted carbon came from. Not a single postulated source has to date been presented with positive evidence for rapid carbon release during the PETM or any other hyperthermal.

In addition, as yet, no model scenario can simultaneously explain the carbon isotope excursion, CCD rise, warming and high background temperatures (e.g., Cui et al., 2011; Meissner et al., 2014; Zeebe et al., 2009). However, plausible explanations for some of these observed perturbations exist. The most prolific hypothesis for explaining the CIE is the destabilization of methane clathrates (Dickens et al., 1995). Clathrates are methane molecules encapsuled in a water cage as a mineral. The formation and stability of these structures strongly depend on temperature and pressure (e.g. Dickens and Quinby-Hunt, 1994; Kvenvolden, 1993). Methane clathrates were possibly present throughout the oceans from ~1 km depth during the Paleocene and Eocene despite warm ocean waters, also at mid and high latitudes (e.g. Dickens, 2001; Dunkley Jones et al., 2010). The formation pathway, involving bacterial methanogenesis, generates an extremely ^{13}C-depleted carbon isotope signature (-60‰, Milkov, 2005) and is thus capable of causing a negative CIE even when a relatively small mass is released (Dickens et al., 1997). Because temperature dependent stability implies that an initial warming or "trigger" is required to destabilize the clathrates (Dickens et al., 1995), the methane clathrate dissociation hypothesis has lead to a discussion regarding cause and effect (Dickens, 2011; Pagani et al., 2006a; Sluijs et al., 2007b).

Another hypothesized carbon source, high latitude permafrost or peat deposits (DeConto et al., 2012), also requires warming to be released. Early warming, which has been regionally observed (e.g., Sluijs et al., 2007b), may have resulted from enhanced volcanism in the North Atlantic Igneous Province (NAIP) (Storey et al., 2007). Alternatively, astronomical forcing in tandem with gradually rising CO_2 could have pushed the system to pass a tipping point (Lourens et al., 2005; Lunt et al., 2011).

Another hypothesis for the origin of ^{13}C-depleted C focuses on hydrothermal activity in the Vøring and Møre Basins in the North Atlantic around the Paleocene – Eocene boundary. Svensen et al., (2004) proposed a scenario where sill intrusion into organic rich sediments leads to thermogenic methane generation. On the surface the expulsion of fluid and gases can be recognized by the presence of at least hundreds, but possibly thousands of craters and hydrothermal vent complexes (Svensen et al., 2004). *Apectodinium augustum*, a dinoflagellate cyst marker species that exclusively occurred during the PETM (Crouch et al., 2001; Schmitz et al., 2004) was found in the only drilled hydrothermal vent system and suggests a direct connection to the PETM.

The most important flaw with assuming any of these sources being that each may explain the CIE, but the volume of these reservoirs are typically inconsistent with the magnitude of either CCD change, or warming, let alone absolute temperatures (Zeebe et al., 2009). This has lead to the hypothesis that carbon was released from multiple reservoirs (e.g., Panchuk et al., 2008; Sluijs et al., 2007b) or a complex short and long-term feedback system affecting one reservoir (Zeebe, 2013), but it remains unknown which reservoir(s).

2.2 Climate model – data mismatch

In addition to the uncertainties in the carbon input source, substantial debate continues on how well climate models can reproduce the reconstructed temperatures. This partially

originates from poor constraints on CO_2 concentrations across the PETM. In addition, we do not know the equilibrium climate sensitivity, defined as temperature rise caused by a doubling of CO_2 equilibrated on geological time scales (Lunt et al., 2010a; Rohling et al., 2012). Temperature change, however, is fairly well constrained in many regions and can hence be used as a target variable for climate modelers (Dunkley Jones et al., 2013).

Absolute temperature during the PETM in mid and high-latitude regions are constrained by a multitude of proxies, using oxygen isotope and Mg/Ca ratios in foraminifera and biomarker-based proxies such as TEX_{86} (e.g. Hollis et al., 2015; Sluijs et al., 2006; Zachos et al., 2006). However, high-quality high-resolution absolute temperature reconstructions from the tropics are extremely rare (Aze et al., 2014). Crucially, none of the existing sites have well-resolved stratigraphy and trustworthy mixed-layer temperature reconstructions.

The tropical band (30 ºN – 30 ºS) not only accounts for 50% of the Earth's surface but also absorbs 75% of the incoming energy. This means that an end-member of the climate system that is crucial to 1) determine global average temperature, 2) the magnitude of global warming during the PETM, and 3) polar amplification of temperature change, remains poorly constrained. In fact, it has been long thought that the tropics were as warm or even cooler than today in greenhouse climates based on planktonic foraminifer oxygen isotope ratios (e.g., Zachos et al., 1994), which presented an impossible task for climate models (Barron, 1987; Sloan et al., 2001). This was used to argue for a tropical thermostat; some physical mechanism that would keep temperatures in tropical regions stable regardless of changing greenhouse gas concentrations, which would have implications for future climate change (Lindzen et al., 2001; Pierrehumbert, 1995). However, evidence has mounted that early studies underestimated tropical temperatures due to carbonate diagenesis (Pearson et al., 2007; Schrag et al., 1995). Recent studies consciously avoiding these diagenetic effects (Aze et al., 2014; Kozdon et al., 2011) have indeed indicated warm tropical regions. This substantially decreased the gap between the data and model studies (Huber and Caballero, 2011). Climate model simulations project tropical sea surface temperatures of more than 35 °C during the PETM. Crucially, however, reconstructions of tropical temperatures based on multiple proxies are still lacking to test this inference.

2.3 Ecological effects of warming in the tropics

Although tropical nannoplankton and foraminifera records (Bown and Pearson, 2009; Kelly et al., 1998, 1996; Mutterlose et al., 2007; Raffi et al., 2005; Tremolada and Bralower, 2004) are available, most of these are from open ocean settings. Very little is known about biotic change and environmental parameters in tropical near-shore environments. Microfossils in general are particularly useful in paleoenvironmental reconstructions due to high biological overturning speed and sensitivity to environmental parameters (Kelly et al., 1998, 1996; Raffi et al., 2005; Sluijs et al., 2005). Dinoflagellates, unicellular protists, are sensitive to environmental changes, such as temperature, salinity, nutrient concentrations and turbulence (Fensome et al., 1996; Zonneveld et al., 2013). A small percentage (10-15%) of dinoflagellate species forms a preservable resting cyst as a mandatory part of their life-cycle (Evitt, 1985). These resting cysts from dinoflagellates (dinocysts) are dominantly organic-walled and have been used successfully at many mid and high latitude sites to provide a continuous record of environmental change across the PETM (e.g., Crouch et al., 2001; Harding et al., 2011; Sluijs and Brinkhuis, 2009).

From this we know several species migrate towards higher latitudes during the PETM, most notably found in quasi-global dominance of the sub-tropical dinoflagellate cyst species *Apectodinium* (Crouch et al., 2001), which is abundant in the Paleocene at low and mid

latitudes (Crouch et al., 2003b; Du Chêne and Adediran, 1984). However, as *Apectodinium* migrated poleward, it remains unknown what happened to biota in tropical regions.

3. Synopsis

In this thesis, the above outstanding issues regarding the PETM are addressed. Dinocysts are used in tandem with organic and inorganic geochemical proxies to reconstruct environmental parameters. The observations are placed in a framework of long-term climate change and perturbation during the PETM, carbon cycle dynamics and ecological response. Data from core and outcrop sections across the globe are discussed (Figure 2).

In **Chapter 2**, we explore whether the warming from 59-52 Ma as recorded in deep waters and the surface of the Southern Ocean occurred also on the northern hemisphere using sediments deposited in the epicontinental West Siberian Sea from a drill site near Omsk, Russia. We reconstruct sea surface temperature change using the molecular temperature proxy TEX_{86}. The warming is found to be remarkably similar to that in the Southern Ocean and global deep waters, suggesting a global signal. Moreover, based on the new and previously published data we determine a minimum sea surface temperature tolerance of 20 °C for Wetzelielloideae, an important Paleogene dinocyst group that also includes *Apectodinium*.

In **Chapter 3**, two sedimentary sections from Nigeria are used for absolute temperature reconstructions during the latest Paleocene and the PETM, using a multi-proxy approach. Three independent temperature proxies (Mg/Ca ratios and $\delta^{18}O$ of planktonic foraminifera and TEX_{86}^{H}) all indicate Paleocene sea surface temperatures of ~33 °C, about 6-7 °C higher than the modern Gulf of Guinea. During the PETM, TEX_{86}^{H} records a temperature rise of ~3 °C. Climate model runs and compiled proxy data shows that the magnitude of warming was dampened relative to that in extratropical regions during the PETM. Especially interesting is the match between the data and the model, which shows that state-of-the-art climate models are able to accurately predict global temperature change, identify regions of enhanced warming and reproduce absolute temperatures, perhaps except for the exceptionally warm polar regions.

I generated another SST record based on TEX_{86}^{H} from offshore Ivory Coast (Ocean Drilling Project (ODP) Site 959), which is presented in **Chapter 4**. Interestingly, both the record from Nigeria and Site 959 indicate exceptionally high SST (~37 °C) during peak PETM warmth. In **Chapters 3 and 5**, we show that most dinocyst taxa did not occur in both these eastern tropical Atlantic Ocean records during peak temperatures. Based on a large and diverse proxy dataset, we link this temporal absence of most dinocyst taxa to heat stress. Taxa belonging to the subfamily Protoperidiniaceae are among the few groups to remain relatively unscathed. This dinoflagellate subfamily is strictly heterotrophic in the modern ocean, and most likely also in the Paleogene, and may thus have dwelled below the mixed layer. In recent years several papers have postulated that heat-stress may indeed play a role during the extreme greenhouse climate of the PETM (e.g. Aze et al., 2014; Huber, 2008), but the PETM sites in Nigeria and ODP Site 959 are the first where it can be demonstrated that other biological stress factors such as extremely low oxygen concentrations, low salinity or acidification did not negatively influence plankton abundance at the same time. At Site 959, none of the eukaryote plankton groups abundant in the Paleocene, including planktonic foraminifera, radiolaria, diatoms and dinoflagellates, persist in large numbers across the PETM. The easiest explanation for this pattern, combined with the findings from Nigeria is that most eukaryotic plankton suffered from heat stress. Interestingly, higher abundance of benthic foraminifera during the PETM at these sites indicates that primary production

persisted, most likely dominated by prokaryotes.

Did the warming cause carbon injection as a positive feedback (e.g., Dickens et al., 1995) or did the carbon cause all the warming (e.g. Pagani et al., 2006a) during the PETM? To resolve this lead and lag relations between temperature and $\delta^{13}C$, I subject the high-resolution SST record from Site 959 and previously published records across the onset of the PETM to time-shifted cross-correlations in **Chapter 4**. It is shown that temperature, on average, leads the CIE by ~2-3000 years. This means that a feedback injecting ^{13}C-depleted carbon as a response to warming is plausible. Interestingly, both destabilization of methane clathrates and permafrost would provide positive feedbacks or self re-enforcing mechanisms (DeConto et al., 2012; Dickens et al., 1995). However, it appears that a substantial portion of the warming (perhaps half) occurred before the onset of the CIE. Moreover, a quasi-global compilation of Barium records from shelf and deep oceans shows that global Ba burial rates increased during the PETM, a feat that can only be accomplished by an anomalous addition of Ba to the oceans. Intriguingly, methane hydrates store large amounts of dissolved Ba. We conclude this combination of features, including initial warming, Ba enrichment and previously recognized spatial patters in carbonate dissolution may only be explained by massive methane hydrate release in the Atlantic Ocean.

The NAIP was very active during the interval encompassing the PETM. Studies have tried to link this activity to the PETM through two different mechanisms. Storey et al., (2007) suggested that it might provide the CO_2 increase needed for the initial warming leading up to the CIE. Svensen et al., (2004) postulated that it might have contributed to warming and possibly caused the CIE through thermogenic methane release from hydrothermal vent systems in the Vøring and Møre Basins. The latter hypothesis is tested in **Chapter 6**. With new stratigraphic insights from dinoflagellate cysts and stable carbon isotope analyses of the palynological residues from the only drilled hydrothermal vent system, it is shown that methane was indeed vented during the PETM. This represents the first solid evidence for ^{13}C-depleted C release during the PETM and indicates that thermogenic methane added to the CIE. However, the timing of venting, during the body phase of the CIE, implies this is an explanation for the exceptional length of the body of the PETM, rather than a direct cause for either the onset of the CIE or the warming. We speculate the initial warming presented in **Chapter 4** may be driven by enhanced volcanism in the NAIP directly before the PETM and enhanced volcanism in the North Atlantic may hence provide a single mechanistic link between three carbon sources; mantle outgassing, methane hydrate dissociation and thermogenic methane.

In **Chapter 7**, the new dinocyst data and proxy data from **Chapters 2,3 and 5** is used to generate a state-of-the-art analysis of ecological affinities of important Paleogene dinocyst taxa. The newly added assemblage and environmental data aids the understanding of ecological signals in dinocyst assemblages at mid and high latitude sections during the PETM, where the environment may have been similar to low latitude regions during the background Paleocene and Eocene. Using a proxy-based approach, we find not only a temperature limitation (>20 ºC) in *Apectodinium*, as presented in **Chapter 2**, but also in *Florentinia reichartii* (>30 ºC) and Goniodomideae (>25 ºC). Furthermore, we find that Peridinioid cysts should be divided in several distinct ecological groups. *Senegalinium* seems to be a low-salinity tolerant genus, whereas *Cerodinium* and *Deflandrea*, although likely also tolerant to low salinities, appear to outcompete other taxa at lower bottom water oxygen levels and high productivity. Moreover, we find that *Apectodinium* responds very differently from other Peridinioid cysts, including the response to proxy records that may be considered closely related to nutrient input. We thus do not find evidence for the

heterotrophic affinity of *Apectodinium*. In general, temperature and geographical bounds are likely more important in controlling distributions of dinocyst groups than was previously thought.

4. Outlook

The data presented in this thesis raises questions regarding tropical ecosystems during the PETM and results in new theories that require further testing. First, the documented eukaryote collapse in (parts of) the tropics raises the need for culture experiments targeting diverse marine primary producers and primary consumers to elucidate the sensitivity of the base of the modern tropical ecosystem to rapid warming from a stable background temperature. Second, although prokaryote driven primary productivity is the most likely driver, this potentially has consequences for the biological pump. Importantly, both the extent and severity of the plankton community reorganisation are unknowns, which in part may be overcome by revisiting previous work, but crucially also needs a quantification of relative amounts of eukaryote and prokaryote primary productivity.

Several carbon sources that may explain part of the PETM are presented in this thesis. Their exact relation remains unknown, but is unlikely due to coincidence alone. A more substantial global Ba compilation may provide insight to the role of methane hydrates. With the role of hydrates quantified it might prove feasible to better estimate other sources in future research. Furthermore, the most active phases of the NAIP need accurate dating to resolve the potential link between pre-CIE warming and volcanism.

It is known that ocean circulation changed across the PETM and this likely explains the pattern of observed global warming. It is however unclear what portion of the oceanographic changes results from the warming and what part drives warming locally. These patterns may be resolved by well-dated high-resolution time slices such as presented in **Chapter 4**, but still focus on sensitive regions as identified in coupled ocean-atmosphere general circulation models is needed.

2

Paleocene - Eocene warming and biotic response in the epicontinental West Siberian Sea

Abstract

We present a Paleocene–Eocene (ca. 60–52 Ma) sea-surface temperature record from sediments deposited in the epicontinental West Siberian Sea. TEX_{86} paleothermometry indicates long-term late Paleocene (~17 °C ca. 59 Ma) to early Eocene (26 °C at 52 Ma) sea-surface warming, consistent with trends previously observed for the Southern Ocean and deep oceans. Photic zone and seafloor anoxia developed as temperatures rose by 7 °C to ~27 °C during the Paleocene–Eocene Thermal Maximum (PETM). Based on paired palynological and TEX_{86} data, we suggest that the minimum temperature for the proliferation of Paleocene and early Eocene members of the dinoflagellate family Wetzelielloideae, which includes the PETM marker taxon *Apectodinium*, was ~20 °C.

Introduction

Southern Ocean surface and global deep-water temperatures rose by ~11 and 7 °C respectively between the late Paleocene, at ~58 Ma and the Early Eocene Climatic Optimum (EECO), 52–50 Ma (Bijl et al., 2013b, 2009; Hollis et al., 2012; Zachos et al., 2008). Superimposed on this long term warming, several transient warming events or "hyperthermals" occurred, including the Paleocene-Eocene Thermal Maximum (PETM; ~56 Ma) and Eocene Thermal Maximum 2 (ETM2; ~54 Ma). These hyperthermals were associated with rapid and massive injections of ^{13}C-depleted carbon into the ocean-atmosphere system, based on pronounced negative carbon isotope excursions (CIEs) in sedimentary components (e.g., Dickens et al., 1995; Lourens et al., 2005).

Early Eocene global climate was ~15 °C warmer than at present based on data and models, with particularly warm polar regions and reduced meridional temperature gradients (e.g., Bijl et al., 2009; Huber and Caballero, 2011). Notably, the gradient changed during the early Paleogene as mid- and high latitude regions cooled, and the limited information from the tropics shows only minor temperature change (Bijl et al., 2009; Pearson et al., 2007). Because of poor spatial coverage, however, the constraints on this gradient are limited. Critically, no record of long-term late Paleocene through the early Eocene sea surface temperature (SST) evolution exists for the Northern Hemisphere apart from the Arctic Ocean (IODP Exp. 302; Arctic Coring Expedition; ACEX; Sluijs et al., 2009, 2008b, 2006).

Both the long-term warming and the hyperthermals were marked by poleward migrations of biota, notably recorded in the (sub-) tropical dinoflagellate cyst (dinocyst) genus *Apectodinium* (Crouch et al., 2001). However, few quantitative temperature constraints exist on plankton biogeography. Here, we present organic geochemical and dinoflagellate cyst data from the southern part of the West Siberian Sea (WSS; Fig. 1) to document regional long-term temperature evolution in relation to plankton biogeography.

Materials

Upper Paleocene sandstones in Well 10 near Omsk, SW Siberia, Russia (53°30'06.37" N, 73°31'35.57" E; paleolatitude ~58°N) are unconformably deposited on the Maastrichtian Gan'kino formation at 260.2 m below surface (mbs; Fig. 2). The Paleocene sandstones fine upwards into mudstones and gaize, a sediment type rich in amorphous silica, indicating a gradual deepening of the basin. A glauconite-rich sandstone from 237.7 to 237 mbs separates the lower and upper Lulinvor subformations. It underlies a sapropelitic bed, which may be correlative to similar lithological units in the Northern Peri-Tethys shown to correspond to the maximum flooding surface (MFS) of the PETM (Gavrilov et al., 2003; Radionova et al., 2003; Fig. 1). The upper Lulinvor subformation consists mainly of siliceous silt and sandstones. The similarity of early Paleogene dinocyst assemblages in the epicontinental

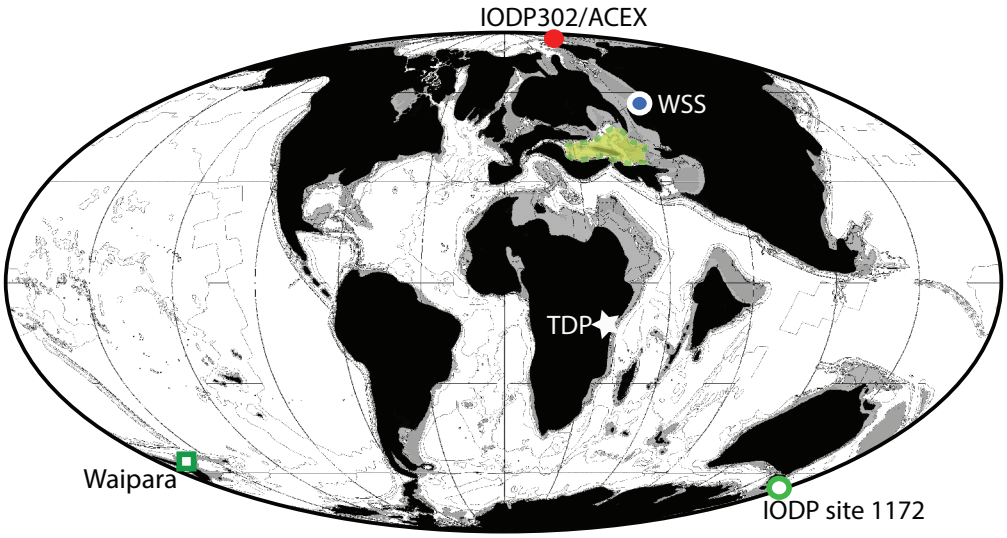

Figure 1. *Paleogeographic map (55 Ma) showing site locations; ACEX (Sluijs et al., 2009, 2008b, 2006), West Siberian Sea (WSS) (this study), Waipara, New Zealand (Hollis et al., 2012), IODP site 1172 (Bijl et al., 2013b, 2009; Sluijs et al., 2011) and Tanzania Drilling Project (TDP) (Pearson et al., 2007). The green shaded area represents the approximate extent of sapropel deposition during the PETM in epicontinental Eurasia (Radionova et al., 2003)*

WSS with those in the North Sea Basin (Heilmann-Clausen, 1985), Atlantic Ocean (Sluijs and Brinkhuis, 2009) and Tethys indicates the WSS was well-connected to the global ocean (Iakovleva, 2011).

Methods

We integrate existing dinocyst biostratigraphy (Iakovleva and Aleksandrova, 2013; Iakovleva and Heilmann-Clausen, 2010) and magnetic polarity reversals (Akhmetiev et al., 2010) with new stable carbon isotope stratigraphy to optimize the age model in Well 10. We apply the organic molecular TEX_{86} proxy (Schouten et al., 2002) to reconstruct temperature and apply dinocyst assemblages as paleoenvironmental indicators.

We measured TOC and $\delta^{13}C_{TOC}$ on ~10 mg of homogenized and decalcified sample using a CNS-analyzer (Fisons) coupled to an isotope ratio mass spectrometer (Finnigan MAT Delta Plus). For TEX_{86} analysis, ~10 g of sediment was extracted by a Dionex Accelerated Solvent Extractor. Extracts were separated into polar and apolar fractions over an Al_2O_3 column. The apolar fractions of the sapropelitic bed and adjacent samples were scanned for isorenieratane by gas chromatography and gas chromatography mass spectrometry. Isoprenoid glycerol dibiphytanyl glycerol tetraethers (GDGTs) and branched GDGTs in the polar fractions were measured on an Agilent 1100 high performance liquid chromatography mass spectrometer. We calculated SST using the most recent high temperature calibration, TEX_{86}^{H}, which yields a calibration error of 2.5 °C (Kim et al., 2010) (see supplementary information for detailed methods and discussion concerning TEX_{86} calibrations and caveats).

Palynological processing included treatment with HCl (10%) for carbonate removal. Clay particles were dispersed with tetra-sodium pyrophosphate ($Na_4P_2O_7.10H_2O$, 10%) and

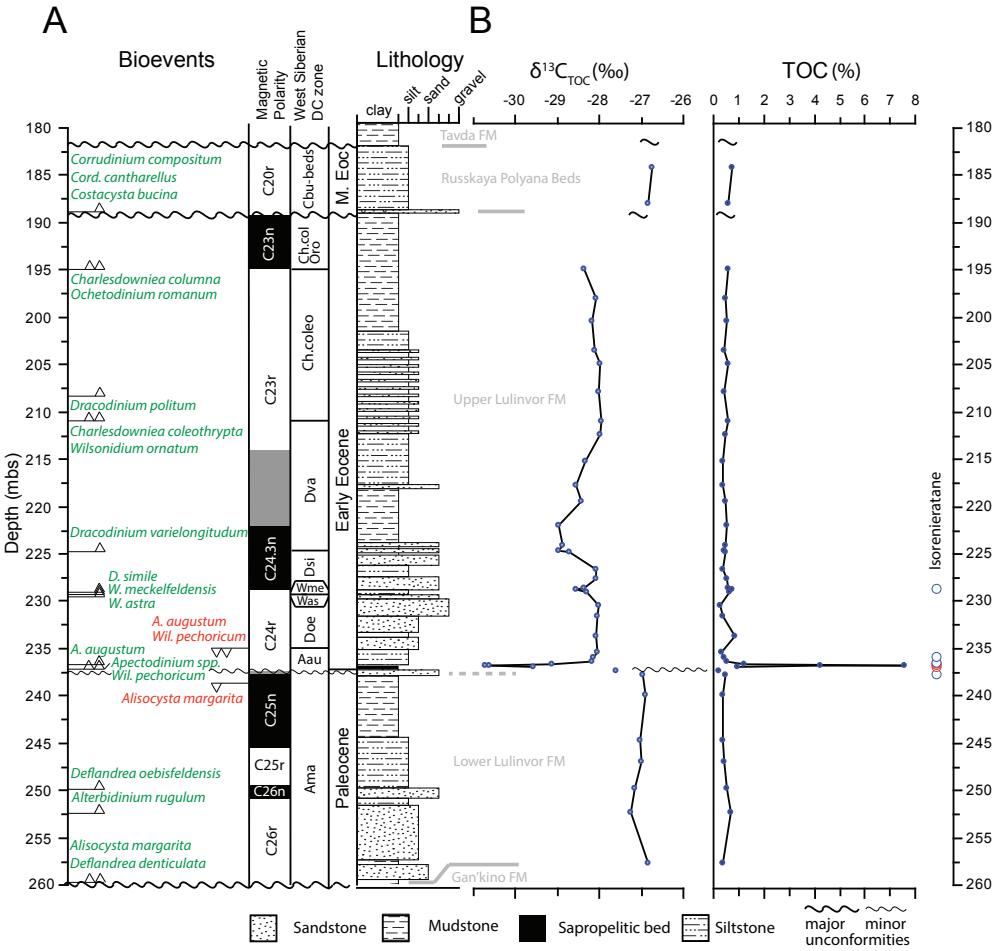

Figure 2. A: *Lithological column of Well 10 and stratigraphic markers. Standard Wentworth grain-size classes are used.* ***B:*** *Stable carbon isotope ($\delta^{13}C_{TOC}$) and total organic carbon (TOC), circles indicate samples tested for isorenieratane (red = present, blue = absent). Depth in meters below surface; mbs. West Siberian dinoflagellate cyst zonation follows Iakovleva and Aleksandrova, (2013). Genus name abbreviations: A.; Apectodinium, Dr.; Dracodinium, Cord.; Cordosphaeridium, W.; Wetzeliella, Wil; Wilsonidium. Dinozone abbreviations: Ama; Alisocysta margarita, Aau; Apectodinium augustum, Doe; Deflandrea oebisfeldensis, Was; Wetzeliella astra, Wme; Wetzeliella meckelfeldensis, Dsi; Dracodinium simile, Dva; Dracodinium varielongitudum, Ch.coleo; Charlesdowniea coleothrypta, Ch.colum; Charlesdowniea columna, Oro; Ochetodinium romanum, Cbu; Costacysta bucina.*

decanted. Residues were centrifuged with heavy liquid (K_2CdI_4) and boiled with HF (10%) to remove heavy particles and silicates, respectively. We applied no exote spiking or sieving. At least 200 dinocysts were counted per sample where possible. Samples yielding <100 dinocysts were excluded from quantitative analyses.

Results and Discussion

Stratigraphy

We apply the dinocyst zonation scheme for Western Siberia (Iakovleva and Aleksandrova, 2013; Iakovleva and Heilmann-Clausen, 2010) to correlate recorded first (e.g., *Alisocysta margarita*, *Deflandrea denticulata*, *Charlesdowniea columna*), and last occurrences (e.g., *A. margarita*, *Apectodinium augustum*, *Wilsonidium pechoricum*), and the magnetic reversals of (Iakovleva et al., 2012) to the global polarity timescale (Fig. 2). This indicates that the section spans the interval from ~60–52 Ma. The combined occurrence of the dinocyst *Apectodinium augustum* and the 3.1 ‰ negative CIE from -27.6 ‰ to -30.7 ‰ indicates that the sapropelitic bed from 237 to 236.4 mbs represents the PETM (Fig. 2; e.g., Crouch et al., 2001; Schmitz et al., 2004). BIT values of ~0.05 indicate low terrestrial contributions to TOC (Hopmans et al., 2004) throughout this interval, excluding a major effect of varying organic matter sources on the recorded $\delta^{13}C_{TOC}$ shift. The 70 cm thick glauconite-rich unit separates the top of Chron 25n and the PETM and marks a ~1 Ma hiatus or condensed interval associated with the unconformity between the lower and upper Lulinvor subformations.

Several first occurrences of Wetzelielliodeae, *Wetzeliella astra-lobisca*, *W. lunaris*, *W. meckelfeldensis* and *Dracodinium simile* around 228.8 mbs suggest an age close to that of ETM2. However, the absence of a CIE suggests a hiatus or insufficient sampling resolution. At 188.2 mbs, an erosional surface marks the boundary between the upper Lulinvor Fm. and middle Eocene Russkaya Polyana beds (Akhmetiev et al., 2010).

Anoxia during the PETM

We recorded the presence of isorenieratane and its derivatives within the PETM (Fig. 2). This provides evidence for the presence of photosynthetic green sulfur bacteria, which implies photic zone euxinia (e.g., Sinninghe Damsté et al., 1995). Concurrent high TOC wt% suggests that anoxia developed in the entire water column. However, given the partially benthic life cycle stage of cyst-forming dinoflagellates that requires oxygen, anoxia likely developed intermittently or seasonally.

Temperature evolution

Regardless of the applied calibration, the TEX_{86} temperature record at Well 10 closely resembles global deep-water temperature trends inferred from the benthic oxygen isotope stack (Zachos et al., 2008) and temperature evolution in the southwest high (Bijl et al., 2013b, 2009) and mid latitude (Hollis et al., 2012) Pacific Ocean for the late Paleocene and early Eocene (~60–52 Ma; Figures 3a, S2). Based on latest Paleocene and earliest Eocene temperatures (~21 °C), SSTs rose by ~7 °C during the PETM (Fig. 3a), consistent with several other mid-latitude sites but somewhat greater than the global average (Dunkley Jones et al., 2013). TEX_{86}^{H} (applied to all records for optimal comparison) shows ~10 °C of long-term warming in both the Northern and Southern hemisphere (NH and SH). Rising atmospheric CO_2 concentrations perhaps caused this warming. However, the only available tropical temperature record suggests stable temperatures throughout the early Eocene, challenging this hypothesis (Pearson et al., 2007).

Contrasting with general assumptions in the literature and SH records (Bijl et al., 2009; Hollis et al., 2012), the Arctic and WSS show stable temperatures or slight cooling between the PETM and ETM2. This is also apparent in various benthic oxygen isotope records (e.g., Zachos et al., 2008) and seems to mark a prolonged (0.8–0.9 Myr) period of comparatively warm temperatures in the NH SST records following the PETM. At ~54.3 Ma, NH-SH temperature gradients are re-established and match the previously observed hemispheric

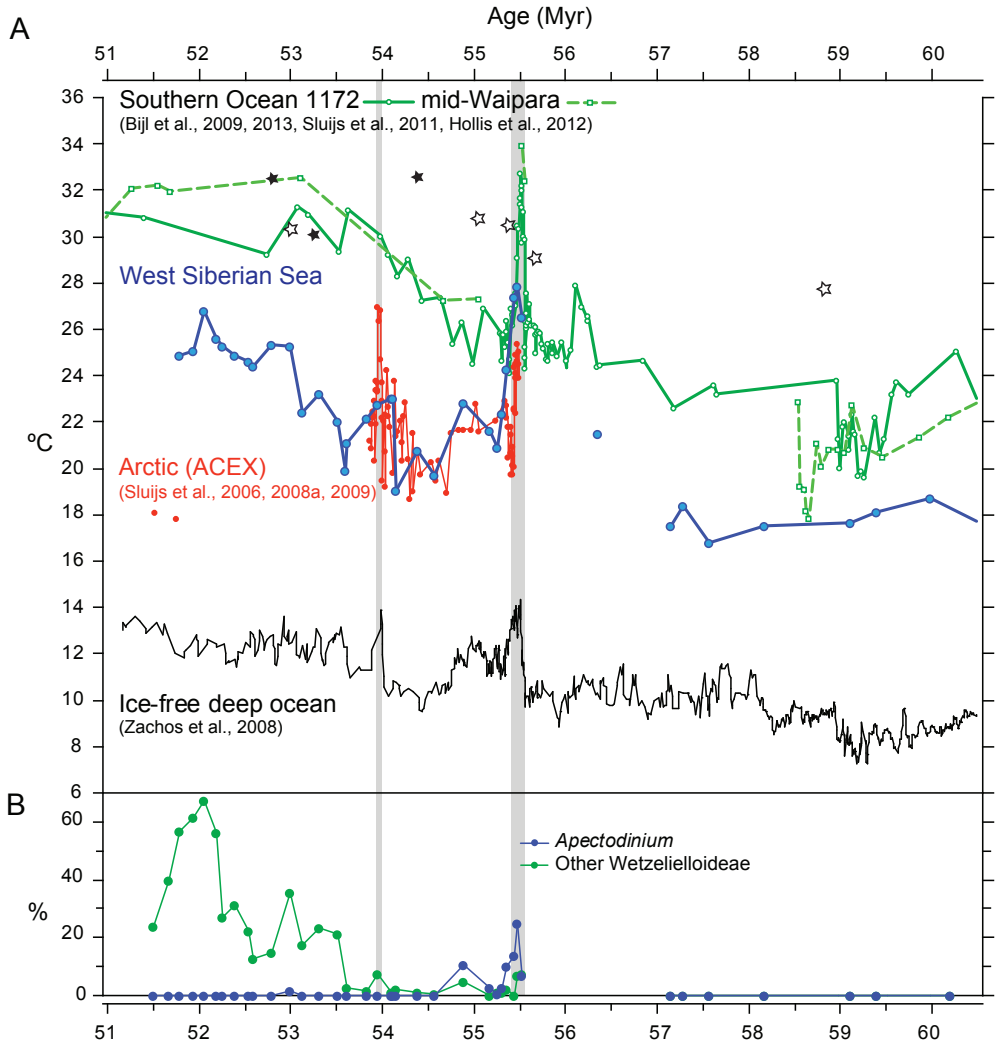

Figure 3. A: *TEX_{86}^{H} reconstructed temperatures. Geological Timescale (GTS) 2012 Age in Ma. Ice-free temperatures represent a 5-point moving average of the Zachos et al. (2008) benthic oxygen isotope stack. Gray bands mark the positions of the PETM (~55.5 Ma) and ETM2 (~54 Ma; latter not recorded in Well 10). Tanzania; closed stars indicate TEX_{86}^{H} data; open stars are maximum foraminifer $\delta^{18}O$ derived temperatures (Pearson et al., 2007). The TEX_{86}^{H} calibration error is 2.5 °C.* ***B:*** *Relative abundances of Apectodinium (blue) and Wetzelielloideae (green) in the Well 10.*

asymmetry, as noted by Bijl et al., (2009).

Remarkably, temperatures in the WSS were nearly identical, in both trend and absolute values to those in the Arctic Ocean during the earliest Eocene (55.5–54 Ma; Fig. 3a), implying the absence of a gradient from 58°N to 85°N. Seasonal and depth biases in the TEX_{86} proxy, as well as impact of genetic differences between archaeal populations are poorly understood

and likely important in higher latitudes and stratified basins, respectively. However, if TEX_{86} truthfully reflects mean annual SST, this implies that mechanisms must have acted that amplified warming in the Arctic (Sluijs et al., 2006) or cooled the WSS.

SST limitation of *Apectodinium* and other Wetzelielloideae

The oldest record of *Apectodinium* is close to the Danian-Selandian boundary in the Tethys Ocean (Guasti et al., 2005) and it has long been hypothesized to be a thermophilic genus (e.g., Bujak and Brinkhuis, 1998) that required a minimum temperature to thrive (Sluijs and Brinkhuis, 2009). If so, *Apectodinium* and its entire subfamily Wetzelielloideae would not be present below this SST threshold in Well 10 (Fig 3). To test this hypothesis, we investigate the relation between SST and the Wetzelielloideae in Well 10 and the ACEX record (Sluijs et al., 2009, 2006 ; Fig. 4), the sites with the lowest TEX_{86}-derived SSTs for the studied time interval and therefore suitable to quantify a lower tolerance limit. We expect this relation to exhibit major scatter; alongside SST, salinity and nutrients were likely important for *Apectodinium* and Wetzelielloideae (Sluijs and Brinkhuis, 2009; Sluijs et al., 2006). Low-salinity tolerant dinocysts (e.g. *Senegalinium*) are only minor components in WSS assemblages during the PETM (see GSA Data Repository1) and co-occur with Wetzelielloideae in the early Eocene suggesting that low salinity was unlikely limiting. Moreover, we find that the correlation of Wetzelielloideae to SSTs is significant ($p = 2.7\times10^{-6}$), whereas the correlation to the BIT is not ($p = 0.015$), which implies that temperature is here more important than terrestrial nutrient and freshwater input. Therefore, we can estimate the lower tolerance limit of Wetzelielloideae, including *Apectodinium* at ~20±2.5 °C (Fig. 4), suggesting this temperature was a minimum prerequisite for their proliferation in the Paleocene and early Eocene.

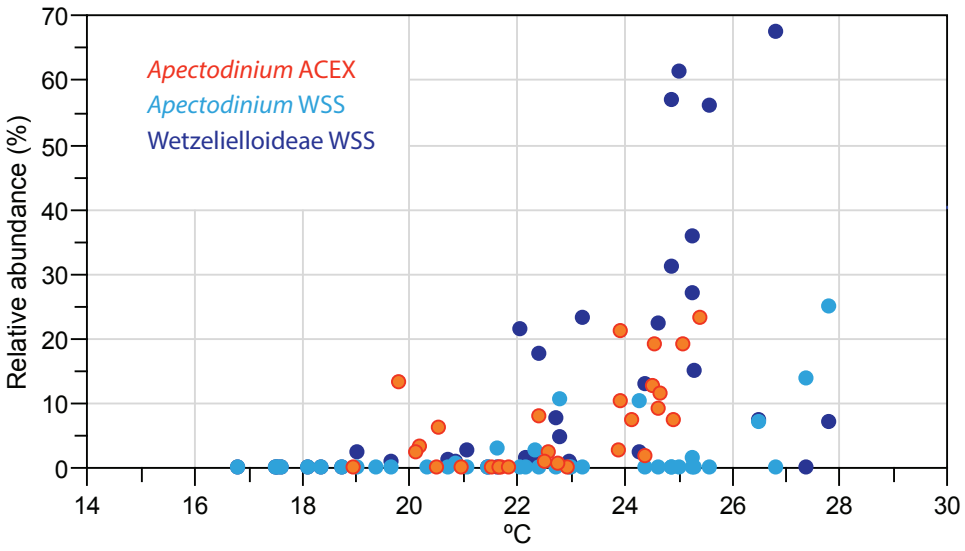

Figure 4. *Relative concentrations of Apectodinium, both in the Well 10 (light blue) and ACEX (orange) and other Wetzelielloideae (Well 10 – dark blue) plotted against reconstructed temperature.*

Conclusions

Upper Paleocene and lower Eocene sediments from the WSS reveal 9 °C of long-term warming from 58 to 52 Ma and 7 °C of warming during the PETM, based on TEX_{86}^{H}. Absolute recorded temperatures are nearly identical to those recorded in the Arctic. Slight cooling occurred in the interval between the PETM and ETM2, consistent with Arctic surface and deep ocean trends. During the PETM, euxinia developed in the photic zone. We quantify the threshold minimum temperature for the proliferation of Paleocene and early Eocene Wetzelielloideae, an extinct dinocyst subfamily that also includes *Apectodinium*, at 20 °C.

Supplementary Information

Organic Geochemistry Methods

We analyzed 38 samples from the Paleocene-Eocene Lulinvor Formation. Total organic carbon (TOC) content is measured on ~10 mg of homogenized and decalcified sample using a CNS-analyzer (Fisons). Stable carbon isotope ratios were determined using an isotope ratio mass spectrometer (IRMS, Finnigan Mat Delta Plus) coupled online to the CNS-analyzer. Based on direct comparison to international and in-house standards, absolute reproducibility for TOC and $\delta^{13}C_{TOC}$ is better than 0.1% and 0.05‰ respectively. For biomarker analysis, ~10 g of freeze-dried powdered sediment was extracted by a Dionex Accelerated Solvent Extractor (ASE) using Dichloromethane (DCM): Methanol (9:1 vol:vol) at 100 °C, 7 x 10^6 Pa. Extracts were separated into polar and apolar fractions over an Al_2O_3 column using Methanol:DCM 1:1 and Hexane:DCM 9:1 as respective eluents. Apolar fractions were measured by gas chromatography (GC) using an Agilent 6890 gas chromatograph and gas chromatography mass spectrometry (GC-MS) using a Thermo DSQ mass spectrometer to identify isorenieratane and its diagenetic derivatives (see Schoon et al., 2011 for further details). These components were detected in 3 samples during the peak of the PETM CIE; 237.0, 236.9 and 236.85 mbs (Fig. 2, Table S3).

To analyze glycerol dibiphytanyl glycerol tetraethers (GDGTs), the polar fraction was dissolved in Hexane:Isopropanol 99:1, filtered over a 0.45 µm PTFE filter and subsequently measured for GDGTs on an Agilent 1100 high performance liquid chromatography-mass spectrometer (HPLC-MS). Based on in-house standards, TEX_{86} reproducibility is better than 0.01, which translates to less than 0.5 °C in our temperature range. The most recent high temperature calibration for the TEX_{86} (Schouten et al., 2002) paleothermometer (TEX_{86}^H) was applied (Kim et al., 2010).

We apply the branched isoprenoid tetraether (BIT) index (Hopmans et al., 2004) and methane indices (MI; Weijers et al., 2011; Zhang et al., 2011) to assess influences of terrestrial, methanotrophic and methanogenic GDGT producers on TEX_{86} (Table S4). BIT values are below 0.3 and we find no significant correlation between TEX_{86} and BIT (r^2 = 0.02). The MI of Zhang et al., (2011) is below the cutoff value (0.3) for all samples except one; 0.302 at 236.9 mbs, where the TEX_{86} value is not anomalous compared to the total dataset. We constrain the influence of diffusive methane fluxes in the sediment using the GDGT-2 over 3 ratio as this is where the largest discrepancies occur according to Weijers et al., (2011). GDGT-2 / GDGT-3 ratios are stable through the entire section and close to normal shallow marine (~2-3) ratios rather than close to GDGT distributions influenced by diffusive methane fluxes (~9).

Age model

The age model (Table S1, Fig. S1) for the Lulinvor Fm. is based on magnetic reversals, first and last occurrences of dinocyst species and the recently updated dinocyst zonation scheme for the West Siberian Sea (Iakovleva and Aleksandrova, 2013; Iakovleva and Heilmann-Clausen, 2010). This scheme has been correlated to North Sea dinocyst zones and is correlated to the Geomagnetic Polarity Time Scale (GPTS) using global nannoplankton zones and global first occurrences of dinocysts. The negative CIE of the PETM is used as complementary stratigraphic marker, from 237-236.7 mbs. We use the GPTS2012 (Vandenberghe et al., 2012) for the absolute ages of magnetic reversals (Table S1), which we identify based on dinocyst biostratigraphy (Williams et al., 2004). Dinocyst taxonomy follows Fensome, (2004).

The sediments of the Lulinvor Formation (Fm) unconformably overlay those of the late Cretaceous Gan'kino Fm. The top of the Lulinvor Fm is marked by an erosional surface and overlain by the Russkaya Polyana beds that are regionally deposited during a middle Eocene (C20r) transgression, and the Tavda Fm which is middle to late Eocene in age (see Akhmetiev et al., 2010; Radionova et al., 2003) for a detailed description of Cretaceous and Paleogene regional stratigraphy). For the purpose of this paper we consider only the age constraints for the Lulinvor Fm in detail.

Based on the number of reversals below the PETM and previous observations from the North Sea (Powell et al., 1996) we calibrate the first occurrence of *Deflandrea oebisfeldensis* at 249.9 mbs to C26n. The first occurrence of *D. oebisfeldensis* reported by Williams et al. (2004) is in C26n, but their reported age (57.8 Ma) is very different due to recent large revisions on the age of C26n itself. We have no calibration points in between 248.5 mbs and the base of the Lulinvor Fm at 260.2 mbs. Assuming that sedimentation rates in this interval were similar to C26n, the base of the section is ~60.2 Ma, closer to the top of C26r than the onset.

A hiatus or period of low sedimentation rates is recognized close to the onset of the PETM, from ~57.0 to 55.53 Ma. This period of glauconitic sandstone deposition between 237.9 and 237 mbs is poorly constrained, due to the lack of tie-points. The data generated for this interval is therefore not considered as part of the age-model. *Apectodinium augustum* is frequently used as a marker for the PETM. We find this dinocyst species occurs from 237 to 233.7 mbs, while the isotope and temperature excursions only occur from 237 to 236.7 mbs.

The resolution of the paleomagnetic measurements is insufficient to identify the several short reversals in C24, but we infer these to be between 212 and 223 mbs. Identification of the underlying C24.3n is based on the first occurrence of *Dracodinium varielongitudum* at 224.9 mbs (Williams et al., 2004). ETM2 initiated in the uppermost part of magnetochron C24r.3r and therefore we expect to record a negative CIE close to this interval. The absence of a CIE suggests a hiatus or insufficient sampling resolution. The first occurrence of *Dr. politum* (~52.3 Ma) identifies C23r at 208 mbs, whereas the first occurrence of *Charlesdowniea columna* at 195 mbs marks the bottom of C23n. Average sedimentation rates suggest that the reversed signal at 212 mbs must be close to the bottom of C23r.

TEX_{86}
Calibrations

The application of TEX_{86} in ancient sediments is complicated by several factors, most of which center on the origin of glycerol dibiphytanyl glycerol tetraethers (GDGTs), export mechanisms and the applied calibration (see detailed review of Pearson and Ingalls, 2013; Schouten et al., 2013; Tierney, 2012). Global core top calibrations of GDGTs in the modern ocean have shown that the original TEX_{86} definition is less responsive towards temperature change in modern high latitude regions. This could partly be due to different Thaumarcheotal populations, which has been source of major debate in recent literature (e.g. Pearson and Ingalls, 2013). However, Thaumarcheotal populations are poorly constrained in the modern ocean let alone the Paleogene ocean. The difference in response resulted in two separate core-top calibrations: TEX_{86}^{H} and TEX_{86}^{L} for high (>15 °C) and low (<15 °C) temperature regimes, respectively (Kim et al., 2010). Recently, an influence of water depth on TEX_{86}^{L} was detected (Taylor et al., 2013). It was suggested that TEX_{86}^{L} should be interpreted as a "shelf" calibration rather than a "low temperature" calibration and that TEX_{86}^{H} is preferred for deep-water settings (Taylor et al., 2013).

Hollis et al., (2012) calibrated the TEX_{86}^{H} for the Eocene Southern Ocean (p-TEX_{86}) using

oxygen isotopes and Mg/Ca ratios to obtain SST estimates in line with foraminifer based proxies. However, this introduces uncertainties related to foraminifer geochemistry and since it is only based on data from the Southern Ocean, the global validity is questionable. Lastly, the TEX_{86}' calibration was developed (Sluijs et al., 2006) for uppermost Paleocene sediments at Lomonosov Ridge, Arctic Ocean (IODP Exp. 302) due to abnormally high abundances of GDGT-3. This calibration excludes GDGT-3 from the original equation and uses an earlier calibration core top dataset (n = 104). Similarly aberrant distributions of lipids are not encountered in any other record.

The existence of all these calibrations for the different parts of the globe makes it difficult to compare TEX_{86} records from different hemispheres, one of the primary goals of our study. Preferably, we apply the same calibration to all TEX_{86} records, as it has the advantage of excluding inter-calibration uncertainties. Below we compare absolute temperature estimates of the two most commonly applied calibrations, TEX_{86}^H and TEX_{86}^L for the different records. Collectively, for the comparison of trends between the discussed sites, TEX_{86}^H is the most suitable option.

Regional evaluation of TEX_{86}^H vs TEX_{86}^L

West Siberian Sea

The TEX_{86} data generated for this study in the WSS was compared to independent regional temperature data and plotted against other TEX_{86}^H and TEX_{86}^L records and deep-ocean temperatures based on benthic foraminifer $\delta^{18}O$ (Figs 3, S1). In the study region, warm temperate to paratropical vegetation elements were persistently present since the early Danian (Akhmetiev and Beniamovski, 2006), indicating both high annual temperatures and low seasonal temperature variability. Furthermore, in the Paleocene TEX_{86}^L in the WSS yields temperatures below that of reconstructed deep-ocean temperatures(Zachos et al., 2008). We consider it unlikely that the WSS Paleocene SSTs were in the order of 7 °C, lower than deep ocean temperatures while thermophilic vegetation grew on adjacent land. In this light we consider TEX_{86}^H-based temperatures for the WSS more realistic.

ACEX

SSTs based on TEX_{86}^H and TEX_{86}^L agree within calibration error during the PETM and ETM2 (compare Figs 3 and S1). However, in the period following the PETM, TEX_{86}^L reconstructed temperatures are on average ~8 °C lower, resulting in extremely high amplitude temperature swings (Fig. 3; S1). The TEX_{86}' calibration typically plots between TEX_{86}^H and TEX_{86}^L. A complicating factor here is the high relative amount of soil-derived lipids, as expressed in the BIT index (Hopmans et al., 2004). Measured BIT values exceed 0.4 in 40 of 67 samples from the top of the PETM CIE recovery to the onset of the ETM2 CIE (Sluijs et al., 2009, 2006). BIT values above 0.3 (Weijers et al., 2006) and 0.4 (Bijl et al., 2013) are often used as cutoff for reconstructing absolute temperatures (Fig. S2). Notably, TEX_{86}^H is not correlated with BIT (r^2 = 0.111) but TEX_{86}^L is (r^2 = 0.414) (Fig. S2). Indeed, high BIT values are associated with rather low TEX_{86}^L in the early Eocene. For our inter-site comparison, we therefore use TEX_{86}^H.

1172 & mid-Waipara

Large differences between the TEX_{86}^H and TEX_{86}^L as seen in the ACEX/WSS have been observed previously from the Southern Ocean (see supplement of Bijl et al., 2013). In contrast to Siberia, Hollis et al., (2012) and Contreras et al., (2014) concluded that TEX_{86}^L better agrees with vegetation derived MAT and Mg/Ca reconstructed water temperatures of planktonic foraminifera in the southwest Pacific Ocean. Crucially, however, trends in

TEX_{86}^{H} and TEX_{86}^{L} are essentially identical so for our inter-site comparison of trends, both TEX_{86}^{H} and TEX_{86}^{L} are applicable. Care should, however, be taken in comparing absolute values.

Dinocyst grouping

Ecological interpretation of dinocyst assemblage data is often carried out by grouping cyst taxa that are considered to have similar ecological affinities. Groups most important to the current paper are reiterated. Generally, we follow Sluijs et al., (2005) and Sluijs and Brinkhuis, (2009) for paleoecological interpretations and dinocyst grouping. The ratio of Peridinioid, dominantly heterotrophic, over Gonyaulacoid, dominantly autotrophic, cysts (P/G ratio) has been used to derive paleo-productivity patterns (see review of Sluijs et al., 2005). Heterotrophic organisms are often found in higher relative abundances in eutrophic areas, leading to the suggestion that these are indicative of eutrophication.

Apectodinium and other Wetzelielloideae

These Peridinioid genera are typically considered thermophilic heterotrophs, although absolute temperature requirements are defined for the first time in this paper. The group consists of the genera *Apectodinium*, *Wetzeliella*, *Dracodinium*, *Charlesdowniea* and *Wilsonidium*. It should be noted that we only consider Paleocene and early Eocene members of the subfamily Wetzelielloideae.

Senegalinium group

This group consists of Peridinioid, i.e. Peridiniales-like, genera with a hexa-2a archeopyle, *Senegalinium*, *Phthanoperidinium*, *Cerodinium*, *Deflandrea* and *Paleocystodinium*. Species from this group are generally considered low-salinity tolerant and heterotrophic (e.g. Barke et al., 2011; Harding et al., 2011; Sluijs and Brinkhuis, 2009).

Gonyaulacoid cysts

These cysts are attributed to the order Gonyaulacales that in the modern ocean is dominated by autotrophic species. Some are considered open marine (e.g. *Impagidinium, Spiniferites*) whereas other are associated with high-energy environments (*Areoligera, Glaphyrocysta*) or lagoons (*Homotryblium*)(Pross and Brinkhuis, 2005). For clarity, we consider only the shared characteristic of autotrophy.

Temperature and dinoflagellate cyst response

Canonical correspondence analysis using PAST v.2.17 (CCA; Fig. S4) plots both TEX_{86} and BIT in the same direction, although no significant correlation between the two exists (r^2 = 0.02). Wetzelielloideae, excluding *Apectodinium*, plot between BIT and TEX_{86}^{H}, indicating a relation of both terrigenous input and SST with the abundance of this group. *Apectodinium* abundances correlate well with %TOC (Fig. S4, axis 2), which is caused by the development of a sapropel during the PETM. In addition, *Apectodinium* plots in the same direction as TEX_{86}^{H} (Fig. S4, axis 1). Crucially, when all Wetzelielloideae are considered together, the correlation with TEX_{86}^{H} is much stronger. It appears that this correlation with temperature starts at ~20 °C, which we interpret as the minimum SST for the occurrence of the group. The correlation with TEX_{86}^{H} is statistically significant ($p = 2.7\times10^{-6}$). The correlation with the BIT index, that would signal a relation with the input of nutrients and low salinity waters from rivers, is much less significant ($p = 0.015$).

Materials

The remaining sediment and palynological slides are stored at the Geological Institute,

Russian Academy of Sciences, Pyzhevsky pereulok 7, 109017 Moscow, Russia. Organic geochemical extracts are stored at the Department of Earth Sciences, Utrecht University, Budapestlaan 4, 3584CD Utrecht, The Netherlands.

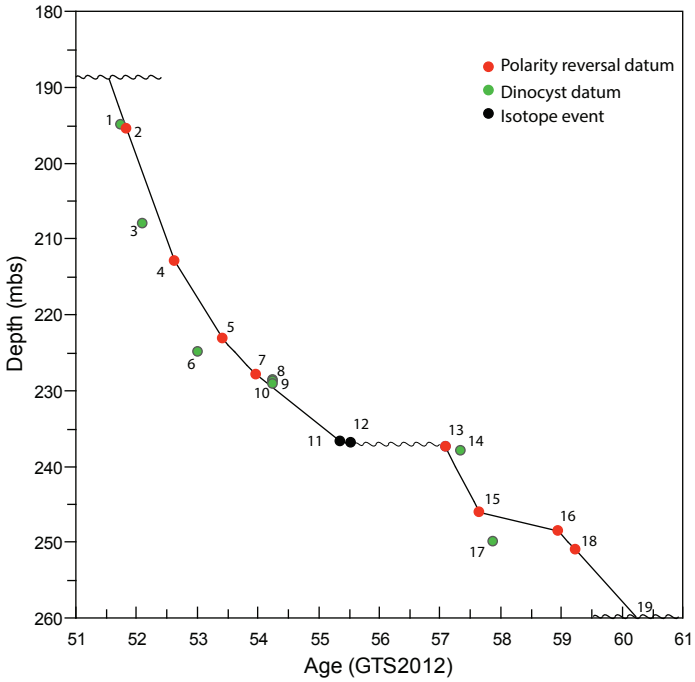

Figure S1. *Age model tie-points and bio-events. Paleomagnetic absolute ages (red) and isotope event (black), used to for the age model, supporting dinocyst events (green). Numbers correspond to event numbers in brackets in Table S1.*

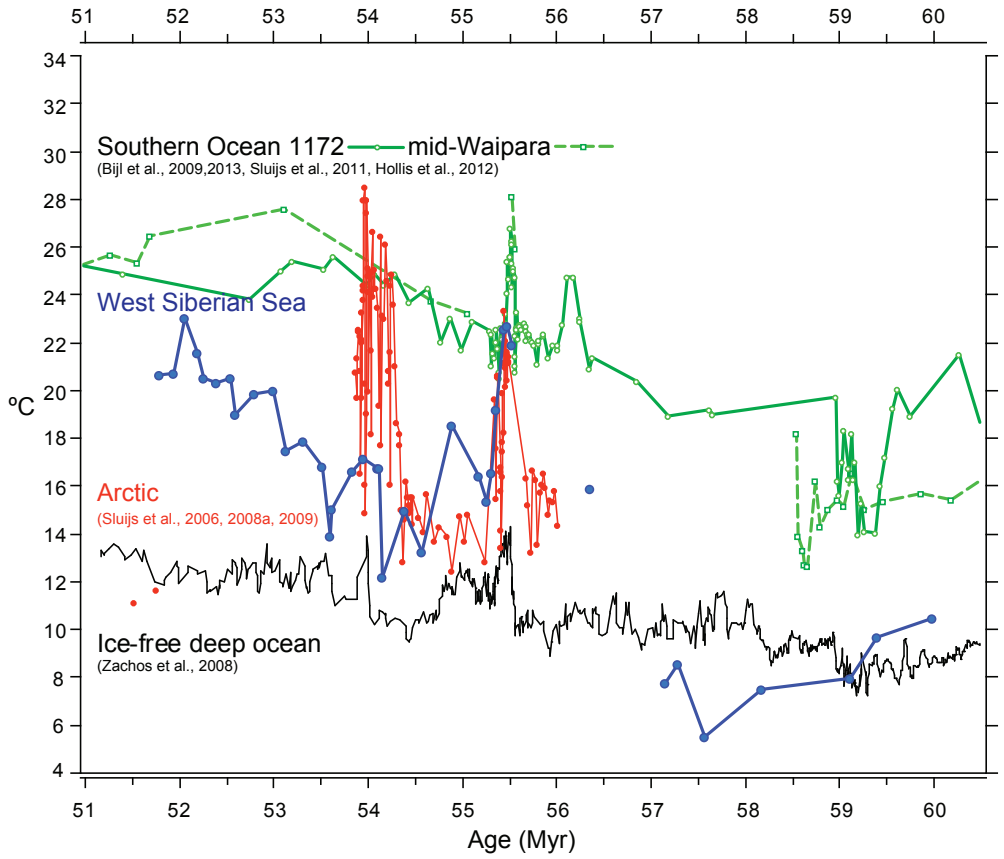

Figure S2. *TEX_{86}^{L} reconstructed temperatures for all sites, including pre-PETM ACEX aberrant lipid distributions. The calibration error for TEX_{86}^{L} is 4°C. Note the large temperature shifts in both the WSS and ACEX record.*

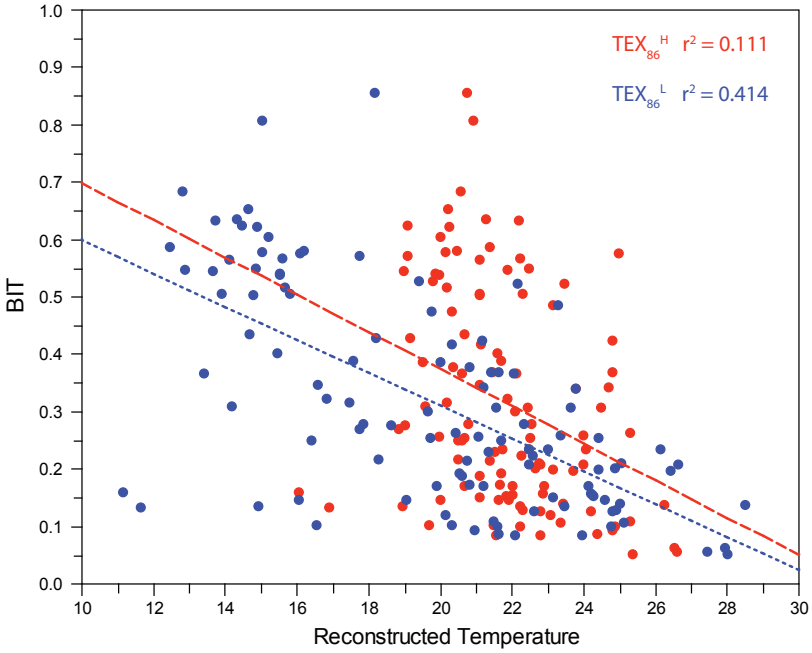

Figure S3. *BIT correlation to TEX_{86}^{L} and TEX_{86}^{H} for the ACEX sediments from the PETM onwards.*

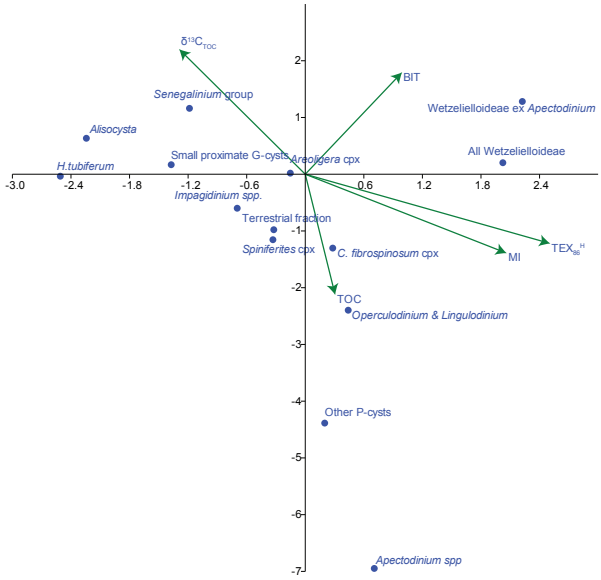

Figure S4. *CCA plot for all dinoflagellate cyst assemblage data from Well 10, WSS. TEX_{86}, BIT, TOC and $\delta^{13}C_{TOC}$, are treated as environmental variables.*

Table S1. *Absolute age of tie-points. *youngest possible age, **oldest possible age. Note that the base and top of the section are extrapolated with sedimentation rates from over and underlying chrons, respectively. Event numbers in parentheses correspond to numbers in Fig. S1. D = Dinocyst event RN = Reverse to Normal NR = Normal to Reverse i = isotope event*

Event(#)	Depth	Chron	Age (GTS2012)	DINO FO/LO	Age model
	189.00	C23.2n	**50.96***		*51.54*
	192.50	C23.2n			*51.70*
D(1)	195.00	C23.2n	51.73	FO *Ch. columna*	*51.81*
RN(2)	195.50	C23r-C23.2n	**51.833**		**51.83**
	198.00	C23r			*51.95*
	200.50	C23r			*52.06*
	203.50	C23r			*52.19*
	205.00	C23r			*52.26*
D(3)	208.00	C23r	52.1	FO *Dr. politum*	*52.40*
	209.00	C23r			*52.44*
	211.10	C23r			*52.53*
	212.50	C23r			*52.60*
NR(4)	213.00	C24.1n-C23r	**52.62**		**52.62**
	215.30	undiff.			*52.80*
	217.80	undiff.			*52.99*
	219.50	undiff.			*53.12*
	220.50	undiff.			*53.20*
	222.00	undiff.			*53.32*
NR(5)	223.25	C24.3n-C24.2r	**53.416**		**53.42**
	224.10	C24.3n			*53.52*
	224.70	C24.3n			*53.59*
D(6)	224.90	C24.3n		FO *Dr. varielongitudum*	*53.61*
	226.70	C24.3n			*53.83*
	227.70	C24.3n			*53.95*
RN(7)	228.00	C24r-C24.3n	**53.983**		**53.98**
D(8)	228.70	C24r		FO *Dr. simile*	*54.09*
D(9)	228.80	C24r		FO *W. meckelfeldensis*	*54.11*
D(10)	229.10	C24r		FO *W. astra-lobisca*	*54.16*
	230.50	C24r			*54.38*
	231.70	C24r			*54.57*
	233.70	C24r			*54.89*
	235.50	C24r			*55.17*
	236.00	C24r			*55.25*
	236.40	C24r			*55.31*
I(11)	236.70	C24r	**55.36**	Top PETM	**55.36**
	236.85	C24r			*55.45*
	236.90	C24r			*55.47*

Table S1. *Cont'd*

Event(#)	Depth	Chron	Age (GTS2012)	DINO FO/LO	Age model
I(12)	237.00	C24r	**55.53**	Onset PETM	**55.53**
	237.00	C25n/C24r?			*57.07*
	237.40	C25n/C24r?			*57.09*
NR(13)	237.50	C25n-C24r?	**57.101***		*57.10*
D(14)	237.90	C25n	57.35	LO *A. margarita*	57.13
	240.00	C25n			57.26
	244.70	C25n			57.57
RN(15)	246.00	C25r-C25n	**57.656**		**57.66**
	247.00	C25r			*58.18*
NR(16)	248.50	C26n-C25r	**58.959**		**58.96**
	248.70	C26n			*58.98*
D(17)	249.90	C26n	57.8	FO *D. oebisfeldensis*	*59.11*
RN(18)	251.00	C26r-C26n	**59.237**		**59.24**
	252.40	C26r			*59.39*
	253.40	C26r			*59.50*
	257.70	C26r			*59.98*
	257.80	C26r			*59.99*
	259.70	C26r			*60.20*
R(19)	260.20	C26r	**62.221****		*60.26*

Table S2. *Well 10 Paleomagnetic measurements. χ; susceptibility, NRM: mA/m, i: inclination (degree)*

Depth	χ	NRM	Inclination (deg)	Depth	χ	NRM	Inclination (deg)
188.0	15.0	0.3	36	228.9	5.6	1.1	-66
188.9	17.2	0.5	45	229.5	8.6	2.2	-64
189.5	12.8	0.6	63	230.7	15.2	2.5	-72
190.5	15.2	0.2	42	231.8	14.0	1.3	-68
191.4	12.8	0.6	21	233.2	15.4	0.9	-70
192.4	17.2	0.4	18	233.8	15.5	1.0	-56
193.0	20.9	1.2	61	234.2	15.6	1.8	-57
194.0	21.0	0.8	62	236.7	20.0	1.3	-24
195.0	25.6	1.6	26	237.5	12.5	2.1	-10
196.0	14.1	0.2	-43	238.7	21.1	1.9	39
198.2	16.0	0.3	-65	239.7	20.9	0.8	27
198.9	9.8	1.0	-63	241.0	20.0	1.2	19
200.9	5.6	0.3	-8	242.8	20.5	2.4	85
201.5	4.0	0.3	-8	243.6	7.1	0.3	65
202.2	3.8	0.2	-29	244.6	8.2	0.4	27
203.3	5.4	0.6	-32	245.6	10.9	0.4	-25
204.2	6.7	0.9	-4	247.0	11.5	1.9	-19
206.0	5.2	0.2	-24	248.3	12.2	1.3	-68
207.2	5.2	0.4	-20	249.5	13.4	1.2	72
208.5	4.6	0.6	-51	250.5	13.6	0.4	63
209.3	5.8	0.3	-34	251.5	8.4	0.9	-82
210.3	7.9	0.8	-66	252.5	8.5	0.5	-38
211.3	17.9	0.7	-25	253.4	8.6	0.5	-69
212.0	14.3	0.4	-27	254.6	9.8	2.4	-78
223.2	16.0	0.4	-30	255.6	8.0	0.8	-45
223.3	20.5	0.6	69	256.6	7.6	0.7	-56
224.0	24.5	1.8	70	257.4	17.0	2.6	-60
225.2	27.1	11.2	83	258.6	11.8	1.5	-57
226.3	13.2	1.1	36	259.3	11.1	0.7	-65
227.2	11.4	1.2	56	260.5	7.0	0.5	-55

Table S3. *$\delta^{13}C_{TOC}$ and TOC(wt%). Isorenieratane / Aromatic Derivative (presence/absence)*

Depth(mbs)	Age (GTS2012)	$\delta^{13}C_{TOC}$	TOC(wt%)	Isor.	A. der.
195.00	51.81	-28.4	0.59		
198.00	51.95	-28.1	0.49		
200.50	52.06	-28.2	0.55		
203.50	52.19	-28.2	0.43		
205.00	52.26	-28.0	0.56		
208.00	52.40	-28.1	0.42		
211.10	52.53	-28.0	0.59		
212.50	52.60	-28.0	0.46		
215.30	52.80	-28.4	0.35		
217.80	52.99	-28.6	0.37		
219.50	53.12	-28.5	0.46		
222.00	53.32	-29.0	0.54		
224.10	53.52	-28.9	0.50		
224.70	53.59	-29.0	0.40		
224.90	53.61	-28.8	0.47		
226.70	53.83	-28.1	0.39		
227.70	53.95	-28.1	0.51		
228.70	54.09	-28.4	0.57		
228.80	54.11	-28.6	0.74	-	-
229.10	54.16	-28.3	0.62		
230.50	54.38	-28.1	0.27		
231.70	54.57	-28.1	0.38		
233.70	54.89	-28.1	0.82		
235.50	55.17	-28.1	0.34		
236.00	55.25	-28.2	0.40	-	-
236.40	55.31	-28.2	0.51		
236.70	55.36	-29.2	1.22	-	-
236.85	55.45	-30.8	7.54	+	+
236.90	55.47	-30.7	4.23	+	+
237.00	55.53	-29.6	0.96	+	+
237.40	57.09	-27.6	0.21		
237.90	57.13	-27.0	0.45	-	-
240.00	57.26	-26.9	0.39		
244.70	57.57	-27.1	0.35		
247.00	58.18	-27.0	0.40		
249.90	59.11	-27.2	0.51		
252.40	59.39	-27.3	0.67		
257.70	59.98	-26.9	0.37		

Table S4. *TEX_{86}^{H} & TEX_{86}^{L} reconstructed temperatures, BIT (Hopmans et al., 2004) and MI (Zhang et al., 2011).*

Depth(mbs)	Age (GTS2012)	TEX_{86}	TEX_{86}^{H}	TEX_{86}^{L}	BIT	MI
195.00	51.81	0.63	24.9	20.7	0.14	0.21
198.00	51.95	0.63	25.0	20.7	0.17	0.21
200.50	52.06	0.67	26.8	23.0	0.13	0.21
203.50	52.19	0.65	25.6	21.6	0.19	0.22
205.00	52.26	0.64	25.3	20.5	0.26	0.21
208.00	52.40	0.63	24.9	20.3	0.16	0.21
211.10	52.53	0.63	24.6	20.5	0.23	0.22
212.50	52.60	0.62	24.4	19.0	0.11	0.22
215.30	52.80	0.64	25.3	19.9	0.14	0.23
217.80	52.99	0.64	25.3	20.0	0.10	0.23
219.50	53.12	0.58	22.4	17.5	0.13	0.21
222.00	53.32	0.60	23.2	17.9	0.15	0.21
224.10	53.52	0.57	22.1	16.8	0.16	0.21
224.70	53.59	0.53	19.9	13.9	0.13	0.20
224.90	53.61	0.55	21.1	15.0	0.12	0.20
226.70	53.83	0.58	22.2	16.6	0.08	0.20
227.70	53.95	0.59	22.7	17.2	0.09	0.21
228.70	54.09	0.59	23.0	16.8	0.09	0.21
228.80	54.11	0.59	23.0	16.7	0.08	0.21
229.10	54.16	0.52	19.0	12.2	0.07	0.19
230.50	54.38	0.55	20.7	15.0	0.10	0.20
231.70	54.57	0.53	19.7	13.2	0.13	0.19
233.70	54.89	0.57	21.8	17.2	0.11	0.18
233.70	54.89	0.61	23.8	19.9	0.10	0.19
235.50	55.17	0.57	21.7	16.4	0.07	0.19
236.00	55.25	0.55	20.9	15.4	0.06	0.19
236.40	55.31	0.58	22.4	16.5	0.07	0.19
236.70	55.36	0.62	24.3	19.2	0.06	0.20
236.85	55.45	0.69	27.4	22.6	0.03	0.21
236.90	55.47	0.70	27.8	22.7	0.08	0.30
237.00	55.53	0.67	26.5	21.9	0.05	0.21
237.40	57.09	0.56	21.5	15.9	0.06	0.19
237.90	57.13	0.49	17.6	7.8	0.13	0.15
240.00	57.26	0.51	18.4	8.5	0.18	0.16
244.70	57.57	0.48	16.8	5.5	0.14	0.14
247.00	58.18	0.49	17.5	7.5	0.15	0.16
249.90	59.11	0.49	17.6	7.9	0.11	0.15
252.40	59.39	0.50	18.1	9.7	0.13	0.17
257.70	59.98	0.51	18.7	10.5	0.12	0.17

Table S5. *Relative dinocyst abundances (% of total dinocysts, i.e. count). Wetzelielliodeae includes genera Wetzeliella, Wilsonidium, Dracodinium, Charlesdowniea. Senegalinium group includes Palaeocystodinium. Both Senegalinium and Deflandrea/Cerodinium groups are considered to be low-salinity-tolerant (e.g. Sluijs et al., 2005, Sluijs & Brinkhuis, 2009). P/P+G ratio is calculated adding all Peridinioid cysts together and dividing that by the sum of all Gonyaulacoid and Peridinioid dinocysts (Sluijs et al., 2005).*

Depth(mbs)	Age(GTS2012)	*Apectodinium*	Wetzelielloideae	*Senegalinium* cpx	P/P+G	Count
189.00	51.54	0	24	34	0.65	211
192.50	51.70	0	40	35	0.84	217.5
195.00	51.81	0	57	23	0.83	216
198.00	51.95	0	61	15	0.78	200.5
200.50	52.06	0	67	9	0.77	237.5
203.50	52.19	0	56	14	0.71	215.5
205.00	52.26	0	27	9	0.37	256.5
208.00	52.40	0	31	9	0.42	280
211.10	52.53	0	22	7	0.32	237.5
212.50	52.60	0	13	6	0.21	239
215.30	52.80	0	15	2	0.18	234
217.80	52.99	1	36	3	0.42	212.5
219.50	53.12	0	17	36	0.62	211.5
222.00	53.32	0	23	43	0.72	225.5
224.10	53.52	0	21	42	0.71	225.5
224.90	53.61	0	3	42	0.49	192
226.70	53.83	0	2	40	0.44	199
227.70	53.95	0	8	16	0.3	200
228.70	54.09	0	1	8	0.11	212.5
228.80	54.11	0	0	3	0.04	259.5
229.10	54.16	0	2	2	0.06	210.5
230.50	54.38	0	1	1	0.02	248
231.70	54.57	0	1	1	0.02	263
233.70	54.89	11	5	11	0.3	190
235.50	55.17	3	0	4	0.08	211
236.00	55.25	0	1	4	0.05	204
236.40	55.31	3	1	5	0.09	197.5
236.70	55.36	10	2	9	0.24	215
236.85	55.45	14	0	2	0.2	136.5
236.90	55.47	25	7	6	0.42	225
237.00	55.53	7	7	7	0.25	215.5
237.40	57.09	0	0	43	0.43	74
237.90	57.13	0	0	30	0.39	172
240.00	57.26	0	0	48	0.52	190
244.70	57.57	0	0	35	0.4	200

Table S5. *cont'd*

Depth(mbs)	Age(GTS2012)	*Apectodinium*	Wetzelielloideae	*Senegalinium* cpx	P/P+G	Count
247.00	58.18	0	0	67	0.69	252
248.70	58.98	0	0	33	0.35	81
249.90	59.11	0	0	69	0.75	225
252.40	59.39	0	0	22	0.27	400
254.30	59.50	0	0	34	0.38	27
257.70	59.98	0	0	17	0.38	53
259.70	60.20	0	0	5	0.07	142

Table S6. *Bio-events as recognized in the Well 10 section. FO; first occurrence. LO; last occurrence. Note that the age is according to the age model and NOT to the actual first or last appearance datum of the species (see Table S1 for relevant absolute datums).*

Depth(mbs)	Age (GTS2012)	Event	Species
188.10	~43-45.xx	FO	*Cordosphaeridium cantharellus*
			Costacysta bucina
			Corrudinium incompositum
195.00	51.81	FO	*Charlesdowniea columna*
			Ochetodinium romanum
208.00	52.40	FO	*Dracodinium politum*
211.10	52.53	FO	*Charlesdowniea coleothrypta*
			Wilsonidium ornatum
224.70	53.59	FO	*Dracodinium varielongitudum*
228.70	54.09	FO	*Dracodinium simile*
228.80	54.11	FO	*Wetzeliella meckelfeldensis*
229.10	54.16	FO	*Wetzeliella astra*
233.70	54.89	LO	*Apectodinium augustum*
		LO	*Wilsonidium pechoricum*
236.70	55.36	FO	*Apectodinium augustum*
237.00	55.53	FO	*Apectodinium spp.*
		FO	*Wilsonidium pechoricum*
237.90	57.16	LO	*Alisocysta margarita*
249.90	59.11	FO	*Deflandrea oebisfeldensis*
252.40	59.39	FO	*Alterbidinium rugulum*
259.70	60.20	FO	*Alisocysta margarita*
			Deflandrea denticulata

3

Extreme warmth and plankton regime shift in the tropics during the Paleocene – Eocene Thermal Maximum

Abstract

Global surface temperatures and the deep ocean rapidly warmed by ~5°C during the Paleocene – Eocene Thermal Maximum (PETM; ~56 million years ago; Ma) (Dickens et al., 1997; Dunkley Jones et al., 2013; Sluijs et al., 2006; Zachos et al., 2006). This warming coincides with a global negative stable carbon isotope excursion (CIE) recorded in terrestrial and marine sedimentary components in conjunction with deep ocean carbonate dissolution, which reflect the injection of ^{13}C-depleted carbon into the ocean-atmosphere system (Dickens et al., 1997). Extratropical sea surface temperatures (SSTs) during the PETM met or exceeded modern subtropical values (Sluijs et al., 2011, 2006; Zachos et al., 2006). In conjunction with such warm extratropical temperatures, climate models (Lunt et al., 2012) predict tropical SSTs >35°C—near upper physiological temperature limits for many organisms (Sherwood and Huber, 2010; Sunday et al., 2011). However, few data are available to test these conjectured extreme tropical temperatures or their potential lethality (Huber, 2008). Such records in the subtropical-to-tropical latitude band (Aze et al., 2014; Kozdon et al., 2011; Zachos et al., 2003), are often stratigraphically complex or incomplete, based on single proxies, or seem to be geochemically altered. Here, we reconstruct equatorial SSTs using paired analyses of planktonic foraminiferal Mg/Ca and oxygen isotope ($\delta^{18}O$) ratios, and TEX_{86} from a shallow marine sedimentary section deposited in Nigeria. We find temperatures ~33 °C in the late Paleocene rising ~3 °C during the PETM, confirming model predictions on the magnitude of polar amplification and refuting the tropical thermostat theories (Williams et al., 2009). Moreover, dinoflagellate cyst abundances and diversity dropped to remarkably low values during peak PETM warming. This suggests that thermal stress was likely the main driver for eukaryotic biodiversity loss in the surface ocean during the PETM implying that tropical marine ecosystems may indeed be vulnerable to future climate change (Solomon et al., 2009).

Introduction

The PETM has been extensively studied, but proxy data from the tropics remains scarce. This means several questions essential for predicting future temperature change in the tropics and globally remain unresolved. For example,tropical temperatures are essential to gauge whether global meridional temperature gradients were diminished during the PETM and to what extent the tropics are affected by the warming, thereby testing tropical thermostat theory and equilibrium climate sensitivity. Furthermore, the biotic response during the severe rapid warming of the PETM in tropical near-shore environments is poorly understood.

To assess concepts as tropical thermostats, polar amplification and limits to biological adaptability to warming and carbon injection during the PETM, we studied samples from boreholes IB10A and B and the Sagamu Quarry (SQ) from the Oshosun Formation, Dahomey Basin, Nigeria (Extended data Figure 1). The Paleocene to lower Eocene sediments of the Oshosun Fm. were deposited on the shelf at ~1 °S paleolatitude (Boyden et al., 2011), and can be traced laterally over the Dahomey Basin (Okosun, 1990). They typically consist of dark-grey mudstones, and are ~100m thick in the IB10B Core. We generated organic and inorganic geochemical and micropaleontological data to locate the PETM and assess environmental change.

Materials

We analysed samples from the Oshosun Formation, from the Nigerian sector of the Dahomey Basin (Extended Data Fig. 1) from the Sagamu Quarry (SQ) and the two drill-cores IB10A and IB10B. An unconformity separates the Oshosun Fm. and the underlying

Paleocene limestones of the Ewekoro Fm. The Ilaro sandstone marks the top of the Oshosun Fm (Okosun, 1990).

Samples from the Oshosun and Ewekoro formations from the SQ (6°48'12.54 N; 3°37'46.11 E) were collected during a field expedition in 2003 and used for foraminifer and dinoflagellate analyses, a.o. for biostratigraphy (Bankole et al., 2007; Gebhardt et al., 2011). From the 13 samples from the Oshosun Formation, we used ~5-10 g for quantitative dinoflagellate cyst analysis, ~10 g for biomarker geochemistry, and 0.3 g for stable bulk organic carbon isotope ($\delta^{13}C_{TOC}$) measurements. Approximately ~600 g was disintegrated, sieved and picked as aliquots or completely for foraminifera (Gebhardt et al., 2011). Well-preserved specimens of *Morozovella acuta, Acarinina spp., Bulimina paleocenica and Lenticulina olokuni*, which are common to abundant throughout the section, were selected for stable isotope and trace element analyses.

The sediments from two drill-cores, IB10A and IB10B (6°53'N, 3°00'E), were recovered during exploration drilling in 1976, targeting the Paleocene limestones of the Ewekoro formation, near Ilaro, Nigeria. Samples from IB10A from an earlier study (Bankole et al., 2007) were used for a pilot. In 2012, we took 73 samples from the 110m long IB10B core. Each sample was split into several fractions; 2 - 10 g for palynological analysis, 5 - 10 g for organic geochemistry, 1 g for major and trace element analyses and 0.3 g for $\delta^{13}C_{TOC}$. The remaining core material is stored at the Nigerian Geological Survey Core Repository in Abuja, Nigeria. Residues of washed samples, SEM-stubs and slides with picked foraminifera are stored in the collection of the Geological Survey of Austria, Vienna, Austria (coll. nos. GBA2010/122/0001 to GBA2010/122/0053). Palynological slides, residues and organic extracts are stored at the Laboratory of Palynology and Paleobotany (LPP), Utrecht University, Heidelberglaan 2, 3584CS Utrecht, The Netherlands.

Methods

Micropaleontology

600 g of air-dried sediment was disintegrated with 5% hydrogen peroxide and washed over a 0.063-mm sieve. Residues were air-dried and split into aliquots and completely picked for foraminifera with a dry paintbrush. Samples with insufficient amounts of sample material were not used for interpretations. For stable isotope and Mg/Ca analyses, we exclusively used pristine (i.e., glassy, hollow) specimens.

Carbonate stable isotope analysis

We picked multiple specimens from each investigated sample. These aliquots comprise about 10 specimens of *Lenticulina olukuni*, about 100 specimens of *Bulimina paleocenica*, about 20 specimens of *Acarinina spp*., and about 10 specimens of *Morozovella acuta*. Foraminiferal tests were treated with 98.8% ethanol, cracked, and ultrasonically cleaned following standard procedures. Stable carbon and oxygen isotopes were measured on a Finnigan MAT 251 mass spectrometer at Leibniz-Labor (Kiel), coupled online to the Carbo-Kiel device I for automated CO_2 preparation. External precision is better than 0.20 ‰ (average 0.04‰) and 0.19 ‰ (average 0.04‰) for oxygen and carbon, respectively. Data are given in conventional delta notation versus Vienna PeeDee Belemnite (V-PDB) standard.

Mg/Ca-ratios

We picked multiple foraminifera from each investigated sample to measure Mg/Ca-ratios. These aliquots comprise about 10 specimens of *Lenticulina olukuni* (0.23-1.53 mg), about 100 specimens of *Bulimina paleocenica* (0.10-0.71 mg), about 20 specimens of *Acarinina spp.* (0.18-0.80 mg), and about 10 specimens of *Morozovella acuta* (0.24-0.89 mg). Foraminiferal

tests were analysed on an ICP-AES instrument with an Mg/Ca intensity ratio calibration according to de Villiers et al., (2002) at Leibniz-Labor (Kiel). Internal analytical precision is better than 0.1-0.2% rsd. The cleaning protocol included several steps for removing adhering clays and siliciclastic particles and a reduction step (anhydrous hydrazine) for the removal of ferro-manganese coatings.

Palynology

We processed and counted a total of 53 samples from IB10B, 19 from IB10A and 7 from the SQ using standard protocols used at the Laboratory of Palaeobotany and Palynology at Utrecht University (Sluijs et al., 2011). In brief, exote spike of *Lycopodium clavatum* spores (n = 18583 ± 762) was added to 5-10g of freeze-dried sample to allow for absolute quantitative analysis. 10% HCl was added to dissolve carbonates. Supernatants were subsequently decanted and residues were treated twice with 38-40% HF and 30% HCl to remove silicates. After decantation, residues were washed with tap water over 250 and 15 μm sieves to remove large and small particles, respectively. One drop of the concentrated residue was mounted on a microscope slide using glycerine jelly and a minimum of 200 dinocysts was counted, if possible. For several samples across the core of the PETM up to 4 microscope slides were fully counted to a total of 18-134 dinocysts. For these samples, assemblages are thus statistically less well constrained than the samples with ≥200 counted dinocysts. This, however, does not affect quantification of absolute numbers of dinocysts per gram sediment.

For stable carbon isotope measurements of the palynological residue ($\delta^{13}C_{PALY}$), after microscope slide preparation, the remaining material was washed over a 40 μm sieve with distilled water, to remove the *Lycopodium* spores and most other pollen and spores to obtain a fraction that mostly contains dinocysts, along with some other palynomorphs. Due to the small amounts of large pollen and spores and low amounts of phytoclasts the fraction typically consists of dinocysts (~90+%) and foraminifer linings (max 10%). The core of the CIE is dominated by organic material from foraminifer linings and minor contributions from dinoflagellates.

Stable carbon isotope analyses

For stable isotope analysis of bulk organic carbon ($\delta^{13}C_{TOC}$), 0.3 g of freeze-dried material was powdered and decalcified using 1 M HCl. Samples were dried in a stove at 50 °C and subsequently total organic carbon (TOC) content was measured on ~10 mg of powdered homogenized residue using a CNS-analyzer (Fisons). Stable carbon isotope ratios were determined using an isotope ratio mass spectrometer (IRMS, Finnigan Delta Plus) coupled online to the CNS analyzer. Absolute reproducibility, based on international and in-house standards, for TOC and $\delta^{13}C_{TOC}$ was better than 0.1% and 0.05‰ respectively. 15-30 μg of the palynological residue was weighed and analyzed on the same IRMS. Samples of sufficient size were measured in duplicate.

Biomarker analyses

For TEX_{86} analysis (51 samples), ~10 g of freeze-dried powdered sediment was extracted by a Dionex Accelerated Solvent Extractor (ASE) using Dichloromethane (DCM): Methanol (9:1 vol:vol) at 100 °C, 7×10^6 Pa. Extracts were separated into polar and apolar fractions over an Al_2O_3 column using Methanol:DCM 1:1 and Hexane:DCM 9:1 as respective eluents. Apolar fractions of 18 samples across the PETM CIE were measured on gas chromatography (GC) using an Agilent 6890 gas chromatograph and gas chromatography mass spectrometry (GC-MS) using a Thermo DSQ mass spectrometer to identify isorenieratane and its diagenetic

derivatives.

To analyze glycerol dibiphytanyl glycerol tetraethers (GDGTs), Hexane:Isopropanol 99:1 was added to the polar fraction, filtered over a 0.45 µm PTFE filter and subsequently measured for GDGTs on an Agilent 1290 ultra high performance liquid chromatography mass spectrometer (UHPLC-MS) at Utrecht University. In addition to measuring in-house TEX_{86} and branched isoprenoid tetraether (BIT) standards, a C_{46} GDGT standard (*m/z* 744) was added to all samples to facilitate quantification of GDGTs. Most samples were measured in duplicate, some in triplicate, to assess reproducibility. Reproducibility was always better than 0.02 TEX_{86} units and 0.1 BIT units respectively, reproducibility of in-house standards was always better than 0.01 and 0.03 for TEX_{86} and BIT.

We use the BIT index (Hopmans et al., 2004) and methane indices (MI) (Weijers et al., 2011; Zhang et al., 2011) to assess influences of terrestrial, methanotrophic and methanogenic GDGT producers on TEX_{86}. BIT values below 0.3 (Weijers et al., 2006) or 0.4 (Bijl et al., 2013) generally yield trustworthy TEX_{86} values. A weak correlation exists between TEX_{86} and BIT ($r^2 = 0.168$; Extended Data Fig. 3), but samples with BIT values >0.3 are not statistically different from samples with BIT <0.3. We therefore use all TEX_{86} data, except for one outlier, i.e. more than 2 standard deviations from the mean, at 93 mbs. GDGT-2 / GDGT-3 ratios are close to normal shallow marine (~2-3) ratios rather than reflecting GDGT distributions influenced by diffusive methane fluxes (~9)(Weijers et al., 2011). Likewise, the cut-off (0.3) for the MI of Zhang et al., (2011) is never reached.

Bulk sediment chemistry

Approximately 125 mg of freeze-dried sediment was dissolved in a 2.5 ml HF (40 %) and 2.5 ml of $HClO_4/HNO_3$ mixture, in a closed Teflon bomb at 90 °C during one night. The acids were then evaporated at 160 °C and the resulting gel was subsequently redissolved in 1M HNO_3 at 90 °C during another night. Subsequently, total elemental concentrations were determined by ICP-OES (Perkin Elmer Optima 3000 Inductively Coupled Plasma - Optimal Emission Spectroscopy). Precision and accuracy was better than 5 %, based on calibration to standard solutions and checked against internal laboratory standard sediments.

Climate Modelling

We carried out a suite of simulations using the new NCAR Community Earth System Model (CESM1), utilizing our well-established boundary conditions. This includes a T31 spectral resolution atmosphere and ~1.8° × 3° horizontal spacing and 25 vertical levels for the oceans. Simulations span a range of radiative forcings equivalent to 1120, 2240, and 4480 ppm CO_2. All these simulations were carried out for >3000 years and are fully equilibrated as indicated by ocean temperature trends, surface and top-of-atmosphere energy imbalance, and trends in ideal age tracers. The higher CO_2 forced experiments produce climates that compare favourably with proxy records for the late Paleocene and early Eocene, which is similar to the results we found previously with the older version of the NCAR model (Huber and Caballero, 2011; Lunt et al., 2012); we will refer to these as the "late Paleocene" and "PETM" simulations. As described previously, the low CO_2 simulations match late Eocene climates well (Goldner et al., 2014). We also conducted short sensitivity studies, utilizing new high-resolution earliest Eocene boundary conditions (Herold et al., 2014) within a model with higher resolution (atmosphere: 2° × 2° horizontal finite volume resolution, ocean: 1° × 1° and 40 vertical levels). While these simulations are not fully equilibrated in the deep ocean, they establish that the upper ocean temperature gradients found in the lower resolution simulations are robust.

All sites within 19 degrees of the equator were averaged to define the tropical mean. In this case, that includes the following sites: Tanzania, Nigeria, and Ocean Drilling Project (ODP) Site 865 (Extended data table 2). The results are qualitatively insensitive to the choice of what to normalise by.

We use standard techniques in ocean data assimilation to create homogenized and interpolated maps of sea surface temperatures based on the sparse data. The proxy records treated according to the standard oceanographic technique of Barnes-Cressman iterated objective analysis implemented in the NCAR Command Language (https://www.ncl.ucar.edu/Document/Functions/Contributed/obj_anal_ic_Wrap.shtml). In this approach each observation is assigned a circular radius of influence, R. In this study we use successive values of R of 10, 2, and 1 degree. A first guess of the value at every grid point is made by including all observations within the region of influence that grid point. A distance weighted average of the differences between the first-guess fields and the actual observations is made and this anomaly is added into the first-guess fields to calculate a second-guess field. Thus observations from beyond the radius of influence are ignored in updating the field and other observations closer to the initial observation are given greater weight. This is done for all grid points under consideration. The resulting fields are used as the basis for the next iteration, which is carried out with a smaller region of influence.

Results & Discussion
Stratigraphy

Planktonic foraminifer zones P4b, P4c and P5 are identified in both the SQ and the IB10B core (Fig. 1, Extended data Fig. 2, see Supplementary Information), based on the presence of *Acarinina soldadoensis*, extinctions of *Morozovella acutispira* and *M. velascoensis*. From 80 to 77 meters below surface (mbs) of the IB10B core, we record a 4‰ negative carbon isotope excursion (CIE) in total organic carbon (TOC). This level corresponds to the lower part of Zone P5 and therefore this CIE represents the PETM.

The general $\delta^{13}C_{TOC}$ pattern is mimicked in the $\delta^{13}C$ measured on the isolated palynological residues ($\delta^{13}C_{PALY}$), which mainly consists of dinoflagellate cysts (dinocysts). However, $\delta^{13}C_{PALY}$ values are up to ~7 ‰ higher than $\delta^{13}C_{TOC}$ in the interval between 80 and 77 mbs (Fig. 1b). This interval has relatively high TOC and dinocyst concentrations 2-50 fold higher compared to previous intervals (Fig 1d). pointing to high marine productivity. This likely caused high $\delta^{13}C_{DIC}$ values which in turn lead to high $\delta^{13}C_{PALY}$ and $\delta^{13}C_{TOC}$, in fact close to the Paleocene value for $\delta^{13}C_{TOC}$. We therefore place the onset of the CIE at ~80 mbs. The onset of the CIE is followed by an interval with stable values, often referred to as the 'core' of the CIE, up to ~70 mbs and a gradual subsequent recovery phase to ~65 mbs, suggesting the PETM in our record is complete.

For the SQ, a 2‰ negative CIE in foraminifer carbonate at the top of the section directly above the P4c/P5 planktonic foraminifer zone boundary suggests the presence of the onset of the PETM (Gebhardt et al., 2011) (Extended data Figure 2). However, not all foraminifer isotope records are consistent with this inference and directly overlying strata are affected by weathering. Therefore, only pre-PETM temperatures can be inferred unambiguously from SQ and for PETM temperatures, we focus on the IB10 core.

Absolute temperatures

For SST reconstructions, we employ the TEX_{86}^{H} calibration (Kim et al., 2010), based on relative abundances of membrane lipids of marine Thaumarchaeota (see Supplementary Information for calibration and potential caveats). TEX_{86}^{H} indicates late Paleocene SSTs

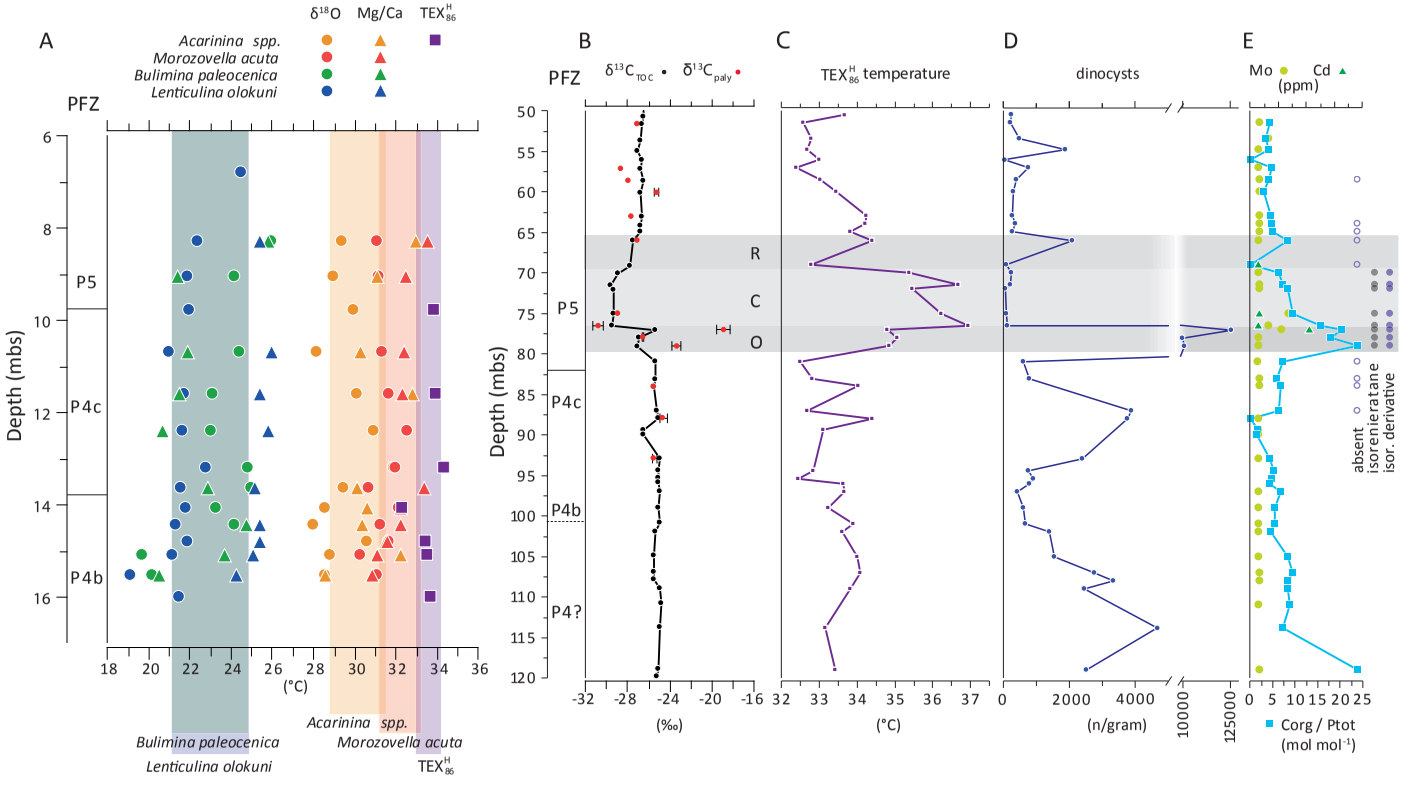

Figure 1. *Temperature and environment for Sagamu Quarry and IB10B core.* ***a.*** *Surface and bottom-water temperature reconstructions based on Mg/Ca (triangles), $\delta^{18}O$ (circles) and TEX_{86}^{H} (squares) for the Sagamu Quarry. Shaded areas represent 1standard deviation around the mean of each species and TEX_{86}^{H}.* ***b.*** *Stable carbon isotope record of total organic carbon ($\delta^{13}C_{TOC}$) and palynological residue ($\delta^{13}C_{PALY}$). The phases of the CIE are denoted O, C and R for Onset, Core and Recovery, respectively.* ***c.*** *TEX_{86}^{H}-based SST.* ***d.*** *Absolute concentrations of dinocysts per gram of dry sediment. Note the scale break between 4,000 and 10,000.* ***e.*** *Indicators of anoxia: Organic carbon over total phosphorus ratio (Corg/Ptot) (bluesquares). Presence of isorenieratane and derivative. Concentrations of redox sensitive trace elements Mo (light green circles) and Cd (dark green triangles) in ppm. Note that Mo concentrations are below the detection limit and absolute values should be treated with caution.*

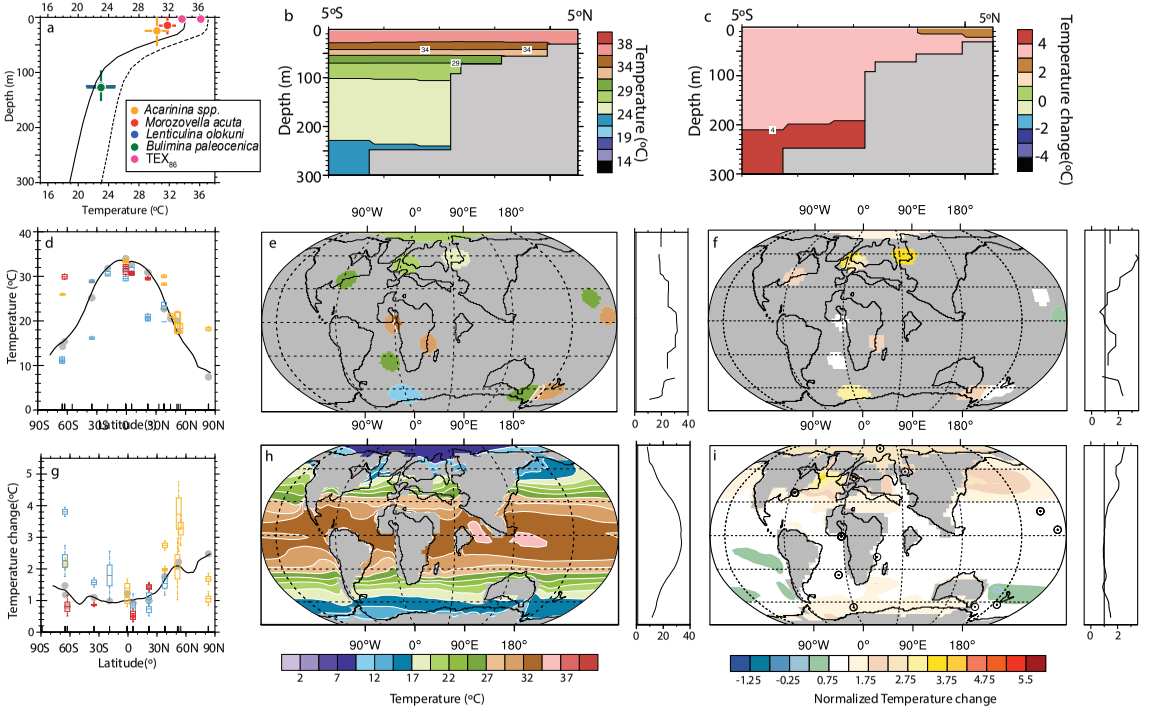

Figure 2. *Model-data comparison for Palaeocene (2240ppm) and PETM (4480ppm) CO_2 scenarios.* ***a.*** *Vertical temperature profile for the site locations, solid and dashed line represent Palaeocene and PETM model estimates, respectively. Data from Fig. 1a & c for comparison, including error bars for depth: Morozovella (0-30m), Acarinina (0-50m), TEX_{86}^H(0m; surface), benthic (100-150m).* ***b.*** *Palaeocene inshore-offshore (5° N - 5° S) transect.* ***c.*** *Temperature change from Palaeocene to PETM inthe same transect.* ***d.*** *TEX_{86}^H(orange), $\delta^{18}O$ (blue) and Mg/Ca (red) derived temperatures and Palaeocene meridional sea surface temperature (SST) gradient from model(solid line). Grey dots represent point-by-pointmodel-data comparisons.* ***e.*** *Absolute temperature reconstructions and interpolations.* ***f.*** *PETM SST change, normalised totropical (20 °N – 20 °S) SST change (2.7 °C) from data.* ***g.*** *TEX_{86}^H(orange), $\delta^{18}O$ (blue) and Mg/Ca (red) derived SST change between late Palaeocene and PETM. Grey dotsrepresent point-by-point model-data comparisons. SST change normalised to tropical SST change from data (2.7 °C).* ***h.*** *Absolute SST in the Palaeocene.* ***i.*** *SST changefrom Palaeocene to PETM normalised to tropical SST change in CESM1 (2.4°C). Black circles indicate site locations.*

of 33.6 ± 0.4 °C (n = 7) based on the samples from the SQ and 33.4 ± 0.2 °C (n = 9) in the IB10B core (Figs 1 a,c).

The reconstructed SSTs exceed the range of the modern ocean core-top calibration by ~4 °C and thus care has to be taken in interpreting these values. However, in mesocosm experiments (Schouten et al., 2007a) archaeal membrane lipids have shown a continuous relation with temperature up to 40 °C which provides support for extrapolating this calibration. If either earlier versions of the linear TEX_{86} calibration or the mesocosm calibration were used, the reconstructed SSTs would be even higher (Supplementary Information).

We also reconstruct Paleocene SSTs by analyses of Mg/Ca ratios and the oxygen isotopic composition ($\delta^{18}O$) of glassy mixed-layer dwelling planktonic foraminifers *Acarinina spp.* (mostly *A. nitida* and *A. soldadoensis*) and *Morozovella acuta* from the SQ. For Mg/Ca, we assume Paleocene seawater Mg/Ca of 2 mol mol^{-1}, correct for non-linear response under changing Mg/Ca (Evans and Müller, 2012), and use calibrations for planktonic (Anand et al., 2003) and benthic (Lear et al., 2002) foraminifera to calculate seawater temperatures. We assume a local seawater $\delta^{18}O$ of -0.39‰, correcting for latitude (+0.61‰) and absence of large ice sheets (-1.0‰) (supplementary information) to calculate seawater temperatures (Kim and O'Neil, 1997). Mg/Ca and $\delta^{18}O$ temperatures derived from *Acarinina* average 31.0 ± 0.6 °C and 29.5 ± 0.5 °C, respectively, whereas *Morozovella acuta* yields 32.2 ± 0.4 °C and 31.4 ± 0.3 °C. *M. acuta* likely had a shallower depth habitat than *Acarinina spp.*, based on their respective $\delta^{13}C$ and $\delta^{18}O$ values (Zachos et al., 2006), which is consistent with our data. Mg/Ca and $\delta^{18}O$ of *M. acuta* and TEX_{86}^{H} therefore provide consistent SST estimates, well within proxy calibration error, of 32-34 °C during uppermost Paleocene zones P4b and P4c (Fig. 1a,c). Mg/Ca and $\delta^{18}O$ of the benthic foraminifera *Bulimina paleoceanica* and *Lenticulina olokuni* indicate seafloor (100-150m) temperatures of ~23 °C (Fig. 1a).

Data - Model comparison

We compare these reconstructions with output from new simulations carried out with the NCAR Community Earth System Model (CESM1) utilizing well-established Eocene boundary conditions (Herold et al., 2014). Similar to work with the older version of the model (Huber and Caballero, 2011), simulations with radiative forcings equivalent to 2240 and 4480 ppm CO_2 compare favourably with proxy records for the late Paleocene and early Eocene; which are referred to as the "late Paleocene" and "PETM" simulations. The late Paleocene simulation reproduces, within proxy calibration error, the Nigerian late Paleocene SSTs reconstructed here, and supports the strong temperature stratification at the core location as inferred from the data (Fig. 1a, 2a,b). The model results furthermore suggest that this basin represents some of the warmest open ocean temperatures in the early Paleogene world (Figure 2h) making this a suitable location to record effects of extreme greenhouse warming on biota during the PETM.

SSTs during the core of the PETM CIE averaged 36.1° C ± 0.7 °C (n = 5) based on TEX_{86}^{H}, implying average warming of ~3 °C relative to the latest Paleocene (Fig. 1c). This is reproduced in the simulations, both in terms of relative change and absolute values (Figure 2a). No mixed-layer planktonic foraminifera and only few poorly preserved thermocline dwelling foraminifera were found in the PETM section of the IB10B core. The temperatures are similar to planktonic foraminifer $\delta^{18}O$ derived SSTs from the western tropical Indian Ocean (Aze et al., 2014) and model results (Figure 2d,e). The maximum recorded absolute SST of 37 °C, about 8 °C warmer than any open ocean at present, is reached at ~76.5 mbs.

Tropical thermostats

Recent modelling work has succeeded in reproducing most proxy reconstructions, with the exception of the Arctic and the southwest Pacific Oceans (Huber and Caballero, 2011). The simulations presented here have the same shortcomings. But, crucially, our SST data for the background latest Paleocene – early Eocene climate state support the very warm tropical oceans of >35 °C that are necessary to approach such warm extratropics in models. In addition, such hot values reject tropical thermostat theory (Williams et al., 2009).

Polar amplification

Our data, together with the few other tropical or subtropical records from a global compilation of proxy records (Supplementary Information), imply that the mean warming of the tropical oceans was ~3°C. Mid and high-latitude regions warmed by 5-8°C (Sluijs et al., 2011, 2006; Zachos et al., 2006), implying that that ocean warming was amplified in the extratropics during the PETM, contrary to prior reconstructions (Sluijs et al., 2006; Zachos et al., 2003). To identify whether the model and data shows the same pattern of polar amplification, we normalise regional temperature changes by the warming observed from 20 °N – 20 °S.

Interestingly, most extratropical regions warm only slightly more compared to the tropics in both data and model (Figure 2g), throughout the Atlantic and in the Central Pacific Ocean. The largest disagreements are around 50-60° North and South latitude, where the proxies show much greater amplification than the models. Interestingly, the only truly polar proxy record, from the Arctic, shows no clear signal of polar amplification, as noted previously (Sluijs et al., 2006), in sharp contrast to the model.

More data, in particular from multi-proxy records are necessary to make a definitive statement about the ability of the current generation of climate models to reproduce past meridional temperature gradients responses to PETM warming, such as we have attempted here, but we believe the normalising approach has merit as the resulting pattern, is a specific 'fingerprint' that may be used as a test of models.

Global Temperature change and climate sensitivity

After using optimal interpolation on the proxy records and taking area-weighted means we find that global tropical mean SSTs increased by 2.7°C across the PETM and global mean SSTs increased by 5.3°C, very close to prior estimates (Dunkley Jones et al., 2013), but without the intervening use of a climate model. CESM1 has a modern equilibrium climate sensitivity of 3.2°C per doubling of CO_2, and we find a nearly identical response of 3.5°C for a doubling under Eocene conditions, but because ocean temperature changes are much less in the Eocene, only 2.8°C per doubling. Consequently, in this model, the observed warming would require two doublings of CO_2 (or equivalent forcing) from a baseline late Paleocene value of 2240 ppm. The required carbon release and CO_2 values are not credible (Panchuk et al., 2008) and any resolution requires a equilibrium climate sensitivity than the model's 3.2 °C value to simultaneously produce a late Paleocene warm enough to agree with proxies and a PETM that is hot enough with a plausible carbon release.

Ecological impact

Finally, to investigate the impact of the extremely high SSTs on biota we investigated dinoflagellate cyst assemblages. Upper Paleocene dinoflagellate cyst assemblages in the IB10 core and SQ represent normal marine assemblages, similar to those in extra-tropical regions during the PETM (Sluijs and Brinkhuis, 2009; Sluijs et al., 2011). At many of these

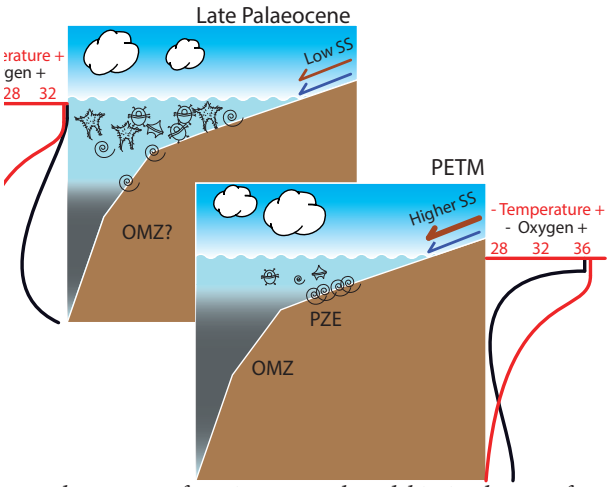

Figure 3. *Conceptual cartoon of environmental and biotic changes from the Palaeocene to the PETM. Differences from Palaeocene to PETM state include; temperature increase (~3ºC), expanded oxygen minimum zone (OMZ) and photic zone euxinia (PZE), higher sediment supply (SS) and suppressed eukaryote productivity in surface waters.*

sites, however, the peak of the PETM is characterized by high productivity of marine dinocysts (Harding et al., 2011; Sluijs and Brinkhuis, 2009). Our data from Nigeria suggests the opposite. At ~77 mbs, we record a decrease from 10^5 to less than 10^2 dinocysts per gram of sediment (Fig. 1d), falling to values far below those of the late Paleocene. Remaining dinocyst assemblages are impoverished with only heterotrophic and generalist genera (Supplementary Information). Anoxia developed at the study site during the PETM, evidenced by the presence of the biomarker isorenieratane and redox sensitive trace elements (Fig. 1e). However, we can exclude anoxia, preservation biases, stratification, and enhanced run-off as main causes for the dinoflagellate crash (Fig. 1, Extended data Figure 6, Supplementary Information). Instead, we argue that conditions became too hot for most dinoflagellate taxa during the core of the PETM, when SSTs rose to values >36°C. Such temperatures are considered uninhabitable for most marine eukaryotic organisms (Somero, 1995) even for hardy dinoflagellates, which are among the most temperature-resilient eukaryote plankton groups (Hallegraeff et al., 1997). Apart from often displaying narrow temperature tolerance ranges (Sunday et al., 2011), many modern thermophilic organisms show a sharp decline in productivity and consequently survival between optimum and (sub-) lethal temperatures (Paerl et al., 2011).

No similar temporal absence of eukaryotic plankton has been observed in tropical regions during the extreme warmth of OAE2, across the Cenomanian-Turonian transition (~94 Ma), where comparable TEX_{86}^{H} temperature estimates were obtained (Forster et al., 2007). This suggests that the rate of change during the PETM was an important factor in creating a heat-induced dead zone in eukaryotic marine plankton at this tropical location. Given that the rates of modern carbon input and warming are estimated to exceed that of the PETM by ~10 times(Zeebe et al., 2014), our results indicate that tropical oceans will be subject to warming and significant biotic change over the coming centuries at rates probably exceeding those of the PETM. Ocean warming on the scale found here has profound negative implications for the terrestrial biosphere as well, because heat stress has been found to scale linearly with tropical mean temperature (Sherwood and Huber, 2010).

Supplemental information

Stratigraphy

Gebhardt et al., (2011) identified planktonic foraminifer zones P4b to P5 and a negative carbon isotope excursion (CIE) in the planktonic foraminifer species *Morozovella acuta*, *Acarinina spp.* and benthic *Bulimina paleocenica* at or around the P4c/P5 boundary in the Sagamu Quarry (SQ) section. In the IB10B core, the lower part of the Oshosun FM is marked by frequent occurrences of mixed late Cretaceous and early Paleocene foraminifera, suggesting significant reworking. In this interval of the IB10B core (~101-137 mbs), we record high abundances of *Apectodinium*, which regularly exceed the typical acme levels (>40%) recorded during the PETM in mid and higher latitudes (Bujak and Brinkhuis, 1998; Crouch et al., 2003b, 2001; Sluijs et al., 2007a). The genus has a (sub-) tropical affinity and has an oldest occurrence around the Danian-Selandian boundary (Guasti et al., 2005) in Egypt and Tunisia (Crouch et al., 2003a). The unconformable surface between the Ewekoro limestones and the shales of the Oshosun formation is thus dated no earlier than the Danian-Selandian boundary based on the presence of *Apectodinium* in the Ewekoro limestones. In addition, we record stratigraphically important taxa: *Muratodinium fimbriatum*, *Kallosphaeridium brevibarbatum* and *Phelodinium magnificum*. All of these are traditionally recorded at mid and high latitude sites during the PETM or around the Paleocene – Eocene boundary (Bujak and Mudge, 1994; Heilmann-Clausen, 1985). Above 101 meters below surface (mbs), planktonic foraminifera are used to correlate to the SQ, which allow for direct correlation between the two (Extended Data Fig. 2).

From 101 mbs upwards, we find foraminifer stratigraphic marker species *Globanomalina pseudomenardii*, *Acarinina soldadoensis*, *Morozovella aequa* and *Morozovella velascoensis*, which indicate an age similar to the Oshosun formation in the SQ, representing planktonic foraminifer zones P4b, P4c and P5 (Berggren and Pearson, 2005; Mancini, 1984; Wade et al., 2011). Unfortunately, first and last occurrence horizons and hence subdivisions of the planktonic foraminifer zone P4 cannot be well constrained in the IB10B. We thus treat P4b and P4c as one zone (101-82 mbs). It should be noted that it is possible that P4b extends further down core. Large fluctuations in sedimentation rate are not expected based on uniform lithology.

The carbon isotope profile of the late Paleocene of IB10A and IB10B (Extended Data Fig. 2a) are characterized by stable values of -25.2 ± 0.4 ‰. At 80 mbs, a first step in $\delta^{13}C_{TOC}$ of -1.2 ‰ occurs, followed by a short plateau stage and a second 2.8‰ step at 76.75 mbs again followed by a plateau stage until recovery starts at 70.75 mbs. The general $\delta^{13}C_{TOC}$ pattern is mimicked in the $\delta^{13}C$ of the palynological residue ($\delta^{13}C_{PALY}$) that mostly consists of dinoflagellate cysts. However, $\delta^{13}C_{PALY}$ values are up to ~7 ‰ higher than $\delta^{13}C_{TOC}$ in the interval between 80 and 77 mbs (Fig. 1b). This interval has relatively high TOC and extremely high dinocyst concentrations (Fig. 1d), suggesting high productivity. This likely skewed $\delta^{13}C_{PALY}$ and $\delta^{13}C_{TOC}$ towards more positive values in this interval as high productivity leads to ^{13}C-enrichment of dissolved inorganic carbon in the surface ocean. We therefore place the start of the CIE at ~80 mbs. The position of this CIE, close to the P4c/P5 boundary and the shape, consisting of a steep decline, core and slow recovery indicate this must represent the PETM (Bains et al., 1999; Cui et al., 2011; John et al., 2008).

Absolute temperature estimates
Mg/Ca temperature estimates

Mg/Ca was measured on planktonic *Acarinina spp.* and *Morozovella acuta*, and benthic Bulimina paleocenica and Lenticulina olokuni. We apply the calibrations of Anand et

al., (2003) and Lear et al., (2002) for planktonic and benthic foraminifera, respectively, corrected for lower Paleocene seawater Mg/Ca ratios.

Eq. 1

$$T = (1/A)^* \ln(Mg/Ca)f/B)^*[(Mg/Ca)_{sw}]^H/[(Mg/Ca)_{sw'}]^H)$$

For planktonic foraminifera A = 0.085, B = 0.38 and for benthic foraminifera A = 0.109 and B = 0.867. Mg/Ca_{test} = foraminiferal test Mg/Ca Mg/Ca_{sw} = Mg/Ca ratio of modern seawater (5.15 mol mol-1), $Mg/Ca_{sw'}$ = Mg/Ca ratio of ancient seawater. We correct for the non-linear behaviour of Mg/Ca_{test} under lower Mg/Ca_{sw} ratios by applying the equation of Evans and Müller, (2012) and use H = 0.42 following (Dunkley Jones et al., 2013). This value obtained for H is derived from cultured *G. sacculifer* and we note that 0.42 is the lowest observed values for H (Evans and Müller, 2012) in any modern genus and hence this may be considered a conservative estimate.

We assume a Paleocene Mg/Ca ratio of 2 mol mol^{-1} in line with recent estimates of early Paleogene Mg/Ca ratios based on non-linear behaviour of foraminifer Mg/Ca ratios under low ambient Mg/Ca (Evans and Müller, 2012). It should be noted that low ambient Mg/Ca increases uncertainties in high temperature environments (Extended Data Fig. 4b) and that previous studies use seawater Mg/Ca above or around 2 mol mol^{-1} (e.g., Coggon et al., 2010; Creech et al., 2010; Dunkley Jones et al., 2013). Furthermore, our reconstructed temperatures are outside the range of the respective calibrations for benthic and planktonic foraminifera. This means values are extrapolated and errors will be larger than the quoted calibration errors (1.13 °C; Anand et al., 2003; 1.7 °C; Lear et al., 2002). Analytical errors are lower than 0.3 °C, which results in very conservative error estimates of ±1.4 and ±2 °C for planktonic and benthic foraminifera respectively.

$\delta^{18}O$ temperature estimates

We measured the same foraminifer species for $\delta^{18}O$ as for Mg/Ca. In order to reconstruct temperatures using the oxygen isotopes from foraminifer carbonate, several assumptions on local $\delta^{18}O_{sw}$ have to be made. First, we assume that no significant ice volume was present during the studied time period. The entire ocean would thus have been more depleted in $\delta^{18}O$ by approximately 1 ‰ (Zachos et al., 1994). Secondly, several local or regional variations in $\delta^{18}O$ can bias the temperature estimates (Zachos et al., 1994). The latitudinal effect on $\delta^{18}O_{sw}$ is fairly well known in modern open marine settings and can be approximated by applying a third order polynomial fit with latitude (x).

Eq.2

$$\delta^{18}O_{sw} = 0.576 + 0.041x - 0.0017x^2 + 1.35^*10^{-5}x^3$$

We correct for latitude by using G-plates (www.g-plates.org) for 55 Ma, using the paleomagnetic reference frame of Seton et al., (2012) and arrive at a paleolatitude for our sites of ~1° S. Combining this with the ice volume effect, we arrive at an estimate of local $\delta^{18}O_{sw}$ of -0.39 ‰. We consider this correction a crude estimate of the local $\delta^{18}O$, and it should be stressed that small changes in paleolatitude near the equator may strongly influence the local $\delta^{18}O_{sw}$.

Salinity fluctuations, which may occur in near shore settings and during periods of major hydrological change such as the PETM, typically lead to variations in $\delta^{18}O_{sw}$. From dinocyst assemblages we infer there are no significant salinity fluctuations which would impact $\delta^{18}O$. The majority of dinocyst species is of normal marine affinity, although some low-salinity tolerant species are present (Supplemental Table 1). Furthermore, symbiont-bearing planktonic foraminifera in the modern oceans are typically restricted to waters with salinity

in excess of 34‰ and hence their presence suggests normal marine salinity (Bijma et al., 1990). We also note that in case of enhanced fresh water supply, the tropical location would dampen the influence relative to a similar hydrological change at higher latitudes (Lachniet, 2009).

Furthermore, in high CO_2 environments, the concentration effect of the carbonate ion [CO_3^{2-}] on $\delta^{18}O$ is important and leads to decreased fractionation and hence underestimation of absolute temperatures (e.g., Zeebe, 2001). If a Paleocene pCO_2 of 1000 ppm is assumed, this results in a pH of 7.88 (pre-industrial 8.16) (Zeebe, 2001). The pH related decreased fractionation ranges from 0.89‰ for symbiont bearing foraminifera to 2.54‰ per pH unit for non-symbiont bearing foraminifera (Uchikawa and Zeebe, 2010). This means that for the pH change relative to the modern, we may underestimate Paleocene absolute temperatures by 1 - 3.5 °C. More importantly, pH changes during the PETM have a similar effect. pH is expected to decrease by about 0.25 unit (e.g. Penman et al., 2014), which could result in underestimated temperature change of 1 - 3 °C. It is difficult to test whether the same pH effect holds on long time scales and long-extinct species. We hence use a conservative approach and only correct for the rapid pH change across the PETM in our data compilation. However, it should be noted that we likely underestimate absolute temperatures if the pH effect in Paleocene and Eocene species is similar to that of extant foraminifera. We subsequently reconstruct temperatures by applying the equation from Kim and O'Neil, (1997) as used by Aze et al., (2014).

Eq.3

$$T = 16.1 - 4.64\,(\delta^{18}O_C - \delta^{18}O_W) + 0.09(\delta^{18}O_C - \delta^{18}O_W)^2$$

In which $\delta^{18}O_C$ is the measured carbonate $\delta^{18}O$ and $\delta^{18}O_W$ is the local seawater $\delta^{18}O$. The equation of (Kim and O'Neil, 1997) is calibrated for inorganic calcite, and the calibration is not limited to oceanic conditions or biotic limitations in foraminifera. The equation is continuous to at least 40 °C, with calibration and analytical errors of ±1.3 and ±0.3 °C respectively. This results in conservative error estimates for $\delta^{18}O$ of ±1.6 °C. Overall, sensitivity is lower for $\delta^{18}O_W$ and values are better constrained than past seawater Mg/Ca ratios (Extended data Figs. 4 a,b).

TEX_{86} temperature estimates

Theoretically, TEX_{86} does not require any assumptions about water chemistry or past paleoenvironmental conditions, although some regions exhibit different responses in the modern ocean (Kim et al., 2010). However, the isoprenoid glycerol dibiphytanyl glycerol tetraethers (GDGTs) used to calculate TEX_{86} are not exclusively biosynthesized by marine Thaumarcheota. Methanogenic organisms living in organic rich sediments and methanotrophic organisms living in and near cold-seeps have been found to produce significant amounts of GDGTs. We apply the Methane Index of (Zhang et al., 2011) and GDGT ratios of (Weijers et al., 2011) and find that these never indicate significant GDGT input of methanotrophic or methanogenic Archaea.

The production of GDGT lipids takes place across the entire water column, potentially complicating the TEX_{86} signal in deep water (>1000 m) settings (Kim et al., 2015). Since our sections are deposited on the continental shelf, with water depths in the order of 100-150m and possibly shallower in the IB10, we surmise that there is little influence from GDGTs produced in deeper water.

TEX_{86} values may also be influenced by terrestrial input and therefore we calculate the relative abundance of terrestrially-derived branched versus marine isoprenoid GDGTs

(BIT-index) (Hopmans et al., 2004), which typically uses a cut off value of 0.3 or 0.4 as limit for TEX_{86} data (Bijl et al., 2013; Weijers et al., 2006). Most samples yield BIT values below 0.3 and we find no correlation between TEX_{86} and BIT (Extended data Fig. 5). However, the topmost part (<50 mbs) of the IB10B core may have suffered from weathering and is associated with relatively high amounts of terrestrial lipids (BIT >0.5) a phenomenon typically observed in oxidized sediments (Huguet et al., 2008). The high TEX_{86} values observed there may therefore be the result of a diagenetic bias.

Recently, debate has focused on GDGT distributions that are similar to modern Red Sea (Inglis et al., 2015). The Red Sea GDGT distribution is notably different from open ocean GDGT distributions and has a different relation to temperature (Trommer et al., 2009). These distributions are often characterised by high relative abundances of the crenarcheol regioisomer (cren') (Inglis et al., 2015; Trommer et al., 2009), which is present in the original TEX_{86} equation. However, our samples do not show such an aberrant distribution during the latest Paleocene and PETM, as the relative abundance of cren' relative to that of cren averages ~10%. Hence, there is no direct potential for temperature overestimation due to Red Sea type Thaumarcheota.

TEX_{86} calibrations

Since the development of the proxy, several calibrations were proposed to calculate SST from TEX_{86} (see reviews of Pearson and Ingalls, 2013; Schouten et al., 2013; Tierney, 2012). We consider several recent calibrations; TEX_{86}^{H}, TEX_{86}^{HC} (Kim et al., 2010) and the Bayesian TEX_{86} calibration (Tierney and Tingley, 2014) to retain clarity in this discussion. TEX_{86}^{H} is based on modern ocean core-top data, TEX_{86}^{HC} is calibrated with mesocosm cultures and the Bayesian TEX_{86} calibration aims to find similar TEX_{86} values from the modern ocean to reconstruct temperature with.

TEX_{86}^{H} derived absolute temperatures agree well with carbonate proxy estimates of upper mixed-layer temperature (Fig. 1a). However, similar to all core-top and modern ocean calibrated proxies, our TEX_{86}^{H} values exceed the calibrated range of the proxy. TEX_{86}^{HC} in contrast is based on mesocosm experiments, extending the upper temperature limit to 40 °C and potentially increasing the range by 10 °C. However, mesocosm studies of Thaumarchaea are limited and do not incorporate population differences and habitat depth, nor taphonomical effects such as diagenesis, burial, and transport, all of which are implicitly included in the core-top calibration.

The Bayesian TEX_{86} calibration is a promising new calibration, although this method is also highly sensitive to the non-modern-analogue setting reconstructed here. We use both default settings to reconstruct temperature and a set of wider calibrations that incorporates most of the modern tropical and subtropical regions. The default setting, which applies search limits of 2 standard deviations (here 0.07 units) from the average TEX_{86} values yields temperatures typically 4 - 5 °C lower than carbonate based proxies. Crucially, however, in the default setting, the calibration utilizes one region from the modern ocean, the Red Sea. The Red Sea is a problematic region in the modern ocean with respect to TEX_{86}, most likely because of a distinctly different population of Thaumarcheota compared to the global ocean (Trommer et al., 2009). The region is often excluded from calibrations (Kim et al., 2010) because in this semi-enclosed basin, the relation between temperature and TEX_{86} is notably different than in the rest of the global ocean.

We stretched the Bayesian approach so that other high temperature tropical regions are incorporated (search limits 0.2, 0.15 and 0.135 TEX_{86} unit). These TEX_{86} calibrations generally yield values similar to those of the mesocosm studies. However, the relative

influence of the Red Sea data is still important and reduces the reconstructed temperatures. It should be noted that, due to the linear nature of the calibrations, the Bayesian TEX_{86} temperatures will nearly always show a larger temperature increase at the high end, in the order of 4-5 °C rather than 2-3 °C derived from TEX_{86}^{H} and TEX_{86}^{HC}. Because we do not see any analogy between the Red Sea and the depositional setting of our analysed sections in any ecological signal, geographical setting or GDGT profiles, we consider the validity of the Bayesian approach to be relatively low for this study.

Based on the convergence with carbonate-based proxies we prefer to use the core-top calibrated TEX_{86}^{H}, with the note of caution that, based on both the mesocosm calibrated TEX_{86}^{H} and the Bayesian calibrations we may underestimate absolute temperatures. Confidence intervals of the Bayesian calibration suggest 90% confidence errors (±7 °C) may be larger than the combined analytical and core-top calibration error (90% confidence ±4.6 °C). It should be noted that this discrepancy is in part due to linear versus logarithmical approaches in the Bayesian TEX_{86} and TEX_{86}^{H}, respectively and due to incorporation of the Red Sea data (Extended Data Figure 6).

In general temperatures derived from $\delta^{18}O$ and Mg/Ca measured on planktonic foraminifera are in excellent agreement with TEX_{86}^{H} derived temperatures in the SQ. Moreover, the possible advantages of other calibrations such as the Bayesian TEX_{86} are either fulfilled by other means, e.g. supplemented by temperature estimates of local carbonate-based proxies or in the case of the Bayesian TEX_{86} calibration, of little added value here. Therefore, we use TEX_{86}^{H} to reconstruct absolute SSTs in the SQ and the IB10B core.

Temperature change data compilation

For our data compilation of SST change across the PETM (hereafter referred to as ΔT), we use several data sources and treat these as follows.

We use the data compilation of Dunkley Jones et al., (2013); DJ2013 and references therein, as a starting point. This compilation contains four different proxies for surface temperatures; $\delta^{18}O$, Mg/Ca, TEX_{86}^{H} and TEX_{86}'. Importantly, TEX_{86}' is only used to reconstruct pre-PETM temperatures from sediments from the Arctic Ocean (Sluijs et al., 2009, 2006). These sediments have very high BIT values, which implies that temperature estimates are likely less trustworthy, regardless of what calibration is used. We thus apply TEX_{86}^{H}, but only use sediments from the Arctic that have low BIT values, to retain consistency in proxies. Then, the only remaining difficulty is that of the estimated ΔT. We here use earliest Eocene sediments as a substitute for latest Paleocene sediments. For all other data, we calculate ΔT from latest Paleocene and PETM sediments. It should be noted that difference between this approach and the previously published ΔT is not large. Reported ΔT of TEX_{86}' temperature is 3.9 °C (Dunkley Jones et al., 2013). In that case, the TEX_{86}' GDGT distribution is calibrated using the Kim et al., (2008) coretop dataset (Kim et al., 2008; Sluijs et al., 2009). Recalibrating TEX_{86}' with a log-transform calibration line and the Kim et al., (2010) coretop dataset yields a ΔT of 3.4 °C. TEX_{86}^{H} reconstructed temperatures are 2.9 °C higher during the PETM compared to post PETM sediments.

A second important change to the DJ2013 data is a pH correction of 0.25 units (0.22‰) for all $\delta^{18}O$ estimates during the PETM. We only use symbiont-bearing foraminifera in our compilation and this increases all $\delta^{18}O$ derived ΔT by ~1 °C.

We further add recently published data from several sections; the West Siberian Sea (Frieling et al., 2014), North Sea area (Schoon et al., 2015), Tanzania (Aze et al., 2014)and the South West Pacific (DSDP277)(Hollis et al., 2015). We subsequently perform a bootstrap (*n* =

1000) approach on the data from each individual site to estimate mean ΔT and 5,25,50,75 and 95% quantiles of ΔT (Extended Data Table 2).

Plankton Regime Shift

Several hypotheses may be posed to explanation the demise in dinocyst abundances across the PETM in Nigeria. First, sedimentation rates increased at many marginal marine sites during the PETM due to hydrological change in the hinterland.
However, the dinocyst abundance drop in the IB10B core cannot be explained by sedimentary dilution. Based on the thickness and duration of P4c (~20 m, ~600 kyr) and the CIE of the PETM (~15 m, ~200 kyr) sedimentation rates average ~3.3 cm kyr^{-1} in the latest Paleocene and ~7.5 cm kyr^{-1} during the PETM (Extended data Fig. 2a), which cannot explain a three order of magnitude decrease ($10^5 > 10^2$ cysts/gram) in absolute dinocyst concentrations.
Second, dinocysts may be subject to oxidation causing low concentrations in sediments. However, cysts of heterotrophic dinoflagellates, which are typically brown-pigmented, become a major part of assemblages during the PETM, although their absolute concentrations remain stable. Crucially, these brown-pigmented cysts are among the least resistant dinocysts (Zonneveld et al., 2008), so their presence, as well as abundant benthic foraminifer linings, indicates optimal palynological preservation. We can therefore exclude oxidation as a cause of the dinocyst demise.
Third, we record isorenieratane throughout the onset and core of the CIE. This is a diagenetic derivative of isorenieratene, a biomarker produced by photosynthetic green sulphur bacteria that need light and free sulphide, and therefore indicate the development photic zone euxinia (PZE) (Sinninghe Damsté et al., 1993), which may have been toxic to dinoflagellates. However, other PETM records where PZE (Frieling et al., 2014; Sluijs et al., 2014, 2008b) developed during the PETM do not yield impoverished assemblages. Moreover, organic linings of benthic foraminifera increase in abundance during peak PETM (Extended data Fig. 6d), suggesting at least intermittent water column oxygenation. In addition, redox sensitive trace metals indicate bottom waters experienced low oxygen conditions during the onset of the PETM (80-77 mbs); this did not hinder dinocyst production, but did apparently affect benthic fauna as indicated by the complete absence of foraminifer linings at 77 mbs. In conclusion, we exclude anoxia/euxinia as a driver for the demise of dinoflagellates.
Fourth, massive freshwater influx from the continent may have caused salinities to drop below tolerance levels of many dinoflagellate species. Under such conditions, high abundances of dinocysts derived from low-salinity tolerant dinoflagellates would be expected in addition to the recorded species, as found in the Arctic Ocean (Sluijs et al., 2008b) and New Jersey Shelf (Sluijs and Brinkhuis, 2009), even under low oxygen and euxinic water column conditions. However, we find no increase in such dinocyst species or fresh water palynomorphs, pollen and spores from terrestrial plants, or shifts in Ti/Al or Zr/Al that could indicate a dramatic increase in runoff and thereby a drop in salinity.

We argue that conditions became too hot for most dinoflagellate taxa during the core of the PETM, when SSTs rose to values between 35°C and 37 °C. Such temperatures are uninhabitable for most eukaryotic organisms because of enzymatic restrictions (Somero, 1995), even for dinoflagellates, which are among the most temperature resilient plankton groups (Hallegraeff et al., 1997). Some modern dinoflagellates produce heat-shock proteins, but these can only mediate short periods of thermal stress (Somero, 1995). Indeed, experiments have shown that temperatures above 35 °C are lethal to dinoflagellates, even while they reside in their cysts (Hallegraeff et al., 1997). Apart from often displaying narrow temperature tolerance ranges (Sunday et al., 2011), many modern thermophilic organisms

show a sharp decline in productivity and consequently survival between optimum and (sub-) lethal temperatures. Collectively, we therefore attribute the recorded loss in dinoflagellate diversity and abundance to heat stress.

Interestingly, the absolute concentration of brown-pigmented cysts appears more or less unaffected. These are, however, exclusively produced by heterotrophic dinoflagellates, which likely resided below the mixed layer. In addition, although preservational biases in foraminifera are difficult to exclude, we recorded no mixed-layer dwelling foraminifera; only the thermocline dwelling *Subbotina spp.* are present in the IB10B core during the PETM.

Burial fluxes of benthic foraminifer linings peaked during the PETM, implying a retained production and flux of decent-quality organic matter to sustain benthic life. Given the known heat stress of many eukaryotic primary produces at the reconstructed SSTs, primary production was likely exclusively performed by prokaryotes in the study area. Consistent with future projections, prokaryotes often outcompete eukaryotes under extreme conditions, including high temperatures (Madigan et al., 2008). Cyanobacteria are the most likely candidates, since these often have high optimum growth temperatures (Paerl et al., 2011) as well as high resistance against other common biological stress factors, e.g. UV radiation, high and low nutrients (Paul, 2008).

Dinoflagellate cysts ecology

We follow Sluijs et al., (2005) for affinity of dinocyst species, unless indicated otherwise.

Normal marine

Assemblages throughout the section are dominated by dinocysts of normal marine affinity and *Apectodinium*. The "normal marine" group includes all genera and taxa that are thought to be representative of normal marine salinity, rather low nutrient environments. There is considerable variance within this group, but only the shared normal marine affinity is important here. This group includes *Spiniferites*, *Achomosphaera*, *Hafniasphaera*, *Areoligera*, *Adnatosphaeridium*, *Glaphyrocysta* and the typically less abundant *Impagidinium* and *Operculodinium*. During the PETM, we find only *Spiniferites spp.*, which is a generalist genus.

Apectodinium

All the species in the genus *Apectodinium* are considered of similar affinity. The genus is thought to be euryhaline, heterotrophic and therefore indicative of near shore, elevated nutrient conditions. The poleward migration of *Apectodinium* during the PETM and temperature-dependant appearance in the fossil record (Frieling et al., 2014) suggests the genus had a fairly high minimum temperature requirement (20 °C) and occurred mostly in (sub-) tropical regions during the late Paleocene and early Eocene at temperatures over ~25 °C. The assemblage during the Paleocene is dominated by aforementioned normal marine species and *Apectodinium spp.*, which combined make up ~80% of the assemblage.

Low-salinity tolerant

This group includes *Senegalinium*, *Phthanoperidinium*, *Paleocystodinium*, *Lejeunecysta* and other minor genera. Some of these, e.g. *Lejeunecysta* and *Paleocystodinium* are also brown-pigmented, as are modern strictly heterotrophic genera. *Senegalinium* and *Phthanoperidinium* were produced in large quantities in the Arctic Ocean when the sea surface was salinity was >5‰ during massive growth of the freshwater fern *Azolla* (Barke et al., 2012). We follow (Sluijs and Brinkhuis, 2009), who considered all so-called 'hexa-

peridinioids' to represent cysts of fresh-water tolerant dinoflagellates.

Protoperidinioids
The genera *Paleocystodinium*, *Lejeunecysta* and *Phelodinium* are primarily considered to represent cysts of heterotrophic dinoflagellates. *Lejeunecysta* and *Phelodinium*, are related to extant Protoperidinioid genera, which are almost exclusively heterotrophic. These cysts are usually considered to be least resistant to oxidation, relative to the normal marine, *Apectodinium* and low salinity tolerant cysts.

Sample	Depth (mbs)	*Apectodinium spp.*	*Brown Peridinioids*	*Senegalinium spp.*	*Cerodinium/other P-cysts*	*Spiniferites cpx*	*Operculodinium*	*C. fibrospinosum cpx*	*Goniodomideae*	*Areoligera cpx*	*Kallosphaeridium spp.*	*Impagidinium spp.*	*Diphyes spp.*	*Florentinia spp.*	*Proximate G-cysts*
SH27	9.80	41	0	0	1	35	2	2	3	0	11	0	2	3	0
SH25	11.60	13	0	0	0	52	0	3	1	0	27	0	0	1	0
SH23	13.20	33	0	1	2	38	3	4	5	2	9	0	0	1	1
SH21	14.10	40	1	1	7	32	0	0	3	0	10	0	0	3	4
SH19	14.80	26	1	2	1	50	1	2	2	0	7	0	0	2	4
SH18	15.10	22	2	2	1	37	1	0	8	0	12	0	0	5	6
SH16	16.00	32	1	1	3	42	1	2	1	0	6	0	0	1	7

Table S1. *Sagamu Quarry Dinoflagellate assemblages. Peridinioid (shaded), Gonyaulacoids (white)*

Table S2 *(Next page). Temperature composite for the Palaeocene and PETM.*

Site	Paleolatitude	Paleolongitude	Paleocene mean	Lower 95%	Upper 95%	PETM mean	Lower 95%	Upper 95%	DeltaT	Lower 95%	Upper 95%	Reported Paleocene	Reported PETM	Delta T	25% Q	Median	75% Q	Proxy	Reference
ACEX	83.2	31.3	18.2	17.8	18.6	22.9	22.5	23.1	4.6	4.1	5.1	18.6	22.4	3.9	4.4	4.6	4.8	TEX_{86}^{L}	Sluijs et al., 2006
	83.2	31.3	21.3	20.9	21.7	24.1	23.7	24.6	2.9	2.3	3.5				2.6	2.9	3.1	TEX_{86}^{H}	Sluijs et al., 2006
West Siberian Sea	54.6	66.0	18.3	17.3	19.4	27.2	26.8	27.7	8.9	7.5	10.1				8.4	9.0	9.5	TEX_{86}^{H}	Frieling et al., 2014
Wilson Lake	38.2	-56.6	28.2	28.0	28.5	35.7	35.4	36.0	7.5	7.1	7.9	28.2	35.7	7.5	7.3	7.5	7.7	TEX_{86}^{H}	Zachos et al, 2006
Bass River	38.1	-56.1	23.4	22.5	24.2	27.7	27.1	28.3	4.3	3.2	5.4	23.2	26.2	3.0	3.8	4.2	4.7	*Acarinina* $\delta^{18}O$	John et al., 2008
	38.1	-56.1	30.0	29.7	30.3	35.5	35.3	35.6	5.4	5.1	5.7	30.0	35.5	5.4	5.3	5.4	5.5	TEX_{86}^{H}	Sluijs et al. 2007
IODP1209	21.7	-157.9	29.4	29.2	29.5	33.2	32.8	33.6	3.9	3.5	4.3	29.4	33.2	3.9	3.7	3.8	4.0	*Acarinina* Mg/Ca	Zachos et al. 2003
	21.7	-157.9	29.6	29.5	29.8	33.6	33.3	33.8	3.9	3.6	4.2	29.6	33.6	3.9	3.8	3.9	4.1	*Morozovella* Mg/Ca	Zachos et al. 2003
	21.7	-157.9	20.6	20.2	21.0	22.6	22.2	22.9	2.0	1.4	2.5	20.4	21.2	0.8	1.7	2.0	2.2	*Acarinina* $\delta^{18}O$	Zachos et al. 2003
	21.7	-157.9	20.8	20.0	21.5	23.9	23.7	24.1	3.1	2.3	3.9	20.6	22.5	1.9	2.8	3.0	3.4	Morozovella $\delta^{18}O$	Zachos et al. 2003
ODP865	5.2	-143.5	31.1	30.2	32.0	33.2	32.3	34.0	2.1	0.9	3.3				1.6	2.1	2.6	Morozovella $\delta^{18}O$	Kozdon et al. 2011
	5.2	-143.5	30.8	30.4	31.1	32.4	32.2	32.6	1.6	1.2	2.0	30.8	32.4	1.6	1.4	1.6	1.8	*Acarinina* Mg/Ca	Tripati & Elderfield, 2004
	5.2	-143.5	30.6	30.3	30.8	31.9	31.7	32.1	1.3	0.9	1.6	30.6	31.9	1.3	1.1	1.3	1.4	*Morozovella* Mg/Ca	Tripati & Elderfield, 2004
Nigeria (IB10B)	-0.7	-1.9	33.4	33.2	33.6	36.1	35.7	36.6	2.7	2.2	3.2				2.5	2.7	3.0	TEX_{86}^{H}	This study
Nigeria (IB10A)	-0.7	-1.9	32.7	32.2	33.1	36.5	35.9	37.1	3.8	3.0	4.6				3.4	3.8	4.2	TEX_{86}^{H}	This study
ODP527	-35.1	-8.1	16.1	15.9	16.4	20.4	20.2	20.8	4.3	3.9	4.7	16.6	19.8	3.1	4.1	4.3	4.5	*Acarinina* $\delta^{18}O$	Thomas et al. 1999
	-35.1	-8.1	28.7	28.6	28.9	31.2	31.1	31.2	2.4	2.2	2.6	28.7	31.1	2.4	2.3	2.4	2.4	*Acarinina* Mg/Ca	Tripati & Elderfield, 2004
DSDP277	-62.7	-173.8	29.9	29.4	30.4	32.2	31.5	33.0	2.2	1.4	3.2				1.8	2.2	2.6	*Acarinina* Mg/Ca	Hollis et al. 2015
IODP1172	-64.8	160.2	25.9	25.8	26.1	31.8	31.3	32.3	5.9	5.4	6.4	25.9	31.8	5.9	5.7	5.9	6.1	TEX_{86}^{H}	Sluijs et al., 2011
ODP690	-65.2	-1.0	11.5	10.9	11.9	17.6	16.4	18.8	6.2	4.8	7.5	11.6	16.6	5.0	5.6	6.2	6.7	*Acarinina* $\delta^{18}O$	Kennett & Stott, 1991
	-65.2	-1.0	10.8	10.5	11.2	21.2	21.0	21.5	10.4	10.0	10.8	11.1	20.0	9.0	10.2	10.4	10.6	*Acarinina* $\delta^{18}O$	Thomas et al., 2002
Tanzania	-19.0	33.7	30.5	30.1	31.1	35.4	33.3	37.4	4.9	2.8	7.0				4.0	4.9	5.8	*Morozovella* $\delta^{18}O$	Aze et al., 2014
Denmark, Fur	52.5	4.1	19.6	17.3	22.0	29.8	28.6	30.9	10.1	7.0	13.0				8.9	10.2	11.6	TEX_{86}^{H}	Schoon et al. 2015
Denmark, Store Baelt	51.2	6.9	19.6	17.3	22.0	25.2	24.2	26.3	5.6	2.8	8.1				4.6	5.6	6.7	TEX_{86}^{H}	Schoon et al. 2015

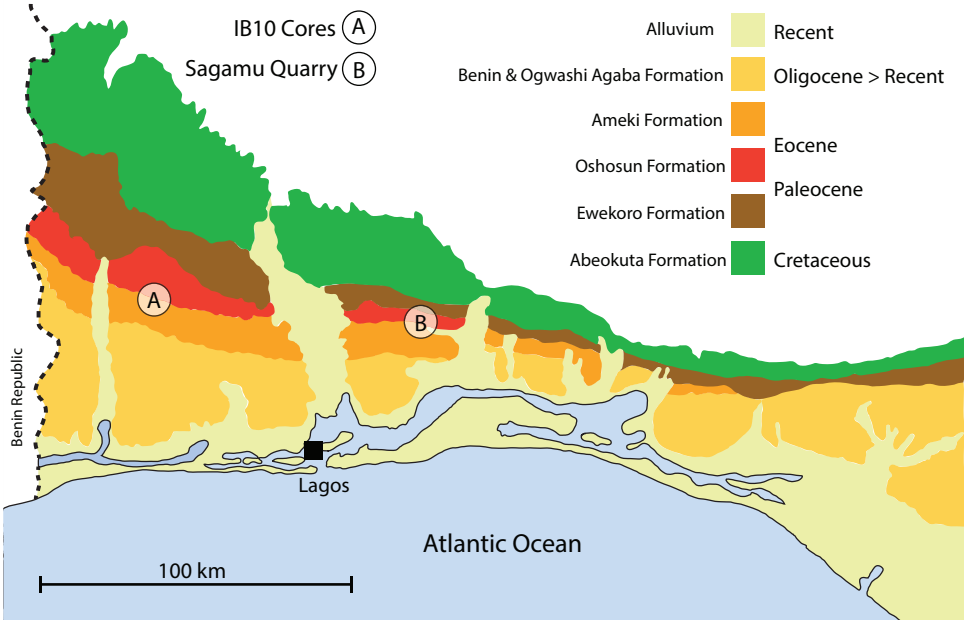

Extended data Figure 1. *Geological map of the Nigerian sector of the Dahomey Basin. A; IB10 cores and B; Sagamu Quarry location.*

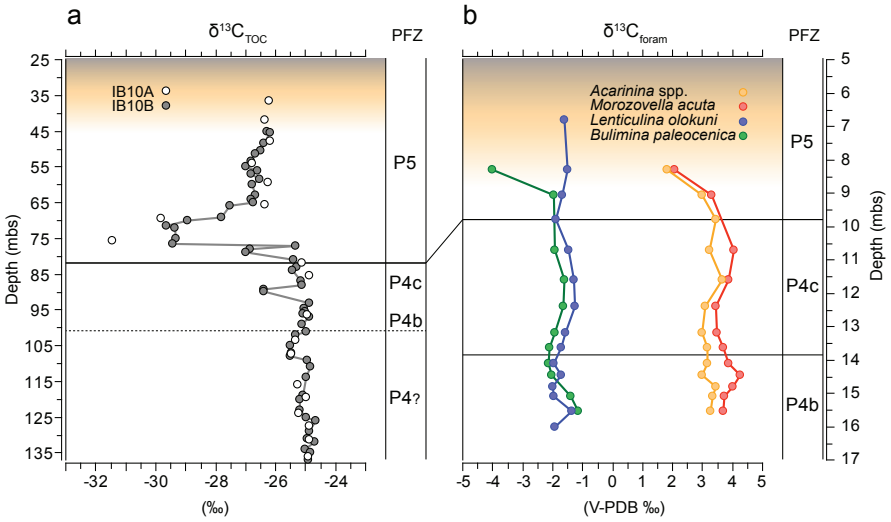

Extended data Figure 2. *Stable carbon isotope records.* ***a.*** *IB10A (open symbols) and B (closed symbols) core stable carbon isotope records of total organic carbon ($\delta^{13}C_{TOC}$).* ***b.*** *Sagamu Quarry stable carbon isotope records of planktonic (Morozovella acuta and Acarinina spp.) and benthic foraminifera (Bulimina paleocenica and Lenticulina olokuni). Planktonic foraminifer zones follows (Berggren and Pearson, 2005). The shaded area indicates the maximum extent of weathering.*

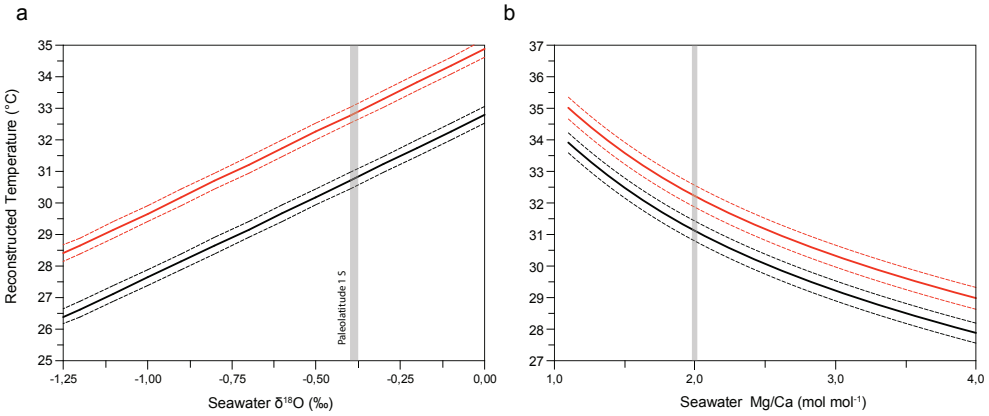

Extended data figure 3. *Sensitivity plots for $\delta^{18}O_{SW}$ and Mg/Ca_{SW}* ***a.*** *Sensitivity plot for $\delta^{18}O$-derived temperature against assumed local $\delta^{18}O_{SW}$. Solid lines indicate average Morozovella acuta (red) and Acarinina sp. (black), plus and minus analytical error (0.05‰) (dashed lines).* ***b.*** *Sensitivity plot for Mg/Ca seawater concentrations, solid and dashed lines same as above.*

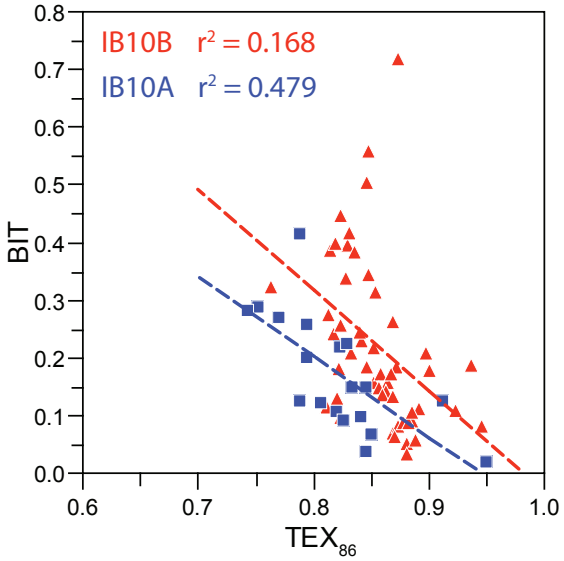

Extended data figure 4. *IB10A and IB10B TEX_{86} and BIT correlations. Note that a large part of the correlation is due to the high-TEX_{86}/low-BIT samples within the PETM interval.*

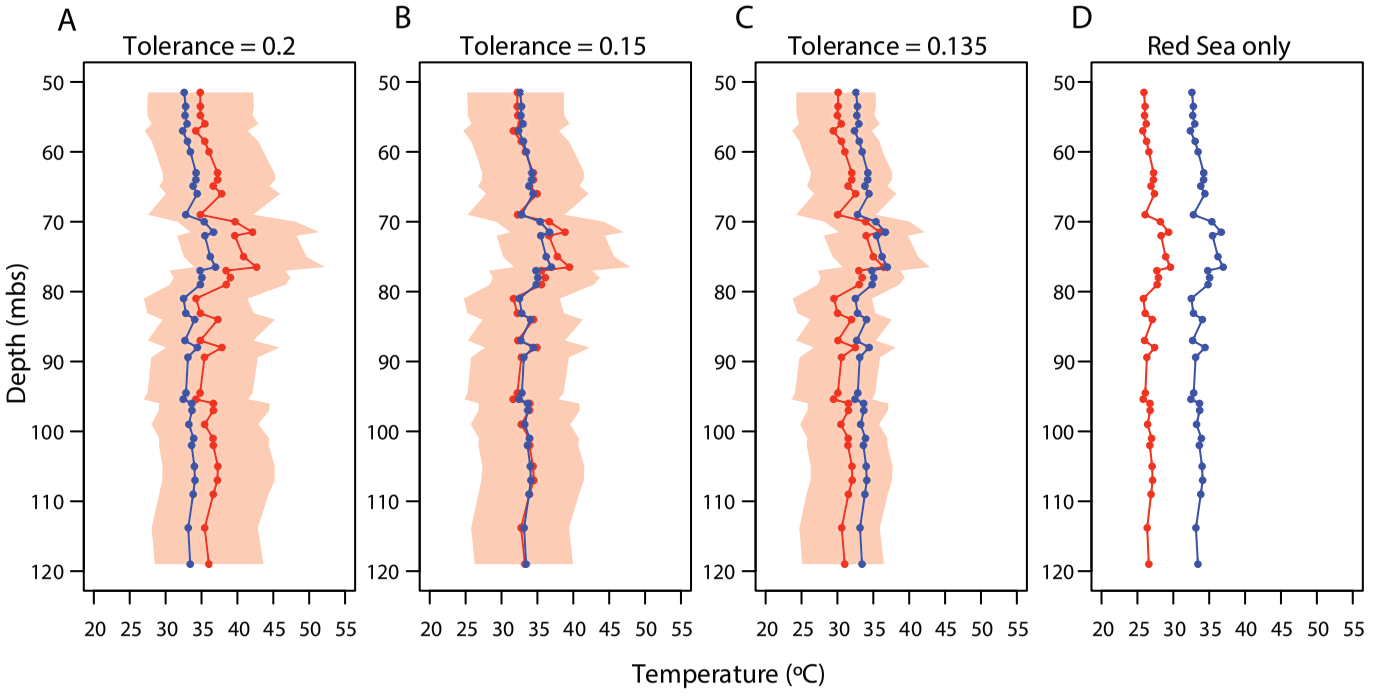

Extended data figure 5. *Bayesian calibrations using the IB10B dataset and BAYSPAR tool (http://bayspar.geo.arizona.edu/) (Tierney and Tingley, 2015, 2014). The blue line is the standard TEX_{86}^{H} core top calibration, while the red lines and areas represent the Bayesian calibrations and 90% confidence intervals thereof.* ***a.*** *Calibration using all regions within 0.2 TEX_{86} units of data average.* ***b.*** *Similar, for 0.15 TEX_{86} units.* ***c.*** *Similar, for 0.135 TEX_{86} units.* ***d.*** *Red Sea (red line) calibration from (Trommer et al., 2009).*

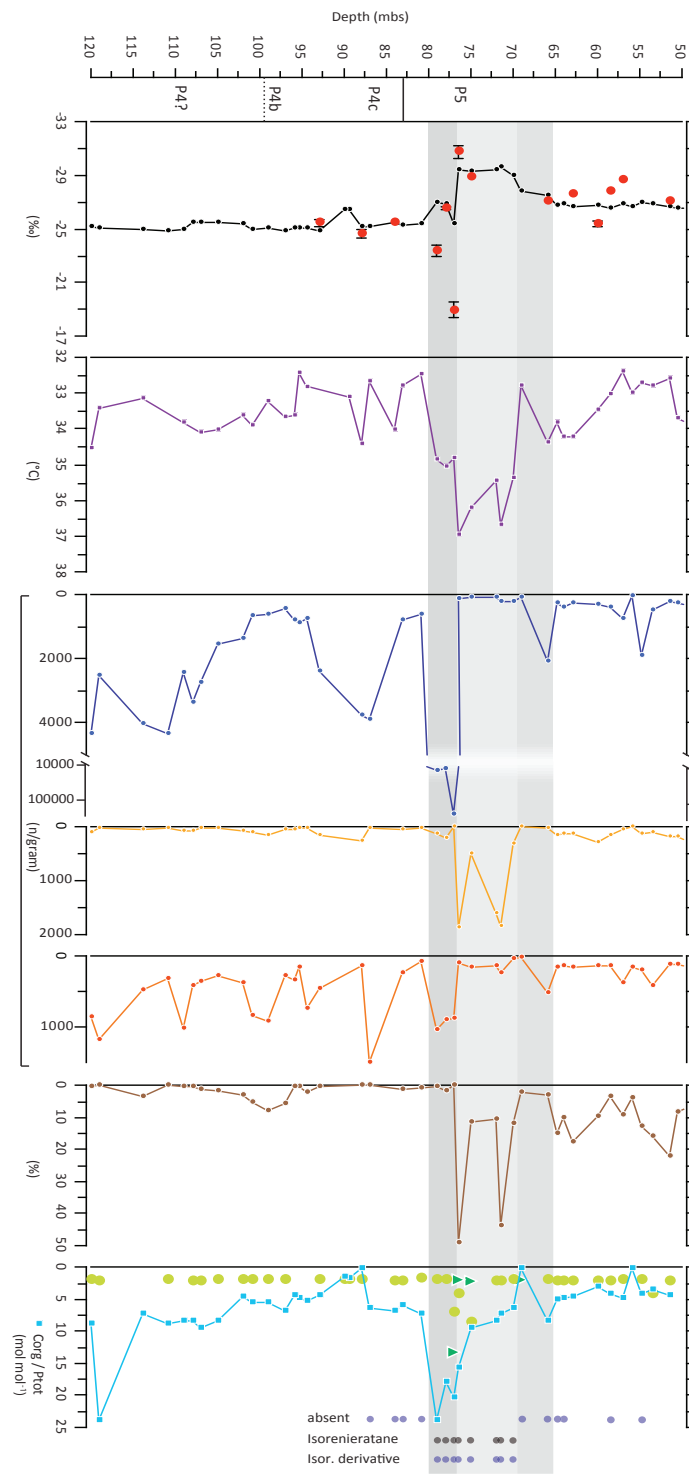

Extended data figure 6. *Environmental reconstructions for the IB10B core.* ***a.*** *Stable carbon isotope record of total organic carbon ($\delta^{13}C_{TOC}$) and palynological residue ($\delta^{13}C_{PALY}$). The phases of the CIE are denoted O, C and R for Onset, Core and Recovery, respectively.* ***b.*** *TEX_{86}^{H} -based SST.* ***c.*** *Absolute concentrations of dinocysts per gram of dry sediment. Note the scale break at 4,000.* ***d.*** *Absolute concentration of organic foraminifera linings.* ***e.*** *Absolute concentration of pollen and spores.* ***f.*** *Relative abundance of Protoperidinioids.* ***g.*** *Indicators of anoxia: Organic carbon over total phosphorus ratio (Corg/Ptot) (light blue squares). Presence of isorenieratane and derivative. Concentrations of redox sensitive trace elements Mo (green circles) and Cd (blue circles) in ppm. Note that Mo concentrations are below the detection limit and absolute values should be treated with caution.*

4

Smoking gun for methane hydrate release during the Paleocene-Eocene Thermal Maximum

Abstract

The Paleocene–Eocene Thermal Maximum (PETM; ~56 Ma), a period of rapid 4-5ºC global warming, is characterized by a massive input of ^{13}C-depleted carbon (>1500 Gt) into the ocean-atmosphere system. Methane from submarine hydrates has long been proposed as the main source, but evidence for methane release is lacking. Here we show, based on new and published data, that substantial global warming led ^{13}C-depleted carbon injection. Moreover, we show that global marine burial fluxes of biogenic Ba approximately doubled, which on PETM time scales can only be explained by a significant Ba addition to the oceans. Submarine hydrates are Ba-rich and require warming to dissociate. The most straightforward explanation for early warming and increased Ba fluxes is that hydrate release acted as a positive carbon cycle feedback during the PETM.

Introduction

In the light of current climate change there is great need for insight in short and long-term global carbon cycle feedbacks (Rohling et al., 2012). Constraints on such feedbacks and their sensitivity may come from past extreme climate events, such as the Paleocene – Eocene Thermal Maximum (PETM; ~56 Ma). The PETM is an extensively studied period of rapid global warming, associated with massive carbon input into the ocean-atmosphere system from a ^{13}C-depleted carbon source (Dunkley Jones et al., 2013; McInerney and Wing, 2011) that released a sufficient mass of carbon to rapidly acidify oceans (Zachos et al., 2005b). This input of ^{13}C-depleted carbon is globally recognized in both carbonate and sedimentary organic matter as a negative carbon isotope excursion (CIE) (McInerney and Wing, 2011). The CIE marks a rapid (millennial scale) onset, a phase of stable low values (often referred to as 'body') and an apparently more gradual recovery, which is similar to the pattern of warming as recorded from temperature proxies (Dunkley Jones et al., 2013) suggesting a causal connection between the two. The PETM was also associated with ocean deoxygenation and marginal marine euxinia (Dickson et al., 2012; Sluijs et al., 2014), sea level rise (Sluijs et al., 2008a), an accelerated hydrological cycle (Handley et al., 2012), and remarkable biotic changes (Sluijs et al., 2007a). The prime candidates for causing the onset of the 3-5‰ CIE are the dissociation of submarine methane hydrates (Dickens et al., 1995) and terrestrial organic carbon reservoirs such as Antarctic permafrost (DeConto et al., 2012). Crucially, these reservoirs might only release large masses of carbon when perturbed beyond background variability; they typically require warming to release carbon as a positive feedback in the climate system (Dickens et al., 1997, 1995).

Previous work has suggested that surface warming preceded the CIE at several locations (Chen et al., 2014; Secord et al., 2010; Sluijs et al., 2007b; Thomas et al., 2002). However, it remains unknown whether early warming was global and, if so, whether the amplitude and timing match a runaway greenhouse scenario. Furthermore, thorough statistical testing of the lead-lag relation between temperature and CIE has not been performed.

We present $\delta^{13}C_{TOC}$ and TEX_{86} data from Ocean Drilling Project (ODP) Hole 959D, in the equatorial Atlantic Ocean. Site 959 is located in the equatorial Eastern Atlantic near the top of a submarine high, the Cote d'Ivoire Ghana Transform Margin (CIGTM; 3°37.656'N, 2°44.149'W) (Supp. Fig. 1). Upper Paleocene and lower Eocene sediments are composed of roughly equal amounts of carbonate, biogenic silica and siliciclastics, with some organic carbon (Wagner, 2002). Based on published biostratigraphy (Shafik et al., 1998) we identified the PETM interval and sampled core sections 41R-6 to Core 42R-2 continuously.

Materials

Hole 959D was drilled on the Cote d'Ivoire-Ghana Transform Margin (CIGTM) in 1995 (3°37.656'N, 2°44.149'W; Fig. 1). Nannoplankton biostratigraphy indicates the presence of late Paleocene and early Eocene CP8a-CP8b zone boundary in the interval from Core 41R-6 to Core 42R-2 mbs (Shafik et al., 1998). We continuously sampled Core Sections 41R-6, 41R-CC, 42R-1 and 42R-2, representing the interval from 800.5 meters below sea floor (mbsf) to 805.58 mbsf at a resolution of 1-3 cm. Between Cores 41R and 42R there is a core gap of ~1 m. Notable lithological changes occur in the interval from 804.1 mbsf to 803.9 mbsf, where siliciclastic sediments are replaced by porcellanite, recrystallized biogenic silicates (Shipboard Scientific Party, 1996). The sediments above Core 41R-6 are recognized by more frequent occurrences of porcellanite (Shipboard Scientific Party, 1996; Wagner, 2002). Sediments below 42R-1 show apparently cyclic dark-light alterations, representing variable amounts of clay, carbonate, organic matter and biogenic silica (Wagner, 2002), which likely indicate precession forcing (e.g., Beckmann et al., 2005).

The tectonic evolution of the CIGTM implies that Site 959 has been located at ~1000 m water depth since the Maastrichtian (Oboh-Ikuenobe et al., 1997). The sedimentary record of Site 959, located on the continental side of the CIGTM, is much more complete than that of Site 960, although the sites are only 5 km apart (Shafik et al., 1998). It was also suggested that significant sediment redeposition has occurred from Site 960 to Site 959 between the early stages of the opening of the Atlantic (120 Ma) and formation of the marginal high (90 Ma) (Pletsch et al., 2001). In general, Site 959 is considered to be above the carbonate compensation depth (CCD) during the entire interval. Progressively higher accumulation rates of biogenic silicates occur from the early Eocene onwards (Wagner, 2002). These silicates are transformed to porcellanites and cherts in the interval above 812 mbsf.

Methods

ICP-OES

Barium concentrations were determined on 50 samples in the CIE interval. Approximately 125 mg of freeze-dried sediment was powdered and then dissolved in 2.5 ml HF (40 %) and 2.5 ml of $HClO_4/HNO_3$ mixture, in a closed Teflon bomb at 90 °C during one night. The acids were then evaporated at 160 °C and the resulting gel was subsequently redissolved in 1M HNO_3 at 90 °C during another night. Total elemental concentrations were determined by Inductively Coupled Plasma - Optimal Emission Spectroscopy (ICP-OES; Perkin Elmer Optima 3000) at Utrecht University. Precision and accuracy was better than 5 %, based on calibration to standard solutions and checked against internal laboratory standard sediments. Biogenic Ba (Babio) concentrations are calculated from ICP-OES data (Reitz et al., 2004) using detrital Ba/Al ratios of 0.0045 as determined for the Congo Fan (Rutsch et al., 1995).

$\delta^{13}C_{TOC}$

Approximately 0.3 g of freeze-dried material was powdered and subsequently decarbonated using two steps of 1M HCl. The residue was neutralized with demineralized water and dried in a stove at 50 °C. TOC content was then measured on ~10 mg of homogenized residue using a CNS-analyzer (Fisons). Stable carbon isotope ratios were determined using an isotope ratio mass spectrometer (IRMS, Finnigan Delta Plus) coupled online to the CNS analyzer. Absolute reproducibility, based on international and in-house standards, for TOC (Fig. 1a) and $\delta^{13}C_{TOC}$ (Fig. 1b) was better than 0.1% and 0.05‰ respectively.

TEX_{86}

For TEX_{86} analysis, ~10 g of freeze-dried powdered sediment was extracted by a Dionex Accelerated Solvent Extractor 200 using Dichloromethane (DCM): Methanol (9:1 vol:vol) at 100 °C, 7×10^6 Pa. Extracts were separated into polar and apolar fractions over an Al_2O_3 column using Methanol:DCM 1:1 and Hexane:DCM 9:1 as respective eluents. To analyze glycerol dialkyl glycerol tetraethers (GDGTs), Hexane:Isopropanol 99:1 was added to the polar fraction, which were then filtered over a 0.45 μm PTFE filter and measured on an Agilent 1290 ultra high performance liquid chromatography mass spectrometer (UHPLC-MS) at Utrecht University following the method of Hopmans et al., (2015). In addition to measuring in-house TEX_{86} and branched isoprenoid tetraether (BIT; Hopmans et al., 2004) standards, 9.9 ng of a C_{46} GDGT standard (*m/z* 744) was added to all samples to facilitate quantification of GDGTs. Fifteen samples were measured in duplicate, and 1 in triplicate, to assess reproducibility. Reproducibility was always better than 0.02 TEX_{86} units and 0.05 BIT units, respectively, and reproducibility of in-house standards was always better than 0.01 and 0.03 for TEX_{86} and BIT. We use the BIT index and methane indices (MI) to assess influences of terrestrial (Hopmans et al., 2004; Weijers et al., 2006), methanotrophic (Zhang et al., 2011) and methanogenic (Weijers et al., 2011) GDGT producers on TEX_{86} and did not encounter evidence for potential biases in any sample.

Data selection and statistical methodology

If the ^{13}C-depleted carbon that caused the CIE was the primary forcing of PETM warming, no time lag is expected between the two parameters since short feedbacks in the climate system operate on time scales (up to 10^2 years) much shorter than the time represented by our sampling intervals. To investigate if warming might have triggered ^{13}C-depleted carbon injection on millennial time scales, we apply cross-correlations on the time-shifted temperature - $\delta^{13}C$ data to determine the optimal lead or lag across a 100 kyr period around the onset of the CIE. Each dataset is resampled at 1 kyr resolution and shifted with 1 kyr increments. The maximum correlation coefficient (r^2) then determines the position of the most likely lead-lag relation. The datasets were also resampled at the resolution of either $\delta^{13}C$ or temperature and subjected to the same analysis. This yielded similar results, implying that the interpolation did not affect the outcome of the analysis.

All r^2 values are highly significant because temperature and $\delta^{13}C$ records are very similar at all sites. However, since the data represents a variable mixture of rescaled and interpolated points, we cannot perform a meaningful Fisher r-to-z transformation on the correlation coefficients for each individual site to address significant differences between correlations. We therefore summarize the lead-lag data from individual sites by plotting kernel densities of the optimal correlations of each site and bootstrapped (n = 1000) means of that data (Figure 2d), with the note of caution that the available data limits the ability to address true confidence intervals of the lead lag relations.

We correct the $\delta^{18}O$ values for ice volume (-1‰), paleolatitude (-0.24‰) and VPDB (0.27‰) and calculate temperatures following Kim and O'Neil, (1997). Due to stratigraphic difficulties at ODP Site 689 and 690, we do not correct for any $\delta^{13}C$ or $\delta^{18}O$ changes as a result of pH decrease across the CIE (Penman et al., 2014). Because $\delta^{18}O$ values are not corrected for pH changes, we potentially underestimate peak PETM temperatures by ~1 °C. This has no qualitative influence on our lead lag relations.

Results
Stratigraphy

Although the $\delta^{13}C_{TOC}$ record might be influenced by changes in organic matter sources, the presence of a 2 ‰ negative step in $\delta^{13}C_{TOC}$ at 804.1 mbsf marks the onset of the CIE,

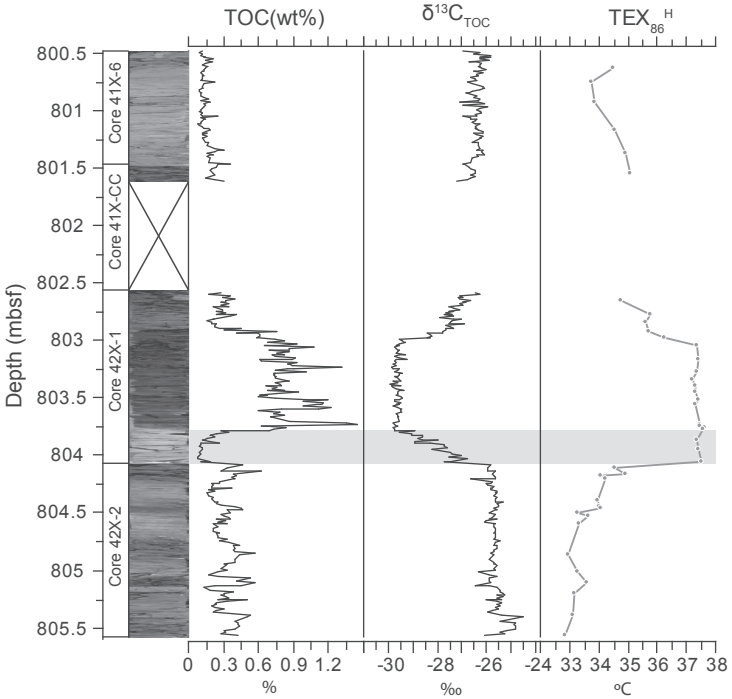

Fig. 1. *Stable carbon isotope data from total organic carbon ($\delta^{13}C_{TOC}$), total organic carbon in weight percentage (TOCwt%) and TEX_{86}^{H} reconstructed temperatures across the Paleocene – Eocene Thermal Maximum at ODP Site 959.*

and stable low values from 803.8 to 803 mbsf indicate the presence of its 'body' (Fig. 1, Supp. Fig. 3 and Supplementary text). The gradual decrease in $\delta^{13}C_{TOC}$ values between the onset and the 'body' of the CIE mark a layer of organic lean allochtonous biogenic silica of Paleocene age, likely deposited by a turbidity current (Supplementary Information). This might suggest a small hiatus at the onset of the CIE. Moreover, this implies that the decreasing $\delta^{13}C_{TOC}$ trend is best explained by bioturbation-mediated mixing of organic rich PETM sediments into the allochtonous biogenic silica. We therefore identify the onset of the PETM at 804.1 mbsf.

PETM temperatures

Average Late Paleocene TEX_{86}^{H} derived SSTs (Kim et al., 2010) are 33.5 (95% confidence interval: 32.9 – 34.3) °C in the late Paleocene. TEX_{86}^{H} shows no relation to the cyclic variations recorded in TOC wt%, implying that observed changes are unrelated to background cyclic variation in climate and weathering. SSTs rise stepwise by 1.2 (95% confidence interval: 0.9-1.6) °C at 804.19 mbsf and by 2.7 (2.4-2.9) °C at 804.1 mbsf to 37.4 (37.2-37.6) °C during the body of the PETM (Fig. 1). Consequently, we estimate a total warming of 3.9 °C (3.6-4.1 °C) across the onset of the PETM. This might be a minimum estimate because TEX_{86}^{H} values within the PETM (0.96) approach the maximum value of 1, which calibrates to 38.6 °C (Kim et al., 2010). Absolute temperatures are in good agreement with late Paleocene and PETM temperatures derived from Mg/Ca, $\delta^{18}O$ and TEX_{86}^{H} in a nearby shelf section from Nigeria (Frieling et al., chapter 3). Although the Paleocene part of the record is marked by gradual warming, we find a step (outside 2σ from the Paleocene mean as well as the

(supplemental text and supp. Fig. 3b).

Regardless of the assumptions used, the position of the maximum correlation is generally robust (see supplemental information) with respect to data quality and correlation window length. Uncertainties for Site 1172 are more pronounced since a large part (3 kyr) of the observed temperature lag (5 kyr) is due to one low TEX_{86}^{H} data point at the onset of the CIE (Supp. Fig. 3a and Sluijs et al., 2011).

Most records show the highest degree of correlation when temperature leads the onset of the CIE (Fig. 2C). Lead-lag relations at Site 689 and 690 are complex since the carbon and oxygen isotope ratios derive from single specimen planktic foraminifer records, which exhibit significant natural scatter and are subject to bioturbation effects (Supp. Fig. 2). However, specimens with high $\delta^{13}C$ (pre-CIE) and low $\delta^{18}O$ (indicating warm conditions) values are present in both *Acarinina* and *Subbotina* records from Site 689 and 690, providing strong evidence for pre-CIE warming (Supp. Fig. 3). This is important for two reasons. Firstly, unlike TEX_{86}^{H} records, the same substrates are measured for both $\delta^{13}C$ and temperature ($\delta^{18}O$), which excludes differences in bioturbation between various substrates. Secondly, although bioturbation effects and sedimentation rates are variable, the time lag between the onset of warming and the onset of the CIE is similar in duration for all TEX_{86}^{H} and $\delta^{13}C$ records we studied, except for ODP Site 1172.

From the position of the optimal correlation of each site we estimate the spread of the mean using a bootstrap approach (Figure 2d). On average, temperature leads the CIE by 1.8 kyr (95% quantiles 4.1 kyr lead to 0.7 kyr lag). If Site 1172 is considered as an outlier, the temperature lead increases to 3 kyr (95% quantiles 4.5 – 1.3 kyr lead; Fig. 2D). Importantly, temperature shows a rise in the order of ~2 °C prior to the CIE, and 3 °C simultaneous with the onset of the CIE.

Discussion

Translation of temperature to a whole-ocean signal

The widespread warming prior to the CIE suggests that this trend was global. To test this, we compare our result to simulations with a fully coupled Atmosphere Ocean General Circulation Model (Hadley Center Model (HadCM) 3) (Lunt et al., 2010b), run at early Eocene geography with 560, 1120 and 1680 ppm CO_2 in the atmosphere. The climate sensitivity (global temperature change under a doubling of atmospheric CO_2 concentrations) in this model is ca. 3.6 °C. Regional changes in the degree of warming between the different CO_2 scenarios occur (Fig. S9) due to oceanographic changes (Frieling et al., chapter 3; Lunt et al., 2010). The excellent agreement between the magnitude of warming from the study sites and that captured by a doubling of CO_2 in the model scenarios (Fig. 3a,b) suggests that the model is quantitatively capable to reproduce spatial variability of warming.

Evidence for methane hydrate dissociation?

At intermediate depths (~1 km) in the tropical Atlantic (Fig. 3C), model results also show enhanced warming (~6 °C per doubling of CO_2). This is crucial, since this is the depth where methane hydrates were most likely to exist in the Paleocene (Dickens et al., 1995). Interestingly, we find circumstantial evidence of the presence of gas hydrates near Site 959 during the late Paleocene and early Eocene. The allochtonous and turbiditic deposition of biogenic silicates at the onset of the CIE suggests slope instability, which can be caused by gas hydrate destabilization (Katz et al., 1999). Also, gas hydrates store large amounts of dissolved Ba (Dickens et al., 2003) and Ba concentrations at Site 959 are extremely high prior to and during the PETM (Fig. S7). We thus speculate based on these two observations

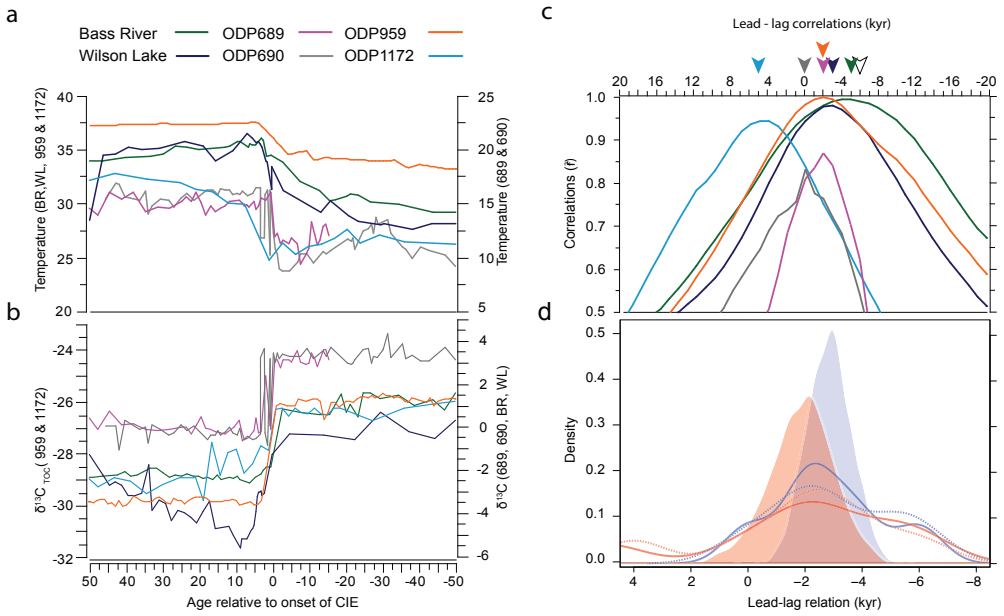

Fig. 2. *Time-shifted cross-correlations between $\delta^{13}C$ and temperature at all sites.* ***A.*** *Temperature records from TEX_{86}^{H} (Bass River, Wilson Lake, ODP 1172 and ODP 959) and $\delta^{18}O$ (ODP 689 and ODP 690).* ***B.*** *Stable carbon isotope records from bulk organic carbon (ODP 1172 and ODP 959), bulk carbonate (Bass River and Wilson Lake) and single specimen Acarinina (ODP 689 and ODP 690).* ***C.*** *Correlation coefficients for each record relative to time-shift. Arrows indicate position of highest value.* ***D.*** *Kernel densities of raw data (lines) and bootstrapped mean (areas). Red line and area includes all data, blue lines and area excludes Site 1172.*

Paleocene trend) in the record at 804.19 mbsf, 10 cm below the first observable change in $\delta^{13}C_{TOC}$. Based on our age model for Site 959, we determine that the initial temperature change leads the $\delta^{13}C_{TOC}$ shift by ~10 kyr (supplementary information).

Lead-lag relation

Similar pre-CIE warming has been observed at two sites along the New Jersey Shelf (Bass River and Wilson Lake (Sluijs et al., 2007b), and the Bighorn Basin in Wyoming (Secord et al., 2010). At ODP Site 690 and 689 in the Southern Ocean, surface warming appears to precede the warming of deeper waters and presumably also the CIE (Thomas et al., 2002). Apart from the terrestrial section in the Bighorn Basin, all of these sites have well-resolved high-resolution chemo- and/or biostratigraphy, temperature and $\delta^{13}C$ data across the onset of the PETM. We refined age models for Bass River, Wilson Lake, ODP Site 1172 and ODP Site 689, which are sites with sediment accumulation rates across the onset of the PETM that are sufficient to extract millennial scale leads and lags (see supplementary information) and resampled each dataset at 1 kyr resolution. The resulting pairs of $\delta^{13}C$ and temperature data were subjected to time-shifted cross-correlations to identify lead-lag relations, assuming a linear relation between temperature and $\delta^{13}C$ (Fig. 2C). Caution should be taken addressing confidence intervals of a lead or lag as the nature of the datasets causes all correlations to be highly significant. For Site 959 we conduct sensitivity experiments where we vary the amount of time covered by the allochtonous biogenic silica layer between 2, 6 and 10 kyr

that gas hydrates near Site 959 leaked methane and Ba during background conditions and dissociated during the PETM.

Dickens et al., (2003) calculated that the release of 2000 Gt of methane hydrate may account for a two-fold increase in global Ba burial rates. This is consistent with the modest increase in Ba concentrations at Site 959 (Supp. Figure 7), and with barite accumulation records from deep sea sediments (Ma et al., 2014). To assess if this represents a redistribution of Ba burial from shelf to deep sea (Ma et al., 2014), we estimate global changes in Ba burial based on previously published data from deep ocean, slope and shelf sites (Fig. S10, Table S2). We find an increase in Ba burial rates at all sites, which implies that global average Ba accumulation rates increased with respect to pre-CIE by a factor 1.6 to 4.6 (95% quantiles).

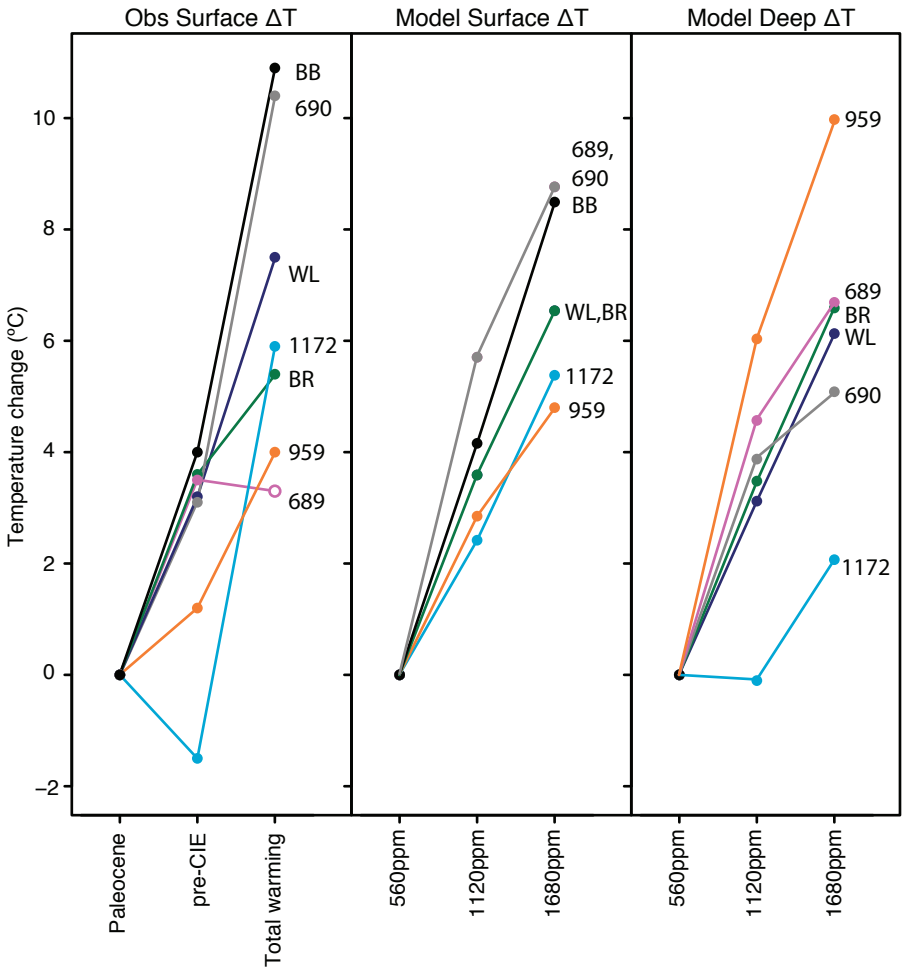

Fig. 3. *Data-model comparison.* ***A.*** *Temperature change as inferred from the data, separated into pre-CIE and full warming.* ***B.*** *Temperature change at surface from model, differences between 1120 ppm and 560 ppm and difference between 1680 ppm and 560 ppm.* ***C.*** *Same for bottom water at these sites.*

Although large uncertainties exist, this is not significantly different from model-based estimates of Ba release from methane hydrates (Dickens et al., 2003) (see supplementary information). This has important implications since Ba has an oceanic residence time (<10 kyr) much shorter than the timescales of the PETM. This implies an input of Ba from an external reservoir and methane hydrates is among the few plausible candidates (e.g., Dickens et al., 2003; Ma et al., 2014).

Crucially, the CCD rose by much more in the Atlantic than in the Pacific, which based on carbon cycle modeling, is only possible with direct CO_2 addition to Atlantic Deep water (Zeebe et al., 2009). Direct carbon addition from methane hydrates may be an important mechanism to explain the difference in CCD rise. Furthermore, pre-CIE warming at many locations (Fig. 3a) was similar in magnitude as the hypothesized warming needed for large scale methane hydrate dissociation (3-4ºC; Archer et al., 2009), which translates well to intermediate and bottom waters (Fig. 3, Lunt et al., 2010). Although early warming might trigger carbon release from several reservoirs (DeConto et al., 2012; Dickens et al., 1995), combined with the globally elevated Ba burial rates and pattern of CCD changes it represents strong evidence of massive methane hydrate dissociation.

A candidate for the initial warming

Based on our data compilation and calculations, warming prior to the injection of ^{13}C-depleted C was most likely global and therefore possibly driven by a rise in CO_2. If so, the magnitude of warming implies that there was significant CO_2 addition in the 10 kyr leading up to the CIE. Previous work (Sluijs et al., 2007b) has hypothesized that early warming resulted from CO_2 input by The North Atlantic Igneous Province (NAIP), which shows enhanced activity during this period (Storey et al., 2007). Sustained magma production rates in the order of 20-160 $km^3\ yr^{-1}$ across 20 kyr, within the limits hypothesized for the most active phase of the NAIP (Storey et al., 2007) may provide upwards of 4000 Gt of CO_2 (supplement and Table S1). Hence, this remains a plausible scenario, particularly because such an input would only minimally affect global exogenice $\delta^{13}C$ during the early warming (Kump and Arthur, 1999).

Conclusions

We conclude, based on new and existing evidence that global warming preceded the PETM carbon isotope excursion by several millennia. The amplitude of pre-CIE surface warming (2-3 ºC), pattern of CCD change and globally increased Ba burial rates represent a combination of features that represent a smoking gun for massive methane hydrate destabilization at the onset of the CIE.

Supplementary Information

Age model Site 959 PETM (Cote d'Ivoire – Ghana Transform Margin, Tropical Atlantic) Refining sedimentation rate estimates and cyclicity

Published nannofossil biostratigraphy has indicated the presence of Rhomboaster bitrifida in the core-catcher of 41R (801.49-801.65 mbsf) used as a biostratigraphic proxy for Campylosphaera eodela and indicates nannoplankton Subzone CP8b. This sample is further marked by the highest occurrence of Fascilithus, also indicating an age close to latest Paleocene (Shafik et al., 1998).

We estimate sedimentation rates at Site 959 on the cyclic occurrence of light and dark banding in the sediments that is accompanied by lower and higher organic matter content, respectively (Fig. 1a). We find 5 cycles in the upper Paleocene of the section (805.58 – 804.2 mbsf). The limited available upper Paleocene and lower Eocene biostratigraphy (Shafik et al., 1998) implies average long-term sedimentation rates of in the order of ~2 cm kyr^{-1}. We identify 5 TOC cycles between 805.6 and 804.2 mbsf, which implies these cycles occur on precessional time scales, similar to a previously studied interval in the Cretaceous at this site (Beckmann et al., 2005). We therefore attribute the TOC cycles to precession, implying compacted sedimentation rates of ~1-1.5 cm kyr^{-1} in the upper Paleocene.

The allochtonous biogenic silica layer is an important feature in this section. It may have caused some scouring and thus there might be some sediment missing, although we have not noted a marked erosional surface during sampling. We also explored three different scenarios with various time gaps for the deposit (2, 6 and 10 kyr, Supp. Fig. 5a). Sedimentation rates during the body of the PETM are assumed to be 1 cm kyr^{-1}, similar to the late Paleocene. This assumption has virtually no influence on further analyses, since values in both TEX_{86}^{H} and $\delta^{13}C_{TOC}$ remain almost unchanged during the entire body phase. The scenario with a 2 kyr hiatus is used for further analyses and Figure 2.

The anomalous shape of the CIE

The onset of the CIE at Site 959 is somewhat anomalous (Fig. 1), with a gradual decrease to PETM values and apparent scatter. The onset of the CIE marks the deposition of biogenic silicates, which have been altered to porcellanite. Since all biogenic silica has been altered to quartz or been replaced by pyrite, detailed micropaleontological analysis is not possible. A step in $\delta^{13}C_{TOC}$, TOC and TEX_{86} suggests a small discontinuity at the base of the porcellanite although this might also be a primary feature of the onset of the CIE.

Only few biogenic silica-rich deposits are known from the late Paleocene and early Eocene and the ocean is generally assumed to be strongly undersaturated with respect to silicate ion during this period (Siever, 1991). Furthermore, the position of the deposit, at the start of the period of warming poses another problem, since warming enhances the solubility of silica. This implies that biogenic silica deposition and burial must have been rapid to prevent dissolution. This suggests that this silica was produced elsewhere and redeposited at the drill site. Low concentrations of siliciclastic material imply that the silica likely did not derive from the African shelf. Rather, the most likely explanation is that it derived from higher elevations on the marginal ridge and deposited through a mass-movement such as a turbidity current. Turbidite deposits and slope failures are common during the PETM, typically associated with increasing sediment supply to marginal marine seas due to intensification of the hydrological cycle (Sluijs et al., 2014), but possibly with submarine hydrate destabilization (e.g., Katz et al., 1999).

Instantaneous deposition of allochtonous biogenic silica at the onset of the PETM also

provides an explanation for the anomalous shape of the CIE onset. The porcellanite yields very low TOC concentrations (Fig. 1). As a consequence, if this layer derives from a turbidity current from shallower depths on the ridge, it must have had low concentrations of organic matter (OM) prior to re-deposition, meaning the source sediments were oxidized, except for a small fraction of highly resistant OM. Such resistant OM is typically clay-bound terrestrial OM (TOM), which in the Paleogene has a much higher $\delta^{13}C$ than marine OM (MOM) (Sluijs and Dickens, 2012). Because the porcellanite is located at the onset of the CIE, it is likely that the original biogenic silica, as well as the resistant OM transported along with the turbidity current is of latest Paleocene age. If so, the low $\delta^{13}C_{TOC}$ values in this layer must reflect a mixture of Paleocene OM with high $\delta^{13}C$ and PETM organic matter that is bioturbated down into the sediment. This is consistent with visual observations of the core material, which shows bioturbation of dark-colored PETM material down into the light porcellanite downcore (Supp. Fig. 2).

We test this hypothesis with a simple sediment mixing model, in which we assume that a small (0.03% TOC) but constant fraction of resistant Paleocene TOM is present in all samples with a $\delta^{13}C$ of -23‰, which is consistent with late Paleocene terrestrial OM (e.g., Sluijs and Dickens, 2012). The BIT-values and kerogen composition from the body of the PETM indicate that PETM organic matter is nearly exclusively marine. This marine organic matter has $\delta^{13}C$ values of around -30‰, which is consistent with published marine organic matter records (Sluijs and Dickens, 2012). Latest Paleocene MOM is assumed to be -26‰, which is consistent with published values (Sluijs and Dickens, 2012). We subsequently calculate $\delta^{13}C_{TOC}$ from measured TOC values (Supp. Fig. 2) with the following equation:

Eq.1 $\delta^{13}C_{TOC} = ((TOM/TOC)^* \delta^{13}C_{TOM})+((TOC-TOM)/TOC)^* \delta^{13}C_{MOM})$

With the exception of one data point (804.07 mbsf), this simple mixing model is capable of accurately predicting the measured $\delta^{13}C_{TOC}$ profile. We hence argue the biogenic silicates that form this porcellanite layer were oxidized, redeposited at the site location and marine PETM organic matter was subsequently bioturbated in from above.

From these inferences it also follows that mixing from above influences reconstructed temperatures. GDGT concentrations during the body of the PETM are much higher than in the uppermost Paleocene and oxidation likely lead to even lower initial concentrations in the porcellanite layer. Therefore, it requires only a very small fraction of allochtonous organic matter to completely overprint the original GDGT signal. The allochtonous deposition of silicates suggests a small amount of sediment may be missing. Due to extensive mixing and allochtonous nature of the layer, we exclude data from the turbiditic deposit (804.1 – 803.8 mbsf) from our lead-lag analyses.

GDGT / TEX_{86} results

Before we use GDGT ratios to reconstruct sea surface temperatures (SSTs) using the Kim et al., (2010) calibration for high temperatures (TEX_{86}^H), we apply several GDGT indices that can indicate biases of the reconstructed temperatures. BIT values are always below ~0.16, signalling that GDGT contributions from sources other than marine thaumarcheota are a minor factor in our samples. Similarly, methane indices that indicate methanotrophic (Zhang et al., 2011) or methanogenic overprints (Weijers et al., 2011) never reach values that suggest a significant contribution to the GDGT pool. Concentrations of GDGTs can be a limiting factor in organic lean sediments, such as encountered here (Schouten et al., 2007b). We selected samples with >5 ng of LCMS injected GDGTs, which amounts to approximately 1 ng g^{-1} sediment. GDGT concentrations during the body of the CIE are ~50 times higher than outside the CIE, signalling enhanced preservation and/or (export)

production. The close correspondence of our SST values with data derived from carbonate proxies and TEX_{86} from Nigeria implies that we can confidently use these TEX_{86}^{H} data to reconstruct temperature.

Evidence for local and global methane hydrate destabilization?

The marine methane hydrate dissociation hypothesis is one of the prime candidates to explain the negative CIE that marks the PETM. Initial warming results in methane hydrate destabilization (e.g., Dickens et al., 1995), which provides a positive feedback to warming. If methane hydrates destabilize, two main pathways can lead to rapid of release gaseous methane from marine sediments. Firstly, if the bubble volume of methane in sediment exceeds a certain threshold value, these bubbles may reach the sediment-water interface, dissolve and oxidize to CO_2 (Archer and Buffett, 2005; Valentine et al., 2001). Although this can happen on small scales (cm-m), this scenario has also been connected to large (km) scale pockmarks, which have been found associated with Paleocene – Eocene sediments (Imbert and Ho, 2012). However, the exact timing of these structures remains uncertain and the gas volume accounted for is equivalent to only ~1% of the total volume required to explain the CIE. The second way of releasing methane is more violent. The continental slopes, where hydrate-rich sediments typically occur (e.g., Kvenvolden, 2002), are also susceptible to sediment destabilization, which can ultimately result in slope failure and turbiditic deposits which release methane more or less instantaneously (Katz et al., 2001, 1999).

The CIGTM was likely deep enough (~1000m) to be within the gas-hydrate stability zone (GHSZ) and at the same time subject to high productivity and organic matter supply, which makes the presence of hydrates more likely (Dickens, 2001). Although circumstantial, two independent lines of evidence may indicate (violent) hydrate release close to Site 959 during and before the PETM. First, the intriguing presence of a single turbiditic deposit precisely at the onset of the PETM may be connected to slope failure similar to that observed at Blake Nose (Katz et al., 1999). Secondly, non-detrital Ba is enriched by a factor 10 relative to average shale. Extremely elevated Ba concentrations are more common during the PETM (e.g., Bains et al., 2000; Ma et al., 2014) and have been attributed to global increase in export productivity.

However, since the residence time of oceanic Ba is short (<10 kyr), this either requires an external source of Ba or a relocation of Ba deposition from the shelf to the open ocean (Paytan et al., 2007), which would be facilitated by enhanced Ba regeneration from extensive anoxic shelf sediments. Although shelf and marginal marine records show evidence for lower oxygen concentrations on a global scale (e.g., Sluijs et al., 2014), Ba burial rates are elevated with respect to background Paleocene in a range of oxic and anoxic shallow sites. We calculate changes in Ba burial rates for sites in Egypt, Southern Tethys (Soliman, 2003), the Well 10 Section in the West Siberian Sea (Iakovleva et al., unpublished data), Wilson Lake, New Jersey Shelf (Zachos et al., unpublished data), ACEX, Lomonosov Ridge, Arctic Ocean (Röhl, unpublished data), Dahomey Basin, Nigeria (Table 4) and Tawanui, New Zealand (Crouch, 2001) (Fig. S10).

Although some sites show a biogenic Ba deficit (i.e. more than 100% detrital), the majority indicates similar or elevated Ba burial from Paleocene to the PETM. Based on previously published data from open ocean settings (Ma et al., 2014) and the slope and shelf sites mentioned above we calculate global average PETM Ba burial rates increase by a factor 1.6 to 4.6 relative to the late Paleocene. It should be noted that we likely underestimate uncertainties in this estimate, as we find strong inter and intra-site variations in Ba burial rates and our compilation (n = 16) may not represent an accurate global picture.

Secondary, but also potentially large, uncertainty arises from complexities in the local stratigraphy, especially at sites that suffer from dissolution, as can be seen in Ma et al., (2014). In comparison uncertainty related to different methodologies used to determine Ba concentrations in previous studies (XRF, ICP-OES) can be neglected, also separating detrital and biogenic Ba is introducing a relative minor uncertainty. That said, we find no evidence for relocation of Ba burial from the shelf or slope to the deep ocean as postulated by Paytan and Griffith (2007), but rather a global increase in Ba burial rates.

Due to short residence time and limited Ba concentrations in the ocean, increasing global Ba burial require an external source, with the most likely source being the destabilization of marine methane hydrates that store large amounts of dissolved Ba (Dickens et al., 2003). Dickens et al., (2003) calculated that a doubling of Ba burial may be accounted for by release of 2000 Gt of methane hydrates. In contrast, Paytan et al., (2007) noted that releasing large amounts of dissolved Ba would supersaturate waters locally and result in subsequent barite precipitation. The precipitation of barite however is strongly dependent on sulfate concentrations and although there is no direct evidence, (Lowenstein, 2001) show that seawater may have evolved from a low sulfate state to a high sulfate state during the Cenozoic linked to contemporary rise of Mg/Ca ratios, implying much lower (10-15 mM; modern = 28 mM) sulfate concentrations in the early Paleogene (see also Kurtz et al., 2003). This could hence result in more widespread deposition of dissolved Ba released from destabilized methane hydrates.
We thus argue that massive methane hydrate destabilization drives a large global increase in Ba burial rates, possibly modulated by productivity changes.

Refined age models from sites used in data compilation
Bass River and Wilson Lake (New Jersey Shelf, North Atlantic)

We use the data for the Bass River and Wilson Lake sites from (Sluijs et al., 2007b).
The age models for the Bass River (BR) and Wilson Lake (WL) sites have been extensively discussed in literature (Gibbs et al., 2006; John et al., 2008; Sluijs and Brinkhuis, 2009; Stassen et al., 2012). We adopt a combination of several methods to calculate the age model for these sites. At BR, we first assume that the percentage of kaolinite in the sediments is directly proportional to the sedimentation rate. The kaolinite is likely Cretaceous in origin and redeposited during the PETM (e.g., Cramer et al., 1999; John et al., 2012). Secondly, we follow Sluijs and Brinkhuis, (2009) and assume sedimentation rates during the PETM in the order of 9 cm kyr^{-1}. Combined with the kaolinite percentages it follows that Paleocene sedimentation rates are on average 2.5-3 cm kyr^{-1}. WL has been correlated to BR using dinocyst assemblage changes (Sluijs and Brinkhuis, 2009) and we here use this correlation to derive the age model for the WL from that of BR.

Sites 689 and 690, Maud Rise (Weddell Sea, South Atlantic)
We use the single specimen *Acarinina* and *Subbotina* data for Site 690 from Kelly, (2002), Kennett and Stott, (1991) and Thomas et al., (2002) and the data for Site 689 from Zachos et al., (2007).

Sedimentation rates at Site 690 (~2000 m water depth) are well constrained by a He^3 age model (Farley and Eltgroth, 2003). We subsequently derive the age model for Site 689 (~1000 m water depth) from direct correlation of the carbon isotope record to that of Site 690. Through the analyzed interval, sedimentation rates seem fairly constant at Site 690 and fitting the Site 689 records using the average sedimentation rate from Site 690 produces satisfying results. Many deeper sites during the PETM show decreased sedimentation rates due to lower carbonate accumulation rates and (partial) carbonate dissolution (Zachos et al.,

2005b). However, dissolution at Site 690 is thought to be relatively minor and if we assume higher sedimentation rates for the shallower Site 689, isotope records start to diverge. A stable and constant sedimentation rate similar to that of Site 690 is therefore used for the Site 689 age model.

In addition to these general remarks, at both sites there are a few foraminifer specimens that are apparently out of stratigraphic context, both above and below the onset. We identify these from other specimens at the same level based on $\delta^{13}C$ and $\delta^{18}O$ values that are characteristic for either CIE or pre-CIE values. For correlations, it matters little if these specimens are included or excluded. We therefore removed only specimens that are obviously out of stratigraphic context.

It should be stressed that, although most foraminifer specimens clearly fall within either peak CIE or pre-CIE groups, there are specimens close to the onset of the CIE that show intermediate $\delta^{18}O$ but pre-CIE $\delta^{13}C$ (Supp. Fig. 3). Even though the lead-lag relations may not be as well resolved as at some other sites due to scarcity of such intermediate specimens, these specimens represent strong evidence for pre-CIE warming at these sites.

Age model Site 1172 (South Tasman Plateau, Southwest Pacific)

We use the data from Sluijs et al., (2011). Upper Paleocene sedimentation rates at site 1172 are resolved from sedimentary thickness from the magnetochron C24r to the CIE that identifies the PETM and are determined to be ~ 0.57 cm kyr^{-1}. Based on the thickness of the CIE, average PETM sedimentation rates are 0.4-0.5cm kyr^{-1} (Sluijs et al., 2011).

Volcanic carbon: a plausible scenario for short term warming?

The mass balance equations used to explain the CIE and CCD changes at the PETM require contributions of two separate ^{13}C-depleted sources (Frieling et al., chapter 6; Zeebe et al., 2009) or the long and short term response of one source (Zeebe, 2013). The pre-CIE warming requires another, ^{13}C-neutral, source that can act on (multi)-millennial scales.

The evidence of enhanced volcanism in the North Atlantic is ample, but it requires large additional amounts of magma production to explain a CO_2 increase. In the long-term carbon cycle, silicate weathering counterbalances volcanically produced CO_2 (Berner, 1990). Therefore, volcanism is usually disregarded as a carbon source for rapid climate events. However, there is evidence that large igneous provinces played a role during the ocean anoxic events of the Cretaceous (Turgeon and Creaser, 2008) and the most active phases of the North Atlantic Igneous Province (NAIP) may have indeed produced some imbalance in the carbon cycle (Storey et al., 2007). We calculate how much carbon could be produced within a short (5, 10 or 20 kyr) period (Table S1). The calculations assume the following constants; magma density is 2750 kg m^3 of which 0.2 to 0.5 weight percent is CO_2, which is degassed completely (Self et al., 2006). The length of the active zone is 2560 km (Eldholm and Grue, 1994). The magma production rates are taken from Storey et al., (2007) and recalculated to rates per kyr. To put these numbers in perspective; the total volume of the flood basalts in the North Atlantic is ~1.8 x 10^6 km^3 (Eldholm and Grue, 1994), maximum and minimum volumes in our calculations are 3.1 x 10^5 km^3 and 2.6 x 10^4 km^3 respectively. It should be noted that the NAIP is emplaced in two phases each spanning several Myr and that our rates are thus much higher than average, consistent with Storey et al., (2007). The modern volcanic CO_2 flux to the atmosphere is approximately 0.26 Gt yr^{-1} (Kerrick, 2001). These scenarios thus require an increase of volcanic CO_2 production, with respect to the modern, of 30-80%.

The degassing parameter is one of the uncertainties; Regardless of the CO_2 content of the

magma contains, it is highly unlikely that all of that CO_2 will be degassed, perhaps even more unlikely when the emplacement time of the flood basalts is rapid. We, therefore, must stress that the emission scenarios here presented are upper estimates and only used to illustrate plausibility. It is however important to note that even the lower estimates of magma production rates produce fairly substantial amounts of CO_2. These scenarios also illustrate that longer (>10 kyr) periods of sustained enhanced activity are required and although it is impossible to connect the earliest warming to the volcanism, we note that first signs of warming are typically observed ~10 kyr before the CIE.

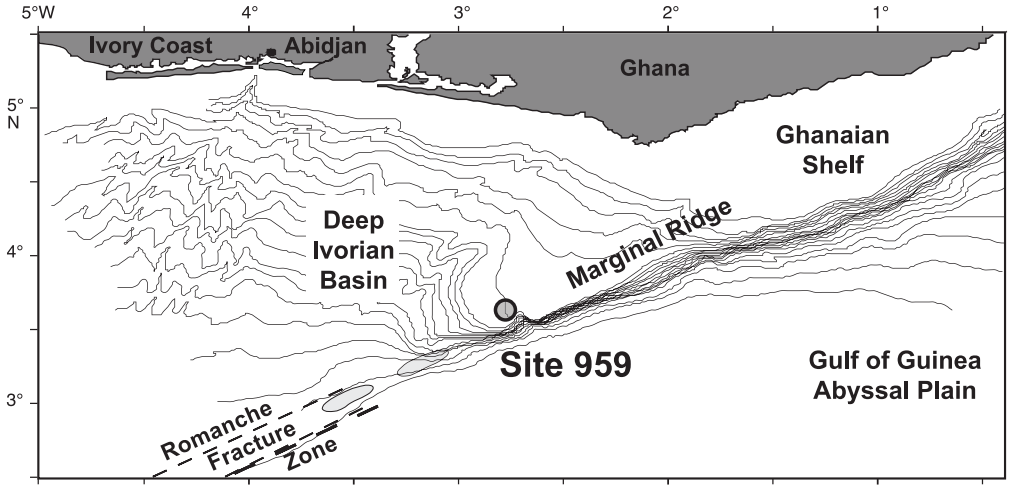

Figure S1. *Site 959 location.*

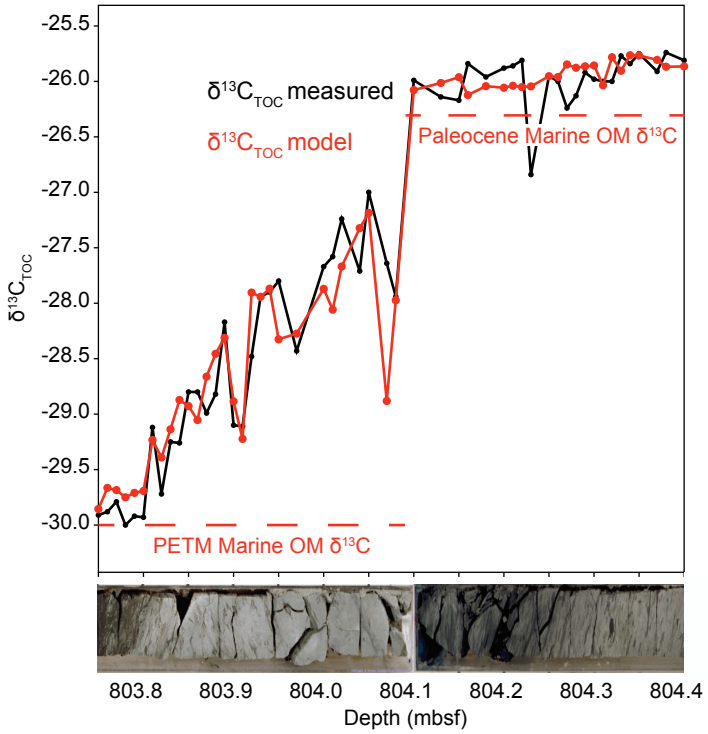

Figure S2. *Organic carbon $\delta^{13}C$ onset mixing model.*

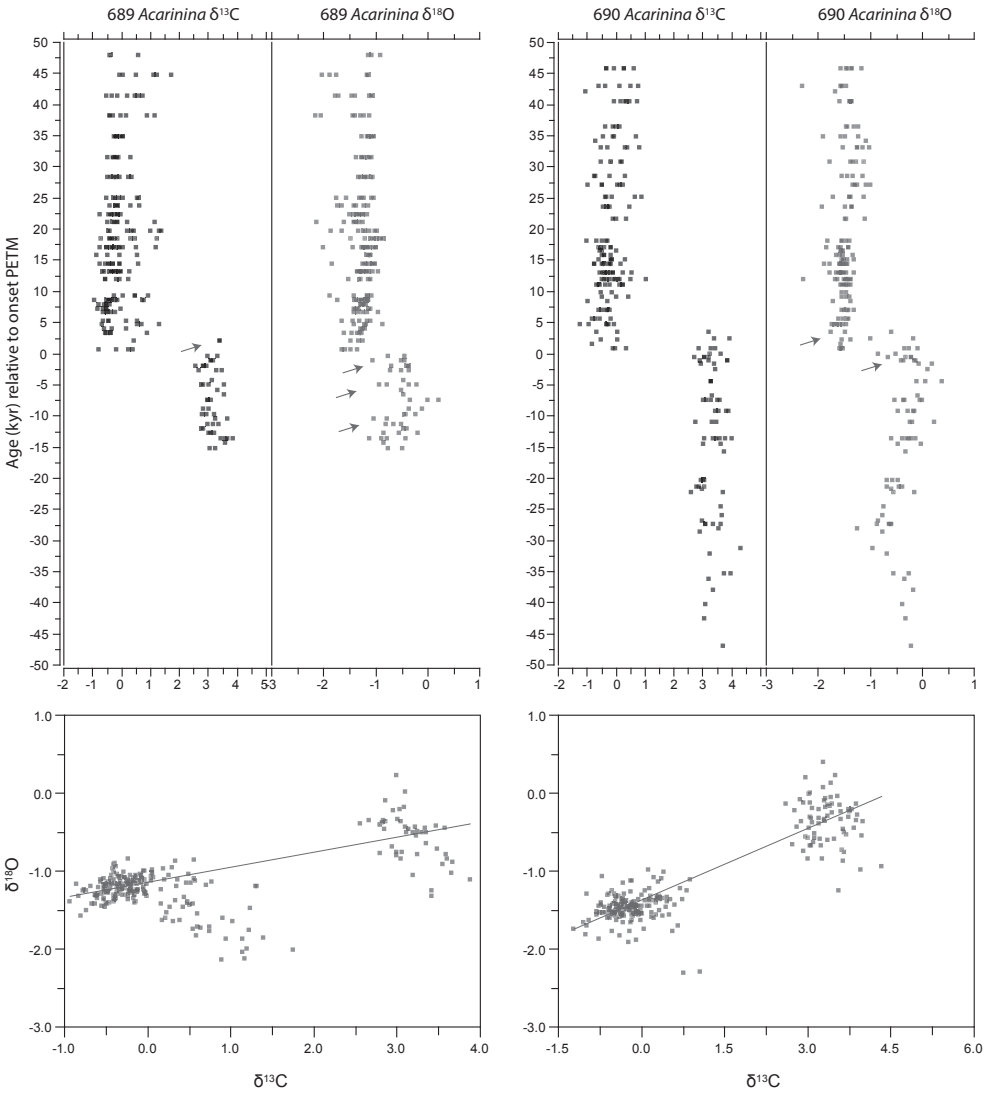

Figure S3. *Acarinina specimens at Site 689 and 690, illustrating the presence of high $\delta^{13}C$ (pre-PETM) and low $\delta^{18}O$ (high temperature) specimens.*

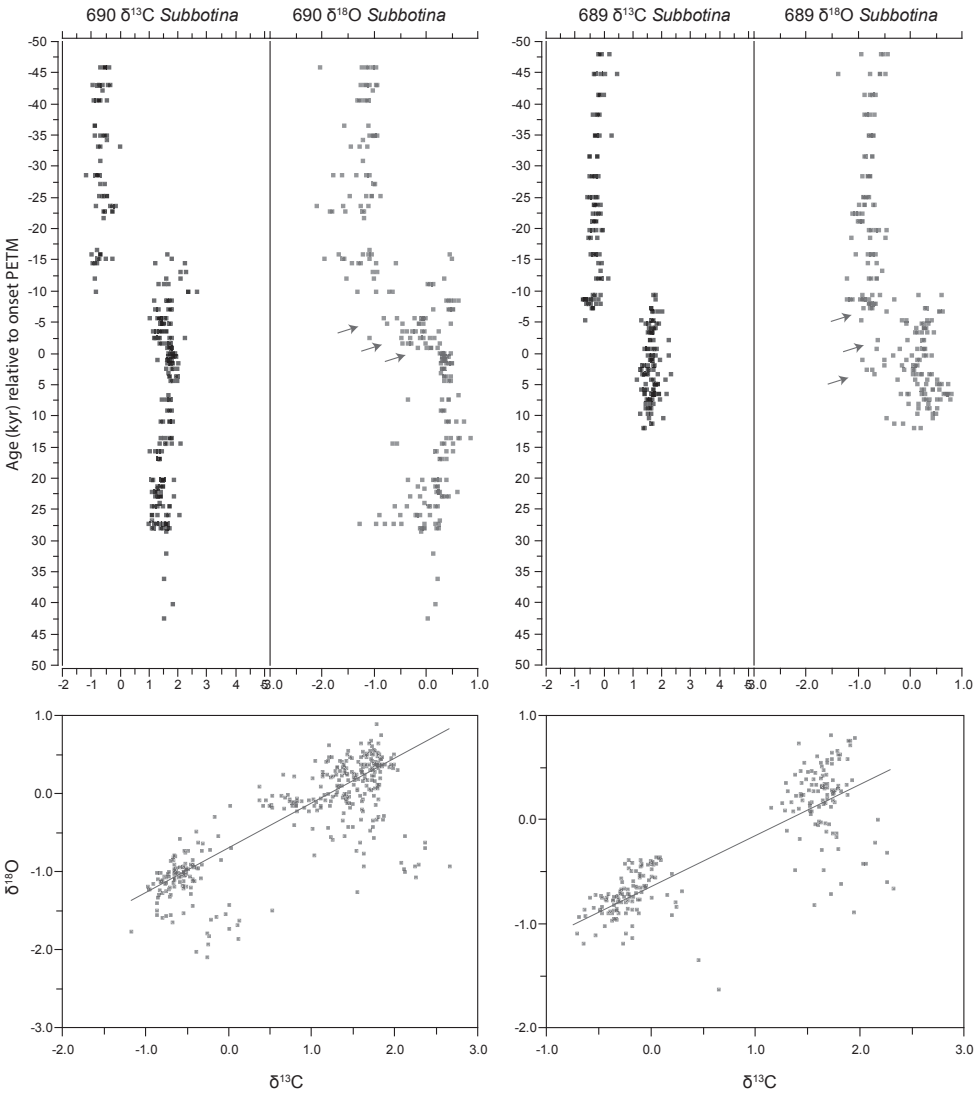

Figure S4. *As Figure S3, for Subbotina specimens.*

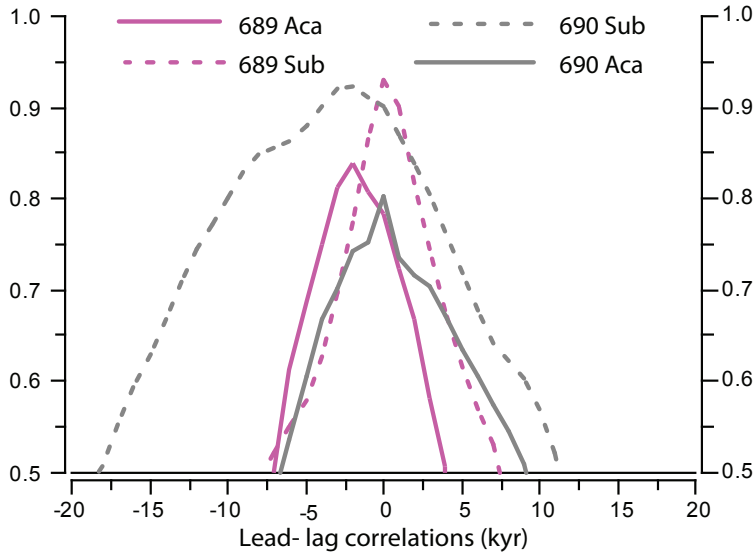

Figure S5. *Correlations of foraminifer datasets at 689 and 690. Surface signal (Acarinina) in solid lines and subsurface signal (Subbotina) in dashed lines.*

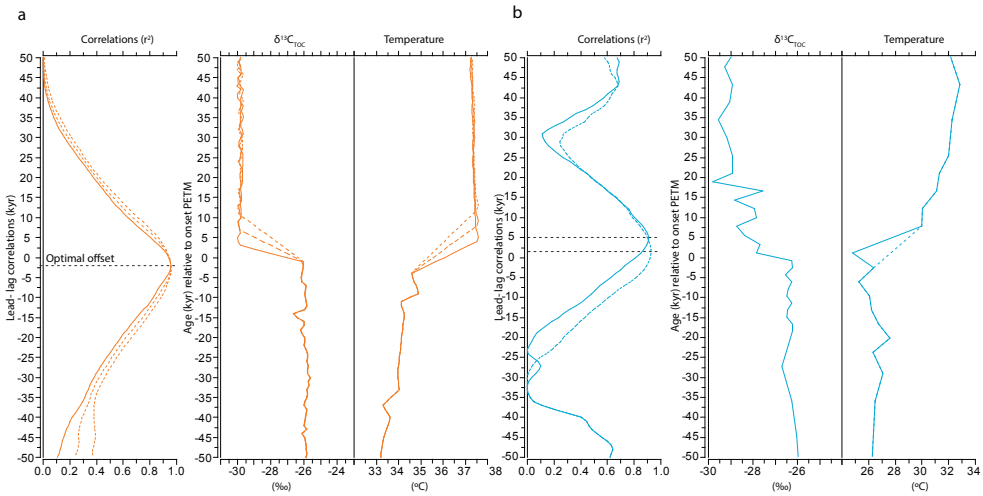

Figure S6. *Sensitivity to data differences: Site 959 and 1172.* ***A.*** *Site 959, lines represent scenarios with 2 kyr (solid line), 6 kyr (dashed line) and 10 kyr (dotted line) missing in turbidite,* ***B.*** *Site 1172 scenario including colder datapoint at the onset (solid line) and excluding this point (dashed line).*

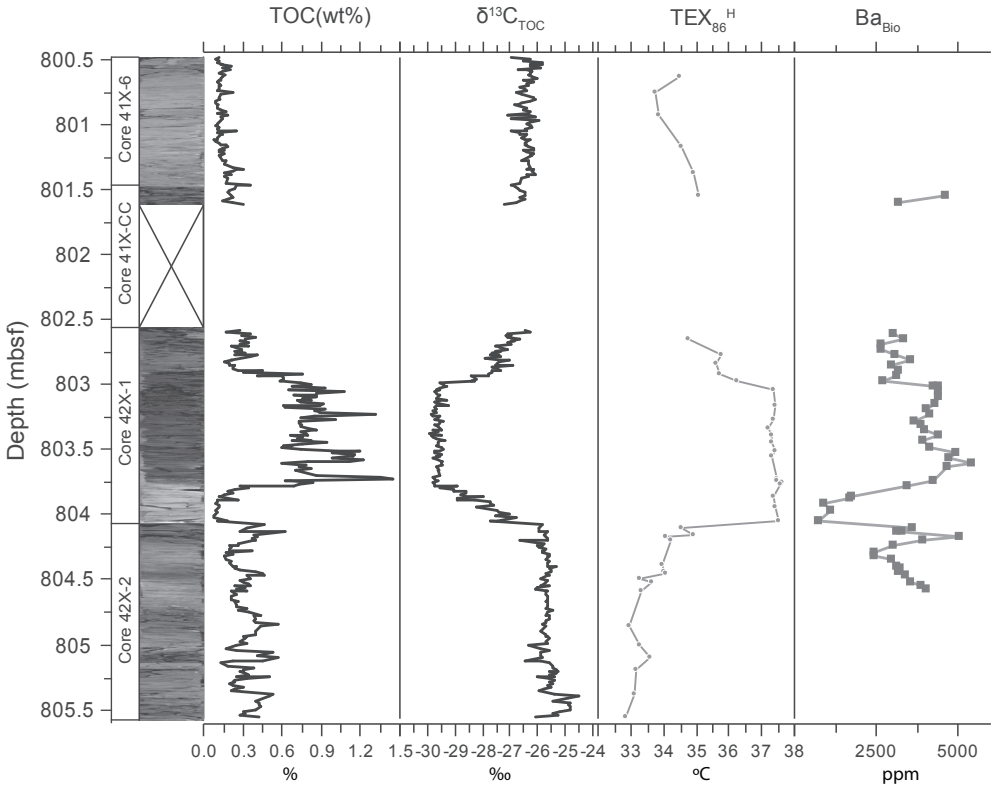

Figure S7. *As Figure 1 including Ba concentrations at Site 959 determined by ICP-OES.*

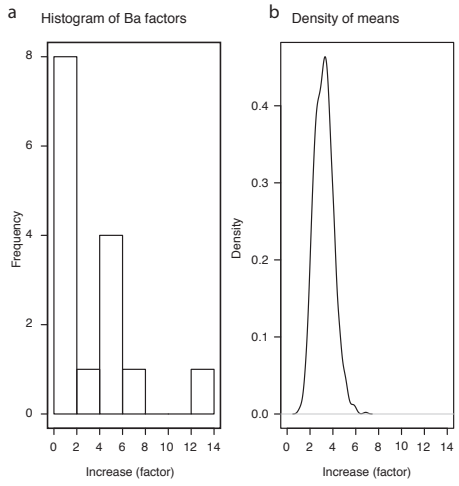

Figure S8. *Global composite of Ba concentration change during the PETM, relative to that of Paleocene.* ***A.*** *histogram of data (n=16).* ***B.*** *Estimate of Ba change using bootstrapped (n=1000) means.*

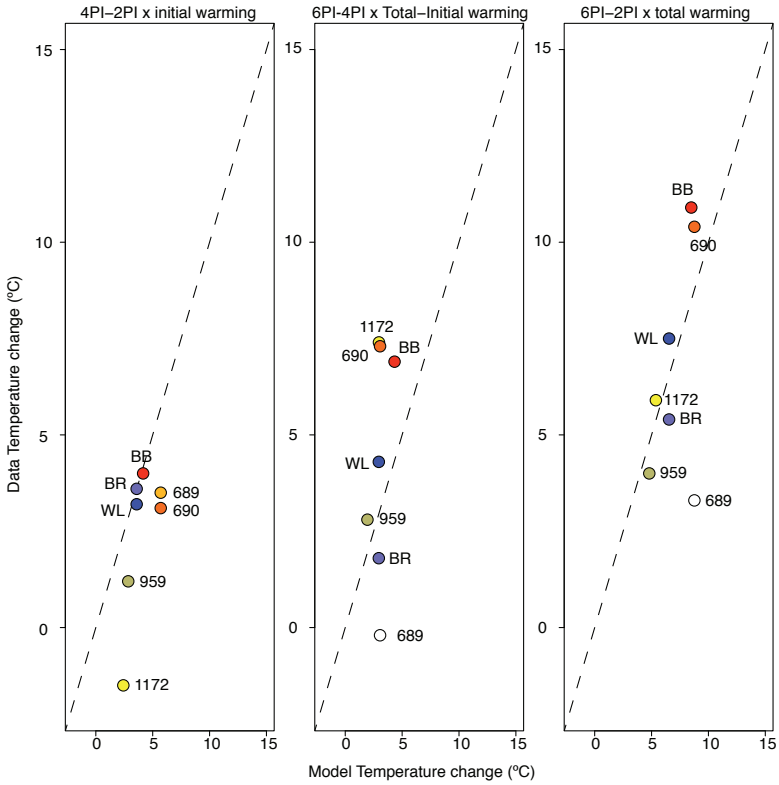

Figure S9. *Model temperature change versus recorded sea surface temperature change.* ***A.*** *1120-560 ppm scenario (4PI-2PI) versus initial warming.* ***B.*** *1680-1120 ppm scenario (6PI-4PI) versus total warming minus initial warming.* ***C.*** *1680-560 ppm (6PI-2PI) versus total warming.*

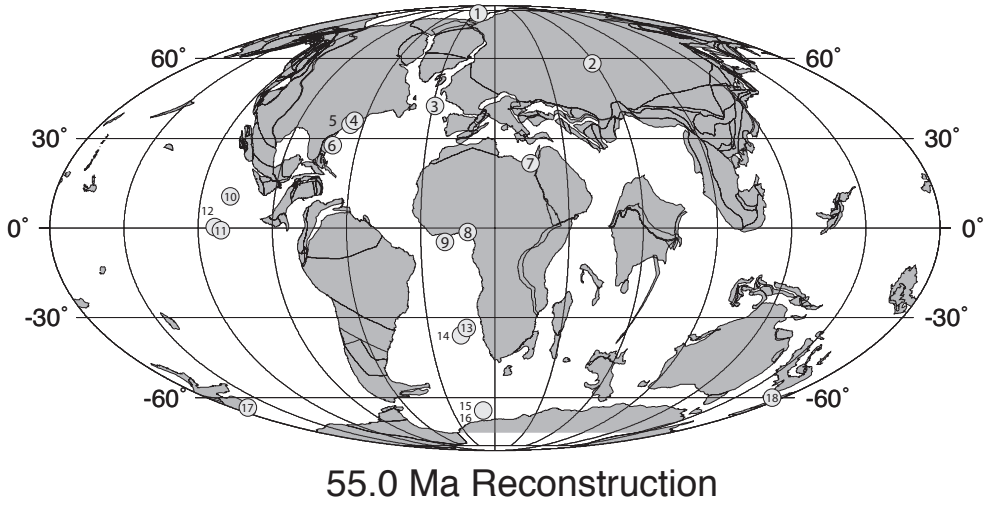

Figure S10. *Sites used for temperature $\delta^{13}C$ relations and/or Ba burial rates. 1. ACEX. 2. West Siberian Sea (Well 10). 3. ODP Site 549. 4. Wilson Lake , New Jersey Shelf. 5. Bass River, New Jersey Shelf. 6. IODP Site 1051. 7. Dababiya quarry, Egypt. 8. Dahomey Basin, Nigeria. 9. ODP Site 959. 10. IODP Site 1215. 11. IODP Site 1220. 12. IODP Site 1221. 13. IODP Site 1262. 14. IODP Site 1263. 15. Tawanui, New Zealand. 16. ODP Sites 690. 17. ODP Site 689. 18. IODP Site 1172.*

Table 1. *Carbon emission rate estimates from enhanced volcanism in the North Atlantic.*

Estimated magma production rate ($km^3\ km^{-1}\ Myr$)	Duration of activity "burst"	Total magma volume	Gt CO_2 (0.5wt%)	Gt CO_2 (0.2wt%)	Maximum Gt yr^{-1} (0.5%)	Maximum Gt yr^{-1} (0.2%)
2000	20	102400	1408	563	0.070	0.028
2000	10	51200	704	282	0.070	0.028
2000	5	25600	352	141	0.070	0.028
3000	20	153600	2112	845	0.106	0.042
3000	10	76800	1056	422	0.106	0.042
3000	5	38400	528	211	0.106	0.042
6000	20	307200	4224	1690	0.211	0.084
6000	10	153600	2112	845	0.211	0.084
6000	5	76800	1056	422	0.211	0.084

***Table 2**. Estimates of Barium accumulation rate changes across the onset of the PETM. Sites and abbreviations. ACEX[1]: Arctic Coring Expedition (1: note that concentrations are XRF counts), WSS: West Siberian Sea Well 10, WL: Wilson Lake, Egypt*: Dababiya Quarry, Egypt**: Gabal el Qreiya, New Zealand: Tawanui, Nigeria: Dahomey Basin. Data from deep sites directly from Ma et al. (2014) , Ba/Al correction from Reitz et al. (2004) . Changes (Ba accumulation, Sedimentation rates) are factors relative to Paleocene. If sedimentation rate changes are unknown, a factor of 1 is applied. Numbers in parentheses are best estimates; in most cases not all data is available (n/a).*

Site	Number on map	Type	Detrital Ba/Al used	Measured Paleocene Ba (ppm)	Measured PETM Ba (ppm)	Babio Paleocene (%)	Babio PETM (%)	Sedimentation rate change	Ba accumulation change
ACEX[1]	1	shelf	n/a	900	3843			?	>4.3
WSS	2	shelf	0.0037	202	1550	75	90	0.17	1.0
WL	4	shelf	0.0037	159	254	12.5	0	4	0
Egypt*	7	shelf	n/a	256	456		-	?	(1.8)
Egypt**	7	shelf	0.0037	106	542	0	62	?	(5.1)
New Zealand	17	shelf	0.0067	1806	1661	90	86	?	0.9
Nigeria	8	shelf	0.0045	107	114	0	0	2.3	(2.3)
ODP959	9	slope	0.0045	3557	4580	95	95	1	1.3
ODP549	3	deep							5.3
ODP690	15	deep							1.9
ODP1051	6	deep							4.9
IODP1215	10	deep							1.4
IODP1220	11	deep							13
IODP1221	12	deep							0.3
IODP1263	13	deep							4.5
IODP1265	14	deep							1
IODP1266	15	deep							0.3

***Table 3**. GDGT measurements. Raw TEX_{86} values, BIT and TEX_{86}^{H} derived temperatures. Samples with insufficient GDGTs indicated in grey.*

Depth (mbsf)	TEX_{86}	TEX_{86}^{H} Temperature	BIT Average	Depth (mbsf)	TEX_{86}	TEX_{86}^{H} Temperature	BIT Average
800.65	0.871	34.48	0.032	804.15			0.013
800.77	0.850	33.75	0.000	804.18	0.884	34.94	0.000
800.94	0.849	33.85	0.038	804.2	0.858	34.05	0.011
800.96				804.22			0.021
801.12				804.23	0.864	34.26	0.013
801.19	0.873	34.56	0.022	804.26			0.021
801.39	0.884	34.93	0.010	804.32			
801.56	0.888	35.06	0.011	804.325			0.080
802.67	0.878	34.74	0.031	804.33			
802.8	0.909	35.75	0.016	804.37			
802.86	0.904	35.59	0.007	804.375			0.100
802.94	0.907	35.70	0.014	804.38			0.087
803	0.925	36.27	0.006	804.4			
803.07	0.959	37.37	0.002	804.41	0.856	33.97	0.087
803.18	0.960	37.39	0.001	804.42			0.059
803.29	0.960	37.37	0.002	804.47	0.857	34.00	0.036
803.36	0.954	37.21	0.001	804.48	0.858	34.06	0.030
803.42	0.958	37.33	0.001	804.52	0.836	33.27	0.020
803.47	0.957	37.30	0.005	804.55	0.847	33.65	0.022
803.53	0.961	37.43	0.002	804.61	0.837	33.31	0.009
803.58	0.958	37.33	0.005	804.7			0.156
803.75	0.962	37.46	0.003	804.73			0.029
803.76	0.963	37.49	0.002	804.76			0.047
803.78	0.967	37.61	0.001	804.89	0.826	32.93	0.016
803.79	0.965	37.55	0.001	805.04	0.835	33.26	0.000
803.88	0.958	37.34	0.001	805.13	0.845	33.61	0.009
803.97	0.961	37.39	0.012	805.22	0.833	33.17	0.014
804	0.964	37.52	0.005	805.41	0.831	33.11	0.016
804.07	0.965	37.53	0.006	805.58	0.825	32.87	0.016
804.13	0.873	34.55	0.015				

Table 4. *Ba concentrations across the PETM at the Dahomey Basin, Nigeria. PETM interval marked in grey.*

Depths	Ba PPM	Depths	Ba PPM
51.5	189	89.4	211
53.5	164	90	173
54.8	177	93	104
56	129	94.5	108
57	184	95.4	104
58.5	209	96	101
60	203	97	92
63	190	99	95
64	185	101	79
64.9	182	102	71
66	143	105	89
69	15	107	92
70	181	108	109
71.5	103	109	110
72	102	111	112
75	102	113.8	110
76.5	99	119	127
77	115	120	138
78	111	123	122
79	114	125	113
81	89	126	127
83.1	95	129	115
84	93	131	109
87	125	132	122
88	80	134	114

5

Tropical Atlantic Climate and Ecosystem Regime Shifts during the Paleocene-Eocene Thermal Maximum

Abstract

The Paleocene – Eocene Thermal Maximum (PETM; 55.5 Ma) was a phase of rapid global warming associated with massive carbon input into the ocean-atmosphere system from a ^{13}C-depleted reservoir. Many mid and high-latitude sections have been studied and document changes in salinity, hydrology, sedimentation, deoxygenation, biotic overturning and migrations, but detailed records from tropical regions are lacking. Here, we study the PETM at Ocean Drilling Program (ODP) Site 959D in the Eastern Tropical Atlantic using a range of organic and inorganic proxies and couple these with dinoflagellate cyst (dinocyst) assemblage analysis. The PETM at Site 959D was previously found to be marked by a ~3.8‰ negative carbon isotope excursion (CIE), and a 3.9 ºC surface ocean warming from the uppermost Paleocene to peak PETM, of which ~1 ºC occurs before the onset of the CIE. We record upper Paleocene dinocyst assemblages that are similar to PETM assemblages as found in extra-tropical regions, confirming poleward migrations of ecosystems during the PETM. The early stages of the PETM are marked by a typical acme of the tropical genus *Apectodinium*, which reaches abundances of up to 95%. Subsequently, dinocyst abundances diminish greatly, as do carbonate and pyritized silicate microfossils. The combined paleoenvironmental information from Site 959D and a close by shelf site in Nigeria leaves heat stress during peak PETM warmth to be the most likely cause for the general absence of eukaryotic surface-dwelling microplankton. Crucially, abundant organic benthic foraminiferal linings imply sustained export production, likely driven by prokaryotes. In sharp contrast, the recovery of the CIE yields rapid (<<10 kyr) fluctuations in the abundance of several dinocyst groups, suggesting extreme ecosystem and environmental variability.

Introduction

Long-term gradual warming during the late Paleocene and early Eocene (~59-53 Ma) is recorded in the deep ocean (Littler et al., 2014; Zachos et al., 2008), as well as mid and high latitude surface oceans (Bijl et al., 2009; Frieling et al., 2014; Hollis et al., 2012). Superimposed, the Paleocene-Eocene Thermal Maximum (PETM) represents a transient period of rapid global warming, associated with the massive input of strongly ^{13}C-depleted carbon into the ocean-atmosphere system (Dickens et al., 1995; Zeebe et al., 2009). This results in a ~2.5-8 ‰ negative carbon isotope excursion (CIE) in carbon-bearing substrates deposited during the PETM (McInerney and Wing, 2011; Sluijs and Dickens, 2012). The CIE has a distinct shape; a rapid "onset" (several millennia; (Zeebe et al., 2014) followed by a prolonged (50-70 kyr) period, the "body", of stable low ^{13}C values and a recovery that lasts 42 - 100 kyr (Abdul Aziz et al., 2008; Murphy et al., 2010; Röhl et al., 2007) to values that remain slightly ^{13}C-depleted (0.5-1 ‰) relative to the latest Paleocene. This pattern is best explained by massive (>>1500 Gt) carbon input from at least 1 but likely multiple reservoirs in the shape of CO_2 and/or CH_4; (Frieling et al., chapter 6, chapter 4; Panchuk et al., 2008; Zeebe, 2013; Zeebe et al., 2009).

The integrated changes in climate and the carbon cycle lead to global average surface warming during the PETM in the order of ~4-5 ºC (Dunkley Jones et al., 2013; Frieling et al., chapter 3), although this warming was not equally distributed across the globe. Regions of enhanced warming are recognized in both the Northern mid and Southern mid and high latitudes, which shows the mechanism underlying extratropical amplification was not fully saturated even in these strong greenhouse climates (Frieling et al., chapter 3). The warming during the PETM is associated with sea level rise (Sluijs et al., 2008a), local photic zone euxinia (Frieling et al., 2014, chapter 3; Sluijs et al., 2014, 2006), global expansion of anoxic waters (Dickson et al., 2012) and an accelerated hydrological cycle (Handley et al., 2012; Pagani et al., 2006b; Schmitz and Pujalte, 2007; Sluijs and Brinkhuis, 2009).

The magnitude of warming during the PETM and environmental and ecological effects have been extensively documented at mid and high-latitude sections (see review in Sluijs et al., 2014). Although micropaleontological studies indicate assemblage shifts and environmental perturbation in several tropical open ocean regions (e.g., Site 865; Kelly et al., 1996, Site 1001; Bralower et al., 1997) the underlying mechanisms remain unclear because causal relations with physicochemical parameters are difficult to establish. Evidence from Tanzania, Nigeria and ODP Site 865 indicates that tropical surface oceans warmed by ~3 °C (Frieling et al., chapter 3). In the modern ocean, a relatively modest (0.5-1 °C) warming already negatively affects biodiversity in tropical regions (Pandolfi et al., 2011). In the Anthropocene migrations to higher latitudes are noted in a multitude of biota (Doney et al., 2012), similar to the PETM (Crouch et al., 2001; Kelly et al., 1996; Sluijs et al., 2007a; Wing et al., 2005), notably in the (sub)tropical dinocyst *Apectodinium*.

Recently, a massive decrease in biodiversity of dinocysts was found during the PETM in Nigeria, which was attributed to heat stress (Frieling et al., chapter 3). The impact and geographical extent of this heat-stress driven biodiversity drop however remain unknown, although a similar heat-stress effects have been suggested for marine biota in tropical sites elsewhere (Aze et al., 2014; Yamaguchi and Norris, 2015). Although other stressors like stratification, salinity fluctuations and acidification may play a role, it should be noted that dinoflagellates typically thrive under such conditions, including very high CO_2 (Hoins et al., 2015). Here, we analyze the PETM from Ocean Drilling Program (ODP) Site 959D in the tropical Atlantic (Figure 1) as recently described using carbon isotope stratigraphy, biostratigraphy and TEX_{86} paleothermometry (Frieling et al., chapter 4). Site 959D is located near the top of the Cote d'Ivoire – Ghana Transform Margin (CIGTM) a submarine high ~150 km offshore Ivory Coast (Shipboard Scientific Party, 1996). Upper Paleocene and lower Eocene sediments were deposited at a paleolatitude of 3 - 7° S (Seton et al., 2012; van Hinsbergen et al., 2015) and are typically composed of roughly equal amounts of carbonate, biogenic silicate and siliciclastics (Shipboard Scientific Party, 1996; Wagner, 2002) with some (0.1-1%) organic matter. We measure bulk magnetic susceptibility and apply inorganic proxies, including, X-ray fluorescence core scanning and bulk sediment chemistry and combine these with dinocyst assemblages and previously published TEX_{86}, Branched versus Isoprenoid Tetraether (BIT) index data (Frieling et al., chapter 4) to reconstruct environments across the PETM.

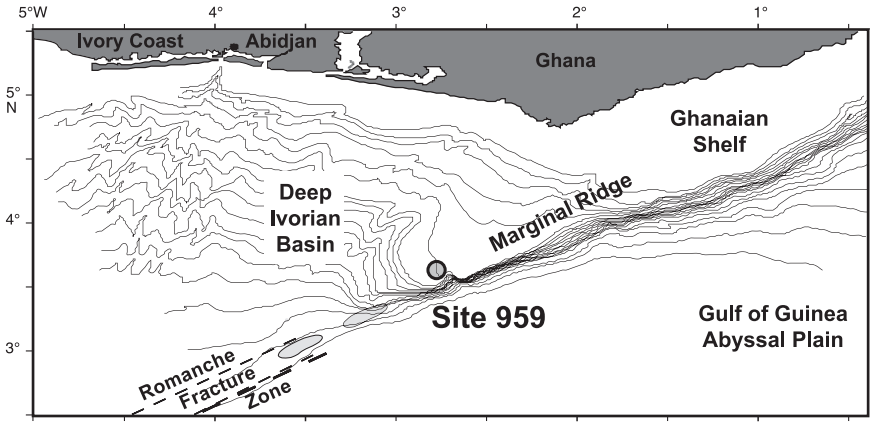

Figure 1. *Map of Eastern Tropical Atlantic and location of ODP Site 959D.*

Material

The Ocean Drilling Program recovered a relatively complete Cretaceous and Cenozoic sediment sequence from Hole 959D, located on the CIGTM, in 1995 (3°37.656'N, 2°44.149'W; Figure 1). From the Early Cretaceous onwards, the submarine high has been subsiding, reaching bathyal depths around the Cretaceous – Paleogene boundary (Oboh-Ikuenobe et al., 1997) and present day water depth is ~2000m. Nannoplankton biostratigraphy indicates the presence of the upper Paleocene CP8a-CP8b zone boundary in the interval from Core 41R-6 to Core 42R-2 mbs (Shafik et al., 1998). The PETM was identified in section 42R-1 and spans the interval 804.1 – 802.6 meters below sea floor (mbsf) based on the identification of the CIE and 4 °C warming (Frieling et al., chapter 4). Unfortunately, the top of the CIE lies within the ~1 m gap between cores 41R and 42R. Notable lithological changes occur in the interval from 804.1 mbsf to 803.9 mbsf, where siliciclastic sediments are replaced by diagenetically altered biogenic silicates (porcellanite) (Shipboard Scientific Party, 1996; Wagner, 2002). The sediments above core 41R-6 are recognized by more frequent occurrences of porcellanite (Shipboard Scientific Party, 1996; Wagner, 2002). Sediments below 42R-1 show apparently cyclic dark-light alterations, likely representing variable amounts of clay, carbonate and biogenic silica (Shipboard Scientific Party, 1996; Wagner, 2002).. The position of the site, near the top of a submarine high, implies that relatively little siliciclastic material reaches the core location. We continuously sampled core sections 41R-6, 41R-CC, 42R-1 and 42R-2 at the Bremen Core Repository of the International Ocean Discovery Program, representing the interval from 800.5 to 805.58 mbsf at a resolution of 1-3 cm (see Frieling et al., chapter 4).

The biogenic silica is likely derived from an allochtonous deposit (Frieling et al., chapter 4) and obscures the exact onset of the carbon isotope excursion (CIE). Carbon isotope stratigraphy of total organic carbon ($\delta^{13}C_{TOC}$) indicates the presence of a 2 ‰ negative step at the base of the porcellanite (804.1 mbsf) and stable low (~ -30 ‰) values from 803.8 to 803 mbsf show the presence of the body phase of the PETM (Frieling et al., chapter 4), Figure 2a). From 803 to 802.6 mbsf there is an increase to values ~1.5 ‰ lower than background Paleocene, which is interpreted as a mixing line between organic matter produced during the Paleocene and the PETM (Frieling et al., chapter 4). A core gap 801.6 - 802.6 mbsf conceals the end of the recovery phase. Core 41R-6 and 41R-CC are characterized by early Eocene values, about 0.7 ‰ lower than late Paleocene. The two distinct steps in the record may indicate small hiatuses; one at 804.1 mbsf and one at 803.0 mbsf (Figure 2). Paleocene accumulation rates are in the order of 1-1.5 cm kyr^{-1}, based on nannoplankton biostratigraphy (Shafik et al., 1998) and a basic cyclostratigraphic age model (Frieling et al., chapter 4).

Methods
Sample handling

All discrete samples taken from the working halves were freeze-dried and measured for bulk magnetic susceptibility before splitting them into fractions for palynology, inorganic and organic geochemical analysis.

Bulk Magnetic susceptibility

Freeze-dried samples were weighed and measured for bulk magnetic susceptibility on an MFK1-FA at the Paleomagnetism laboratory, Fort Hoofddijk, Utrecht University. Reproducibility was determined by replicate measurements and was always better than 1%.

Palynology

We processed and counted a total of 155 samples, using standard protocols used at the Laboratory of Palaeobotany and Palynology at Utrecht University (Sluijs et al., 2003). In brief, a spike of exote *Lycopodium clavatum* spores (n = 20848 ± 691) was added to 1-10 g of freeze-dried sample to allow for absolute quantitative analysis (Stockmarr, 1971). To dissolve carbonates, sediments were first treated with 10% HCl, after which supernatants were decanted. This was followed up by two steps of 38-40% HF and 30% HCl to dissolve silicates. Samples were centrifuged and neutralized with tap water before sieving over 250 and 15 µm sieves to remove large and small particles, respectively. Subsequently, residues were concentrated in glycerine water and mounted on microscope slides using glycerine jelly. We followed dinocyst taxonomy of Fensome, (2004) and the paleoecological grouping of (Sluijs and Brinkhuis, 2009). Unlike Sluijs and Brinkhuis, (2009), we separate Protoperidinioid dinocysts from the other Peridinioid types with hexagonal 2a archeopyles. Where possible, a minimum of 200 dinocysts was counted. For samples with very low numbers of dinocysts, slides were fully counted to a total of ~10-100 dinocysts. We qualitatively estimated the abundance of pyritized remains of biogenic silica relative to organic particles in each sample. A full list of encountered taxa is given in Table 1. All materials are stored in the collection of the Laboratory of Palaeobotany and Palynology, Utrecht University.

XRF Core Scanning

XRF Core Scanner data were collected every 1 cm down-core over a 1 cm^2 area with slit size of 10 mm using generator settings of 10 kV and 50 kV, a current of 0.2 mA and 1.0 mA respectively, and a sampling time of 30 seconds directly at the split core surface of the archive halves of Cores 41R-6, 42R-2 and lower part of 42R-1with XRF Core Scanner III at the MARUM - University of Bremen. The split core surface was covered with a 4 m thin SPEXCerti Prep Ultralene foil to avoid contamination of the XRF measurement unit and desiccation of the sediment. The dark-colored interval from 803.8 mbsf to 803 mbsf and directly overlying sediment in Core section 42R-1 was too fragmented for acquiring reliable core scanning measurements. The here reported data have been acquired by a Canberra X-PIPS Detector (X-PIPS SXP5C-200-1500 from Canberra) with 150eV X-ray resolution, the Canberra Digital Spectrum Analyzer DAS 1000 and an Oxford Instruments 100W Neptune X-ray tube with rhodium (Rh) target material. Raw data spectra were processed by the Analysis of X-ray spectra by Iterative Least square software (WIN AXIL) package from Canberra Eurisys.

Bulk sediment chemistry from Inductively Coupled Plasma - Optimal Emission Spectroscopy (ICP-OES)

Bulk sediment chemistry was determined on 50 samples in the interval that could not be used for XRF core scanning and 22 samples from intervals with XRF scanning data to assess consistency between the two methods. Approximately 125 mg of powdered freeze-dried sediment was dissolved in 2.5 ml HF (40 %) and 2.5 ml of $HClO_4/HNO_3$ mixture, in a closed Teflon bomb at 90 °C during one night. The acids were then evaporated at 160 °C and the resulting gel was subsequently redissolved in 1M HNO_3 at 90 °C during another night. Subsequently, total elemental concentrations were determined by ICP-OES (Perkin Elmer Optima 3000 Inductively Coupled Plasma - Optimal Emission Spectroscopy) at Utrecht University. Precision and accuracy was better than 5 %, based on calibration to standard solutions and checked against internal laboratory standard sediments. All elemental ratios are normalized to Al, except for organic carbon over total phosphorus (Corg/Ptot), which is reported in mol mol^{-1}.

Carbonate percentage measurements

The carbonate concentration of Site 959D samples was determined at the University of Southampton using a UIC CM5015 coulometer operated with a UIC CM5011 emulator and coupled to an AutoMateFX autosampler and carbonate digestion system. The samples were oven-dried at 50°C, crushed with an agate mortar and pestle, placed in a glass vial, and oven dried again after crushing. Each vial was capped immediately after removal from the oven to prevent the samples from taking on moisture. Depending on estimated carbonate content, 10–40µg of bulk dry sample was weighed out on a Sartorius ME5 microbalance and placed in a septum-capped autosampler vial prior to each run. A total of 59 samples were analysed across six runs on separate days, with repeat analyses performed on ~25% of the samples. Each run was calibrated using blank-corrected counts for a calcium carbonate standard (Acros Organics, 99.999% pure) spanning a mass range of 2–10µg. External precision is estimated at ±0.6% $CaCO_3$ based on results from a consistency standard that was included in all runs (average = 73.1%; n = 12). The detection limit was determined from a compilation of blank analyses from all runs (n = 24), and using the average blank counts plus 3×s.d., the detection limit for a typical 15mg sample was calculated to be 0.08% $CaCO_3$.

Results
Palynology

Dinocysts typically dominate the palynological residues. Pollen and spores derived from terrestrial higher plants are present but in very low abundances (average ~1%; 40 g^{-1}). The body of the PETM CIE and the corresponding interval with higher TOC is marked by high abundances of organic linings of benthic foraminifera. Upper Paleocene dinocyst assemblages are composed of three major components (Figure 2c). The most abundant component is the generalist group *Spiniferites*, followed by *Apectodinium* and Goniodomideae with an epicystal archeopyle (hereafter referred to as Goniodomideae; see Sluijs and Brinkhuis, (2009), for taxonomic descriptions of the groups and complexes). Within the uppermost Paleocene, representatives of the *Areoligera* cpx increase in abundance. The onset of the PETM is marked by an acme of *Apectodinium*, reaching highest abundances (>90%) between 803.89 and 803.77 mbsf. The body of the PETM CIE yields extremely low abundances of dinocysts (100-200 $gram^{-1}$) so that percentages are based on counts below 200 specimens and should hence be interpreted as rough estimates (open circles in Figure 2). Regardless, assemblages within the body of the CIE are mostly composed of Goniodomideae, *Spiniferites* and *Apectodinium*. *Senegalinium* and Protoperidinioid cysts occur almost exclusively during the body of the CIE. High cyst concentrations (>10^4 $gram^{-1}$) and a series of ~10 subsequent acmes of different dinocyst groups mark the recovery of the CIE (Figure 2c). Towards the top of the analyzed interval, *Florentinia reichartii* becomes the dominant species. Several groups show abundance peaks in the interval following the recovery of the CIE.

Carbonate weight%

Apart from sediments close to the PETM, the studied interval typically comprises 10-30 weight % $CaCO_3$ (Fig. 3). However, $CaCO_3$ is below the detection limit in an interval starting just below the CIE, at 804.2 mbsf. Various methods, i.e. weight loss during decalcification, ICP-OES analysis of Ca concentrations and dedicated $CaCO_3$ measurements show similar trends (Figure 3f). We use the weight loss during HCl-treatment as a high-resolution approximation for $CaCO_3$ outside the PETM. Especially across the PETM the weight loss during decalcification is strongly influenced by dissolution of HCl-soluble salts and minerals, especially gypsum, which accounts for 5-10% of sediment weight in some parts

of the CIE.

Bulk sediment chemistry (XRF and ICP-OES)

We use elemental ratios to reconstruct hinterland hydrology and redox sensitive trace elements to reconstruct bottom water oxygenation for the core location. The Ti/Al ratios from XRF core scanning and ICP-OES analysis show identical trends, with a gradual rise in the upper Paleocene and rapid second increase at the base of the porcellanite that marks the onset of the CIE (804.1 - 803.8 mbsf, Figure 3g). Hereafter, values drop and remain consistently lower than in the upper Paleocene within the body and recovery phases of the CIE. K/Al ratios correlate well with TOCwt%. Concentrations are slightly higher within the CIE than in the upper Paleocene and interrupted by a sharp drop in the porcellanite layer. The CIE is also marked by elevated concentrations of Cr, S, Ni, V, Zn and progressively higher Corg / Ptot ratios (Cu/Al, Cr/Al, V/Al and Corg/Ptot; Figure 3i).

Magnetic susceptibility

Magnetic susceptibility is anti-correlated with carbonate percentages in the upper Paleocene. At 804.2 mbsf, before the onset of the CIE, this relation disappears. The porcellanite layer is marked by low magnetic susceptibility and the body of the CIE is marked by stable high values. A maximum is reached during the recovery phase, at 802.97 mbsf, followed by a second maximum at 802.81 mbsf. Bulk magnetic susceptibility measurements closely resemble Fe concentrations derived from both ICP-OES and XRF (Figure 3j) and correlates to %TOC in the upper Paleocene and lower part of the CIE.

Discussion
Background cyclic variability

The latest Paleocene at the core location is characterized by cyclic variations in proxy records, including total organic carbon content (TOC), dinocysts per gram of sediment, magnetic susceptibility and $CaCO_3$ content (Figure 3). (Frieling et al., chapter 4), attributed the cycles to climatic precession (21 kyrs). Implied late Paleocene average accumulation rates are 1-1.5 cm kyr^{-1}, which is consistent with the limited available nannofossil biostratigraphy. During the PETM we find 2 potential additional precession cycles recorded in K/Al ratios (Figure 3g), which may imply a two-fold accumulation rate increase. Notably, however, cyclic variability is apparently absent in dinocyst assemblages, $\delta^{13}C_{TOC}$, TEX_{86}^{H} derived temperatures and Ti/Al ratios. This observation is important since we can, although with caution, use these as indicators of environmental change that is not associated with background cyclic variability.

Depositional setting, sea level, bottom water oxygen levels
Late Paleocene Background State

Dinocyst assemblages in the Paleocene are characterized by abundant *Spiniferites spp*. and *Apectodinium spp.* Absolute numbers of dinocysts correlate well with TOCwt%, but also with K/Al ratio. In tropical regions, K/Al ratios vary with wet-dry cycles due to variations in provenance, which suggests precession forcing may be an important driver of productivity in the study region. We also find that some of the cycles show a "notch" at the peak, which, given the paleolatitude (3 – 7 °S), may be interpreted to result from the double overpass of the intertropical convergence zone (ICTZ) (Verschuren et al., 2009).

Occasionally, Goniodomideae are present in great abundance. In the modern ocean (Zonneveld et al., 2013) and in the Paleogene (Sluijs and Brinkhuis, 2009), high abundances of Goniodomideae are typically associated with warm, stratified waters and very high and/

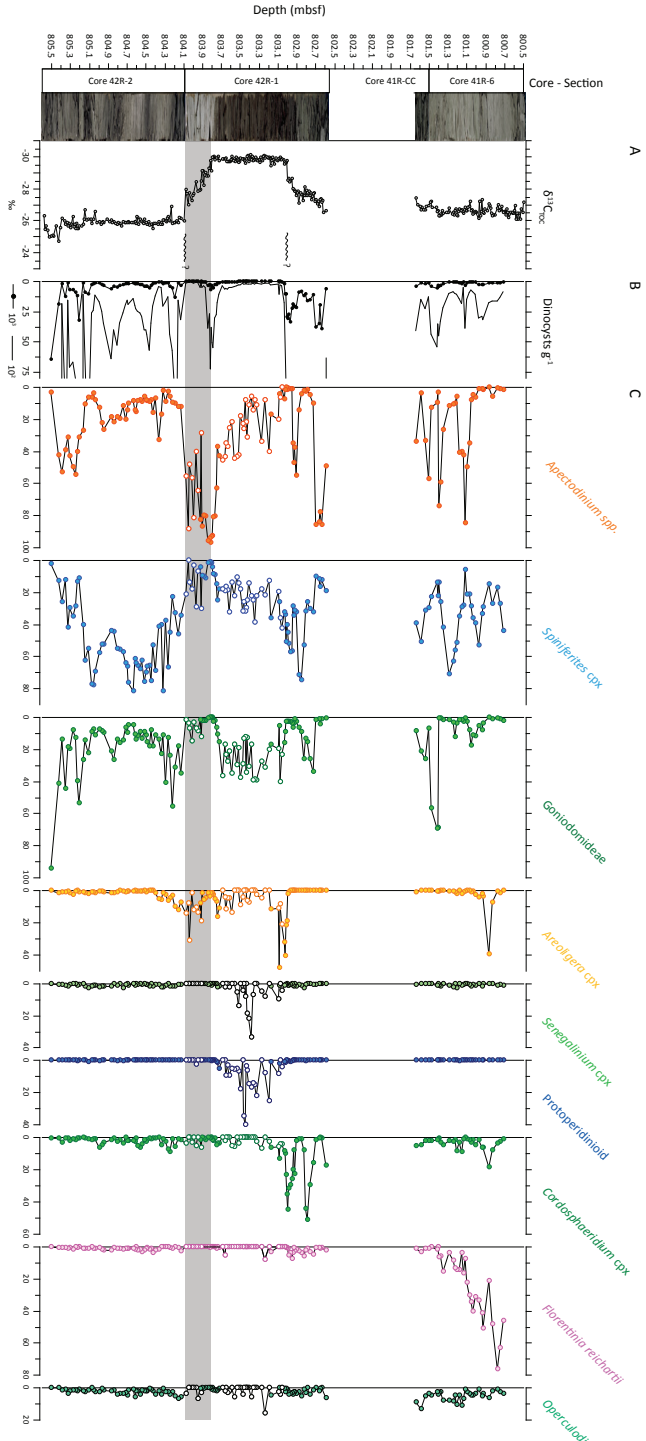

Figure 2. *The PETM as recorded by dinoflagellate cysts at Site 959D.* ***A.*** $\delta^{13}C_{TOC}$ *in permil.* ***B.*** *Concentration of dinocysts per gram dry sediment.* ***C.*** *Dinocyst groups in percentage of total dinocysts. The grey band marks the porcellanite. Symbols in white indicate counts <100.*

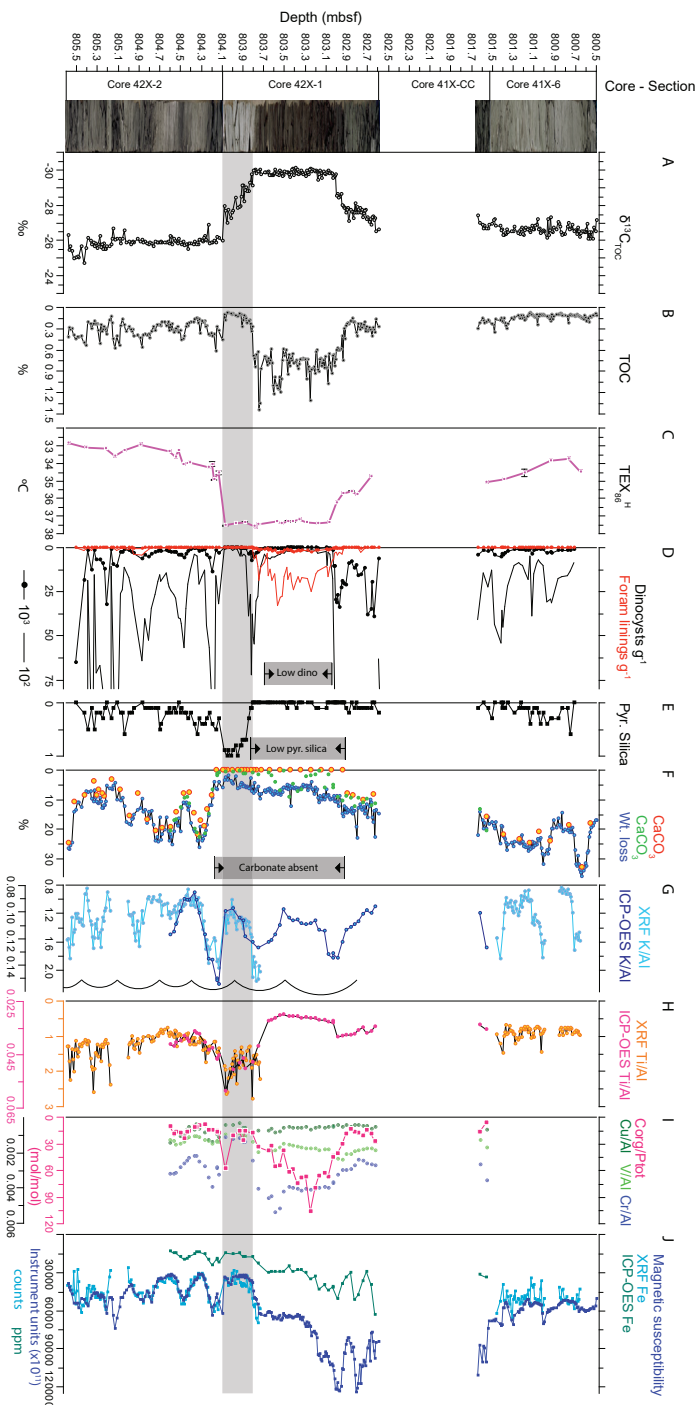

Figure 3. *The PETM as recorded by multiproxy at Site 959D.* ***A.*** *$\delta^{13}C_{TOC}$ in permil.* ***B.*** *Total organic carbon (TOC) in weight percentages.* ***C.*** *TEX_{86}^{H} derived temperature.* ***D.*** *Dinoflagellate cyst and organic linings of benthic foraminifera in n g^{-1} of dry sediment.* ***E.*** *Fraction of pyritized silica particles in palynological residue.* ***F.*** *Weight loss during decalcification (Wt. loss) as indication of $CaCO_3$ content; $CaCO_3$ calculated from Ca concentration ICP-OES (green) and selected samples analyzed for $CaCO_3$ on a coulometer (orange).* ***G.*** *K/Al ratio from XRF (light blue) and ICP (dark blue).* ***H.*** *Ti/Al ratio from XRF (orange) and ICPOES (pink).* ***I.*** *Cu/Al (dark green), Cr/Al (blue) and V/Al (light green) and Corg/Ptot ratio (pink) in mol mol^{-1}.* ***J.*** *Magnetic susceptibility in instrument units (x1011) (dark blue), XRF Fe counts (light blue) and ICP-OES Fe concentrations in ppm (green). The grey band (804.1 – 803. 83 mbsf) marks the porcellanite. $\delta^{13}C_{TOC}$, TOC and TEX_{86}^{H} data from Frieling et al., in prep. Chapter 4.*

or seasonally fluctuating salinity. In open ocean settings the group can be indicative of strong stratification (Reichart et al., 2004). Considering the offshore location of Site 959, and relatively low abundances of low-salinity-tolerant taxa, we interpret high abundances of Goniodomideae to indicate seasonally strong stratification, either by temperature or salinity.

From 804.4 mbsf, we find an increase in abundance of dinocysts belonging to, or closely related to the genus *Areoligera* (*Areoligera* complex *sensu* Sluijs and Brinkhuis, 2009). A relative abundance increase of this genus was previously interpreted to reflect sea level rise at several shelf and slope sites during the PETM (Sluijs et al., 2008a). However, Site 959 is located in an open ocean setting, which means water depth and shore proximity proportionally do not change as much as may be expected from sites on the continental shelf, especially if estimates of the amplitude of sea level rise across the onset of the PETM (5-20m, e.g., (Sluijs et al., 2008a; Speijer and Morsi, 2002) are considered. The increase in *Areoligera* is further associated with a decrease in *Spiniferites*, consistent with other PETM records (e.g., Sluijs et al., 2008), including a recent record from Nigeria (Frieling et al., chapter 3). Since we cannot distinguish between transported and local signals, we may either record a signal that is transported off the shelf, or a local signal that is similar to, but not related to sea level change.

The onset of the PETM and the *Apectodinium* acme

The quasi-global acme of the tropical dinocyst genus *Apectodinium* has long been used as a Paleocene-Eocene boundary marker in biostratigraphic studies (Bujak and Mudge, 1994; Heilmann-Clausen, 1985) and later discovered to be connected to the PETM (Bujak and Brinkhuis, 1998; Crouch et al., 2001). However, some sections show relatively low percentages of *Apectodinium* during the PETM (Frieling et al., 2014; Sluijs et al., 2006).

In addition to the acme of *Apectodinium*, through entire North Atlantic, Arctic and Northern Tethys, the marker species *Apectodinium augustum* is present during the PETM (Harding et al., 2011; Heilmann-Clausen, 1985; Iakovleva et al., 2001; Sluijs and Brinkhuis, 2009; Sluijs et al., 2006) although other species are often the dominant representatives of the genus. Recent taxonomic revision of several taxa has removed *Apectodinium augustum* from *Apectodinium* and moved it to *Axiodinium* (Williams et al., 2015). This would imply that there is an acme of *Apectodinium* outside the North Atlantic and an acme of *Axiodinium* only in some places in the North Atlantic. We consider all these dinocysts to be similar in nature and origin and for practical purposes we hence continue to refer to this as "*Apectodinium*" acme. *A. augustum* was not recorded here.

The abundance of *Apectodinium* appears to be largely controlled by temperature in higher latitude regions across the PETM (Crouch et al., 2001; Frieling et al., 2014; Sluijs et al., 2006), but it was abundant to dominant in tropical and sub-tropical material already in the late Paleocene (Crouch et al., 2003; Du Chêne and Adediran, 1984; Frieling et al., chapter 3; Sluijs et al., 2014) (Figure 2). Furthermore, the required minimum temperature of ~20 °C (Frieling et al., 2014) was widespread in many mid latitude sections well before the PETM (Dunkley Jones et al., 2013; Frieling et al., chapter 3), signaling other environmental factors were more important in controlling the distribution of *Apectodinium* at low and mid latitudes (Sluijs and Brinkhuis, 2009; Sluijs et al., 2007b).

At Site 959D, *Apectodinium* is abundantly present in the Paleocene, which is not surprising given the tropical location. This is similar to the Paleocene in Nigeria (Du Chêne and Adediran, 1984; Frieling et al., chapter 3), Cameroon (Mbesse, 2013) and Tunisia (Crouch et al., 2003a), indicating *Apectodinium* was already common along African margins before

the PETM. More surprising is perhaps the general lack of an *Apectodinium* acme at these low latitude sites during the PETM, although some caution must be placed due to poor preservation at the Tunisian site (Crouch et al., 2003a) and the low sampling resolution of the section in Nigeria (Frieling et al., chapter 3).

At Site 959D, we find the highest abundance (95%) of *Apectodinium*, close to the onset of the body of the PETM (803.89 mbsf). This is perhaps later than at many mid and high latitude sites where the highest abundance of *Apectodinium* often slightly precedes the CIE (Kender et al., 2012; Sluijs et al., 2011, 2007b). However, like many of these sites the assemblages recorded here are nearly monospecific. We thus infer this high abundance of *Apectodinium* is the tropical equivalent of an *Apectodinium* acme. The high percentages of *Apectodinium* in the porcellanite (804.1 - 803.9mbsf) are most likely mixed in from above (803.85 - 803.75 mbsf) (see Frieling et al., chapter 4), since assemblages and species are very similar.

Microfossil decline and deoxygenation during peak PETM

The dinocyst assemblages, but also other microfossil groups, in mid-latitudes have been successfully used for detailed environmental reconstructions (e.g., Gibbs et al., 2006; Hollis, 2007; Sluijs and Brinkhuis, 2009; Stassen et al., 2012). Here, extremely low numbers of dinocysts (100-200 g^{-1}, relative to late Paleocene average of >5000 g^{-1}), carbonate and siliceous microfossils during the body of the CIE, which, since accumulation rates increase by at most a factor 2 (Fig. 3g), is appreciably beyond the effect of sediment dilution. This hampers detailed a paleoenvironmental reconstruction.

A few dinocyst genera however are present. The CIE is notably marked by higher relative abundances of Protoperidinioid cysts, as well as *Senegalinium* and related genera. Importantly, these are the only groups that increase in abundance with respect to the late Paleocene. Protoperidinioid dinocysts are produced by heterotrophic dinoflagellates in the modern ocean (Jacobson and Anderson, 1986) and most likely also in the Paleogene. Also *Senegalinium* cysts were likely produced by heterotrophic dinoflagellates (Sluijs et al., 2007b, 2005), which implies that a larger proportion of the dinoflagellate production was heterotrophic. This suggests that autrotrophic dinoflagellate species were stressed, but that a food source, locally produced or imported from elsewhere, was abundantly present. Notably, based on empirical information, the species in these groups were tolerant to relatively low salinity (Barke et al., 2011; Sluijs and Brinkhuis, 2009; Sluijs et al., 2006). Although lower Ti/Al ratios suggest that hinterlands were been more humid during the body of the CIE (Fig. 3), a large drop in salinity ~150 km offshore seems unlikely. Low-salinity tolerant dinocysts species, i.e. *Senegalinium* cpx, are abundant in many high latitude sections during the PETM (Harding et al., 2011; Sluijs et al., 2006), but the high relative abundance of Protoperidinioid cysts is only found in two sites in the eastern tropical Atlantic (Frieling et al., chapter 3). This is surprising given the high abundances of Protoperidinioid cysts in sediments deposited in nutrient-rich sectors of the modern ocean. Although other groups are consistently present within the peak of the CIE, absolute numbers are much lower than in the late Paleocene and we cannot exclude that these specimens are reworked.

Many sites globally show decreased bottom-water oxygen content during the PETM and at some shelf sections the photic zone became euxinic (Frieling et al., 2014, chapter 3; Schoon et al., 2015; Sluijs et al., 2014, 2006). Deep ocean waters were affected by deoxygenation but anoxia did not develop in the deep sea (Pälike et al., 2014). At Site 959, we find strong indications of decreased oxygen concentrations in bottom waters in the form of increased organic matter burial fluxes, as assessed through reconstructed accumulation rates and TOCwt%. Moreover, increasing Corg/Ptot ratios (Fig. 3i) relate to preferential regeneration

of phosphorus from sediments under anoxic conditions (Algeo and Ingall, 2007; Slomp et al., 2002). The PETM interval is also associated with slightly elevated concentrations of redox sensitive elements (e.g., Cr) (Figure 3i). In apparent contrast is an increase in the abundance of organic linings of benthic foraminifera. Some benthic foraminifera however can tolerate low oxygen concentrations for substantial periods (Langlet et al., 2014) and may outcompete other metazoans at such oxygen concentrations (Woulds et al., 2007). This signal is surprisingly similar to that found in shelf sections of the Gulf of Mexico (Sluijs et al., 2014) and Nigeria (Frieling et al., chapter 3). The combined information from Site 959 and Nigeria suggests that oxygen minimum zones during the PETM expanded upwards onto the shelf and downwards to the paleodepth of Site 959 (~1000 m) in the eastern tropical Atlantic, a phenomenon very similar to modern trends (e.g., Stramma et al., 2008).

Recovery after the PETM

At 803.0 mbsf, a small (~1‰) positive step in $\delta^{13}C$ possibly indicates a period of non-deposition, which is followed by the start of the recovery of the CIE. About 15 cm above the start of the CIE recovery, carbonate accumulation resumes. Dinocyst diversity and abundance directly recover and exceed upper Paleocene levels at the start of the CIE recovery. Remarkably ~10 distinct acmes of different dinocyst groups occur within ~30 cm of sediment within the ~100 kyr recovery phase. These events are hence limited to a maximum duration of 10 kyr, but are likely much shorter since bioturbation smoothed the signal. Moreover, the recovery of the PETM at Site 959 is truncated by a core gap and perhaps preceded by a small hiatus, which leads to overestimates of accumulation rates in our approach. SST drops concomitantly with the increase in $\delta^{13}C$ (Fig. 3), but does not show a clear relation with any of the individual dinocyst groups. No such short-term extreme biotic variation is known for any PETM site across the globe, certainly not for the recovery interval, and indicates highly variable environmental conditions. We observe high transient abundances of cosmopolitan (*Cordosphaeridium*) and generalist genera (*Spiniferites*), species indicative of stratified waters (Goniodomideae), high-energy environments (*Areoligera* cpx) and *Apectodinium* (Figure 3). Although environmental preferences of many of these groups are known, it is difficult and perhaps pointless to disentangle the highly dynamic assemblages into individual environmental signals.

Only the variability of dinocyst assemblages during the 'body' of the CIE at the New Jersey Shelf sites Bass River and Wilson Lake resemble the results at Site 959 (Sluijs and Brinkhuis, 2009). However, Bass River and Wilson Lake are shallower and closer to the paleoshore and therefore more prone to local changes. The strong variation at Site 959, representing a fully open ocean setting is therefore much more surprising.

Potentially, the recorded variability at Site 959 is related to sub-Milankovitch climate variability, which has been observed in a range of tropical sections from the Proterozoic onwards (Wilson et al., 2014; Wu et al., 2012) and also within the PETM (Abdul Aziz et al., 2008) and in dinocyst records (Reichart and Brinkhuis, 2003). However, we observe no cyclic recurrence of these dinocyst assemblage variations, nor do we find the far more obvious cyclic (likely precession-scale) variation in the upper Paleocene in the dinocyst assemblages. Therefore this explanation appears unlikely. Unfortunately, none of our proxy records show similar variability in this period so we cannot resolve the underlying cause of such extreme variations in dinocyst assemblages.

Post PETM assemblages

Early Eocene dinocyst assemblages and thus presumably environmental circumstances are similar to those found in the Paleocene. Only *Florentinia reichartii* increases towards the top

of the analyzed interval. Although this species seems to be associated with somewhat higher temperatures and fresh-water input along the New Jersey shelf (Sluijs and Brinkhuis, 2009), and relates to occurrences of *Apectodinium* at southwest Pacific ODP Site 1172 (Sluijs et al., 2011), it here thrives under apparently relatively stable, open ocean conditions that prevail in the earliest Eocene. In addition to *F. reichartii*, *Apectodinium* is occasionally abundant, as are *Spiniferites* and Goniodomideae. Carbonate accumulation is similar or slightly higher than in the upper Paleocene (10-30%) and bottom waters appear to be well ventilated. Remarkably, the clear correlations between TOC and dinocyst numbers that exists in the upper Paleocene did not return, but dinocyst numbers and K/Al ratios continue to show cyclicity at similar intervals to that in the upper Paleocene, suggesting that hydrology of the hinterland remained an important factor governing plankton assemblages at Site 959 (see also section 5.2.1).

Absolute temperature and temperature change in a global perspective

The recorded warming across the onset of the PETM (3.9 °C) is similar to the global average (4-5 °C, e.g., (Dunkley Jones et al., 2013; Frieling et al., chapter 3). However, the few sampled tropical regions typically warmed slightly less (Kozdon et al., 2011; Tripati, 2003; Zachos et al., 2003) than global average due to persistent extratropical amplification of temperature change (Frieling et al., chapter 3). The isoprenoid glycerol dialkyl glycerol tetraether (iGDGT) distribution we find here is somewhat similar to modern Red Sea distributions and may therefore behave slightly different from the global calibration, with a different slope and offset (Trommer et al., 2009). The Red Sea calibration of Trommer et al., (2009) yields a warming of 3.4 °C, only slightly smaller than the 3.9 °C recorded by TEX_{86}^{H}, which uses a global calibration dataset (Kim et al., 2010). Furthermore, although iGDGT distributions may look similar, there is no reason to assume that Site 959 was subject to a similar setting or that Thaumarcheota communities were similar to those in the modern Red Sea. We note that Paleocene TEX_{86}^{H} reconstructed absolute temperatures are in the same range as were previously reported from this region (Frieling et al., chapter 3), which are supported by planktonic foraminifer $\delta^{18}O$ and Mg/Ca derived temperature estimates from the same section. Even though these temperatures are outside the calibration interval (5-30 °C) for TEX_{86}^{H}, the relation with temperature continues to at least 40 °C, based on mesocosm culture experiments (Schouten et al., 2007a; Wuchter et al., 2004). Importantly, the maximum temperature that can be reconstructed by TEX_{86}^{H} is 38.6 °C. The reconstructed temperatures are close to this maximum and we may actually approach the limit of the proxy and underestimate maximum PETM temperatures.

Suppression of eukaryote productivity in surface waters

Sediments typically contain less than 30% $CaCO_3$ in the latest Paleocene, but already from 804.2 mbsf, just below the onset of the CIE, $CaCO_3$ is completely absent (Figure 3f). We explore several factors that might explain this feature. First, it could be due to post-depositional carbonate dissolution through PETM ocean acidification as recorded in deep ocean basins (Zachos et al., 2005). However, at no single site described so far, the carbonate compensation depth (CCD) rose above the reconstructed paleodepth (~1000m, Oboh-Ikuenobe et al., 1997) for this site, so this scenario seems unlikely. Second, carbonates can be dissolved locally through enhanced oxic organic matter (OM) decomposition at the sea floor, producing CO_2. However, the dinocyst concentrations (~10^4 $gram^{-1}$) or TOC (~0.5%) content in this interval are not anomalous compared to the entire upper Paleocene, so this factor is unlikely the sole explanation. Finally, there may be a general suppression of carbonate (export-) production because of biotic stress, either through acidification or warming (Aze et al., 2014; Frieling et al., chapter 3). We surmise that low carbonate

production, possibly associated with the (pre-CIE) warming (Frieling et al., chapter 3) played a pronounced role in the absence of carbonate throughout the PETM.

After carbonate accumulation ceased, without apparent change in other proxies or large changes in sediment accumulation rates, dinocyst concentrations decrease from 5000 g^{-1} to 100-200 g^{-1} at 803.70 mbsf (Figure 3d). Organic linings of benthic foraminifera continue to increase in abundance indicating that export productivity did not collapse. This signal is identical to that found in a shelf section from Nigeria (Frieling et al., chapter 3); both sections show very low (100 - 200 g^{-1}) abundances of dinocysts during peak PETM warmth. We also note that pyritized biogenic silica, which is abundantly present in the upper Paleocene and early Eocene, is largely absent above the porcellanite and only reappears during the recovery (Figure 3e).

In addition to these overall similarities, the assemblages of dinocyst at Site 959D are very similar to those found at the PETM in Nigeria. Both sections are marked by relatively high percentages of Protoperidinioid dinocysts within the body of the PETM, which is an exclusively heterotrophic group (Jacobson and Anderson, 1986). Oxidation experiments show Protoperidinioid cysts are usually less resistant to oxidation than, e.g. *Spiniferites* cysts (Zonneveld et al., 2008, 1997a). However, the absence of a relation between the abundance of these taxa and TOC content suggests that preservation is not a major factor. We speculate that these species resided in slightly deeper waters, possibly near the thermocline.

The combined information suggests that eukaryote activity in the mixed layer was suppressed not only in Nigeria (Frieling et al., chapter 3) but also at the more offshore Site 959. Similar to Nigeria, there is hence no evidence that the low numbers of dinocysts resulted from severe stratification and anoxia, strong variations in salinity or biases resulting from preservation. Although the initial absence of carbonate is perhaps related to a secondary factor, we attribute the drop in eukaryote production in this region to heat stress, as this is among the few physicochemical factors that can generate the same effect in both the open ocean (Site 959) and on the shelf (Nigeria).

It should be emphasized that primary productivity did not collapse due to the lack of eukaryotes. Organic linings of benthic foraminifera are abundant within the PETM interval at Site 959 and in Nigeria, which suggests that food supply was likely of similar quality and quantity as before the PETM. Both sections are characterized by enhanced organic carbon content and burial. This apparently prokaryote dominated ecosystem, with enhanced organic carbon burial hence bears some similarities with tropical ecosystems during the Cretaceous Ocean Anoxic Events (OAEs) (Kuypers et al., 2001).

Conclusions

The Paleocene – Eocene transition at Site 959 is marked by a warming of 3.9 °C. Absolute TEX_{86}^{H} temperatures at 37.4 °C are unprecedented for the PETM, although similar to recent estimates from Nigeria and in good agreement with climate model estimates. Based on our multi-proxy records, we conclude that these extreme temperatures caused a remarkable drop in dinocyst abundances, and most likely also in the production of biogenic carbonate and opal during the PETM. Crucially, only heterotrophic dinoflagellate species, which likely resided somewhat deeper in the water column, increased in abundance. Together with relatively abundant organic benthic foraminifer linings this indicates sustained primary production, likely dominated by prokaryotes. Combined evidence from dinocysts and inorganic chemistry points to an altered hydrological cycle at the PETM, resulting in fluctuations in stratification. Furthermore, progressively less oxygenated bottom waters characterize the body phase of the PETM. In sharp contrast to the general absence of

eukaryotes during the body phase of the PETM, the recovery phase of the PETM is highly dynamic, with several groups of dinocysts dominating assemblages on timescales shorter than 10 kyr.

6

Thermogenic Methane as a cause for the long duration of the PETM

Abstract

The Paleocene-Eocene Thermal Maximum (PETM; ~56 Ma ago) was a ~170 kyr period of global warming associated with rapid and massive injections of ^{13}C-depleted carbon into the ocean and atmosphere, reflected in sedimentary components as a negative carbon isotope excursion (CIE). Carbon cycle modelling has indicated that the shape and magnitude of this CIE are best explained by an initial large pulse, followed by ~50 kyr of slow ^{13}C-depleted carbon release. Suggested sources include submarine methane hydrates, terrigenous organic matter, and thermogenic methane and CO_2 from hydrothermal vent complexes. Here, we test the contribution of carbon release associated with volcanic intrusions in the North Atlantic realm. We use dinoflagellate cyst and stable carbon isotope stratigraphy to date the active phase of a hydrothermal vent system and find it to post-date massive carbon release at the onset of the PETM. Crucially, however, it correlates to a period within the PETM associated with additional carbon injection. This finding represents the first actual proof of PETM carbon release from a particular reservoir. Based on carbon cycle box model (LOSCAR) experiments, we show that pulsed carbon input from several vent systems over a prolonged period suggested from the vent-literature (4-12 pulses within 60 kyr; total volume of 1,480 Pg) matches the CIE and deep ocean carbonate dissolution as recorded in sediment records. We therefore surmise that CH_4 and CO_2 from the Norwegian Sea vent complexes were the main source of carbon during the PETM, following its dramatic onset.

Introduction

The Paleocene – Eocene Thermal Maximum (55.93 Ma) was a period of rapid global warming (Dunkley Jones et al., 2013) associated with massive injections of ^{13}C-depleted carbon into the global exogenic carbon pool and extensive environmental upheaval, including ocean acidification (Zachos et al., 2005), global expansion of oxygen minimum zones, local photic zone euxinia, sea level rise (Sluijs et al., 2014), species migrations (Sluijs et al., 2007a), and an accelerated hydrological cycle (Schmitz and Pujalte, 2007). The carbon injection is recognised as a negative carbon isotope excursion (CIE) of 2.5-8‰ in sedimentary components (Dickens et al., 1995). The CIE associated with the PETM as recorded in sedimentary records has a rapid onset, likely in the order of millennia, followed by 80-100 kyr of stable values, referred to as the "body" of the PETM, and a recovery phase (50-100 kyr) to pre-event conditions (Abdul Aziz et al., 2008; Murphy et al., 2010; Röhl et al., 2007; Zeebe et al., 2014). This particular shape, which distinguishes it from other early Eocene transient carbon cycle perturbations (Stap et al., 2009), is best explained by rapid and massive additions of ^{13}C-depleted carbon at the onset (3000 Pg within millennia), slow continuous release (1480 Pg) across the body and subsequent sequestration (Zeebe, 2013; Zeebe et al., 2009). Several mechanisms have been proposed to explain the CIE, either in combination or alone, including the dissociation of gas hydrates (Dickens, 2011; Dickens et al., 1995) and organic matter oxidation (Kurtz et al., 2003), possibly from permafrost thawing (DeConto et al., 2012). However, it remains unclear if carbon was released from these proposed source reservoirs during the PETM and if any of the reservoirs may have acted as a positive feedback in the carbon cycle to cause the long duration of the PETM.

This puzzle is further complicated by potential carbon addition from the North Atlantic Igneous Province (NAIP), which was active during the late Paleocene and early Eocene (Storey et al., 2007) and may have been the main driver of long term warming (Zachos et al., 2008). A period of intense volcanism also occurred close to the PETM (Storey et al., 2007) and two pathways have been proposed to link this to ^{13}C-depleted carbon input.

Svensen et al., (2004) proposed the release of thermogenic CH_4 from the Norwegian Sea as

a possible trigger and carbon source for the PETM. This hypothesis strongly depends on the timing of sill-intrusion in the Vøring and Møre Basins. These sills are extensive (2 x 10^6 km^2) and partly emplaced in organic rich rocks (Planke et al., 2005) and roughly coincide with the PETM based on radiometric dating (Svensen et al., 2010; Westerhold et al., 2012). Numerous (>>700) hydrothermal vents (Figure 1a) are directly linked to the sill intrusions and provide evidence for large-scale degassing (Supplemental Figure 2). Furthermore, 95% of the vents terminate at the top-Paleocene reflector (Planke et al., 2005) and *Apectodinium augustum*, a dinoflagellate cyst marker species that is correlated to the PETM CIE (Eldrett et al., 2014; Schmitz et al., 2004; Sluijs et al., 2006) was found in the only drilled hydrothermal vent complex.

Rampino, (2013) suggested that melting of organic rich sediments may have generated even more methane and CO_2 than was calculated by Svensen et al., (2004). As much as 3000-6000 Pg of carbon may be released based on volumetric calculations of igneous deposits and intrusions across the North Atlantic. Correlations between deposits are made by radiometric dating and correlated to the PETM via dinoflagellate cyst biostratigraphy, most notably the presence of *A. augustum* in sediments interbedded in a basalt sequence at Ocean Drilling Program (ODP) Site 642E (Boulter and Manum, 1989). However, there is no CIE associated with the presence of *A. augustum* at Site 642E indicating the specimens of *A. augustum* are reworked into early Eocene sediments (Abdelmalak et al., 2016).

To test for a causal link between sill intrusion, generation of thermogenic methane and the PETM, we analysed samples recovered in the wildcat 6607/12-1 borehole, drilled in 1986 at 390 m water depth reaching 3521 m below sea surface (mbss) in the central part of a hydrothermal vent complex in the Vøring Basin (Svensen and Jamtveit, 2010) (Figure 1).

Materials

Drilling chips from 6607/12-1 were sampled at the Norwegian Petroleum Directorate in Stavanger, Norway. Here we focus on 22 samples from the 1640-1770 m interval, from the Maastrichtian – Paleocene unconformity to the top of the eye structure. The chips were originally collected and grouped from five-meter intervals during drilling. We sampled washed chips and hand-picked them for bulk rock total organic carbon, Rock Eval and vitrinite reflectivity measurements.

Methods

Rock-Eval and vitrinite reflectance

Total organic carbon (TOC) contents, Rock-Eval and vitrinite reflectance (%Ro) analyses were carried out on powdered samples using a Rock-Eval 6 instrument at Applied Petroleum Technology (APT), Kjeller, Norway. Rock-Eval pyrolysis is used to identify the type and maturity of organic matter. The TOC and Rock-Eval analyses are performed at temperatures between 300 °C and 850 °C during 25 min. The vitrinite reflectance is a widely used parameter to define the thermal maturity of organic matter in shales and coals. The vitrinite reflectance was determined at APT from polished slabs analyzed on a Zeiss Standard Universal research microscope-photometer (MPM01K) equipped with a tungsten-halogen lamp (12 V, 100 W) and an Epiplan-Neofluar 40/0.90 oil objective. Quality ratings reported in Table 1 are based on various important aspects which may affect the measurements, like abundance of vitrinite, uncertainties in the identification of indigenous vitrinite, type of vitrinite, particle size and particle surface quality.

Palynology

Of each sample, 5-15g was processed for palynology, using standard procedures (Sluijs

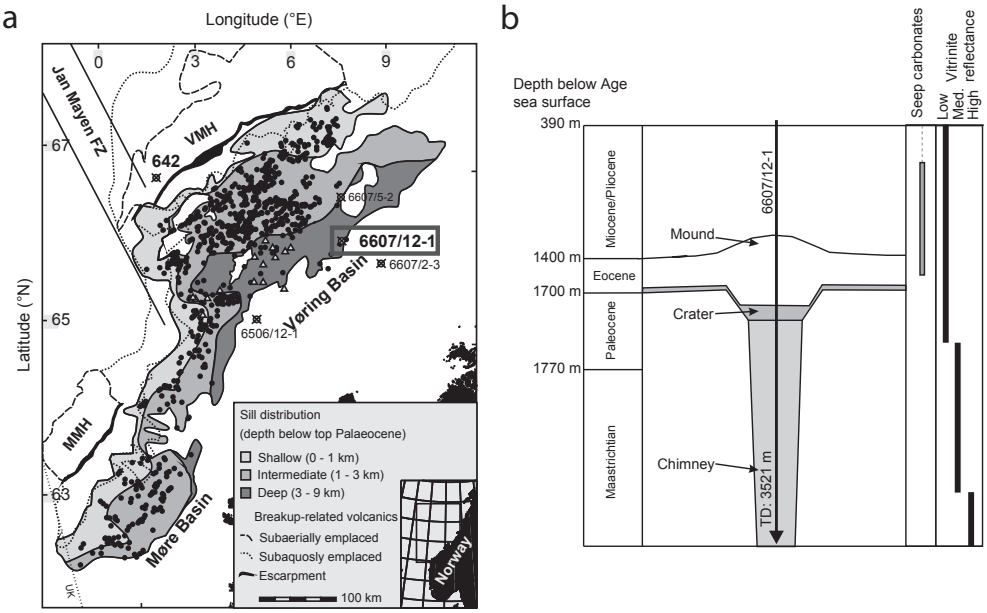

Figure 1. *Bore hole location and schematic view* ***a.*** *Location of wildcat 6607/12-1 (red rectangle) and other vent complexes (black dots and white triangles) and volcanics in the Vøring and Møre basins, redrawn from Svensen et al. (2004).* ***b.*** *Schematic view of bore hole 6607/12-1 structures. Ages of important regional sedimentary formations are indicated on the left, maturity of the organic matter on the right. Note that the base of the vent complex is at 1730 m below sea floor/surface, ~30m lower than the average depth of the Top Paleocene horizon outside the vent complex. TD: Total Depth.*

et al., 2011), including the addition of one *Lycopodium* spore tablet (*n* = 18583±764) (Stockmarr, 1971) for absolute quantitative analyses and treatment with HCl and HF. Afterwards, samples were sieved with water over a 250 and 15 µm sieve to remove large and small particles, respectively. Residues were concentrated in glycerine water and mounted on microscope slides using glycerine jelly. Slides were analyzed at 400x magnification to a minimum of 200 dinocysts, where possible. We follow dinocyst taxonomy of Fensome, (2004). All material is stored in the collection of the Laboratory of Palaeobotany and Palynology, Utrecht University.

Stable isotope analysis of palynological residues

Palynological residues from the 6607/12-1 bore hole were used for stable carbon isotope analyses. Splits of the residue were again washed with distilled water to remove glycerin. Samples were dried in a stove at 50 °C and subsequently total organic carbon (TOC) content was measured on ~1 mg of homogenized residue using a CNS-analyzer (Fisons). Stable carbon isotope ratios were determined on 15-30 µg of residue using an isotope ratio mass spectrometer (IRMS, Finnigan Mat Delta Plus) coupled online to the CNS analyzer. We correct our $\delta^{13}C_{PALY}$ for variable marine influences to obtain $\delta^{13}C_{POLLEN}$ using the equation of (Sluijs and Dickens, 2012), which assumes a constant offset of 4.4‰ between marine and terrestrial organic matter, the latter being the heavier fraction. Absolute reproducibility, based on international and in-house standards, for TOC and $\delta^{13}C_{PALY}$ is better than 0.1%

and 0.05‰ respectively.

LOSCAR

A detailed description of the LOSCAR model can be found in Zeebe, (2012). Primarily, this box model simulates the cycling of carbon through oceanic and atmospheric reservoirs (modified from (Walker and Kasting, 1992), coupled to a sediment module. Concentrations of several biogeochemical tracers are calculated for each box, including dissolved inorganic carbon (DIC), total alkalinity, $\delta^{13}C$, oxygen and phosphate. The Paleogene model ocean consists of four main ocean basins (Atlantic, Indian, Pacific, Tethys), which are in turn separated into surface (0-100 m water depth), intermediate (100-1000 m) and deep (>1000 m) boxes. Thermohaline circulation and ocean mixing are prescribed. For our simulations, we use default parameter settings (Zeebe, 2012), and alter the PETM body background conditions following (Zeebe et al., 2009; see also supplement thereof).

Vent stratigraphy

The vent complex is characterized by a 2 km wide eye-shaped upper part, at the top of the Paleocene series (crater and mound), above a zone in which seismic data indicate disrupted sediments (chimney structure) (Svensen et al., 2004) (Extended Data Figure 2). The chimney can be divided into two parts, where the upper part has low to intermediate organic maturity and a lower part with high maturity, based on vitrinite reflectance (Figure 1b). The chimney connects the upper part of the vent complex to the termination of a high-amplitude seismic event at 5.0 s two way travel time, regionally interpreted as a sill intrusion (Extended Data Figure 2). The strata above the vent complex are domed. We performed detailed analysis of palynology, stable carbon isotopes of isolated palynological residue, Rock-Eval and vitrinite reflectance on 22 cutting samples from the chimney and eye structure (1640-1745 m) at 6607/12-1. For borehole 6607/12-1 we correlate our dinocyst biostratigraphy to regional dinoflagellate cyst zonations (Bujak and Mudge, 1994), which confirms an earliest Eocene age for all studied samples (Figure 2c and SI).

We also record the presence and abundance of *A. augustum*. Crucially, stable carbon isotope ratios of palynological residue ($\delta^{13}C_{PALY}$) are extremely low at -31 ‰ in between 1710 and 1745 m, during the *Apectodinium* acme, and subsequently rise to -27 ‰ at 1660 m. However, changes in organic matter sources, here represented by the fractions of marine and terrestrial palynomorphs, can significantly influence the isotopic signal (Freeman and Hayes, 1992; Sluijs et al., 2012). Palynological assemblages are dominated by pollen grains, with variable marine contributions (5-30 %; Figure 2b), which could lead to biases in $\delta^{13}C_{PALY}$ values (Sluijs and Dickens, 2012). We can correct for this potential bias using end-member modelling of terrestrial and marine organic matter $\delta^{13}C$ and the relative abundance of terrestrial and marine contributions to the palynological assemblages (Sluijs and Dickens, 2012) (SI). The correction leads to a synthetic $\delta^{13}C$ record of terrestrial palynomorphs ($\delta^{13}C_{POLLEN}$, Figure 2a,b). The trends in this record follow those of the $\delta^{13}C_{PALY}$ record, although the thickness of the body of the PETM CIE is reduced. Collectively, biostratigraphy and carbon isotope stratigraphy imply the presence of the body and recovery phases of the PETM CIE (Figure 2a).

The new stratigraphic constraints indicate that both *A. augustum* and very low $\delta^{13}C$ are prevalent from below the base of the vent system (1730 mbss). Moreover, the previously recorded thermally mature specimens of *A. augustum* (Svensen et al., 2004) suggest that the vent system blew through PETM sediments, in line with our simple sedimentation model which indicates activity is limited to a short period during the body of the CIE (SI).

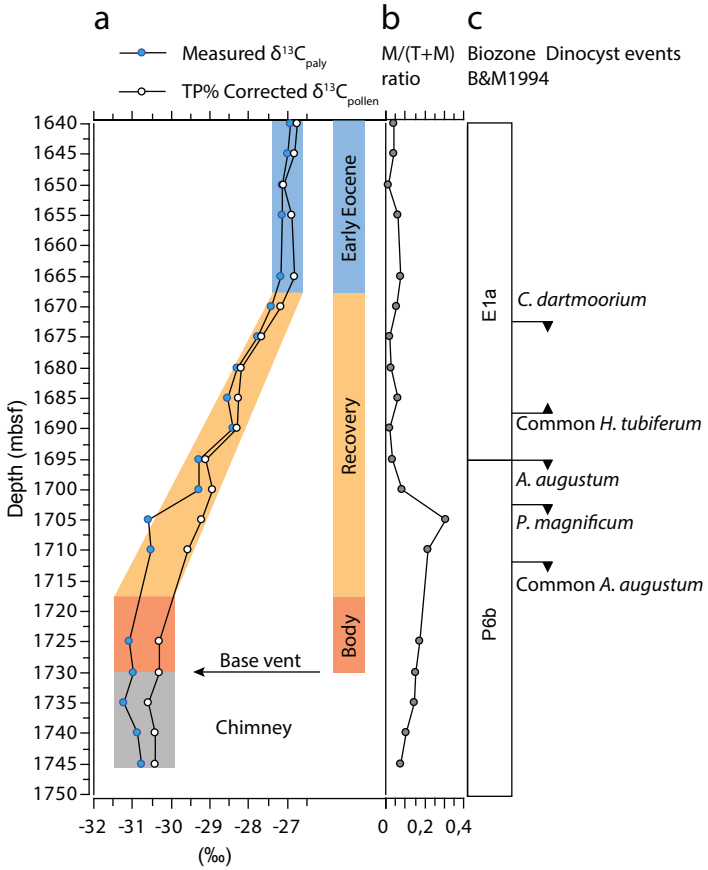

Figure 2. *Stratigraphy of the 6607/12-1 bore hole* ***A.*** *Isotope records of isolated palynological residue (δ[13]C paly) and corrected for marine organic matter (δ[13]C pollen) plotted against depth.* ***B.*** *Fraction of marine palynomorphs calculated as marine / marine + terrestrial (M/(T+M)).* ***C.*** *Dinocyst zonation based on Bujak and Mudge (B&M; 1994) and stratigraphically important dinocyst events.*

Implications for PETM carbon cycling

The body of the PETM CIE is an enigmatic and unique feature among the early Eocene hyperthermals and has been attributed to slow carbon addition, possibly through a slow carbon cycle feedback (Zeebe, 2013; Zeebe et al., 2009). To test whether pulsed release of thermogenic methane and CO_2 could have produced a 60-70 kyr period of stable $\delta^{13}C$ values in the sedimentary record, we conducted simulations with the Long-term Ocean atmosphere-Sediment CArbon cycle Reservoir carbon cycle model (LOSCAR) (Zeebe, 2012). We inject a total of 1480 Pg of carbon with a carbon isotope value of -45‰ (cf. Zeebe et al., 2009; 1480 Pg, -50‰) spread over 4, 8 and 12 pulses within 60 kyr, directly following the initial massive carbon injection at the onset of the PETM (Figure 3, Supplemental Figure 3, see Supplementary Information for detailed model run descriptions). With respect to the changes in pCO_2, pH and carbonate compensation depth (CCD) and overall $\delta^{13}C$ trends, our results are similar to the scenario explored by Zeebe et al., (2009). However, the

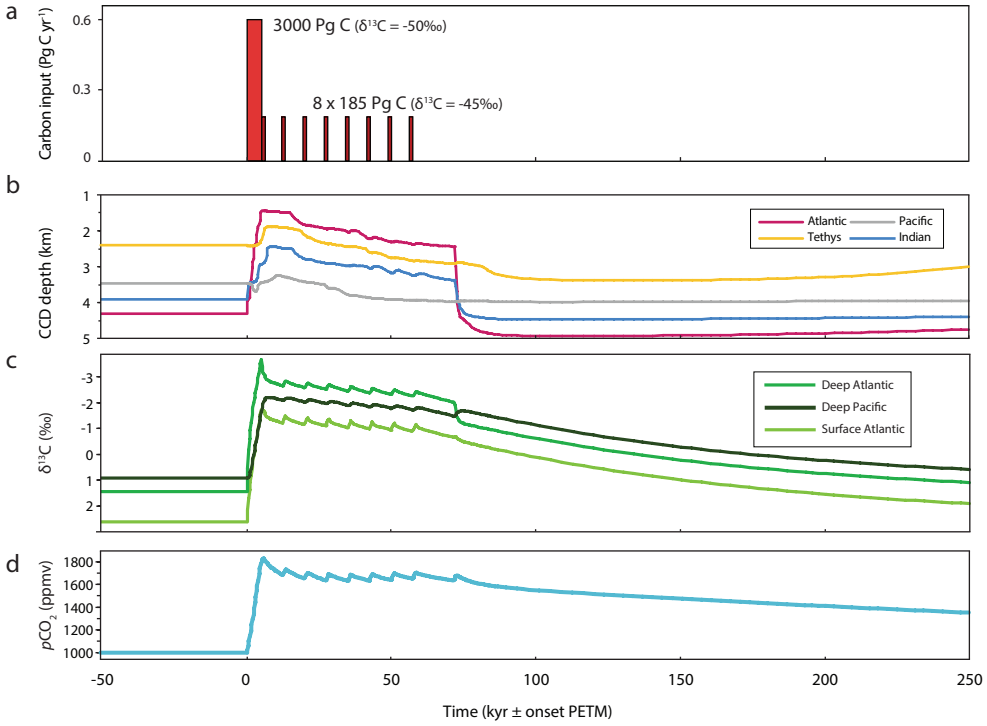

Figure 3. *LOSCAR model output of pulsed carbon release.* ***a.*** *Emission scenario showing the release of carbon with 8 distinct pulses of 185 Pg following an initial release of 3,000 Pg.* ***b.*** *Response of carbonate compensation depth (CCD) in different ocean boxes.* ***c.*** *Response of $\delta^{13}C$ in different ocean boxes.* ***d.*** *Atmospheric CO_2 concentrations in ppm.*

pulsed carbon input is recorded in $\delta^{13}C$ as short-lived, distinct spikes. Ocean-mixing time dampens these spikes in the deep basins and even in most shallow marine sites bioturbation is expected to completely remove millennial scale $\delta^{13}C$ fluctuations from bulk isotope records. Intriguingly, some high-resolution terrestrial (Bowen and Zachos, 2010) and laminated marine sections (Luciani et al., 2007) record high-frequency variability during the body of the CIE, which can perhaps be attributed to pulsed thermogenic methane release from the Vøring and Møre basins. Futhermore, we cannot exclude activity in some of the hydrothermal vent complexes close to the onset of the PETM. Taking into account the recent discovery of a precursor event (Bowen et al., 2015), we speculate some other vents may have indeed released carbon close to the onset and perhaps provided a trigger for the release of submarine hydrate dissociation.

We conclude that carbon release from this particular vent system cannot have triggered the PETM. Most importantly, we find that the pulsed release of methane and CO_2 from these vent complexes may have prolonged the body of the CIE, as well as environmental effects such as warming and ocean acidification during the PETM.

Supplementary information

North Atlantic Paleogene volcanism

The Large Igneous Province in the Northeast Atlantic Ocean that was active from about 61 to 55 Ma is preserved as a wide range of volcanic deposits in both onshore (Greenland, Great Britain, Denmark) and offshore settings (East and West Greenland, the Vøring and Møre basins, the Faroe-Shetland Basin). In addition to abundant volcanic centers and large areas covered by flood basalts, sills intruded into the sedimentary basins around the NE Atlantic (Figure 1a) (Berndt et al., 2000; Planke et al., 2005; Svensen et al., 2010).

Heating of organic-bearing sedimentary rocks in contact with the sills generated methane and carbon dioxide. This process has been suggested as the trigger for the Paleocene-Eocene Thermal Maximum (PETM; ~56 Ma) (Svensen et al., 2010, 2004), and perhaps widespread melting could account for even more carbon input during this period (Rampino, 2013).

The NE Atlantic Paleocene and early Eocene volcanism co-occurs with a long term gradual rise in global temperatures (Bijl et al., 2013b, 2009; Frieling et al., 2014; Zachos et al., 2008). Seismic data reveal the presence of lava flows and a few hydrothermal vent complexes in the central part of the Paleocene sequence (Planke et al., 2005). A reduction or cease of volcanic activity during right after the magnetochron C25n-C24r boundary is implied by the presence of a coal sequence in the Faroes that overlies late Paleocene lava flows (Storey et al., 2007). A short period (< 1 Myr) of voluminous breakup volcanism started at about 56 Ma. Seismic interpretations show that the breakup volcanism began with a period of intrusive activity in the Vøring and Møre basins, forming at least 700 (Figure 1a), but most likely thousands of hydrothermal vent complexes terminating at the reflector that represents the top Paleocene horizon (Planke et al., 2005; Svensen et al., 2004). It is well documented that sill intrusions alter the light element geochemistry of the intruded sediments (Aarnes et al., 2010; Galushkin, 1997), forming CH_4 and CO_2 followed by overpressure generation and in some cases explosive venting (Aarnes et al., 2012; Jamtveit et al., 2004). The contact metamorphic volume of sedimentary rocks is usually twice the sill volume, which can be used to calculate the mass of carbon generated (Aarnes et al., 2011). The gas venting was followed by the emplacement of dominantly subaerially erupted lavas represented by the Inner Flows, Lava Delta, Landward Flows, and Seaward Dipping Reflectors seismic facies units (Berndt et al., 2001; Planke et al., 2000). The estimates of carbon release during the main period of intrusive volcanism in the Vøring and Møre Basins is 300-3500 Pg (Aarnes et al., 2010; Svensen et al., 2004), and the latest conservative estimate is 1100 Pg (Aarnes et al., 2015). Large uncertainties remain concerning the amount of released carbon due to the extrapolation of data over a large (200,000 km^2) area and the assumption of synchronicity of 95% of these vent systems based on seismic profiles (Planke et al., 2005).

The voluminous phase of breakup volcanism was followed by decreasing volcanic activity during the next 6 million years, reaching normal sea floor spreading magma production rates in the Norwegian Sea at about 50 Ma (Fig. S1). Shallow marine explosive volcanism forming the Outer High seismic facies units characterizes the transition from subaerial to deep marine volcanism (Planke et al., 2000). Seismic and magnetic anomaly data show that this transition occurred at about 52 Ma (Breivik et al., 2006).

Stable carbon isotope and dinocyst stratigraphy of 6607/12-1

Although our analyses did not reach down to the onset of the negative carbon isotope excursion (CIE), extremely low $\delta^{13}C$ paly values of ~31 ‰ and subsequent recovery to -27‰, combined with the presence of *Apectodinium augustum* confidently ties the lower part of

the analyzed interval to the core and recovery of the PETM (Eldrett et al., 2014; Schmitz et al., 2004; Sluijs et al., 2012, 2007a, 2006). However, changing composition of organic matter often complicates a detailed interpretation of an organic carbon isotope record (Sluijs et al., 2012). In particular the ratio between terrestrial and marine organic matter (OM) can be a determining factor. Since we measured isotopes of the bulk palynological residue and analyzed palynology on the same samples, we can use the composition of the palynological residue to correct for the composition of the organic matter. The difference in carbon isotopic signature between terrestrial and marine OM is relatively well constrained for the Early Palaeogene (Hayes et al., 1999; Magioncalda et al., 2004; Sluijs and Dickens, 2012). With the present dataset, we cannot correct for varying contributions of angiosperm and gymnosperm pollen (Schouten et al., 2007c), carbon dioxide effects on ^{13}C fractionation of marine (Freeman and Hayes, 1992) and terrestrial organisms (Schubert and Hope Jahren, 2013), or changes in trophic state of the ecosystem. However, we can correct for the fractions of marine and terrestrial OM by using the total pollen versus total marine counts (TP%) as a proxy for the proportion of terrestrial organic matter in the palynological residue, and by assuming marine OM is 4.4‰ more depleted in ^{13}C than terrestrial OM (Sluijs and Dickens, 2012)(Fig. 2).

The resulting $\delta^{13}C_{POLLEN}$ shows two distinct plateaus, like the $\delta^{13}C_{PALY}$, although the lower plateau phase is substantially shortened. Sediments below 1730m are interpreted to be part of the chimney structure (Figure 1a) and therefore not taken into account in the stratigraphic assessment. The body of the PETM hence spans 1730 to ~1717.5 m and the upper plateau spans 1665-1640 m. The very depleted stable values (-31‰) during the lower plateau imply a relation to the "body" of the PETM CIE, globally recognized in isotope records as a ~70-130 kyr period of relatively small $\delta^{13}C$ changes (Murphy et al., 2010; Röhl et al., 2007). Such low absolute values are unlikely to be associated with the "recovery" phase of the PETM. Based on a gradual rise in $\delta^{13}C$ in both $\delta^{13}C_{PALY}$ and $\delta^{13}C_{POLLEN}$, we ascribe the interval from 1717.5 to 1667.5 m to the recovery phase of the PETM. The plateau at the top of the section is characterized by typical early Eocene $\delta^{13}C$ values of around -27‰.

Following the North Sea dinocyst zonation of Bujak and Mudge, (1994)(Fig. 2c), the last occurrence of *A. augustum* (1695 m) defines the start of earliest Eocene biozone E1a. Our findings are consistent with aspects of this zonation; *sensu scricto*, this zone is characterized by last occurrences of *Phelodinium magnificum* (1700 m), *Cerodinium speciosum* and *C. dartmoorium* (1670 m), and the first occurrence of common to abundant *Hystrichosphaeridium tubiferum* (here 1685-1640 m), which we also record near the top of *A. augustum*. The last occurrence of *C. speciosum* is not recorded, suggesting this subzone extends further up section. A single specimen of *Wetzeliella meckelfeldensis* at 1730m indicates some caving has occurred. However, the dinocyst assemblages show continuous events characteristic of the early Eocene North Sea and it is hence concluded that caving is a minor factor.

Summarizing, the PETM interval is at least 80 meters thick (Fig. 2), which given a total duration of ~170-230 kyr for the PETM (Murphy et al., 2010; Röhl et al., 2007) amounts to minimum average sedimentation rates ~35-47 cm kyr^{-1}. Sedimentation rates immediately following crater formation were likely even higher to due to newly available accommodation space, possibly much higher than 50 cm kyr^{-1}.

Vent system sedimentation constraints

The base of the vent is interpreted to be at ~1730 m depth, based on seismic profiles and velocity/density hole logs (Fig. 1b, Fig. S2). During the main activity phase, continuous

flow largely inhibits normal sedimentation in the vent system. This implies that sediments above the base of the vent were deposited after the vent was active. Sediments below this level were deposited in and around the study location prior to vent activity and re-deposited in the chimney. The presence of mixed immature and mature *A. augustum* specimens in the top of the chimney structure are of interest (Svensen et al., 2004). Importantly, there are no other records of thermally altered *A. augustum* nearby, suggesting the signal is very local, perhaps in situ. There are two scenarios for immature and mature *A. augustum* to be present in the lower parts of the crater and the top of the chimney structure. 1) The vent system penetrated PETM sediments, thereby thermally altering the organic matter, including *A. augustum*. Part of this material fell back into the chimney structure and was mixed with immature PETM material from just outside the crater and perhaps also with new sediments. 2) The vent system penetrated PETM sediments and after a short hiatus thermally immature organic matter is deposited on top of mature organic matter. Mature and immature specimens are then in the same sample due to caving. Crucially, either of these two, or a combination thereof requires PETM sediments to be present at the time of explosive venting. This means that also this line of evidence implies that the vent system postdates the onset of the PETM.

We test a simple sedimentation model, based on the thickness of the recovery to test when sedimentation in the crater resumed after the vent was active. We use average duration of the body (100 kyr) and recovery (85 kyr) of the CIE based on estimates of both astronomical (Röhl et al., 2007) and extraterrestrial He^3 (Murphy et al., 2010) age models for the PETM. We take the length of the recovery as determined from the $\delta^{13}C_{POLLEN}$ record (50 m). Assuming constant sedimentation rates of 60.7 cm kyr^{-1}, sedimentation on top of the base of the vent re-initiated 85 kyr after the onset of the PETM.

Alternatively, if the entire body of the PETM CIE would be present in our section, it would mean 100 kyr is represented by 20-25 (maximum 40) m of sediment. The resulting sedimentation rates of 20 - 25 (maximum 40) cm kyr^{-1} may appear very high, but this would require sedimentation rates to further increase by a factor 1.6 - 3.3 during the recovery phase. In contrast, we expect sedimentation rates to be generally decreasing towards the top of the structure as the accommodation space is being filled. When the activity ceases, infilling is very rapid due to newly available accommodation space, as is the case with any topographic depression. This is also reflected in the thickness of formations in the crater, which are a factor 3-4 thicker than the regional average (Blunck and Blanchet, 1986; Mattson, 2006). Even though this age model is crude, it suggests sedimentation started well after the onset of the PETM, most likely during the second half of body of the CIE.

LOSCAR experimental setup

In our model experiments, we use the LOSCAR model (Zeebe et al., 2009), a relatively simple box model designed to resolve large-scale processes and perturbations in the carbon cycle, described in detail in (Zeebe, 2012). We use the Zeebe et al., (2009), scenario (Z09) as a starting point and further refine with our constraints from detailed dinoflagellate biostratigraphy, $\delta^{13}C$ records, sedimentation and previous research on thermogenic methane generation around sills. In all of our experimental scenarios, the system is first perturbed by the input of 3000 Pg of ^{13}C-depleted (-50‰) carbon over 5 kyr. Following to the Z09 scenario, we invoke changes in ocean circulation and a deep ocean-to-shelf shift in the locus of carbonate deposition during the body of the PETM. Contrasting with Z09, we then impose a pulsed input of ^{13}C-depleted (-45‰) carbon, representing discrete, short lasting (1 kyr) episodes of methane venting in the Vøring and Møre basins. All scenarios are set up so that the first pulse always directly follows the initial 3000 Pg perturbation and the

first and last pulse are always 60 kyr apart.

We conduct a series of sensitivity experiments where we change the locus of carbon input, the number of pulses and the total mass of released carbon. We note that it is highly unlikely that methane was vented in equally spaced, equally sized pulses, but at present the data does not allow for constraints on size and timing of individual pulses or on the exact number of pulses and different scenarios would not change the conclusions significantly.

Locus of the carbon input

In the original Z09 scenario carbon from methane hydrates at the start of the PETM is released into the atmosphere (60%) and the deep Atlantic (40%). We keep this ratio constant in the initial 3000 Pg perturbation, but 90% of the subsequent pulsed 1500 Pg enters the atmosphere directly. We feel this approach is more realistic when considering violent releases of methane, as witnessed by the presence of numerous large craters in the Vøring and Møre basins. As a consequence, the scenario in which 40% of the carbon input enters the Atlantic directly shows more variability in deep Atlantic carbonate compensation depth and $\delta^{13}C$. However, the observed differences are only noticeable on a millennial scale and hardly affect $\delta^{13}C$ in the other ocean basins (Figure S6 b,c).

4, 8 or 12 pulses

We conduct three experiments with 4, 8 and 12 individual pulses of 1 kyr each, as constrained by seismic profiles (Svensen et al., 2004) and sill cooling time (Aarnes et al., 2010) (Fig. S4), while total carbon input is held constant at 1480 Pg (following Z09). All the pulses are represented by discrete, albeit small, $\delta^{13}C$ excursions. The largest excursions are found in the Atlantic, the smallest in the Pacific. In the Atlantic, the amplitude of the $\delta^{13}C$ changes ranges from 0.6‰ in the 4-pulse scenario to 0.2‰ in the 12-pulse scenario. However, these excursions are smoothed in the Pacific, resulting in output that is practically indistinguishable from the continuous input scenario (Z09) (Fig. S6a). Arguably, $\delta^{13}C$ excursions of ~0.6‰ would have been recorded in some of the high-resolution shallow marine PETM records. However, after deposition, mixing processes, such as bioturbation, usually smooth out the largest excursions. Indeed, high-resolution terrestrial (Bowen and Zachos, 2010; Chen et al., 2014) and marine PETM records without substantial bioturbation (Luciani et al., 2007) typically show more variability in $\delta^{13}C$. In the 8 and 12-pulse scenarios, $\delta^{13}C$ excursions are limited to <0.2 and <0.1‰ in the deep Atlantic and deep Pacific, respectively. Such small excursions would not be picked up in any $\delta^{13}C$ record.

Uncertainties in the amount of released carbon: 300, 1480 or 3000 Pg

The proposed 1,480 Pg of carbon as continuous input was tuned to the CCD data from different ocean basins (Zeebe et al., 2009) and close to the average estimate of methane release from the Vøring and Møre basins (Aarnes et al., 2010; Svensen et al., 2004). However, large uncertainties remain in the latter due to extrapolation over a large area (~200,000 km^2) and the assumption that 95% of the craters is synchronous with the top-Paleocene reflector. Therefore, we explore what the effects are of releasing 300 Pg and 3,000 Pg, the minimum and maximum estimated mass of released thermogenic methane, respectively. A total release of 300 Pg is unable to produce the observed prolonged excursions in $\delta^{13}C$ and pH (Penman et al., 2014; Zeebe, 2013) (Fig. S5a). Contrasting with this, 3,000 Pg would cause a continued decrease of $\delta^{13}C$ (Fig. S5 c), whereas most records show stable or slightly increasing $\delta^{13}C$ values within the body of the PETM.

Dinocyst ecology

The dinoflagellate cyst assemblages indicate a rather uniform paleoecological signal in the 1745-1640 m interval. Notably, it represents a mixture of open ocean, oligotrophic and more proximal eutrophic species (Fig. S7). Such mixtures of distal and proximal species are usually interpreted as transported signals (Sluijs et al., 2005), in line with high sediment supply at the site location. *Senegalinium* and related genera, usually associated with (seasonally) lower than normal marine salinities and eutrophic conditions (Barke et al., 2011; Brinkhuis et al., 2006; Sluijs and Brinkhuis, 2009) make up ~25% of the assemblage on average, perhaps slightly more in the lower part (1705-1745 m). This could indicate the prevalence of lower salinities during the greenhouse warmth of the PETM, as was previously found in Spitsbergen (Harding et al., 2011) and the Arctic Ocean (Pagani et al., 2006b; Sluijs et al., 2006).

We further find close to 30% *Apectodinium spp.* at 1725-1730 m, a (sub-) tropical, euryhaline genus that is usually associated with warm and eutrophic waters (Frieling et al., 2014; Sluijs and Brinkhuis, 2009). *Deflandrea* and *Cerodinium* species substitute for *Apectodinium* from 1700 m upward, arguably representing a similarly eutrophic, albeit somewhat colder, environment. More open marine *Spiniferites* account for ~35% of the assemblage, with a maximum of 60% at 1695m. Together with a maximum in marine over terrestrial palynomorphs at 1705m this represents a period of more distal influences.

Pollen assemblages

We record the typical late Paleocene and early Eocene *Taxodiaceaepollenites hiatus* acme (Bujak and Mudge, 1994), derived from extensive coastal *Taxodium* swamps. Concomitant with abundant *Apectodinium spp.*, we find higher percentages (~40%) of *Caryapollenites spp.*, possibly again related to warmer conditions during this period. Other common pollen includes *Alnipollenites spp.* and *Momipites spp.*, which is closely related to *Caryapollenites*. Bisaccate pollen, indicative of cooler, drier conditions make up ~10% of the pollen total higher up in the section (1675-1640 m). Although we mainly focus on dinoflagellates here, these findings are in general congruent with (Eldrett et al., 2014).

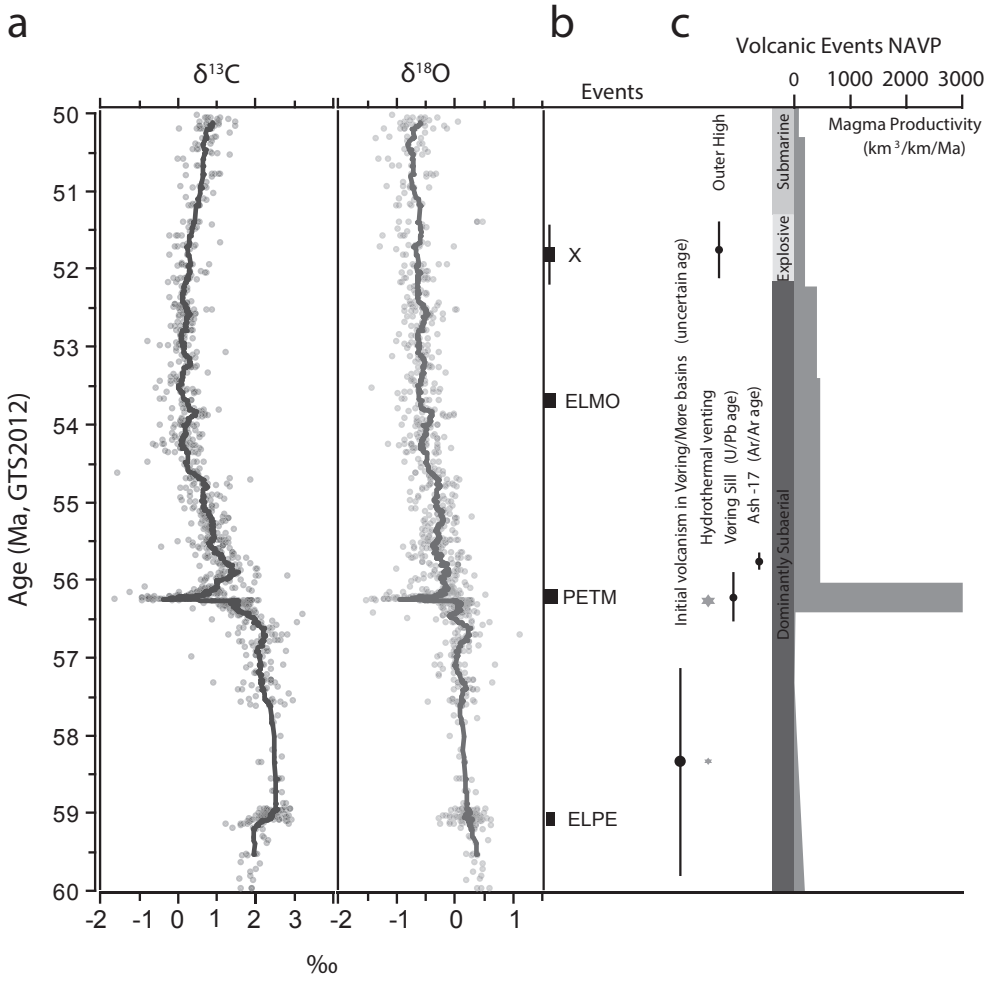

Figure S1. *North Atlantic Volcanism and long term Paleocene – Eocene climate.* ***a.*** *Oxygen a carbon isotope data from Zachos et al. (2008) showing long-term warming from 60-51 Ma.* ***b.*** *Significant climatic and biological events.* ***c.*** *Volcanic events and approximate magma production from Storey et al. (2007).*

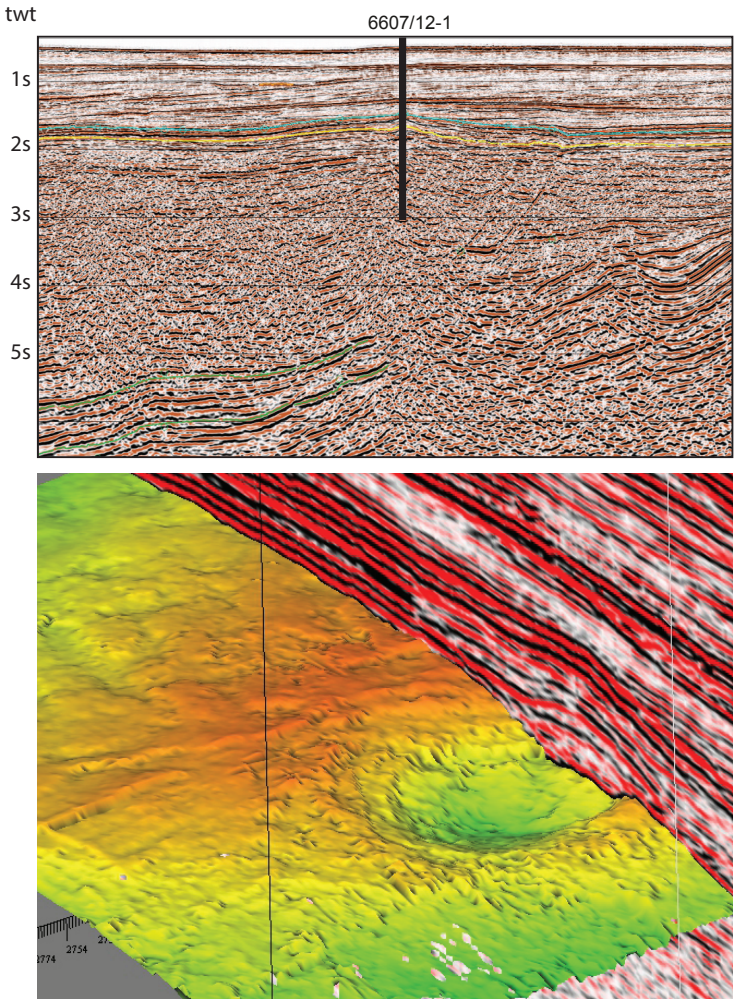

Figure S2. *Seismic data for 6607/12-1 and surroundings.* ***a.*** *Seismic profile across the hydrothermal vent system penetrated by 6607/12-1, green lines indicate sill intrusions and the yellow line represents the top Paleocene reflector. Two-way travel time (twt) indicated.* ***b.*** *3D visualisation of the hydrothermal vent system, with pronounced crater and overlying eye-structure.*

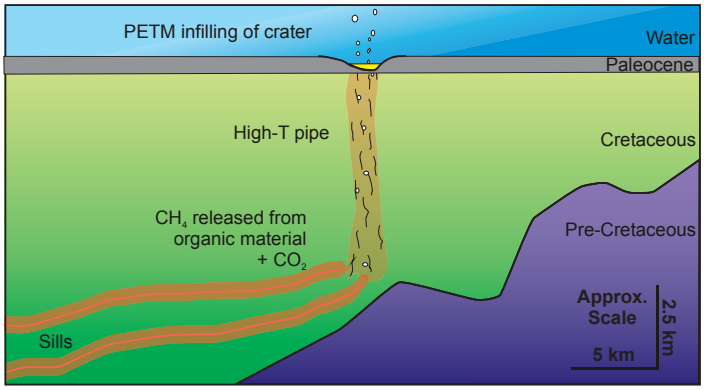

Figure S3. *Conceptual image of carbon release through hydrothermal venting.*

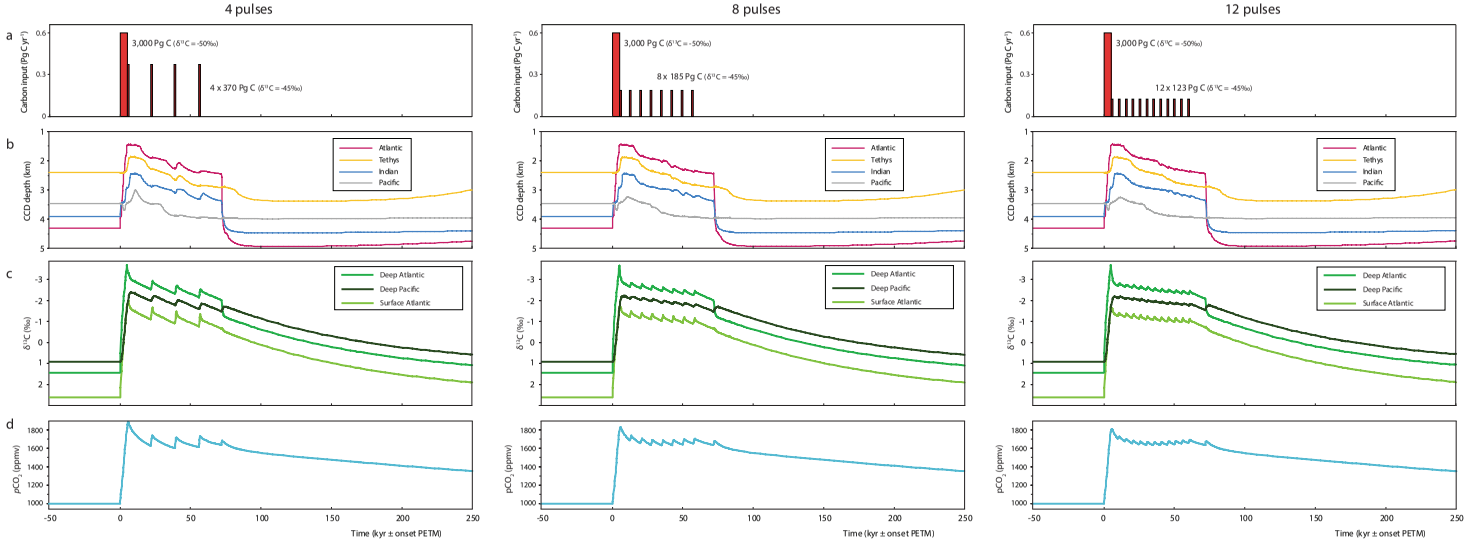

Figure S4. *LOSCAR model output of carbon release (1480 Pg) in 4, 8 and 12 pulses.* ***a.*** *Emission scenario showing the release of carbon with 4, 8 and 12 distinct pulses totalling 1480 Pg following an initial release of 3,000 Pg.* ***b.*** *Response of carbonate compensation depth (CCD) in different ocean boxes.* ***c.*** *Response of* $\delta^{13}C$ *in different ocean boxes.* ***d.*** *Atmospheric* CO_2 *concentrations.*

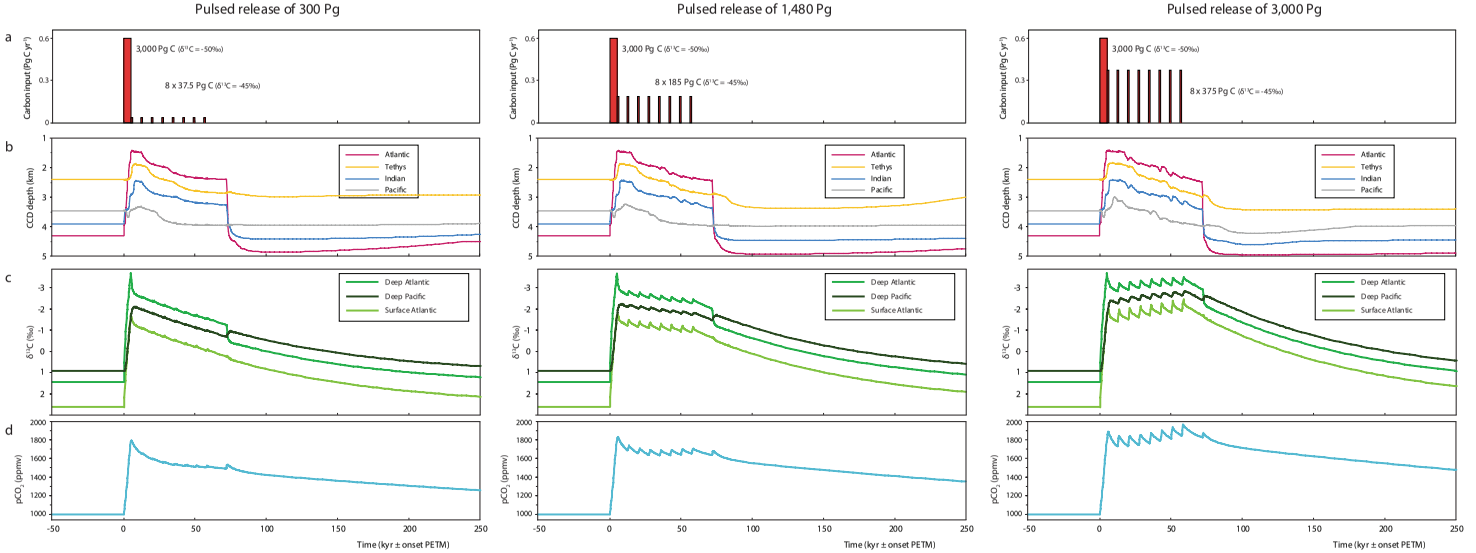

Figure S5. *LOSCAR model output of variable carbon release (300, 1480 and 3000 Pg) in 8 pulses.* ***a.*** *Emission scenarios showing the release of carbon with 8 distinct pulses of 37.5, 185 and 350 Pg following an initial release of 3000 Pg.* ***b.*** *Response of carbonate compensation depth (CCD) in different ocean boxes.* ***c.*** *Response of $\delta^{13}C$ in different ocean boxes.* ***d.*** *Atmospheric CO_2 concentrations.*

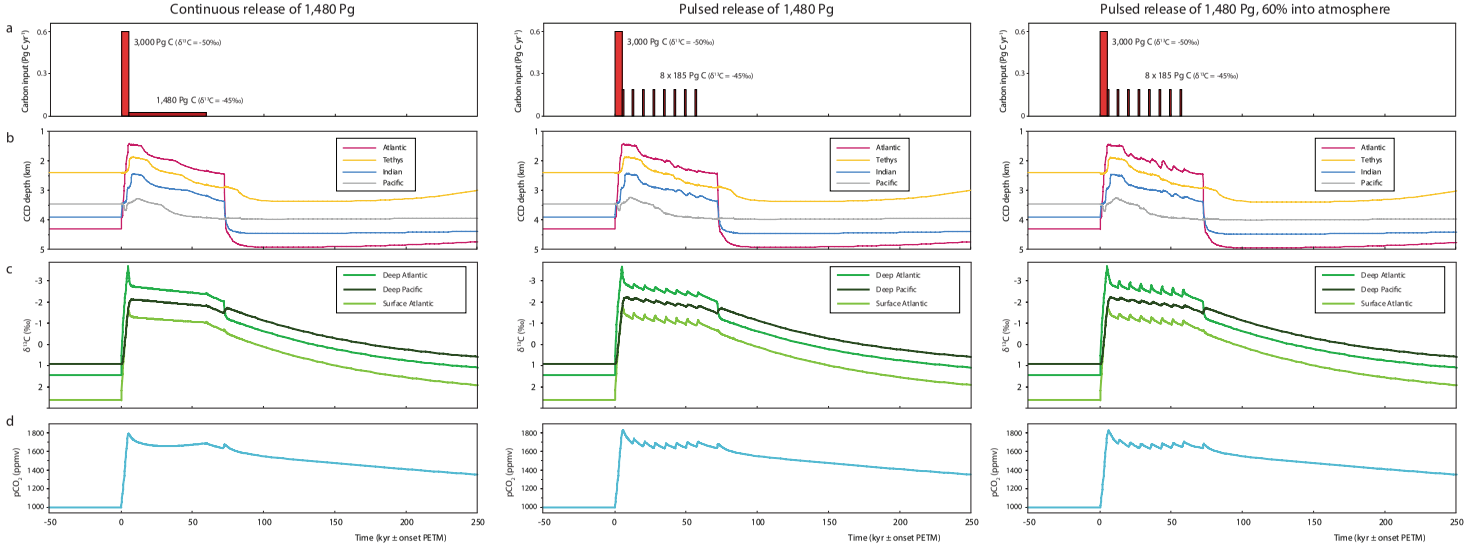

Figure S6. *LOSCAR model output of continuous carbon release and pulsed carbon release.* ***a.*** *Emission scenarios showing the continuous release of carbon, 8 distinct pulses of 185 Pg (90% into the atmosphere) and 8 distinct pulses of 185 Pg (60% into the atmosphere) following an initial release of 3,000 Pg.* ***b.*** *Response of carbonate compensation depth (CCD) in different ocean boxes.* ***c.*** *Response of $\delta^{13}C$ in different ocean boxes.* ***d.*** *Atmospheric CO_2 concentrations.*

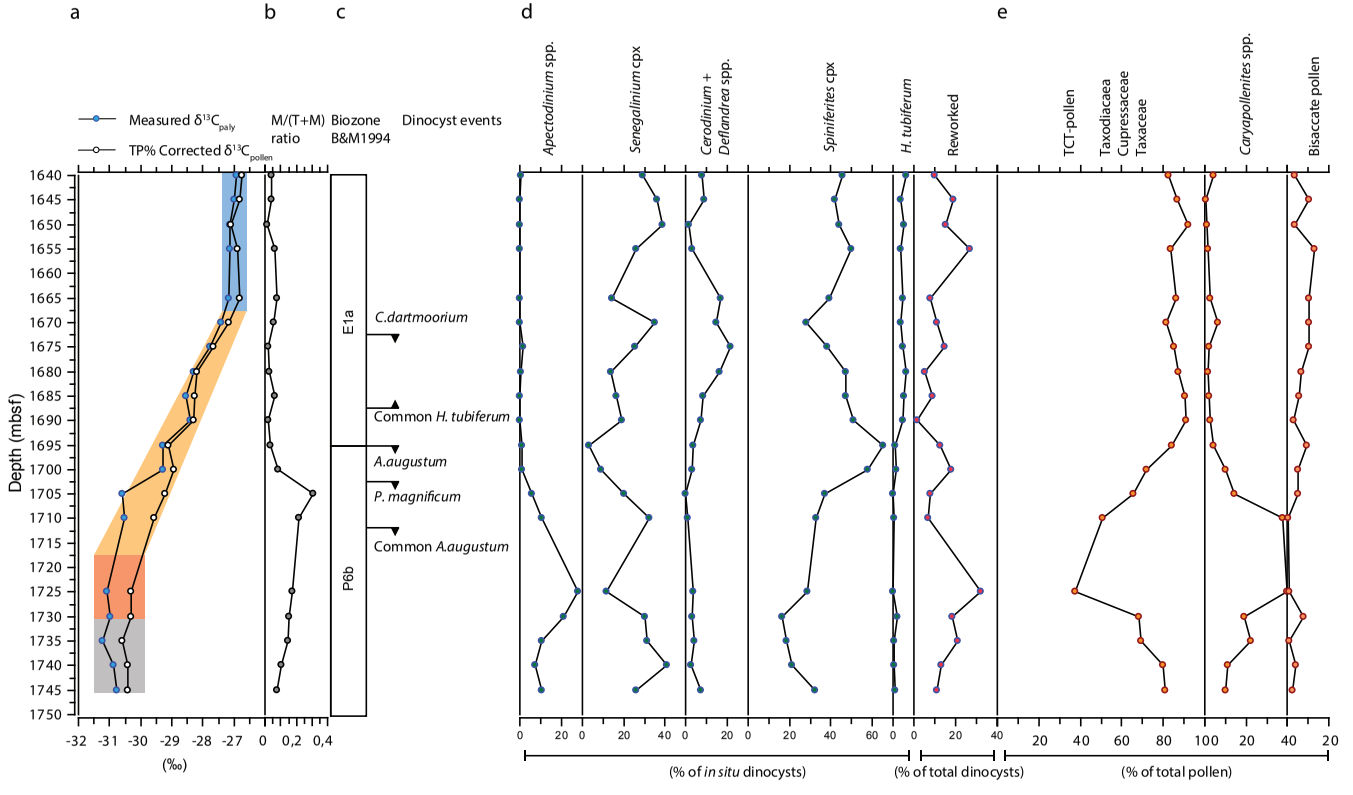

Figure S7. a. *$\delta^{13}C$ records, color coded as in Figure 2a; chimney (grey), body of the CIE (red), recovery (orange) and Early Eocene (blue).* ***b.*** *Fraction of marine palynomorphs calculated as marine / marine + terrestrial (M/(T+M)).* ***c.*** *Dinocyst zonation based on Bujak and Mudge (B&M; 1994) and stratigraphically important dinocyst events.* ***d.*** *Dinoflagellate cyst assemblages.* ***e.*** *Pollen assemblages.*

Table S1. *$\delta^{13}C$, palynological and organic matter analyses. Abbreviations: mbss = meters below sea surface, $\delta^{13}Cpaly$ = $\delta^{13}C$ palynological residue, C. fibrospinosum cpx = Cordosphaeridium fibrospinosum complex. TAI = Thermal Alteration Index*

Depth(mbss)	δ^{13}Cpaly (‰)	Marine fraction	"Marine bias" (‰)	δ^{13}C pollen (‰)	*Apectodinium*	*Senegalinium*	*Deflandrea/Cerodinium cpx*	Protoperidinioids	*Spiniferites cpx*	*Areoligera cpx*	*Operculodinium spp.*	Goniodomaceae	*H.tubiferum*	*C.fibrospinosum cpx*	Reworked (very high TAI)
1640	-26.93	0.04	-0.15	-26.77	1	29	8	1	45	1	1	0	6	0	15
1645	-27.00	0.04	-0.17	-26.83	0	36	9	1	42	2	0	0	4	0	11
1650	-27.14	0.01	-0.04	-27.10	0	39	2	0	44	2	2	0	5	0	9
1655	-27.13	0.06	-0.24	-26.90	0	26	3	0	50	7	5	0	4	0	17
1665	-27.18	0.08	-0.31	-26.86	0	14	17	1	39	2	0	0	5	0	4
1670	-27.42	0.06	-0.23	-27.18	0	35	15	0	28	5	0	0	4	0	6
1675	-27.75	0.02	-0.09	-27.66	2	25	22	0	38	2	1	0	5	0	11
1680	-28.31	0.03	-0.12	-28.19	0	14	16	0	47	3	3	0	6	1	6
1685	-28.56	0.06	-0.25	-28.31	0	17	8	1	47	1	12	0	5	0	5
1690	-28.39	0.02	-0.08	-28.31	0	19	7	0	51	1	5	0	5	4	1
1695	-29.27	0.04	-0.15	-29.13	1	3	4	4	65	0	7	0	1	2	7
1700	-29.29	0.08	-0.32	-28.97	1	9	3	2	58	1	8	1	2	1	10
1705	-30.58	0.31	-1.20	-29.38	6	20	0	7	37	1	6	2	0	0	4
1710	-30.52	0.21	-0.84	-29.68	11	33	1	2	33	1	0	0	0	0	3
1720															
1725	-31.07	0.18	-0.69	-30.38	28	12	4	6	29	1	2	0	0	2	34
1730	-30.99	0.15	-0.60	-30.40	21	30	3	3	16	0	4	1	2	1	12
1735	-31.22	0.15	-0.57	-30.65	11	31	4	6	19	3	2	1	1	1	14
1740	-30.88	0.10	-0.41	-30.47	7	41	3	3	21	0	2	1	0	2	12
1745	-30.77	0.08	-0.31	-30.46	10	26	7	2	32	0	2	2	1	0	9
1755															
1770															

Table S1. *Cont'd. Abbrevations: TCT = Taxodiaecaea, Cuppressaeuae, Taxacaeae, PP = production potential, PI = Production Index, HI = Hydrogen Index, OI = Oxygen Index, TOC = Total Organic Carbon, Ro% = Reflectance in oil.*

Depth(mbss)	TCT	Bisaccate pollen	*Caryapollenites spp.*	S1 (mg/g)	S2 (mg/g)	S3 (mg/g)	Tmax ºC	PP (mg/g)	PI (wt ratio)	HI (mg)*	OI (mg)**	TOC (wt%)	Vitrinite reflectivity (%Ro)	stdev reflectivity
1640	83	4	4	0.22	0.99	2.04	398	1.2	0.18	43	89	2.3	0.24	
1645	87	10	1											
1650	92	4	1	0.18	0.92	1.67	406	1.1	0.16	177	321	0.52	0.23	0.03
1655	84	13	2	0.24	0.95	1.63	398	1.19	0.2	44	76	2.15	0.28	
1665	86	10	3	0.29	0.71	2.35	396	1	0.29	42	139	1.69	0.26	
1670	82	11	7	0.18	0.9	1.51	400	1.08	0.17	57	96	1.57	0.29	0.02
1675	85	11	2											
1680	88	7	2	0.12	0.6	1	403	0.72	0.16	63	104	0.96	0.28	0.04
1685	90	6	2	0.11	0.73	1.5	398	0.84	0.13	54	110	1.36	0.22	0.04
1690	91	3	3	0.12	0.72	1.27	400	0.84	0.14	56	98	1.29	0.24	0.04
1695	84	9	4	0.1	0.44	1.26	405	0.54	0.19	33	93	1.35	0.3	0.05
1700	72	5	10	0.11	0.62	1.26	408	0.73	0.15	295	600	0.21	0.24	0.03
1705	66	5	14	0.12	0.69	1.94	399	0.82	0.15	43	120	1.62	0.24	0.02
1710	51	0	38	0.12	0.72	0.94	402	0.84	0.14	76	99	0.95	0.26	0.03
1720				0.21	1.8	1.45	396	2	0.1	101	82	1.77	0.25	0.07
1725	38	1	40	0.26	4.8	1.27	398	5.06	0.05	186	49	2.58	0.22	0.07
1730	68	8	19	0.6	5.71	1.2	397	6.31	0.09	381	80	1.5	0.25	0.03
1735	69	1	22											
1740	80	4	11	0.74	9.4	0.73	390	10.13	0.07	267	21	3.52	0.26	0.03
1745	81	3	10											
1755													0.27	0.04
1770				0.27	2.43	1.33	394	2.7	0.1	91	50	2.67		

7

Ecological preferences of Paleocene - Eocene dinoflagellates

Abstract

Organic dinoflagellate cysts (dinocysts) are widely used in shelf and open marine settings for biostratigraphy and reconstructions of past environments and environmental change. For the recent past this can be done with relative confidence as the ecology of extant species is reasonably well known, but this is less certain for the early Cenozoic. Recent progress in geochemical and sedimentological environmental proxy development and applications in tandem with dinocyst assemblages allows us to review early Paleogene dinocyst records and assess the environmental preferences of their associated dinoflagellates. Here we aim at extracting empirical relations for the abundance of previously proposed paleoecological dinocyst groups as a function of independent environmental proxies for, e.g., sea surface temperature and terrestrial organic matter input. For this, we use published dinocyst assemblage data from 10 sections worldwide spanning the Paleocene – Eocene transition, for which independent environmental proxy data is available. As expected, much of the variability in the assemblages cannot unequivocally be tied to unique environmental variables. Many dinocysts show some relation to one or several of the reconstructed environmental variables. However, qualitatively, the available independent proxy data support most, although not all, of the traditional paleoecological interpretations of dinocyst ecogroups. Notably, we confirm earlier views that *Apectodinium* required Sea Surface Temperature (SST) in excess of 20 °C, but also show that epicystal Goniodomideae are largely restricted to SST above 25°C and *Florentinia reichartii* is only abundant between 30 and 35 °C. Other groups apparently favor either a limited (*Spiniferites*) or high (*Senegalinium*) amount of terrestrial input, which can be related to multiple factors, such as salinity, nutrient levels or suspended sediment load (i.e. murkiness). Crucially, the validation of ecological signals by independent environmental proxies puts additional emphasis on the unique value of dinoflagellate cyst assemblage ecology studies in deep time.

1. The Paleogene and Paleocene – Eocene Thermal Maximum

The early Paleogene greenhouse has climatological and environmental characteristics that may serve as analogues for future climate change and for these purposes has been extensively studied (e.g., Zachos et al., 2008). Most well known is the Paleocene – Eocene Thermal Maximum (PETM, 56 Ma), a period of geologically brief (170 kyr) global warming of 4-5 °C (e.g., Dunkley Jones et al., 2013), associated with massive input of ^{13}C-depleted carbon (Dickens et al., 1995). The PETM is further characterized by ocean acidification (Penman et al., 2014; Zachos et al., 2005), globally expanded oxygen minimum zones (Dickson et al., 2012; Sluijs et al., 2014), local photic zone euxinia (Frieling et al., 2014; Sluijs et al., 2014, 2006) and an intensified hydrological cycle (Pagani et al., 2006b; Schmitz and Pujalte, 2007). In recent years, significant progress has been made in dinoflagellate cyst assemblage studies and several high-resolution records across the globe have been generated across the PETM (Frieling et al., chapter 5; Harding et al., 2011; Kender et al., 2012; Sluijs and Brinkhuis, 2009; Sluijs et al., 2011). These records typically rely on dinoflagellate cyst assemblage characteristics to infer ecological signals.

The amount of dinocyst species found for the extended period of time from the late Paleocene through the Early Eocene is often impractical for use in paleoenvironmental reconstructions, especially in periods of high diversity such as the early Paleogene (MacRae et al., 1996). Therefore authors have attempted to group dinocysts in so-called eco-groups or select species to which specific affinities are attributed (e.g., Brinkhuis, 1994; Pross and Brinkhuis, 2005; Sluijs et al., 2005; Torricelli et al., 2006). The groups or complexes are usually centered around one genus, and include genera and species with similar taxonomical affinities. For example, the *Senegalinium* complex is thought to be tolerant of lower than

marine salinity (e.g., Barke et al., 2011; Sluijs and Brinkhuis, 2009).

Here, we aim to expand the already significant knowledge of Paleocene – Eocene dinocyst paleoecology by compiling data from published PETM sites in the mid and high latitudes on both hemispheres (Figure 1, Table 1), supplemented by data from the equatorial Atlantic (Frieling et al., chapter 3, chapter 5). For many of the sites used here, independent environmental proxy data is available, which allows for direct comparison to environmental variables and dinocyst response. We aim to qualitatively review the traditional ecological views of Paleogene dinocyst groups by directly comparing global dinocyst assemblage data to independent environmental proxies for parameters such as temperature, terrestrial influence and shore proximity.

2.1. Dinocyst Paleoecological Potential

Dinoflagellates are an ecologically diverse unicellular eukaryote plankton group. They inhabit essentially all aquatic environments from fresh water to hypersaline lagoons, from oligotrophic gyres to upwelling zones, and some thrive in tropical waters whereas others have colonized sea ice systems (Zonneveld et al., 2013). Many free-living dinoflagellates have complex and often poorly understood life cycles; a fraction (13-16%) of free-living (i.e. planktonic) dinoflagellates produce preservable organic hypnozygotic cysts, or dinocysts, as an obligatory part of their sexual reproduction cycle (Evitt, 1985; Fensome et al., 1996). Although temporary (month scale) encystment may occur in some dinoflagellates, typically induced by stress, these temporary cysts are markedly different from the resting cysts and usually have few morphological features (e.g., Peña-Manjarrez et al., 2005). The hypnozygotic cysts have species-dependent characteristic morphologies, are often highly resistant to oxic and acid degradation and show excellent preservation potential. Palynomorphs that can be confidently identified as dinocysts have been preserved in deposits as old as the early Triassic (MacRae et al., 1996), although molecular evidence suggests dinoflagellates were

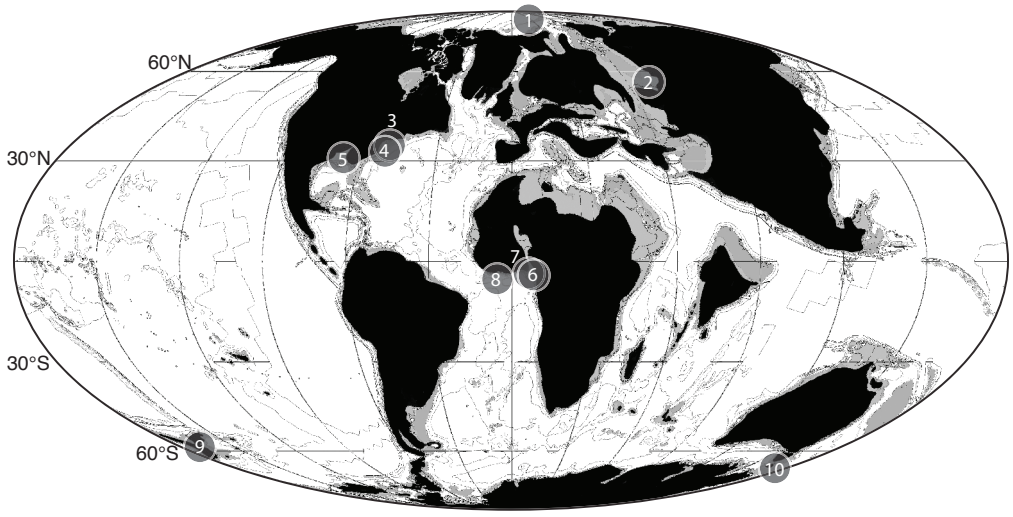

Figure 1. *Map of sites used in this study. 1. Arctic Coring Expedition (ACEX), Lomonosov Ridge 2. Well 10, West Siberian Sea, 3. Wilson Lake, New Jersey 4. Bass River, New Jersey 5. Harrell Core, Gulf of Mexico 6. IB10 cores, Nigeria, 7. Sagamu Quarry, Nigeria 8. ODP Site 959D, Cote d'Ivoire Ghana Transform Margin 9. Tawanui, New Zealand 10. IODP Site 1172D, South Tasman Plateau. See Table 1 for references.*

likely around before this time (Moldowan et al., 1996).

The very rich fossil record and the high turnover rates make the group an excellent biostratigraphic tool, particularly in marginal marine settings and polar environments (e.g., (Bijl et al., 2013b; Eldrett et al., 2004; Gradstein et al., 2012). In recent years, significant progress was made in revealing the molecular composition of the cysts (Bogus et al., 2014, 2012) and efforts to analyze their stable carbon isotope composition are in progress (Sluijs et al., 2007b). In addition, dinocysts are widely used as paleoenvironmental indicators on all time scales (De Vernal et al., 2005; Donders et al., 2009; Matthiessen et al., 2005; Sluijs et al., 2005). Because of the high diversity in ecological preferences within dinoflagellates, dinocyst paleoecology is regarded as a valuable and widely applicable method, especially suitable for marginal marine deposits, in which carbonate microfossils are often scarce or poorly preserved.

2.2 Taxonomic dinocyst classification

For extant dinoflagellates many cell-cyst relations are now known (e.g., Head, 1996; Zonneveld et al., 2013), but for extinct species, this relation is impossible to resolve. Therefore, distinct nomenclature is in use for both the motile and resting cyst stages (Evitt, 1985). Paleontological dinocyst taxonomy is based on morphological characteristics of the cyst, which tracks morphological characteristics in its motile dinoflagellate. Dinoflagellate cell membranes are typically built up from a number of plates (20-30). These plates are typically copied onto the dinocyst during encystment (e.g., Kokinos and Anderson, 1995). Morphological variations in these plates and their configuration compose the backbone of the dinoflagellate and dinocyst taxonomies. For example, the number of plates on the antapex of the cyst is one criterion to define the order (Peridiniales or Gonyaucales). In cysts, the position and shape of the archeopyle, which is the gap left by the plate(s) that (partially) detach when the cell leaves the cyst, is a criterion often associated with taxonomical separations on the family to genus level (e.g., (Evitt, 1985). Genera and species are then often determined based on position, shape and size of ornamentations on the cysts. Particularly with extinct taxa, however, it remains uncertain to which extent morphological variability truly reflects species diversity, or rather phenotypic plasticity or in some cases even preservation (e.g., Sluijs et al., 2005). Indeed, morphological variations in ornamentation often mark a morphological continuum between endmembers. In several modern species, these are related to environmental changes such as salinity and temperature (e.g., Ellegaard et al., 2002) and may therefore serve to reconstruct environmental parameters (Mertens et al., 2009). Dinocyst paleoecology in the early Cenozoic has, hence, dominantly been applied on the level of dinocyst genera or groups of related genera (e.g., Harding et al., 2011; Schiøler et al., 1997; Sluijs and Brinkhuis, 2009).

2.3 Translation of dinoflagellate communities and ecological signals to sedimentary records

In addition to taxonomic challenges, the dinocyst fossil record presents some important limitations. Cyst assemblages in sediments reflect a small part of the production of cyst-producing dinoflagellates in the overlying water column, while this underlies the environmental parameters that most studies aim to reconstruct.

Part of this discrepancy is connected to the actual production of the cysts in the upper water column, e.g. oceanic and neritic species are likely to have different encystment and excystment strategies (Dale and Dale, 1992; Dale, 1983; Matthiessen et al., 2005).
As of yet, it is also not completely clear how dinoflagellate cysts reach the sediment. Most organic matter reaches the sediment water interface via flocculates (marine snow) or fecal

pelleting of zooplankton, and although dinoflagellate cysts are not ubiquitous in marine snow or fecal pellets (Alldredge et al., 1998; Bursa, 1963; Mudie, 1996; Reid and Boalch, 1987) this remains the most likely transport mechanism. Alternatively, empty cysts may be transported to the sediment as dinoflagellates complete their life cycle in the water column (e.g., Harland, 1983) although this trait is likely more common in oceanic species. In addition, encystment in species is governed by a diverse set of factors including nutrient concentration, light and temperature (Anderson et al., 1985, 1984; Blanco, 1995; Nagai et al., 2004). Upon reaching the sediment, oxidation may bias the assemblage (Kodrans-Nsiah et al., 2008; Zonneveld et al., 1997b).

It should also be emphasized that although many dinoflagellates show very strong seasonal responses to light, nutrients, temperature and salinity and interact with biota that show equally strong relations to these parameters, typically none of these seasonal signals can be extracted from the sedimentary record. Depending on local factors, bioturbation may erase up to millennial scale variations. In more distal regions, notably on the outer shelf, slope and continental rise, transport often plays a role in shaping the sedimentary plankton record and dinocysts are not an exception (e.g., Dale and Dale, 1992).

Improving insights in the relation between motile dinoflagellate cells in an ecosystem, the production of dinocysts and their incorporation in the sediment record increasingly allows to resolve smaller scale, i.e. species interactions and affinities (e.g., de Souza et al., 2014; Jephson et al., 2012). For example, the proportion of heterotrophic cysts is likely related to the production of prey in the surface waters and thus nutrient supply (e.g., Naustvoll, 2000; Sherr and Sherr, 2007). Absolute numbers of cysts have therefore been used to track productivity in surface waters (Dale, 2009). However, heterotrophic cyst production likely also depends on complex interactions and competition with other (heterotrophic) plankton groups. This may lead to biases in the proxy.

Despite these limitations, dinocyst assemblages have yielded valuable and unique reconstructions of paleoenvironments. The strength of the relations between species and environment can be further established by determining empirical relations with environmental parameters (De Vernal et al., 2005). Indeed, many species have distinct environmental affinities in the modern ocean (Zonneveld et al., 2013). Transfer functions derived from core-top sediment assemblages and environmental parameters have been successfully applied to the recent past (De Vernal et al., 2005). For deep time, however, we have to rely on the relation of dinocysts and dinocyst groups to independent environmental proxy data. In this contribution, we aim to deduce environmental preferences of Paleogene dinoflagellates and their cysts by using proxies for environmental parameters, although it is obvious that these proxies have uncertainties as well.

3. Data and methodology

3.1. Available dinocyst assemblage and proxy data

We use published data from 10 sections (Table 1, Figure 1), each with independent stratigraphic control in the form of carbon isotope stratigraphy. The stratigraphic distinction we make for this study is between Paleocene, Eocene and PETM data, which is taken from the published literature. For each of the 10 sections, there is dinocyst data available with determinations at least to the genus level and in most instances to the species level (n of samples = 624). In order to use statistically sound measurements of dinocyst assemblages, we typically include only samples with at least 200 counted cysts (n = 544), which can then be used for direct comparison between dinocyst assemblages and proxy records.
As can be seen from Table 1, only a limited number of proxy data has been generated on all

included sites. Also, for some records, two or more independent proxies have been applied to reconstruct the same environmental parameter. We therefore discuss the variability of assemblages in relation to the environmental variable the proxy record represents, i.e., TEX_{86} > Sea Surface Temperature (SST).

Furthermore, it is important to note that especially the tropical sections show a marked drop in diversity and dinocyst numbers during the PETM, which is likely caused by heat-stress (Frieling et al., chapter 3, chapter 5). The counts for these samples are often low and hence would be typically excluded from quantitative analyses. In contrast with other dinocyst assemblage studies we choose to include these samples in our analyses as they reflect meaningful ecological information and do not simply represent bad data.

Dinocyst assemblage studies typically normalize the abundance of dinocysts relative to the total, resulting in relative abundances. The most important disadvantage of this method is the closed-sum effect, i.e. the relative increase in one species could in fact be due to a decrease in the absolute abundance of another species and vice versa. Ideally, intra-site assemblage studies should therefore be supplemented by quantitative numbers or fluxes, rather than only relative abundances. We here use the relative abundance because it allows for straightforward comparisons between sites, with the note of caution that in some cases the closed-sum effect may play a role in observed trends. However, absolute quantitative data (in cysts per gram of sediment) presented in the source studies (Table 1) typically mimic the trends recorded in the relative abundances (e.g., Sluijs and Brinkhuis, 2009) indicating that the closed-sum effect is a minor factor. Regardless, future work may focus on dinocyst accumulation rates, allowing for quantitative comparisons of several sites although this remains difficult at marginal marine sites with variable sediment accumulation rates.

3.2 Independent environmental proxies

For all study sites, independent geochemical and sedimentological environmental proxy data is available, generated in parallel with the dinoflagellate assemblages, typically although not exclusively, on the same samples. Each proxy is linked to one environmental parameter using biogeological experiments or core top calibrations from the modern ocean. Reconstructions based on these data are not always unambiguous because of potential diagenesis (e.g. remobilization of trace elements under anoxic conditions), uncertainties regarding calibrations (for proxies with modern core calibrations top such as the glycerol dibiphytanyl glycerol tetraether (GDGT) based proxy TEX_{86}), or the potential influence of environmental parameters other than the target parameter. Therefore, it is important to note that we assume that the independent proxy data correctly reflect their target parameter. However, we present these data in bins reflecting a range of values, which is expected to minimize this uncertainty.

We use TEX_{86} for temperature reconstructions (Schouten et al., 2002). The BIT index is used (Hopmans et al., 2004), in tandem with other proxies, such as terrestrial (pollen and spores) over marine (here dinocysts and organic linings of foraminifera), palynomorphs (e.g. Sluijs and Dickens, 2012) to reconstruct terrestrial input. Weight percent total organic carbon (TOC wt%) and organic carbon over total phosphorus ratio (Corg/Ptot) (Ingall and Van Cappellen, 1990) provide insight into productivity and seawater oxygen concentrations. The weight percent carbonate (carb%) and coarse fraction (% >63 μm) are used as a proxy for shore proximity and/or sea level (e.g., Sluijs and Brinkhuis, 2009). We also explore the use of the potential stratification proxy based on the relative abundance of the crenarcheol regioisomer relative to that of GDGT-0 (e.g., Inglis et al., 2015).

3.3 Methodology

3.3.1 Dinocyst grouping

As a starting point for our analyses, we use the grouping of dinocysts as defined by Sluijs and Brinkhuis, (2009), who studied the PETM in two sections from the New Jersey Shelf. We apply some minor modifications and additions to better accommodate variability of all sections included here (see Table 2 for groups and selected genera). These include sections from polar to equatorial regions, and from coastal to open marine settings. This should, hence, include most of the important groups from this time interval, enabling a complete analysis on which environmental factors were dominant in determining the distribution of cyst-forming dinoflagellates.

The ecological grouping from Sluijs and Brinkhuis, (2009) is itself largely derived from previous work (Brinkhuis, 1994; Pross and Brinkhuis, 2005; Schiøler et al., 1997; Sluijs et al., 2005). In addition to the grouping of Sluijs and Brinkhuis, (2009), the diversity in our data allows us to separate Peridinioid cysts in 4 groups: Protoperidinioids (cf., Guasti et al., 2005) (as *Lejeunecysta*-group), *Cerodinium*, *Phthanoperidinium* and *Senegalinium*. The remaining cysts, mostly Gonyaulacoid cysts with low ornamentation are divided on morphological parameters. We group G-cysts with proximal ornamentation according to archeopyle shape (apical or precingular). Groups and genera are listed in Table 2.

3.3.2 Proxy binning

To optimally test for ecological preferences, we have divided the full range of proxy values

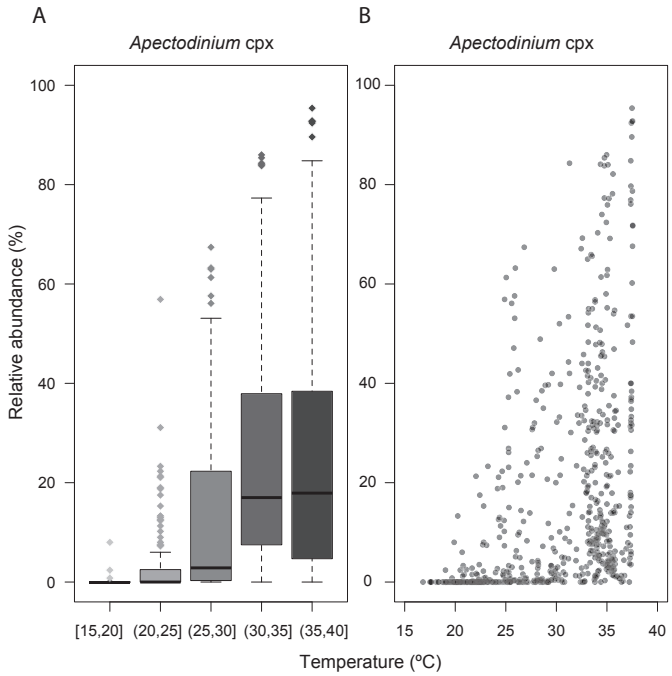

Figure 2. *Example of data binning: Relative abundance of Apectodinium versus TEX_{86} temperature.* ***A.*** *Data in bins.* ***B.*** *Raw data.*

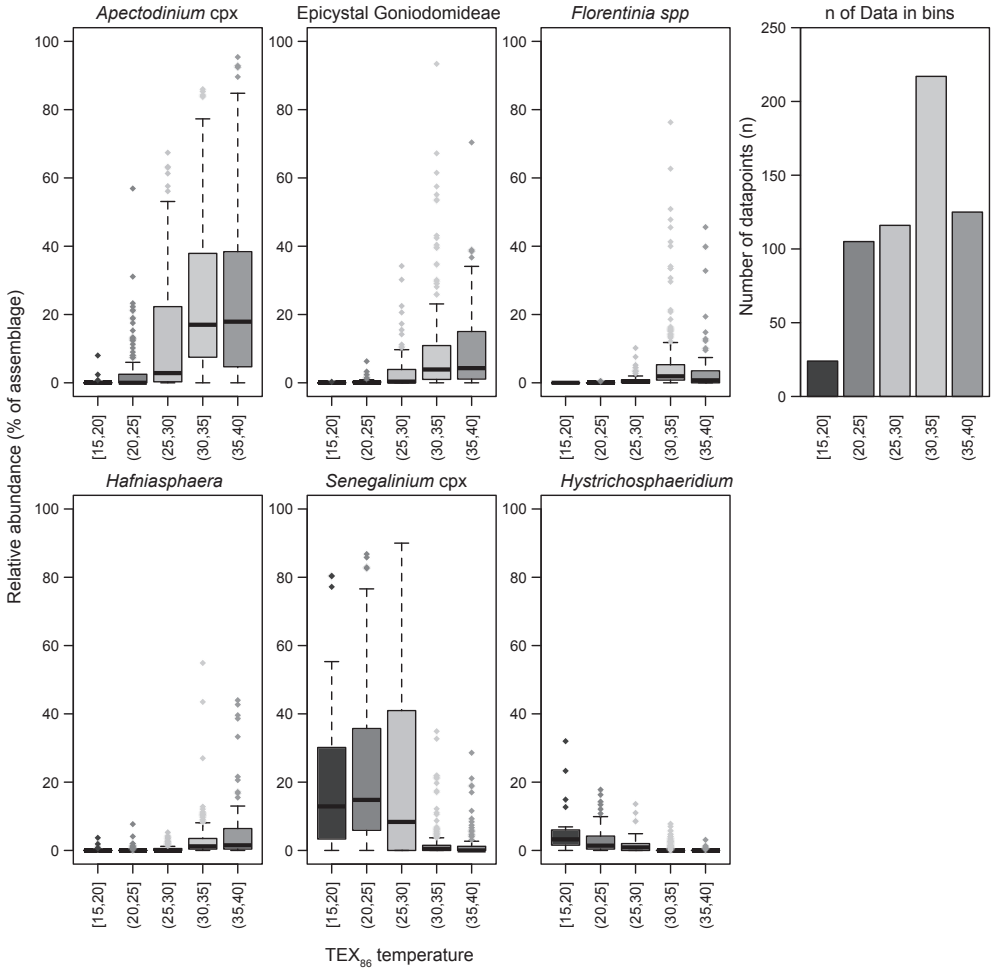

Figure 3. *Relation of selected species with TEX_{86} and number of data in TEX_{86} bins*

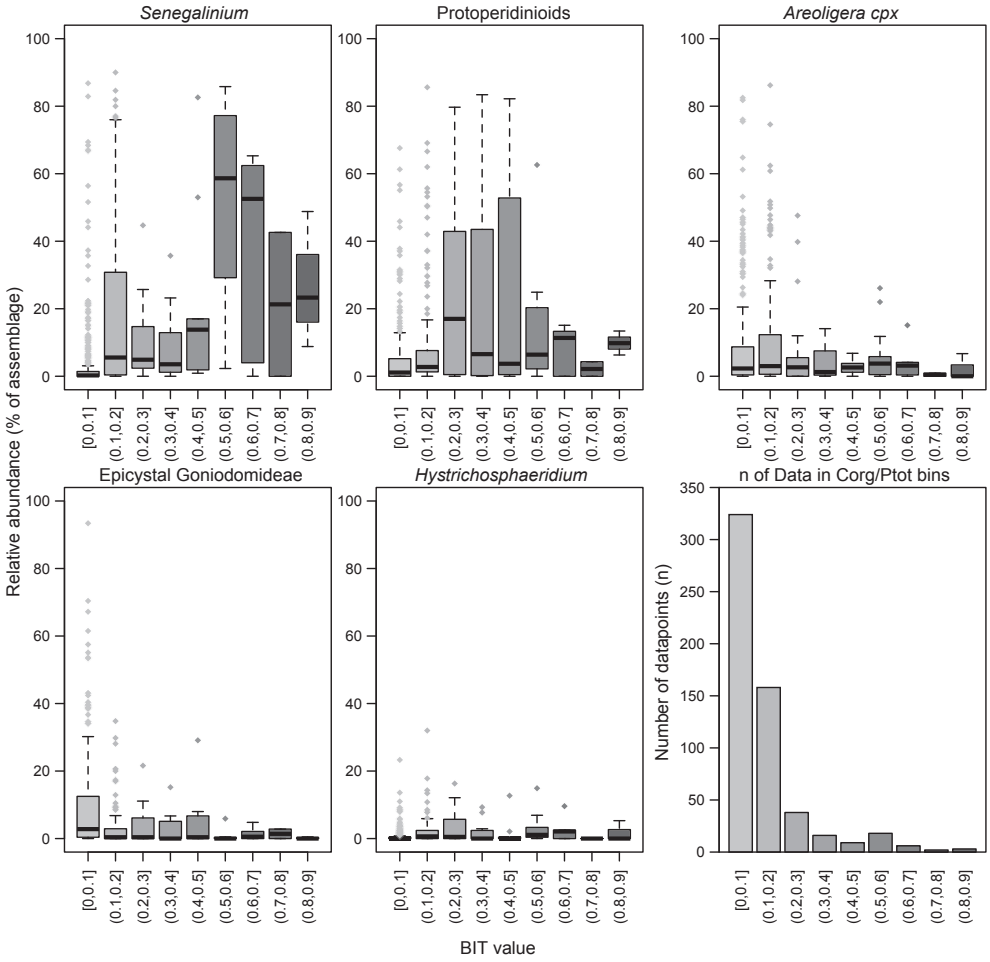

Figure 4. *Relation of selected species to BIT and number of data points in each bin.*

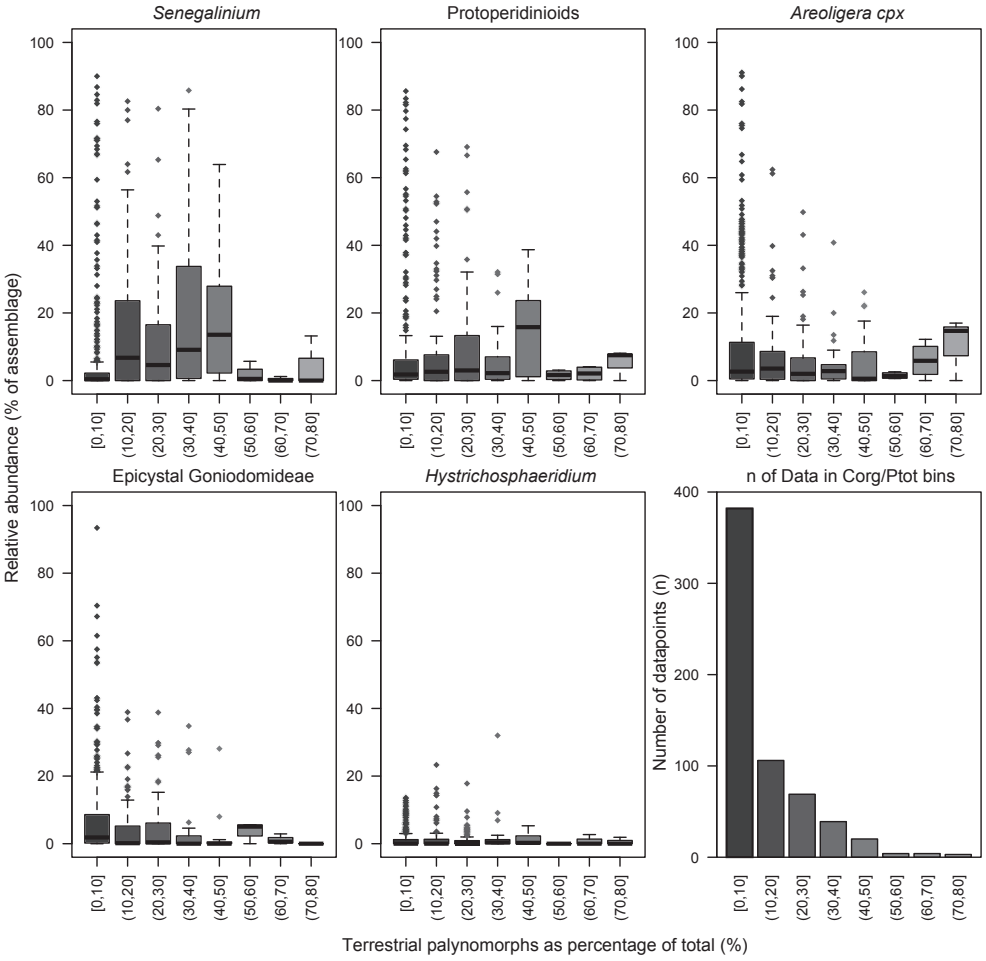

Figure 5. *Relation of selected species to Marine Terrestrial ratios and number of data points in each bin.*

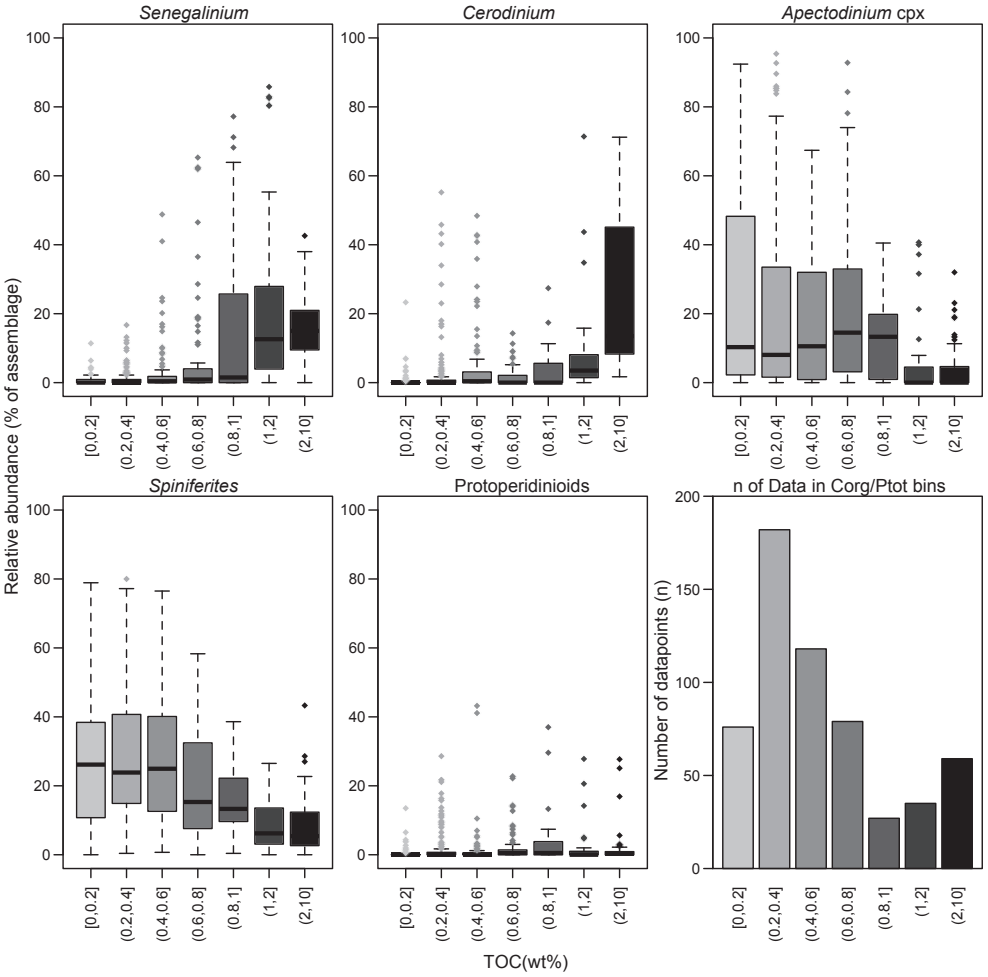

Figure 6. *Relation of selected species to Total organic carbon content (TOC) Number of data points in each bin.*

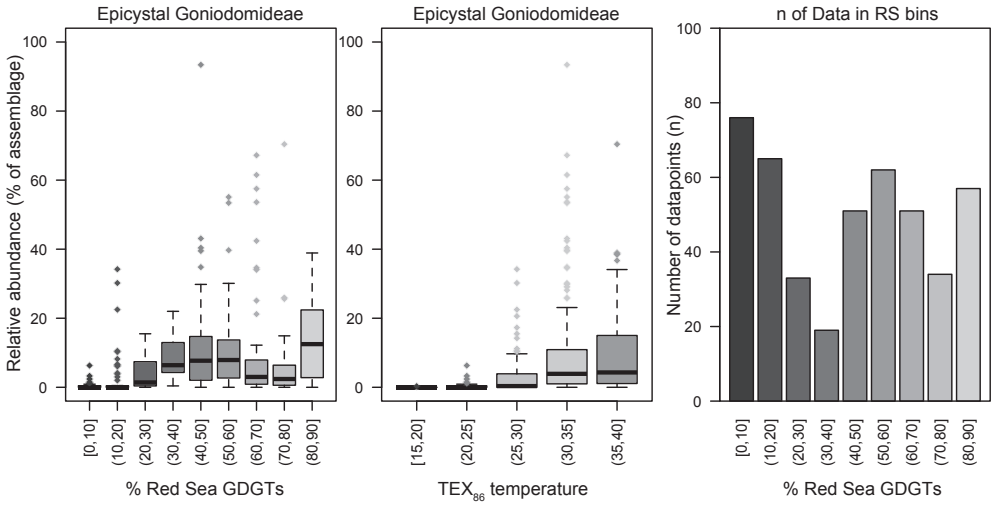

Figure 7. *Epicystal Goniodomideae relation to %Red Sea GDGTs and TEX_{86} and Number of data points in %Red Sea bin, for number of data in TEX_{86} bin, see Figure 2.*

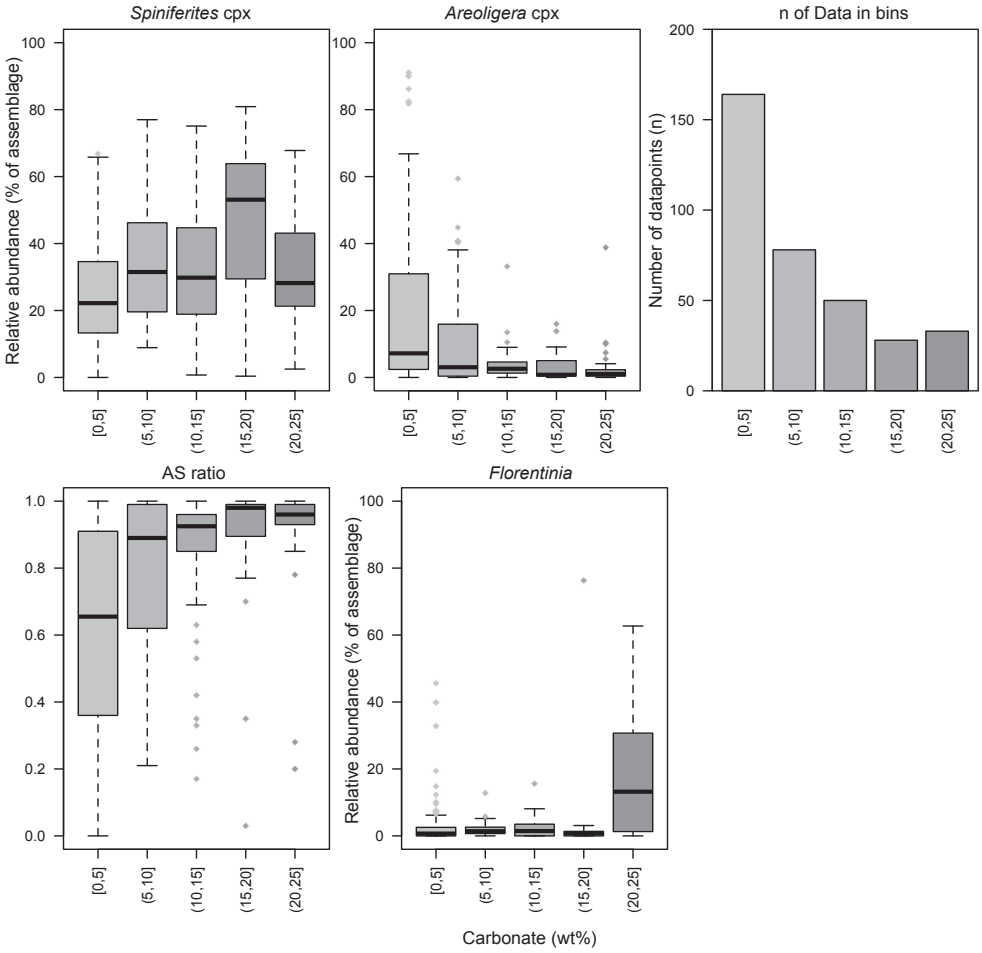

Figure 8. *Relation of selected species to carbonate content and number of data points in each bin.*

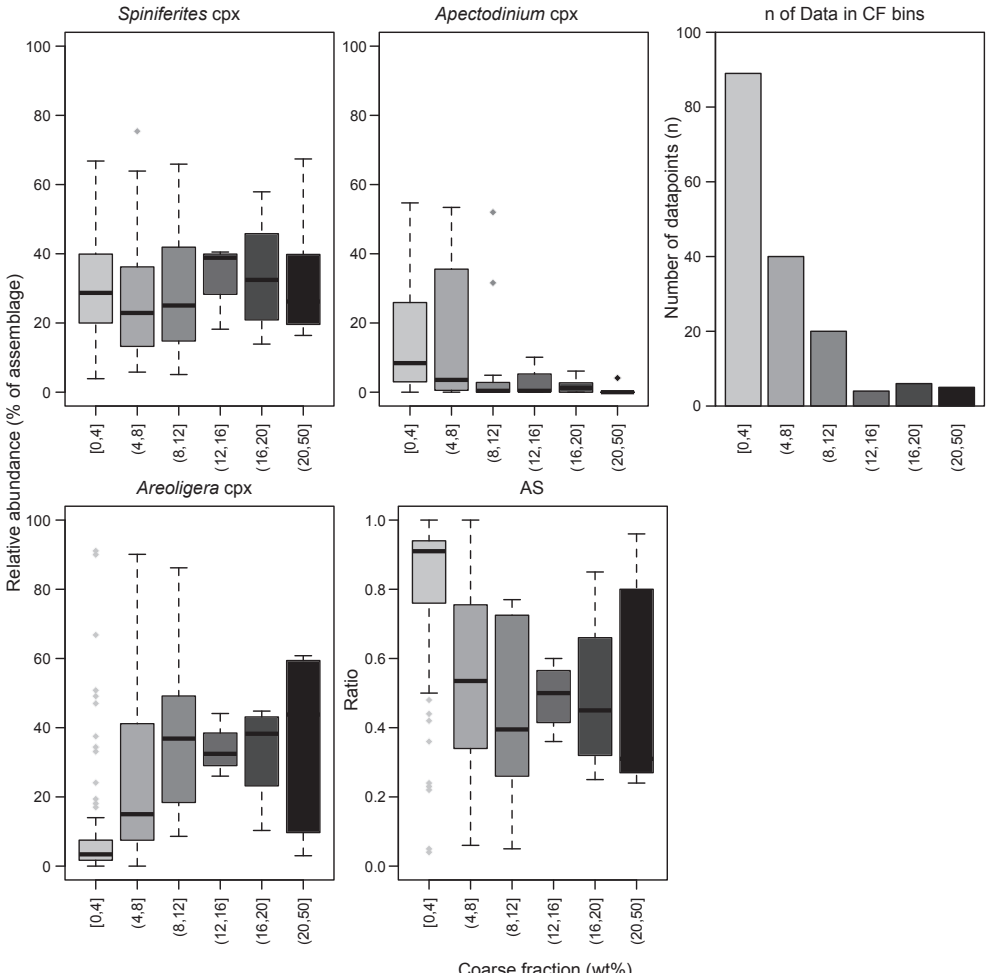

Figure 9. *Relation of selected species to coarse fraction (>63µm) and number of data in each bin.*

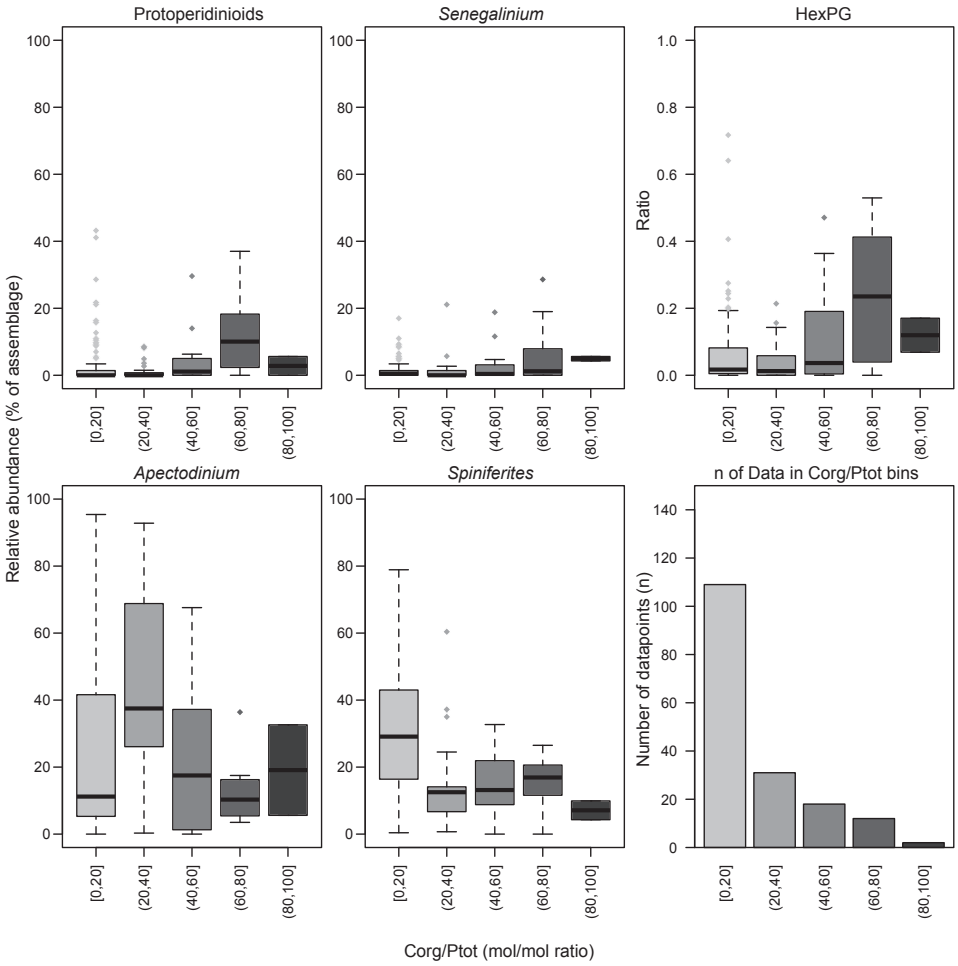

Figure 10. *Relation of selected species to Corg/Ptot ratio and number of data in each bin.*

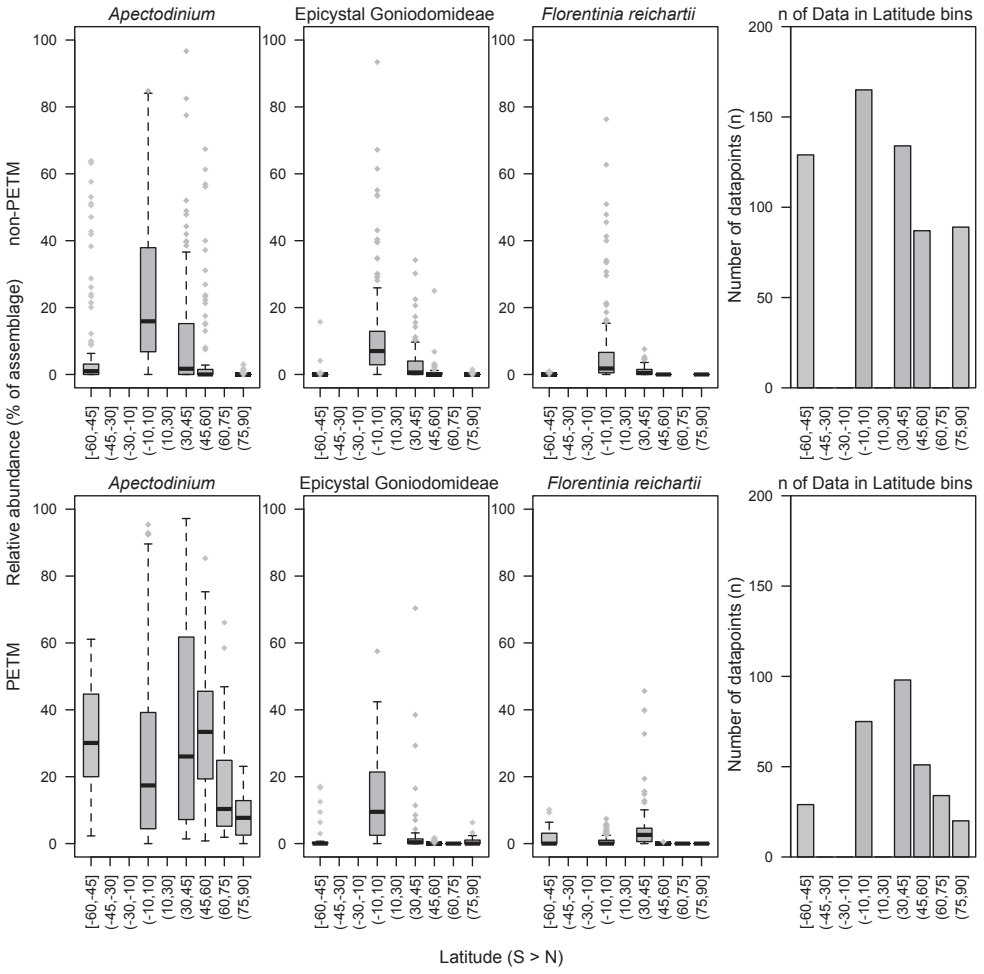

Figure 11. *Relation of selected species to latitude and number of data in each bin. Top row represents data outside the PETM, bottom row within the PETM.*

into 5-10 bins. This allows for proper readability of illustrations as well as a simple definition of uncertainty in the recorded relations between abundance and environmental parameter (see Fig. 2a and b). Due to the strong non-normal distribution of some proxy data, the bins are not of equal sizes and hence we include the number of data in each bin in the plots. Similarly, for some proxies (e.g. TOCwt%), the high and low values have proportionally likely very different impacts. Log-transformation of the data could counteract these effects, but we choose to separate the data into bins of unequal width.

4. Discussion and results

4.1 Temperature

Temperature dependent behavior is well known for many biota and species of dinocysts have been successfully employed as relative temperature indicators in a number of sections both in recent and deep time sediments (Brinkhuis et al., 1998). Indeed, a number of dinocyst groups in our data appear temperature limited (Figure 3a, b, c). For example, *Apectodinium* does not occur in great abundance below 20 °C (Figure 3c). *Apectodinium* expanded its geographical range polewards (Bujak and Brinkhuis, 1998; Crouch et al., 2001; Sluijs et al., 2007a), which has been explained as a direct response to temperature (Bujak and Brinkhuis, 1998). For some locations and periods, this may indeed be the case (Frieling et al., 2014), but for most locations other environmental factors are considered more important in controlling its' abundance (Sluijs and Brinkhuis, 2009).

Epicystal Goniodomideae and *F. reichartii* are even less low-temperature resilient and have not been recorded below 25 °C (Figure 3b) and 30 °C (Figure 3c), respectively. It is implicit from our data that these lower temperature bounds play a vital role in poleward species migrations during the PETM such as that of *Apectodinium*. Epicystal Goniodomideae and *F. reichartii* show a similar temperature response and both arguably have even higher optimal temperatures than *Apectodinium*. Notably, *F. reichartii* exhibits a narrow distribution of optimal temperatures, which may imply that it is more sensitive to small temperature changes and less well adapted to fluctuating or adverse environmental conditions. In this light, *Apectodinium* has a much wider optimal temperature range, suggesting high adaptability to such conditions, which partly explains its global expansion during the PETM.

Some genera within complexes show specific relations to temperature, most notably seen in *Hafniasphaera* in the *Spiniferites* complex. *Hafniasphaera* has a high optimal temperature and does not occur in great abundance below 25 °C. This observation is important since *Hafniasphaera* is considered a tropical species and also migrates during the PETM.

Limitations to high temperature also appear from our data set, although much less obvious than the low temperature bound. However, this is not necessarily surprising from a modern ocean perspective as taxa that tolerate high-latitude temperatures are often not intolerant to conditions at lower latitudes (Sunday et al., 2011). As a consequence, higher temperatures for high latitude species typically prove less of a challenge than low temperatures for low latitude species (Tewksbury et al., 2008).

Senegalinium is more abundant at lower temperatures (Fig. 3f). However, this result is almost certainly influenced by the, in our dataset, unique combination of relatively low salinity and low temperature in the Arctic Ocean (Sluijs et al., 2008b); salinity likely played a more crucial role (see section 3.2). An affinity to lower temperatures is also observed in *Hystrichosphaeridium* (Fig. 3g), which unlike the trend observed in *Senegalinium*, cannot be explained by lowered salinity, as it negatively correlates to the terrestrial organic matter input proxies BIT and marine terrestrial (MT) palynomorph ratio (Fig. 4e, 5e).

4.2 Salinity and terrestrial input

Several groups show a relation with BIT (Fig. 4) and terrestrial palynomorph fraction (MT) (Fig. 5). As expected, periods of high terrestrial input tend to favor species in the *Senegalinium* complex (*sensu* Sluijs and Brinkhuis, 2009), a group that is particularly abundant in the Arctic. The opposite appears to be true for the *Areoligera* complex (cpx), which supports previous studies that report high abundance of this group associated with transgressive systems tracts (Iakovleva et al., 2001; Schiøler et al., 1997; Sluijs et al., 2008a). Also Epicystal Goniodomideae show a weak anti-correlation with BIT and MT. This is intriguing since Epicystal Goniodomideae have been associated with transgressive system tracts (e.g., Sluijs et al., 2008b) and very high salinity environments (Zonneveld et al., 2013) in the modern and the Paleogene (Pross and Brinkhuis, 2005). Considering the weak anti-correlation with BIT and MT we surmise that high relative abundances of this group in Paleogene sediments are thus particularly associated with elevated salinity levels, likely because they are among the few dinoflagellates producing cysts under such (seasonal) conditions. Notably, Gonyaulacoid cysts with an apical archeopyle show highest abundances in samples with intermediate values for BIT and TM ratios (Fig. 4b,5b). This could indicate a certain degree of tolerance to lower than marine salinity in this group.

4.3 Nutrient levels and productivity

Sluijs et al., (2005) reviewed the application of the relative abundance of Peridinioid (P) cysts relative to Gonyaulacoid (G) cysts to reconstruct the availability of nutrients. This PG ratio is based on the observation that in the modern ocean, many P taxa are heterotrophic, while G dinoflagellates are autotrophic. Originally, however, the ratio between P and G cysts was defined as the number of species rather than specimens, to assess salinity (Harland, 1973). Indeed, P-cysts *Senegalinium*, *Phthanoperidinium*, *Deflandrea* and *Cerodinium* were tolerant to low salinity (Barke et al., 2011; Brinkhuis et al., 2006; Sluijs et al., 2006). But they were presumably heterotrophic feeding on primary producers in coastal or upwelling environments (e.g., Brinkhuis, 1994; Firth, 1996; Sluijs et al., 2005), similar to many, although not all (Dale and Fjellså, 1994), of their modern Peridinioid counterparts.

The *Protoperidinium* family of obligate heterotrophic dinoflagellates produces typical brown-pigmented cysts, are an exclusively heterotrophic group in the modern ocean and often found in higher abundances in upwelling zones (e.g., Marret, 1994; Zonneveld et al., 2013). Across the PETM, and in the entire early Paleogene, however, Protoperidinioid dinocysts are usually not very abundant. Evolution and/or expansion of Protoperidinioid-dominated systems such as found in Arctic and Antarctic regions was likely tightly coupled to the availability of niches (e.g. sea ice) and prey species (e.g. diatoms) (Houben et al., 2013) and the same is possibly true for upwelling zones.

We also find that some sections, particularly in the tropical Atlantic are characterized by higher relative abundances of Protoperidinioid cysts during the PETM. Although relative percentages are high, the absolute abundances are low and hence this may represent a subsurface signal during extreme warming rather than an indication of elevated nutrient concentrations. Therefore, it can be that, in general, the ratio of heterotrophic over autotrophic cysts tracks total productivity (Dale, 1996), but not necessarily dinoflagellate productivity.

Using terrestrial input (marine terrestrial ratio) and TOC content as general indicators for the amount of nutrients and productivity, it appears that *Apectodinium* behaves differently from other Peridinioid genera (Fig. 6). The abundance of *Apectodinium* has previously been used to argue that productivity was enhanced during the PETM(e.g., Sluijs et al., 2007b).

However, the nutrient or trophic affinity of *Apectodinium*, the most abundant P-cyst genus in many PETM sections, is not well resolved. *Apectodinium* morphologically stands out relative to other Peridinioid genera analyzed here by shape of the archeopyle. Although *Apectodinium* may occur in great abundance during the PETM, it apparently does not particularly favor environments with very high terrestrial input or high organic carbon percentages (Fig. 6c & Supp. Fig. 1 & 5) in contrast to Peridinioid cysts with a hexagonal archeopyle (HexP). We argue that, in the light of uncertainty involved in the affinity of *Apectodinium*, using the HexP over Gonyaulacoid cysts in addition to the traditional P/G ratio provides a range estimate for the relative abundance of the heterotrophic group and hence nutrient availability.

4.4 Stratification and turbulence

Inglis et al., (2015) showed a remarkable co-occurrence of "Red Sea"-type iGDGT distributions (%RS) and Epicystal Goniodomideae at ODP Site 1172. Representatives of Epicystal Goniodomideae are still abundant in the modern ocean and typically occupy warm stratified, hyperhaline, but also meso- and polyhaline waters (Zonneveld et al., 2013). Although there are some pitfalls, this is potentially one of the first molecular tools for the identification of hyperhaline and/or stratified waters.

Although the match between Epicystal Goniodomideae and %RS at Site 1172 is very intriguing, the translation to global dinoflagellate assemblages is more complex (Fig. 7). In general the Epicystal Goniodomideae are indeed associated with higher %RS, but both the fractional abundance of GDGT-0 and the Crenarcheol regioisomer are also strongly correlated to temperature (Schouten et al., 2002). Furthermore, high %Red Sea is not exclusively associated with Epicystal Goniodomideae and absence of either one does not preclude the presence of the other. High temporal abundances of Epicystal Goniodomideae are recorded at both Site 959 and Dahomey Basin sites, but Site 959 is characterized by continuous presence of high %RS, whereas the Dahomey Basin sites record more normal marine distributions. Contrasting with the view of stratification, Sluijs et al., (2011) speculated that the high transient abundance of the Epicystal Goniodomideae at Site 1172 may be the result of increased storminess. This hypothesis is based on the notion that modern epicystal Goniodomidaea blooms may relate to sediment resuspension during a storm (Siringan et al., 2008; Villanoy et al., 2006, 1996). Combined, the high abundance of Epicystal Goniodomideae may result from stratification and/or high storm activity, both of which are fairly common in tropical regions and may become more common at higher latitudes at higher temperatures.

4.5 Oxygen levels

Anderson et al., (1987) found that absence of oxygen often prevents excystment, but the extent of the effects of very low oxygen concentrations may vary between species (Keafer et al., 1992). Anoxic zones in the modern ocean are expanding and therefore economic and public interest in reconstructing anoxia in past environments has risen (Stramma et al., 2008). In the modern oceans, dinoflagellates inhabit a wide range of oxygen levels in bottom waters (Zonneveld et al., 2013).

The TOC relation with the *Senegalinium* cpx (Fig. 6a) is perhaps not surprising given its preference for high terrestrial input and nutrient levels (Fig. 4a, Fig. 5a). However, some differences exist between genera within this complex, which may give some clues about the reaction of different species to oxygen levels. We find that *Cerodinium* (Fig. 6b) is markedly more abundant at extremely high organic carbon levels (>2wt%) than would be expected based on terrestrial input alone. This suggests that this genus was relatively well

accommodated to deal with low bottom water oxygen concentrations.

In contrast, both *Spiniferites* and *Apectodinium* show higher affinity to lower TOC (Fig. 6c, d), suggesting a preference for well-ventilated bottom waters. For *Spiniferites* this is consistent with the traditional view of open marine outer neritic affinity (e.g., Sluijs et al., 2008a). *Apectodinium* however shows a more surprising trend. Organic carbon concentrations typically increase during the PETM (John et al., 2008; Sluijs et al., 2006) as does *Apectodinium*, but we find a weak anti-correlation instead. Such an affinity for slightly higher oxygen concentrations may explain why *Apectodinium* was not extremely abundant in some localities that show extremely low oxygen conditions during the PETM such as the Arctic (Sluijs et al., 2006) and the West Siberian Sea (Frieling et al., 2014).

The relatively uniform distribution of Protoperidinioids (Fig. 6e), a notoriously degradation-sensitive group, shows that preferential oxic degradation of these cysts is unlikely an important factor in our dataset. However, there appears to be an increase in Protoperinioids towards higher Corg/Ptot values (Fig. 10a), which may be related to lower oxygen conditions. It should be noted, though, that there is relatively few Corg/Ptot data available and that most of the data is from the PETM of the tropical Atlantic, a record that is biased towards high relative Protoperidinioid cysts due to the absence of other taxa, likely because of heat stress.

4.6 Shore proximity & sea level

Notably, the *Areoligera* group was found associated with relatively high-energy environments in the Paleogene (Sluijs et al., 2008a). As a result, an index was derived from the relative abundance of this group to that of *Spiniferites*, a generalist taxon with a more open marine affinity. These inferences are consistent with carbonate percentage of the sediments. Higher abundances of *Areoligera* are correlated to lower carbonate and higher amounts of the coarse fraction (Fig. 8b, Fig. 9b). The *Spiniferites*/(*Spiniferites* + *Areoligera* (AS) ratio was originally formulated to reconstruct sea level fluctuations. However, from a global perspective the relation for the AS ratio is virtually identical to the relative abundance of *Areoligera* due to the uniform distribution of *Spiniferites* (Fig. 8a, Fig. 9a) and indeed is only useful when concentrations of both *Areoligera* and *Spiniferites* are low.

4.7 Migrations

Many poleward migrations of species took place during the PETM, including but not limited to mammals, nannoplankton, dinoflagellates, foraminifera and flora (Sluijs et al., 2007a), most notably *Apectodinium*. To expand on the mechanisms behind these migrations, (sub) tropical sections are crucial for elucidating species affinities independently of the PETM. We identify at least two other groups present in the Paleocene and Eocene in the tropics that are found almost exclusively during the PETM at higher latitudes, although relative concentrations are generally much lower (Figure 11).

Notably, *F. reichartii* shows a minimum temperature requirement around ~30 °C, much higher than that of *Apectodinium*. During the PETM, *F. reichartii* is found at Bass River and Wilson Lake on the New Jersey shelf and at Site 1172 in the Southern Ocean, at ~55 °S. Remarkably, the occurrence of *F. reichartii* and it's apparent narrow high temperature tolerance (Figure 3c) may provide additional support for the extremely high temperatures (>30 °C) recorded in the Southern Ocean during the PETM (Hollis et al., 2015; Sluijs et al., 2011). Although additional factors, such as stratification, storminess and nutrient levels may also play a role, a similar temperature driven migration effect is apparent from Epicystal Goniodomideae. These occur only during the warmest periods of the Paleogene, i.e. the

Early Eocene Climate Optimum (EECO) and PETM in the Southern Ocean (Brinkhuis et al., 2003; Sluijs et al., 2011).

The temperature driven responses implies these groups are potentially suitable to identify high temperature intervals in mid and high latitude sections without the use of additional molecular or isotopic tools. Some caution should be taken as stratification and salinity fluctuations, although likely a result of higher temperatures, were likely more prevalent during the PETM than during the Paleocene, implying an indirect mechanism to temperature driven migrations may be important. *Senegalinium* mainly occurs in the Arctic Ocean during the latest Paleocene, but occurs abundantly at mid latitudes during the PETM, which may have been supported by fluctuating and locally decreases in salinity (Sluijs and Brinkhuis, 2009).

5. Conclusions & Outlook

We present a compilation of environmental proxy data and Paleogene dinocyst assemblages and document ecological preferences of specific dinocyst groups. Binning of the environmental proxy data allows us to semi-quantitatively assess optimal conditions as well as tolerance levels of extinct dinoflagellates for multiple specific ecological parameters. Although it is at this point not possible to distinguish between primary, secondary or even further removed indirect relations, we find strong indications that temperature-driven migrations during the PETM were more widespread than previously thought. In addition to *Apectodinium*, Epicystal Goniodomideae and *F. reichartii* and perhaps other species migrated polewards. This vast latitudinal overhaul in species is further connected to increased stratification and nutrient input, possibly from enhanced run-off.

We further find that specific Peridinioid cysts, most notably *Cerodinium* but possibly also Protoperidinioid cysts, may tolerate low bottom water oxygen conditions as evidenced by their relatively high abundance at high TOC content and high Corg/Ptot ratios. In addition, low bottom water oxygen concentrations are often found below high-productivity regions, which matches the occurrence of previously recognized abundances of Peridinioid cysts. However, we find that *Apectodinium* behaves differently from the other Peridinioids to terrestrial input and lower oxygen conditions. This may imply that *Apectodinium*, unlike other Peridinioid cysts is not heterotrophic, resulting in potential bias in the use of the P/G ratio. Therefore the use of HexP over Gonyaulacoid ratio as a supplement to the classic P/G ratio is advised until the trophic affinity of *Apectodinium* is resolved.

Table 1: *Sites and available data. References and proxy annotations:* ***Reference****: a(Sluijs et al., 2006), b(Sluijs et al., 2008b), c(Sluijs et al., 2009), d(Harding et al., 2011), e(Sluijs and Brinkhuis, 2009), f(Eldrett et al., 2014), g(Frieling et al., 2014), h(Sluijs et al., 2014), j(Crouch and Brinkhuis, 2005), i(Sluijs et al., 2011), k(Frieling et al., chapter 5), l(Frieling et al., chapter 3) b).* ***Proxy annotations****: 1: TOC(wt%), 2: TEX_{86}^{H}, 3: BIT, 4: Cren'/cren, 5: GDGT-2/cren, 6: Fraction of terrestrial palynomorphs, 7: Fe (counts per second, cps), 8:Ti/Al (XRF), 9: Ba/Al (XRF) 10: carbonate (%),11: Magnetic susceptibility, 12: Sand fraction >63um, 13: Ti/Al (ICP-OES), 14: Ba/Al (ICP-OES), 15: Fe (%), 16: Ca (cps), 17: Corg/Ptot*

Site	Refs	Paleolatitude	Proxy data	Remarks
ACEX	a,b,c	76.5	1,2,3,4,5,6,7,8,9	Early Eocene very restricted basin
Bass River	e	34.6	1,2,4,6,10,11,12	
Wilson Lake	e	34.8	1,2,3,4,5,6, 10,12,13,14	
Well 10	g	51.3	1,2,3,4,5,6,8, 9,13,14,15	Contains early Eocene
GoM	h	31.1	1,2,4,5,6,10,11	Only one Paleocene sample
Tawanui	i	-47.4	1,6,10,13	
IODP1172	j	-58	2,3,4,5,6,7,16	
ODP 959	k	-9.5	1,2,3,4,5,6,7,8,9, 10,11,13,14,16,17	
BH10 & SQ, Nigeria	l	-7.3	1,2,3,4,5,6,11,13,14,17	

Table 2. *Most abundant dinocyst genera and grouping. These genera comprise on average 96.3% (95% confidence interval +3.7 to -13.0%) of the assemblage encountered in all samples.*

Group	Genera	Group	Genera
Senegalinium complex	*Senegalinium*	*Areoligera* complex	*Areoligera*
			Glaphyrocysta
	Phthanoperidinium		*Adnatosphaeridium*
	Cerodinium		
	Deflandrea	*Cordosphaeridium* complex	*Cordosphaeridium*
	Lentinia		
	Vozzhennikovia		*Lanternosphaeridium*
	Manumiella		*Carpatella*
	Alterbidinium		*Thalassiphora*
	Spinidinium		*Muratodinium*
Protoperidinioids	*Lejeunecysta*		*Ifecysta*
	Phelodinium		*Kenleyia*
	Paleocystodinium		*Fibrocysta*
	(bp Senegalinium*)		*Turbiosphaera*
	Trithyrodinium		
		Diphyes	
Apectodinium complex	*Apectodinium*		
		F. reichartii	
	Wetzeliella		
	Dracodinium	Proximal G-cysts (apical archeopyle)	*Batiacasphaera*
	Rhombodinium		
	Wilsonidium		*Elytrocysta*
Epicystal Goniodomideae	*Eocladopyxis*		*Membranosphaera*
			Kallosphaeridium
	Polysphaeridium		*Alisocysta*
	Homotryblium		*Eisenackia*
	Heteraulacacysta		
Spiniferites complex	*Spiniferites*	Proximal G-cysts (precingular arch.)	*Cerebrocysta*
			Pyxidinopsis
	Achomosphaera		*Cribroperidinium?*
	Spiniferella		*Microdinium*
	Hafniasphaera		*Tectatodinium*
Impagidinium			*Leptodinium*
			Trichodinium

Table 3. *Group and species affinities. *** indicates clear affinity, ** likely affinity, * possible affinity.*

Group	Affinity
Senegalinium complex	***Low salinity
	**High nutrients
	*Low temperature
Protoperidinioids	***High nutrients
	**Prey species
	*High temperature?
	*Upwelling
Apectodinium complex	***High temperature
Epicystal Goniodomideae	***High temperature
	**Stratification
	*Fluctuating salinity
Spiniferites complex	*Low nutrients
	*Open marine
Hafniasphaera	**High temperature
Cordosphaeridium complex	*Open Marine?
	*High temperature?
Diphyes	?
F. reichartii	***Very high temperature
	*Open marine
Proximal G-cysts (apical archeopyle)	*Below marine salinity
	*High terrestrial input
Proximal G-cysts (precingular)	*Open marine
Impagidinium	***Oceanic
Areoligera complex	*Proximal systems
	*Low terrestrial input
	*Normal Salinity

Supplementary Figures

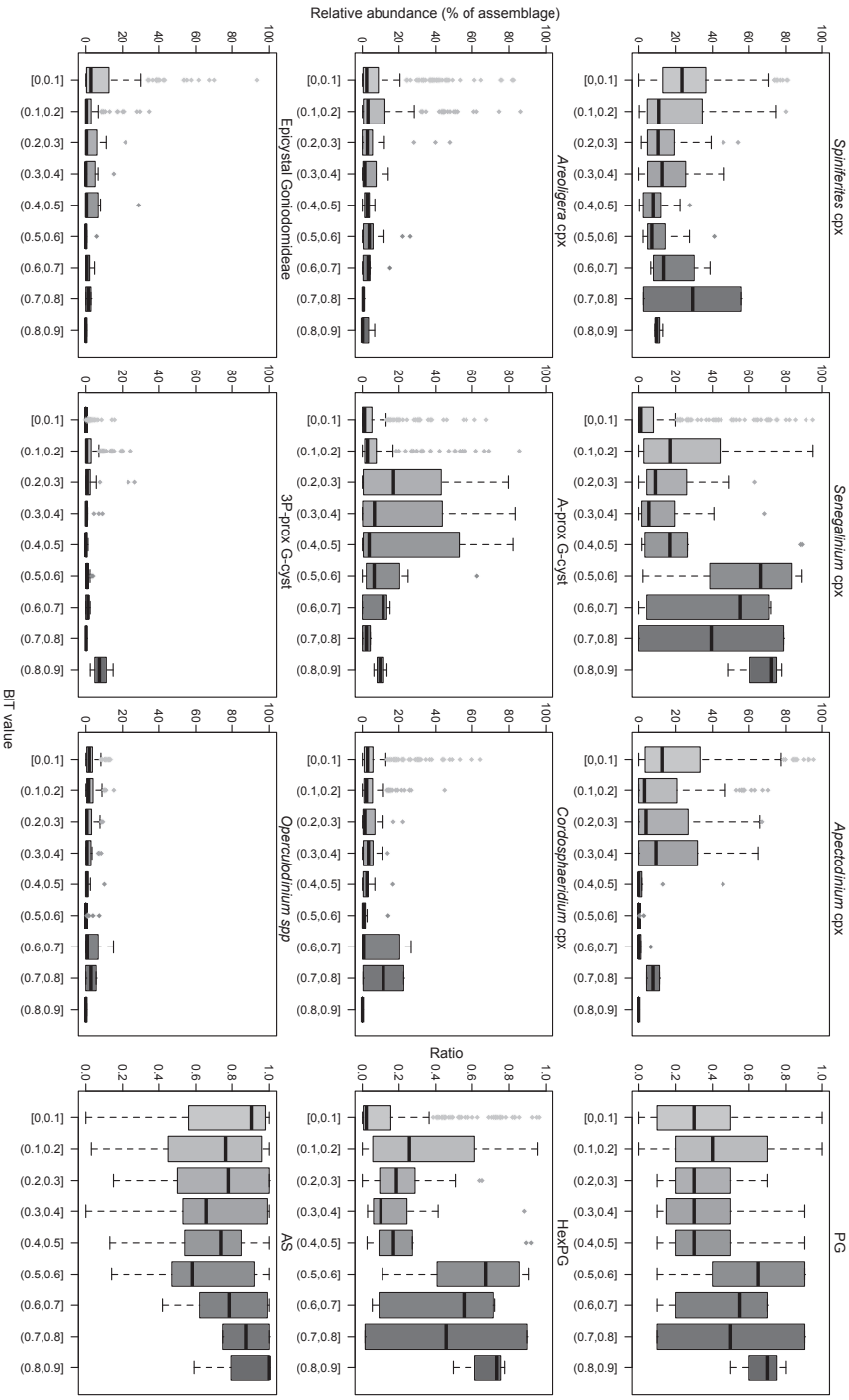

Supplementary Figure 1. *Relation of 9 most abundant species and 3 indices (PG ratio, HexP/G ratio and AS ratio) relative to BIT.*

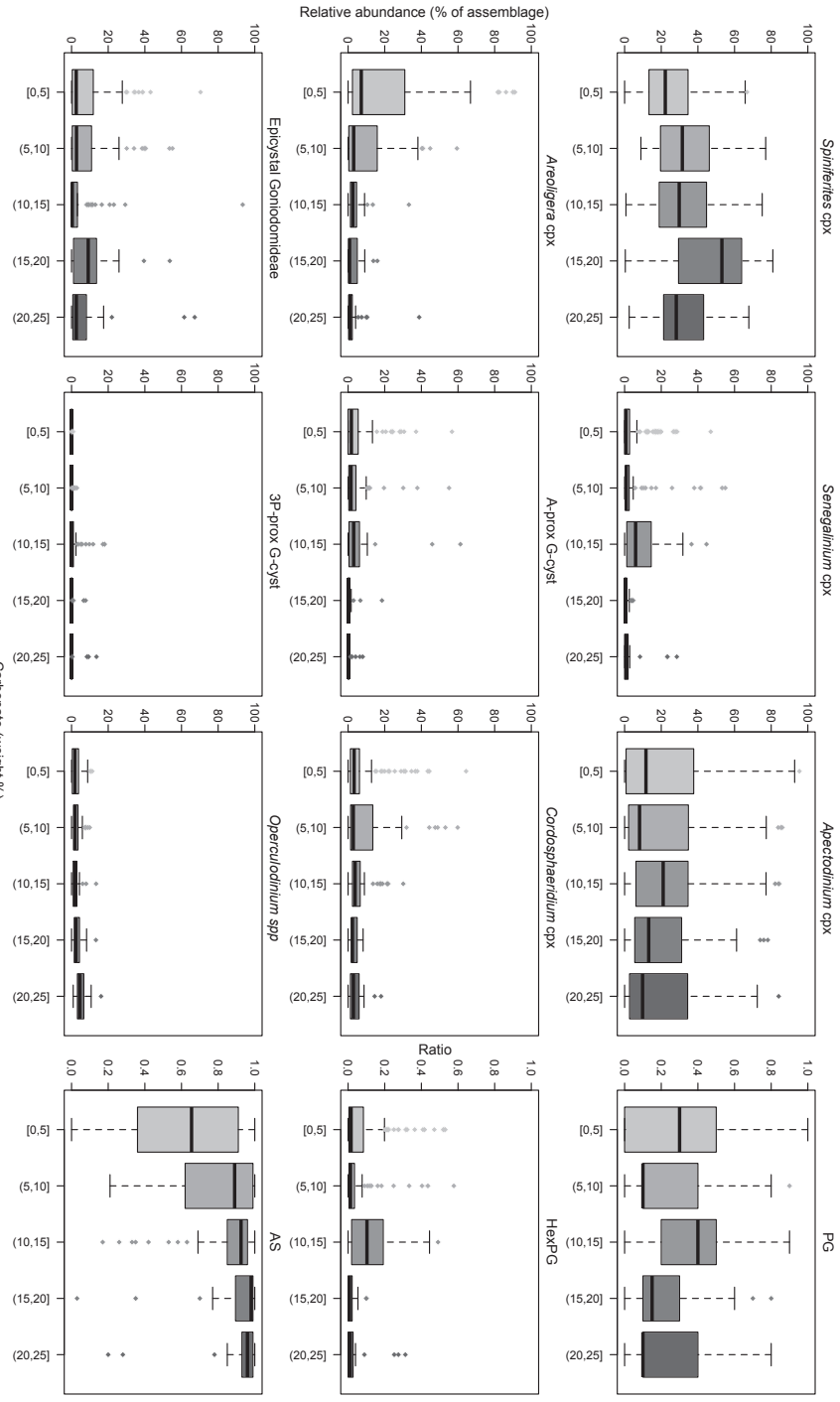

Supplementary Figure 2. *Relation of 9 most abundant species and 3 indices (PG ratio, HexP/G ratio and AS ratio) relative to carbonate percentage (Carb%)*

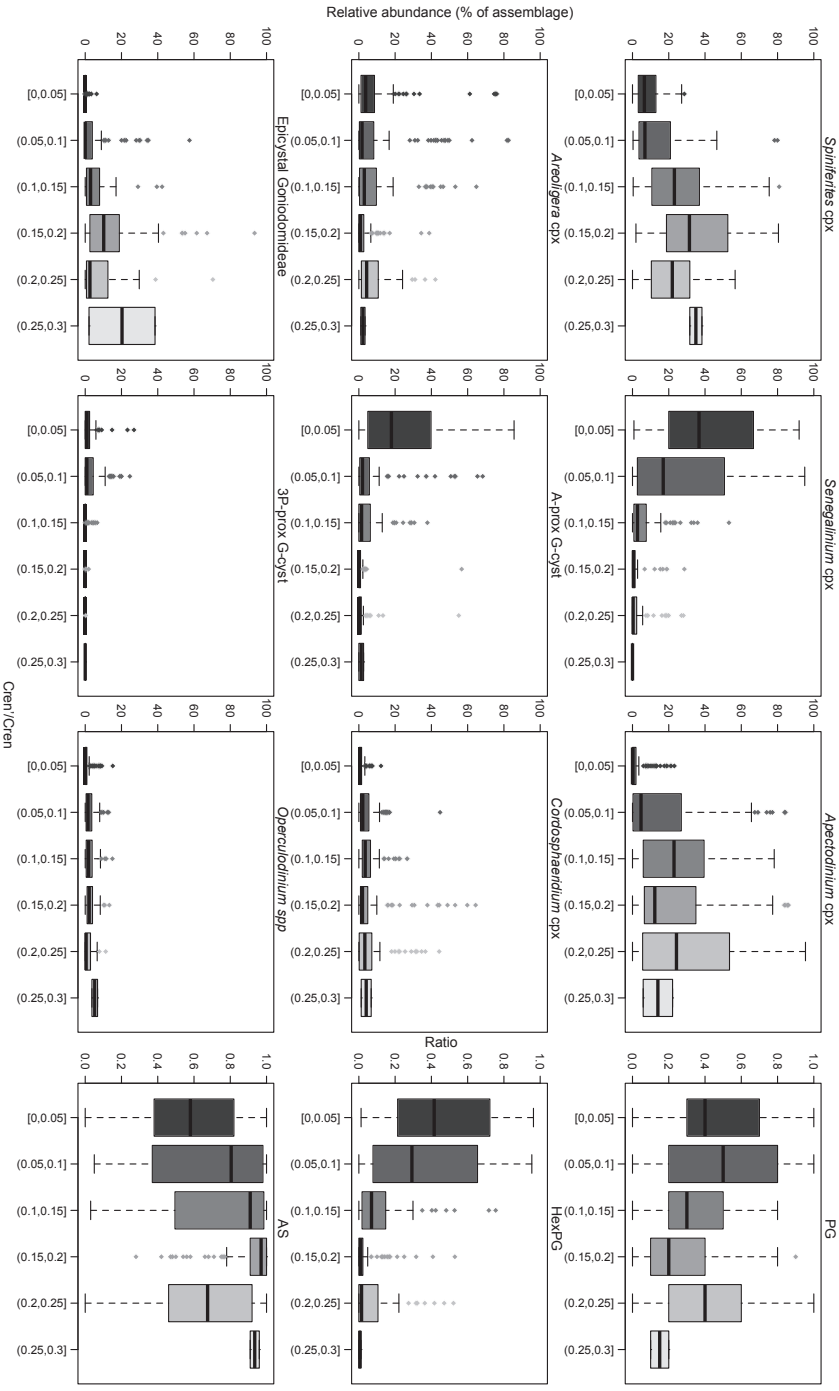

Supplementary Figure 3. *Relation of 9 most abundant species and 3 indices (PG ratio, HexP/G ratio and AS ratio) relative to relative abundance of crenarchaeol regioisomer (Cren'/Cren)*

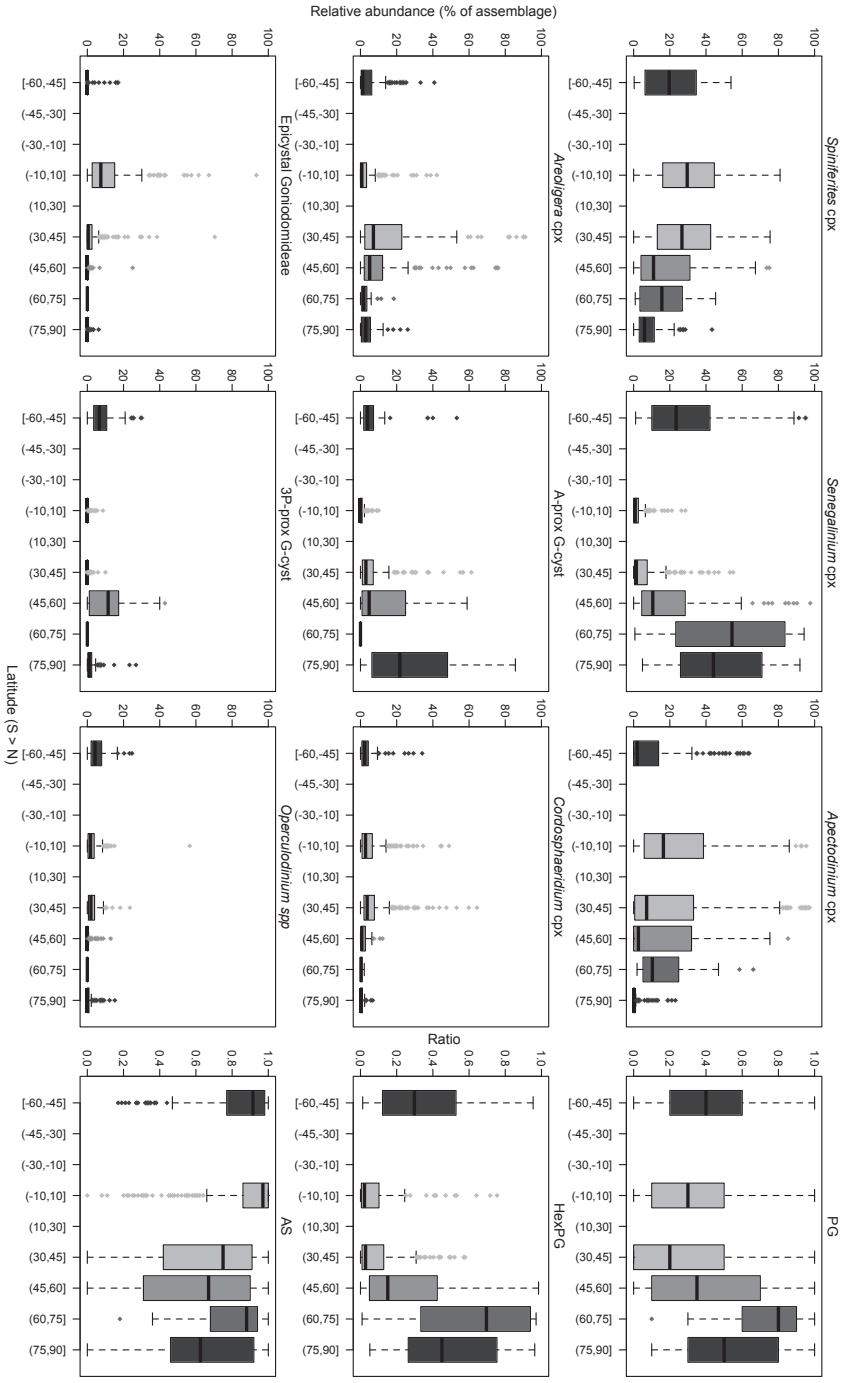

Supplemental Figure 4. *Distribution of 9 most abundant species and 3 indices (PG ratio, HexP/G ratio and AS ratio) relative to latitude.*

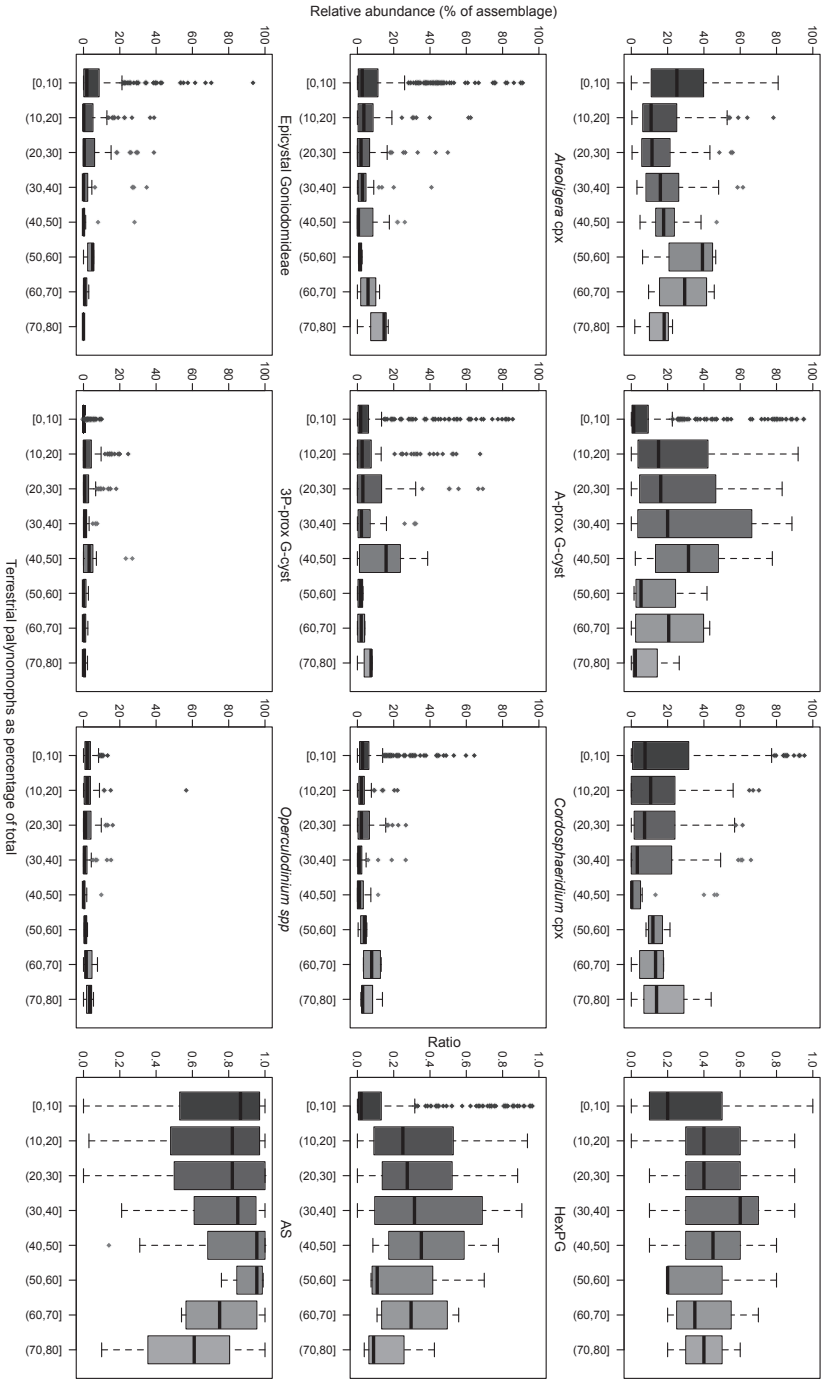

Supplemental Figure 5. *Relation of 9 most abundant species and 3 indices (PG ratio, HexP/G ratio and AS ratio) relative to terrestrial over total palynomorphs (TM ratio).*

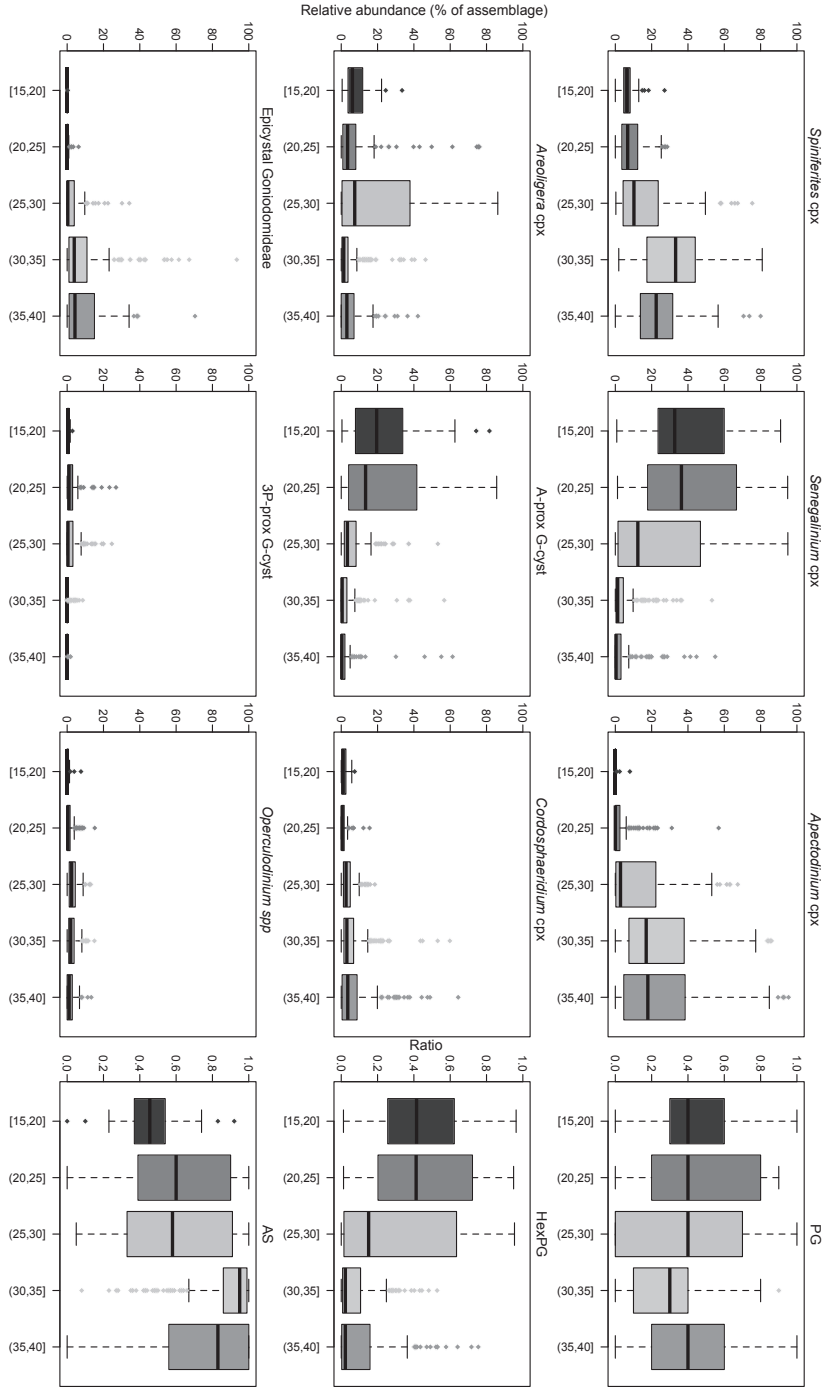

Supplemental Figure 6. *Relation of 9 most abundant species and 3 indices (PG ratio, HexP/G ratio and AS ratio) relative to* TEX_{86}.

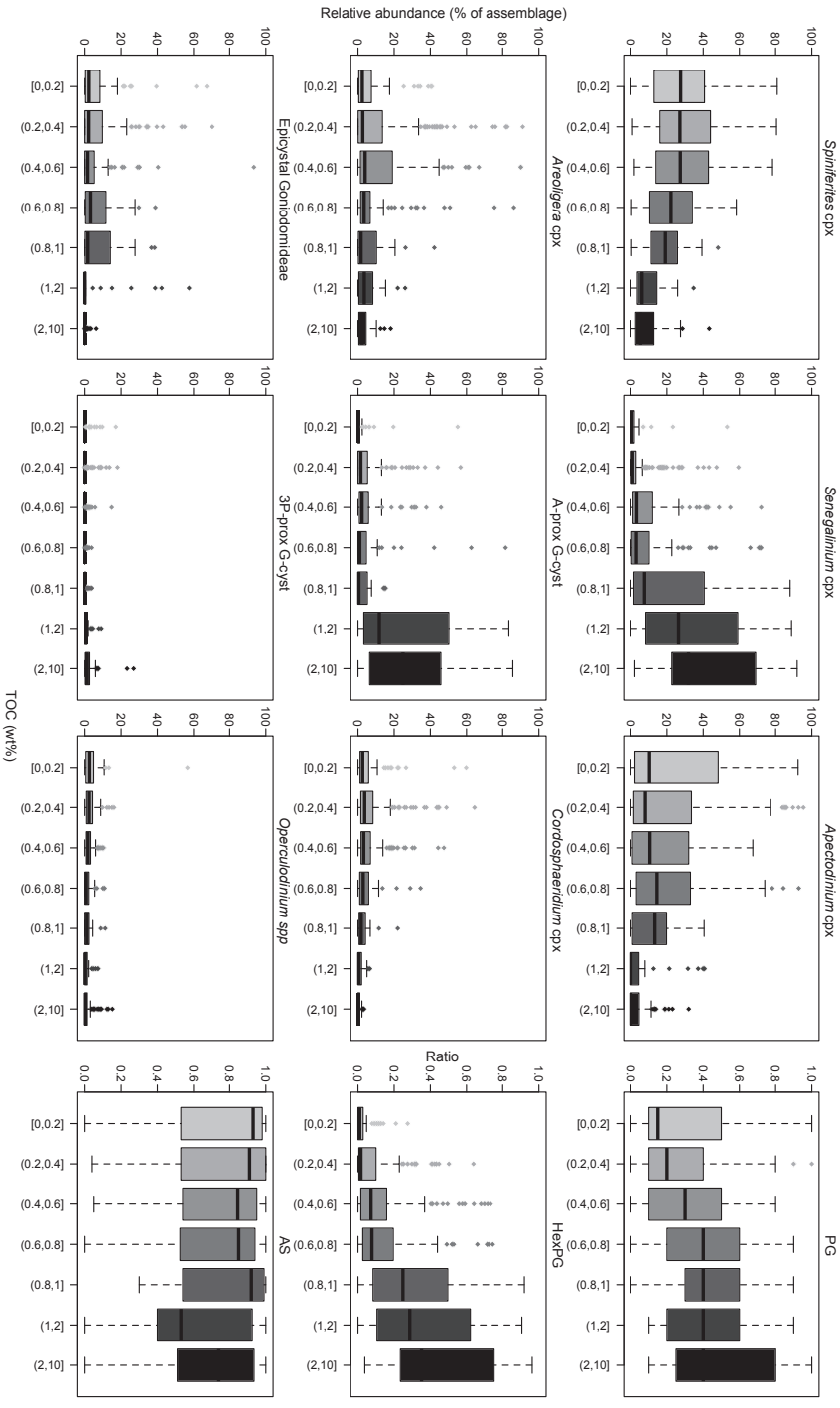

Supplemental Figure 7. *Relation of 9 most abundant species and 3 indices (PG ratio, HexP/G ratio and AS ratio) relative to weight percent Total Organic Carbon (TOCwt%).*

References

Aarnes, I., Planke, S., Trulsvik, M., Svensen, H., 2015. Contact metamorphism and thermogenic gas generation in the Vøring and Møre basins, offshore Norway, during the Paleocene–Eocene thermal maximum. J. Geol. Soc. London. 172, 2014–2098. doi:10.1144/jgs2014-098

Aarnes, I., Podladchikov, Y.Y., Svensen, H., 2012. Devolatilization-induced pressure build-up: Implications for reaction front movement and breccia pipe formation. Geofluids 12, 265–279.

Aarnes, I., Svensen, H., Connolly, J.A.D., Podladchikov, Y.Y., 2010. How contact metamorphism can trigger global climate changes: Modeling gas generation around igneous sills in sedimentary basins. Geochim. Cosmochim. Acta 74, 7179–7195. doi:http://dx.doi.org/10.1016/j.gca.2010.09.011

Aarnes, I., Svensen, H., Polteau, S., Planke, S., 2011. Contact metamorphic devolatilization of shales in the Karoo Basin, South Africa, and the effects of multiple sill intrusions. Chem. Geol. 281, 181–194. doi:http://dx.doi.org/10.1016/j.chemgeo.2010.12.007

Abdelmalak, M.M., Meyer, R., Planke, S., Faleide, J.I., Gernigon, L., Frieling, J., Sluijs, A., Reichart, G.-J., Zastrozhnov, D., Theissen-Krah, S., Said, A., Myklebust, R., 2016. Pre-breakup magmatism on the Vøring margin: Insight from new sub-basalt imaging and results from Ocean Drilling program hole 642E. Tectonophysics. doi:10.1016/j.tecto.2016.02.037

Abdul Aziz, H., Hilgen, F.J., van Luijk, G.M., Sluijs, A., Kraus, M.J., Pares, J.M., Gingerich, P.D., 2008. Astronomical climate control on paleosol stacking patterns in the upper Paleocene-lower Eocene Willwood Formation, Bighorn Basin, Wyoming. Geology 36, 531–534. doi:10.1130/G24734A.1

Akhmetiev, M.A., Beniamovski, V.N., 2006. The Paleocene and Eocene in the Russian part of west Eurasia. Stratigr. Geol. Correl. 14, 49–72. doi:10.1134/S0869593806010047

Akhmetiev, M.A., Zaporozhets, N.I., Iakovleva, A.I., Aleksandrova, G.N., Beniamovski, V.N., Oreshkina, T. V., Gnibidenko, Z.N., Dolya, Z.A., 2010. Comparative analysis of marine paleogene sections and biota from West Siberia and the Arctic Region. Stratigr. Geol. Correl. 18, 635–659. doi:10.1134/s0869593810060043

Algeo, T.J., Ingall, E., 2007. Sedimentary Corg:P ratios, paleocean ventilation, and Phanerozoic atmospheric pO2. Palaeogeogr. Palaeoclimatol. Palaeoecol. 256, 130–155. doi:10.1016/j.palaeo.2007.02.029

Alldredge, A.L., Passow, U., Haddock, H.D., 1998. The characteristics and transparent exopolymer particle (TEP) content of marine snow formed from thecate dinoflagellates. J. Plankton Res. 20, 393–406.

Anand, P., Elderfield, H., Conte, M.H., 2003. Calibration of Mg/Ca thermometry in planktonic foraminifera from a sediment trap time series. Paleoceanography 18, 21–28. doi:10.1029/2002PA000846

Anderson, D.M., Coats, D.W., Tyler, M.A., 1985. Encystment of the Dinoflagellate Gyrodinium uncatenum: Temperature and Nutrient Effects. J. Phycol. 21, 200–206.

Anderson, D.M., Kulis, D.M., Binder, B.J., 1984. Sexuality and Cyst Formation in the Dinoflagellate Gonyaulax tamarensis: Cyst Yield in Batch Cultures. J. Phycol. 20, 418–425.

Anderson, D.M., Taylor, C.D., Armbrust, E.V., 1987. The effects of darkness and anaerobiosis on dinoflagellate cyst germination1, 2. Limnol. Oceanogr. 32, 340–351. doi:10.4319/

lo.1987.32.2.0340

Archer, D., Buffett, B., 2005. Time-dependent response of the global ocean clathrate reservoir to climatic and anthropogenic forcing. Geochemistry, Geophys. Geosystems 6.

Archer, D., Buffett, B., Brovkin, V., 2009. Ocean methane hydrates as a slow tipping point in the global carbon cycle. Proc. Natl. Acad. Sci. 106, 20596–20601. doi:10.1073/pnas.0800885105

Aze, T., Pearson, P.N., Dickson, A.J., Badger, M.P.S., Bown, P.R., Pancost, R.D., Gibbs, S.J., Huber, B.T., Leng, M.J., Coe, A.L., Cohen, A.S., Foster, G.L., 2014. Extreme warming of tropical waters during the Paleocene–Eocene Thermal Maximum. Geology 42, 739–742. doi:doi:10.1130/G35637.1

Bains, S., Corfield, R.M., Norris, R.D., 1999. Mechanisms of Climate Warming at the End of the Paleocene. Science (80-.). 285, 724–727. doi:10.1126/science.285.5428.724

Bains, S., Norris, R.D., Corfield, R.M., Faul, K.L., 2000. Termination of global warmth at the Palaeocene/Eocene boundary through productivity feedback. Nature 407, 171–174. doi:10.1038/35025035

Bankole, S.I., Schrank, E., Erdtmann, B.D., 2007. Palynology of the Paleogene Oshosun Formation in the Dahomey Basin , southwestern Nigeria. Rev. Española Micropaleontol. 39, 29–44.

Barke, J., Abels, H.A., Sangiorgi, F., Greenwood, D.R., Sweet, A.R., Donders, T., Reichart, G.-J., Lotter, A.F., Brinkhuis, H., 2011. Orbitally forced Azolla blooms and Middle Eocene Arctic hydrology: Clues from palynology. Geology 39, 427–430. doi:10.1130/G31640.1

Barke, J., van der Burgh, J., van Konijnenburg-van Cittert, J.H.A., Collinson, M.E., Pearce, M.A., Bujak, J.P., Heilmann-Clausen, C., Speelman, E.N., van Kempen, M.M.L., Reichart, G.-J., Lotter, A.F., Brinkhuis, H., 2012. Coeval Eocene blooms of the freshwater fern Azolla in and around Arctic and Nordic seas. Palaeogeogr. Palaeoclimatol. Palaeoecol. 337-338, 108–119. doi:10.1016/j.palaeo.2012.04.002

Barron, E.J., 1987. Eocene equator-to-pole surface ocean temperatures: A significant climate problem? Paleoceanography 2, 729–739.

Beckmann, B., Flögel, S., Hofmann, P., Schulz, M., Wagner, T., 2005. Orbital forcing of Cretaceous river discharge in tropical Africa and ocean response. Nature 437, 241–244. doi:10.1038/nature03976

Berggren, W. a., Pearson, P.N., 2005. A revised tropical to subtropical Paleogene planktonic foraminiferal zonation. J. Foraminifer. Res. 35, 279–298. doi:10.2113/35.4.279

Berndt, C., Mjelde, R., Planke, S., Shimamura, H., Faleide, J.I., 2001. Controls on the tectono-magmatic evolution of a volcanic transform margin: the Vøring Transform Margin, NE Atlantic. Mar. Geophys. Res. 22, 133–152.

Berndt, C., Skogly, O.P., Planke, S., Eldholm, O., Mjelde, R., 2000. High-velocity breakup-related sills in the Vøring Basin, off Norway. J. Geophys. Res. Solid Earth 105, 28443–28454.

Berner, R.A., 1990. Atmospheric carbon dioxide levels over phanerozoic time. Science 249, 1382–1386. doi:249/4975/1382 [pii]

Bijl, P.K., Bendle, J.A.P., Bohaty, S.M., Pross, J., Schouten, S., Tauxe, L., Stickley, C.E., McKay, R.M., Rohl, U., Olney, M., Sluijs, A., Escutia, C., Brinkhuis, H., Klaus, A., Fehr, A., Williams, T., Carr, S.A., Dunbar, R.B., Gonzalez, J.J., Hayden, T.G., Iwai, M., Jimenez-

Espejo, F.J., Katsuki, K., Kong, G.S., Nakai, M., Passchier, S., Pekar, S.F., Riesselman, C., Sakai, T., Shrivastava, P.K., Sugisaki, S., Tuo, S., van de Flierdt, T., Welsh, K., Yamane, M., 2013a. Eocene cooling linked to early flow across the Tasmanian Gateway. Proc. Natl. Acad. Sci. 110, 9645–9650. doi:10.1073/pnas.1220872110

Bijl, P.K., Schouten, S., Sluijs, A., Reichart, G.-J., Zachos, J.C., Brinkhuis, H., 2009. Early palaeogene temperature evolution of the southwest Pacific Ocean. Nature 461, 776–779.

Bijl, P.K., Sluijs, A., Brinkhuis, H., 2013b. A magneto- and chemostratigraphically calibrated dinoflagellate cyst zonation of the early Palaeogene South Pacific Ocean. Earth-Science Rev. 124, 1–31. doi:http://dx.doi.org/10.1016/j.earscirev.2013.04.010

Bijma, J., Faber, W.W., Hemleben, C., 1990. Temperature and salinity limits for growth and survival of some planktonic foraminifers in laboratory cultures. J. Foraminifer. Res. 20, 95–116.

Blanco, J., 1995. Cyst production in four species of neritic dinoflagellates. J. Plankton Res. 17, 165–182.

Blunck, T.D., Blanchet, H., 1986. 6607/12-1 final report: Elf Aquitane Norge.

Bogus, K., Harding, I.C., King, A., Charles, A.J., Zonneveld, K.A.F., Versteegh, G.J.M., 2012. The composition and diversity of dinosporin in species of the Apectodinium complex (Dinoflagellata). Rev. Palaeobot. Palynol. 183, 21–31. doi:10.1016/j.revpalbo.2012.07.001

Bogus, K., Mertens, K.N., Lauwaert, J., Harding, I.C., Vrielinck, H., Zonneveld, K.A.F., Versteegh, G.J.M., 2014. Differences in the chemical composition of organic-walled dinoflagellate resting cysts from phototrophic and heterotrophic dinoflagellates. J. Phycol. 50, 254–266.

Boulter, M.C., Manum, S.B., 1989. The Brito-Arctic igneous province flora around the Paleocene/Eocene boundary. Proc. Ocean Drill. Program, Sci. Results 104, 663–680.

Bowen, G.J., Maibauer, B.J., Kraus, M.J., Röhl, U., Westerhold, T., Steimke, A., Gingerich, P.D., Wing, S.L., Clyde, W.C., 2015. Two massive, rapid releases of carbon during the onset of the Palaeocene-Eocene thermal maximum. Nat. Geosci. 8, 44–47.

Bowen, G.J., Zachos, J.C., 2010. Rapid carbon sequestration at the termination of the Palaeoceneg €"Eocene Thermal Maximum. Nat. Geosci. 3, 866–869.

Bown, P.R., Pearson, P.N., 2009. Calcareous plankton evolution and the Paleocene/Eocene thermal maximum event: new evidence from Tanzania. Mar. Micropaleontol. 71, 60–70.

Boyden, J.A., Müller, R.D., Gurnis, M., Torsvik, T.H., Clark, J.A., Turner, M., Ivey-Law, H., Watson, R.J., Cannon, J.S., Cark, J.A., Turner, M., Ivey-Law, H., Watson, R.J., Cannon, J.S., 2011. Next-generation plate-tectonic reconstructions using GPlates. Geoinformatics cyberinfrastructure solid earth Sci. 95–114. doi:10.1017/CBO9780511976308.008

Bralower, T.J., Thomas, D.J., Zachos, J.C., Hirschmann, M.M., Röhl, U., Sigurdsson, H., Thomas, E., Whitney, D.L., 1997. High-resolution records of the late Paleocene thermal maximum and circum-Caribbean volcanism: is there a causal link? Geology 25, 963–966.

Breivik, A.J., Mjelde, R., Faleide, J.I., Murai, Y., 2006. Rates of continental breakup magmatism and seafloor spreading in the Norway Basin–Iceland plume interaction. J. Geophys. Res. Solid Earth 111.

Brinkhuis, H., 1994. Late Eocene to Early Oligocene dinoflagellate cysts from the Priabonian type-area (northeast Italy): Biostratigraphy and paleoenvironmental interpretation.

Palaeogeogr. Palaeoclimatol. Palaeoecol. 107, 121–163.

Brinkhuis, H., Bujak, J.P., Smit, J., Versteegh, G.J.M., Visscher, H., 1998. Dinoflagellate-based sea surface temperature reconstructions across the Cretaceous–Tertiary boundary. Palaeogeogr. Palaeoclimatol. Palaeoecol. 141, 67–83.

Brinkhuis, H., Schouten, S., Collinson, M.E., Sluijs, A., Damsté, J.S.S., Dickens, G.R., Huber, M., Cronin, T.M., Onodera, J., Takahashi, K., Bujak, J.P., Stein, R., Van Der Burgh, J., Eldrett, J.S., Harding, I.C., Lotter, A.F., Sangiorgi, F., Cittert, H.V.K.-V., De Leeuw, J.W., Matthiessen, J., Backman, J., Moran, K., Clemens, S., Eynaud, F., Gattacceca, J., Jakobsson, M., Jordan, R.W., Kaminski, M.A., King, J., Koc, N., Martinez, N.C., Mcinroy, D., Moore Jr, T.C., O'Regan, M., Pälike, H., Rea, B., Rio, D., Sakamoto, T., Smith, D.C., St. John, K., Suto, I., Suzuki, N., Watanabe, M., Yamamoto, M., 2006. Episodic fresh surface waters in the Eocene Arctic Ocean. Nature 441, 606–609.

Brinkhuis, H., Sengers, S., Sluijs, A., Warnaar, J., Williams, G.L., Exon, N.F., 2003. Latest Cretaceous–earliest Oligocene and Quaternary dinoflagellate cysts, ODP Site 1172, East Tasman Plateau, in: Proceedings of the Ocean Drilling Program, Scientific Results. pp. 1–48.

Bujak, J.P., Brinkhuis, H., 1998. Global warming and dinocyst changes across the Paleocene/Eocene epoch boundary. Berggren al 277–295.

Bujak, J.P., Mudge, D.C., 1994. A high-resolution North Sea Eocene dinocyst zonation. J. Geol. Soc. London. 151, 449–462.

Bursa, A., 1963. Phytoplankton in coastal waters of the Arctic Ocean at Point Barrow, Alaska. Arctic 239–262.

Chen, Z., Wang, X., Hu, J., Yang, S., Zhu, M., Dong, X., Tang, Z., Peng, P., Ding, Z., 2014. Structure of the carbon isotope excursion in a high-resolution lacustrine Paleocene–Eocene Thermal Maximum record from central China. Earth Planet. Sci. Lett. 408, 331–340.

Coggon, R.M., Teagle, D.A.H., Smith-Duque, C.E., Alt, J.C., Cooper, M.J., 2010. Reconstructing Past Seawater Mg/Ca and Sr/Ca from Mid-Ocean Ridge Flank Calcium Carbonate Veins. Science (80-.). 327, 1114–1117. doi:10.1126/science.1182252

Colosimo, A.B., Bralower, T.J., Zachos, J.C., 2006. Evidence for lysocline shoaling at the Paleocene/Eocene thermal maximum on Shatsky Rise, northwest Pacific, in: Proceedings of the Ocean Drilling Program, Scientific Results. College Station Texas, pp. 1–36.

Contreras, L., Pross, J., Bijl, P.K., O'Hara, R.B., Raine, J.I., Sluijs, A., Brinkhuis, H., 2014. Southern high-latitude terrestrial climate change during the Palaeocene–Eocene derived from a marine pollen record (ODP Site 1172, East Tasman Plateau). Clim. Past 10, 1401–1420.

Cramer, B.S., Aubry, M.-P., Miller, K.G., Olsson, R.K., Wright, J.D., Kent, D. V., 1999. An exceptional chronologic, isotopic, and clay mineralogic record of the latest Paleocene thermal maximum, Bass River, NJ, ODP 174AX. Bull. la Soc. Geol. Fr. 170, 883–897.

Cramer, B.S., Wright, J.D., Kent, D. V., Aubry, M.-P., 2003. Orbital climate forcing of d13C excursions in the late Paleocene-early Eocene (chrons C24n-C25n). Paleoceanography 18, 21.

Creech, J.B., Baker, J.A., Hollis, C.J., Morgans, H.E.G., Smith, E.G.C., 2010. Eocene sea temperatures for the mid-latitude southwest Pacific from Mg/Ca ratios in planktonic and benthic foraminifera. Earth Planet. Sci. Lett. 299, 483–495. doi:10.1016/j.epsl.2010.09.039

Crouch, E.M., 2001. Environmental Change at the time of the Paleocene - Eocene Biotic Turnover. Utrecht University.

Crouch, E.M., Brinkhuis, H., 2005. Environmental change across the Paleocene–Eocene transition from eastern New Zealand: a marine palynological approach. Mar. Micropaleontol. 56, 138–160.

Crouch, E.M., Brinkhuis, H., Visscher, H., Adatte, T., Bolle, M.-P., 2003a. Late Paleocene-early Eocene dinoflagellate cyst records from the Tethys: Further observations on the global distribution of Apectodinium. Spec. Pap. Geol. Soc. Am. 369, 113–131. doi:10.1130/0-8137-2369-8.113

Crouch, E.M., Dickens, G.R., Brinkhuis, H., Aubry, M.-P., Hollis, C.J., Rogers, K.M., Visscher, H., 2003b. The Apectodinium acme and terrestrial discharge during the Paleocene-Eocene thermal maximum: New palynological, geochemical and calcareous nannoplankton observations at Tawanui, New Zealand. Palaeogeogr. Palaeoclimatol. Palaeoecol. 194, 387–403.

Crouch, E.M., Heilmann-Clausen, C., Brinkhuis, H., Morgans, H.E.G., Rogers, K.M., Egger, H., Schmitz, B., 2001. Global dinoflagellate event associated with the late Paleocene thermal maximum. Geology 29, 315–318.

Crouch, E.M., Visscher, H., 2003. Terrestrial vegetation record across the initial Eocene thermal maximum at the Tawanui marine section, New Zealand. Geol. Soc. Am. Spec. Pap. 351–364.

Cui, Y., Kump, L.R., Ridgwell, A.J., Charles, A.J., Junium, C.K., Diefendorf, A.F., Freeman, K.H., Urban, N.M., Harding, I.C., 2011. Slow release of fossil carbon during the Palaeocene–Eocene Thermal Maximum. Nat. Geosci. 4, 481–485. doi:10.1038/ngeo1179

Dale, B., 2009. Eutrophication signals in the sedimentary record of dinoflagellate cysts in coastal waters. J. Sea Res. 61, 103–113.

Dale, B., 1996. Dinoflagellate cyst ecology: modeling and geological applications. Palynol. Princ. Appl. 3, 1249–1275.

Dale, B., 1983. Dinoflagellate resting cysts:"benthic plankton." Surviv. Strateg. algae 69–136.

Dale, B., Dale, A.L., 1992. Dinoflagellate contributions to the deep sea. Woods Hole Oceanographic Institution.

Dale, B., Fjellså, A., 1994. Dinoflagellate cysts as paleoproductivity indicators: state of the art, potential, and limits, in: Carbon Cycling in the Glacial Ocean: Constraints on the Ocean's Role in Global Change. Springer, pp. 521–537.

de Souza, K.B., Jephson, T., Hasper, T.B., Carlsson, P., 2014. Species-specific dinoflagellate vertical distribution in temperature-stratified waters. Mar. Biol. 161, 1725–1734. doi:10.1007/s00227-014-2446-2

De Vernal, A., Eynaud, F., Henry, M., Hillaire-Marcel, C., Londeix, L., Mangin, S., Matthiessen, J., Marret, F., Radi, T., Rochon, A., Solignac, S., Turon, J.L., 2005. Reconstruction of sea-surface conditions at middle to high latitudes of the Northern Hemisphere during the Last Glacial Maximum (LGM) based on dinoflagellate cyst assemblages. Quat. Sci. Rev. 24, 897–924. doi:10.1016/j.quascirev.2004.06.014

de Villiers, S., Greaves, M., Elderfield, H., Villiers, S. De, Greaves, M., Elderfield, H., 2002. An intensity ratio calibration method for the accurate determination of Mg/Ca and Sr/Ca of

marine carbonates by ICP-AES. Geochemistry, Geophys. Geosystems 3, Paper number 2001GC000169. doi:10.1029/2001GC000169

DeConto, R.M., Galeotti, S., Pagani, M., Tracy, D., Schaefer, K., Zhang, T., Pollard, D., Beerling, D.J., 2012. Past extreme warming events linked to massive carbon release from thawing permafrost. Nature 484, 87–91. doi:10.1038/nature11424

Dickens, G.R., 2011. Down the Rabbit Hole: toward appropriate discussion of methane release from gas hydrate systems during the Paleocene-Eocene thermal maximum and other past hyperthermal events. Clim. Past 7, 831–846. doi:10.5194/cp-7-831-2011

Dickens, G.R., 2001. The potential volume of oceanic methane hydrates with variable external conditions. Org. Geochem. 32, 1179–1193.

Dickens, G.R., Castillo, M.M., Walker, J.C.G., 1997. A blast of gas in the latest Paleocene: simulating first-order effects of massive dissociation on oceanic methane hydrate. Geology 25, 259–262.

Dickens, G.R., Fewless, T., Thomas, E., Bralower, T.J., 2003. Excess barite accumulation during the Paleocene-Eocene Thermal Maximum: Massive input of dissolved barium from seafloor gas hydrate reservoirs. Geol. Soc. Am. Spec. Pap. 369, 11–24. doi:10.1130/0-8137-2369-8.11

Dickens, G.R., O'Neil, J.R., Rea, D.K., Owen, R.M., 1995. Dissociation of oceanic methane hydrate as a cause of the carbon isotope excursion at the end of the Paleocene. Paleoceanography 10, 965–971.

Dickens, G.R., Quinby-Hunt, M.S., 1994. Methane hydrate stability in seawater. Geophys. Res. Lett. 21, 2115–2118.

Dickson, A.J., Cohen, A.S., Coe, A.L., 2012. Seawater oxygenation during the Paleocene-Eocene Thermal Maximum. Geology 40, 639–642.

Donders, T., Weijers, J.W.H., Munsterman, D.K., Kloosterboer-van Hoeve, M.L., Buckles, L.K., Pancost, R.D., Schouten, S., Damsté, J.S.S., Brinkhuis, H., 2009. Strong climate coupling of terrestrial and marine environments in the Miocene of northwest Europe. Earth Planet. Sci. Lett. 281, 215–225.

Doney, S.C., Ruckelshaus, M., Duffy, J.E., Barry, J.P., Chan, F., English, C.A., Galindo, H.M., Grebmeier, J.M., Hollowed, A.B., Knowlton, N., 2012. Climate change impacts on marine ecosystems. Mar. Sci. 4.

Du Chêne, J., Adediran, S.A., 1984. Late Paleocene to early Eocene dinoflagellates from Nigeria. Cah. Micropaléontologie 3, 5–38.

Dunkley Jones, T., Lunt, D.J., Schmidt, D.N., Ridgwell, A.J., Sluijs, A., Valdes, P.J., Maslin, M.A., 2013. Climate model and proxy data constraints on ocean warming across the Paleocene–Eocene Thermal Maximum. Earth-Science Rev. 125, 123–145. doi:http://dx.doi.org/10.1016/j.earscirev.2013.07.004

Dunkley Jones, T., Ridgwell, A., Lunt, D.J., Maslin, M.A., Schmidt, D.N., Valdes, P.J., 2010. A Palaeogene perspective on climate sensitivity and methane hydrate instability. Philos. Trans. R. Soc. A Math. Phys. Eng. Sci. 368, 2395–2415. doi:10.1098/rsta.2010.0053

Eldholm, O., Grue, K., 1994. North Atlantic volcanic margins: dimensions and production rates. J. Geophys. Res. Solid Earth 99, 2955–2968.

Eldrett, J.S., Greenwood, D.R., Polling, M., Brinkhuis, H., Sluijs, A., 2014. A seasonality trigger for carbon injection at the Paleocene–Eocene Thermal Maximum. Clim. Past 10, 759–769.

Eldrett, J.S., Harding, I.C., Firth, J. V., Roberts, A.P., 2004. Magnetostratigraphic calibration of Eocene–Oligocene dinoflagellate cyst biostratigraphy from the Norwegian–Greenland Sea. Mar. Geol. 204, 91–127.

Ellegaard, M., Lewis, J., Harding, I.C., 2002. Cyst–Theca Relationship, Life Cycle, and Effects of Temperature and Salinity on the Cyst Morphology of Gonyaulax baltica sp. nov. (Dinophyceae) from the Baltic Sea area. J. Phycol. 38, 775–789.

Evans, D., Müller, W., 2012. Deep time foraminifera Mg/Ca paleothermometry: Nonlinear correction for secular change in seawater Mg/Ca. Paleoceanography 27.

Evitt, W.R., 1985. Sporopollenin dinoflagellate cysts: their morphology and interpretation. Amer Assn of Stratigraphic.

Farley, K., Eltgroth, S.F., 2003. An alternative age model for the Paleocene–Eocene thermal maximum using extraterrestrial 3 He. Earth Planet. Sci. Lett. 208, 135–148.

Fensome, R.A., 2004. The Lentin and Williams Index of Fossil Dinoflagellates 2004 Edition, 909 pp. Am.Assoc.of Strat. Coll. Station. Tex.

Fensome, R.A., Riding, J.B., Taylor, F.J.R., 1996. Dinoflagellates, in: Jansonius, J., McGregor, D.C. (Eds.), Palynology: Principles and Applications. . American Association of Stratigraphic Palynologists Foundation, pp. 107–169.

Firth, J. V., 1996. Upper middle Eocene to Oligocene dinoflagellate biostratigraphy and assemblage variations in Hole 913B, Greenland Sea, in: Proceedings of the Ocean Drilling Program. Scientific Results. Ocean Drilling Program, pp. 203–242.

Forster, A., Schouten, S., Moriya, K., Wilson, P.A., Damsté, J.S.S., 2007. Tropical warming and intermittent cooling during the Cenomanian/Turonian oceanic anoxic event 2: Sea surface temperature records from the equatorial Atlantic. Paleoceanography 22.

Freeman, K.H., Hayes, J.M., 1992. Fractionation of carbon isotopes by phytoplankton and estimates of ancient CO2 levels. Global Biogeochem. Cycles 6, 185–198.

Frieling, J., Iakovleva, A.I., Reichart, G.-J., Aleksandrova, G.N., Gnibidenko, Z.N., Schouten, S., Sluijs, A., 2014. Paleocene-Eocene warming and biotic response in the epicontinental West Siberian Sea. Geology 42, 767–770.

Galeotti, S., Krishnan, S., Pagani, M., Lanci, L., Gaudio, A., Zachos, J.C., Monechi, S., Morelli, G., Lourens, L., 2010. Orbital chronology of Early Eocene hyperthermals from the Contessa Road section, central Italy. Earth Planet. Sci. Lett. 290, 192–200. doi:10.1016/j.epsl.2009.12.021

Galushkin, Y.I., 1997. Thermal effects of igneous intrusions on maturity of organic matter: a possible mechanism of intrusion. Org. Geochem. 26, 645–658.

Gavrilov, Y.O., Shcherbinina, E.A., Oberhansli, H., 2003. Paleocene-Eocene boundary events in the northeastern Peri-Tethys. Spec. Pap. Geol. Soc. Am. 369, 147–168.

Gebhardt, H., Adekeye, O.A., Akande, S.O., 2011. Late Paleocene to Initial Eocene Thermal Maximum (IETM) Foraminiferal Biostratigraphy and Paleoecology of the Dahomey Basin, Southwestern Nigeria. Jahrb. der Geol. Bundesanstalt 3, 407–419.

Gibbs, S.J., Bralower, T.J., Bown, P.R., Zachos, J.C., Bybell, L.M., 2006. Shelf and open-ocean

calcareous phytoplankton assemblages across the Paleocene-Eocene Thermal Maximum: Implications for global productivity gradients. Geology 34, 233. doi:10.1130/G22381.1

Goldner, A., Herold, N., Huber, M., 2014. Antarctic glaciation caused ocean circulation changes at the Eocene-Oligocene transition. Nature 511, 574–577.

Gradstein, F.M., Ogg, J.G., Schmitz, M., Ogg, G., 2012. The Geologic Time Scale 2012 2-Volume Set. elsevier.

Guasti, E., Kouwenhoven, T.J., Brinkhuis, H., Speijer, R.P., 2005. Paleocene sea-level and productivity changes at the southern Tethyan margin (El Kef, Tunisia). Mar. Micropaleontol. 55, 1–17.

Hallegraeff, G.M., Valentine, J.P., Marshall, J.-A., Bolch, C.J., 1997. Temperature tolerances of toxic dinoflagellate cysts: application to the treatment of ships' ballast water. Aquat. Ecol. 31, 47–52.

Handley, L., O'Halloran, A., Pearson, P.N., Hawkins, E., Nicholas, C.J., Schouten, S., McMillan, I.K., Pancost, R.D., 2012. Changes in the hydrological cycle in tropical East Africa during the Paleocene-Eocene Thermal Maximum. Palaeogeogr. Palaeoclimatol. Palaeoecol. 329-330, 10–21. doi:10.1016/j.palaeo.2012.02.002

Harding, I.C., Charles, A.J., Marshall, J.E.A., Pälike, H., Roberts, A.P., Wilson, P.A., Jarvis, E., Thorne, R., Morris, E., Moremon, R., Pearce, R.B., Akbari, S., 2011. Sea-level and salinity fluctuations during the Paleocene–Eocene thermal maximum in Arctic Spitsbergen. Earth Planet. Sci. Lett. 303, 97–107. doi:http://dx.doi.org/10.1016/j.epsl.2010.12.043

Harland, R., 1983. Distribution maps of recent dinoflagellate cysts in bottom sediments from the North-Atlantic Ocean and adjacent seas. Palaeontology 26, 321–387.

Harland, R., 1973. Dinoflagellate cysts and acritarchs from the Bearpaw Formation (Upper Campanian) of southern Alberta, Canada. Palaeontology 16, 665–706.

Hayes, J.M., Strauss, H., Kaufman, A.J., 1999. The abundance of 13C in marine organic matter and isotopic fractionation in the global biogeochemical cycle of carbon during the past 800 Ma. Chem. Geol. 161, 103–125.

Head, M.J., 1996. Modern dinoflagellate cysts and their biological affinities. Palynol. Princ. Appl. 3, 1197–1248.

Heilmann-Clausen, C., 1985. Dinoflagellate stratigraphy of the uppermost Danian to Ypresian in the Viborg 1 borehole, central Jylland, Denmark. I Kommission hos CA Reitzels forlag.

Herold, N., Buzan, J., Seton, M., Goldner, A., Green, J.A.M., Müller, R.D., Markwick, P.J., Huber, M., 2014. A suite of Early Eocene (~ 55 Ma) climate model boundary conditions. Geosci. Model Dev. 7, 2077–2090.

Higgins, J.A., Schrag, D.P., 2006. Beyond methane: towards a theory for the Paleocene–Eocene thermal maximum. Earth Planet. Sci. Lett. 245, 523–537.

Hoins, M., Van de Waal, D.B., Eberlein, T., Reichart, G.-J., Rost, B., Sluijs, A., 2015. Stable carbon isotope fractionation of organic cyst-forming dinoflagellates: Evaluating the potential for a CO2 proxy. Geochim. Cosmochim. Acta 160, 267–276. doi:10.1016/j.gca.2015.04.001

Hollis, C.J., 2007. Radiolarian faunal turnover through the Paleocene-eocene transition, Mead Stream, New Zealand, in: Radiolaria. Springer, pp. 79–99.

Hollis, C.J., Hines, B.R., Littler, K., Villasante-Marcos, V., Kulhanek, D.K., Strong, C.P., Zachos,

J.C., Eggins, S.M., Northcote, L., Phillips, A., 2015. The Paleocene–Eocene Thermal Maximum at DSDP Site 277, Campbell Plateau, southern Pacific Ocean. Clim. Past 11, 1009–1025. doi:10.5194/cp-11-1009-2015

Hollis, C.J., Taylor, K.W.R., Handley, L., Pancost, R.D., Huber, M., Creech, J.B., Hines, B.R., Crouch, E.M., Morgans, H.E.G., Crampton, J.S., Gibbs, S.J., Pearson, P.N., Zachos, J.C., 2012. Early Paleogene temperature history of the Southwest Pacific Ocean: Reconciling proxies and models. Earth Planet. Sci. Lett. 349-350, 53–66.

Honisch, B., Ridgwell, A., Schmidt, D.N., Thomas, E., Gibbs, S.J., Sluijs, A., Zeebe, R., Kump, L., Martindale, R.C., Greene, S.E., Kiessling, W., Ries, J., Zachos, J.C., Royer, D.L., Barker, S., Marchitto, T.M., Moyer, R., Pelejero, C., Ziveri, P., Foster, G.L., Williams, B., 2012. The Geological Record of Ocean Acidification. Science (80-.). 335, 1058–1063. doi:10.1126/science.1208277

Hopmans, E.C., Schouten, S., Sinninghe Damsté, J.S., Damsté, J.S.S., 2015. The effect of improved chromatography on GDGT-based palaeoproxies. Org. Geochem. 93, 1–6. doi:10.1016/j.orggeochem.2015.12.006

Hopmans, E.C., Weijers, J.W.H., Schefuß, E., Herfort, L., Sinninghe Damsté, J.S., Schouten, S., 2004. A novel proxy for terrestrial organic matter in sediments based on branched and isoprenoid tetraether lipids. Earth Planet. Sci. Lett. 224, 107–116. doi:10.1016/j.epsl.2004.05.012

Houben, A.J.P., Bijl, P.K., Pross, J., Bohaty, S.M., Passchier, S., Stickley, C.E., Rohl, U., Sugisaki, S., Tauxe, L., van de Flierdt, T., Olney, M., Sangiorgi, F., Sluijs, A., Escutia, C., Brinkhuis, H., 2013. Reorganization of Southern Ocean Plankton Ecosystem at the Onset of Antarctic Glaciation. Science (80-.). 340, 341–344. doi:10.1126/science.1223646

Huber, M., 2009. Climate change: Snakes tell a torrid tale. Nature 457, 669–671.

Huber, M., 2008. A hotter greenhouse? Science (80-.). 321, 353–354.

Huber, M., Caballero, R., 2011. The early Eocene equable climate problem revisited. Clim. Past 7, 603–633. doi:10.5194/cp-7-603-2011

Huguet, C., De Lange, G.J., Gustafsson, O., Middelburg, J.J., Sinninghe Damsté, J.S., Schouten, S., 2008. Selective preservation of soil organic matter in oxidized marine sediments (Madeira Abyssal Plain). Geochim. Cosmochim. Acta 72, 6061–6068.

Iakovleva, A.I., 2011. Palynological reconstruction of the Eocene marine palaeoenvironments in south of Western Siberia. Acta Palaeobot. 51, 229–248.

Iakovleva, A.I., Aleksandrova, G.N., 2013. To the question on dinocyst zonation of Paleocene-Eocene in Western Siberia. Bull. Moscow Soc. Nat. Geol. Ser. 88, 59–82.

Iakovleva, A.I., Aleksandrova, G.N., Gnibidenko, Z.N., 2012. Updating of Paleogene Lulinvor Formation age in southern Western Siberia by palynological and paleomagnetic data. Bull. Moscow Soc. Nat. Geol. Ser. 87, 53–87.

Iakovleva, A.I., Brinkhuis, H., Cavagnetto, C., 2001. Late Palaeocene–Early Eocene dinoflagellate cysts from the Turgay Strait, Kazakhstan; correlations across ancient seaways. Palaeogeogr. Palaeoclimatol. Palaeoecol. 172, 243–268.

Iakovleva, A.I., Heilmann-Clausen, C., 2010. Eocene dinoflagellate cyst biostratigraphy of research borehole 011-BP, Omsk Region, southwestern Siberia. Palynology 34, 37–41. doi:10.1080/01916121003629974

Imbert, P., Ho, S., 2012. Seismic-scale funnel-shaped collapse features from the Paleocene-Eocene of the North West Shelf of Australia. Mar. Geol. 332, 198–221. doi:10.1016/j.margeo.2012.10.010

Ingall, E.D., Van Cappellen, P., 1990. Relation between sedimentation rate and burial of organic phosphorus and organic carbon in marine sediments. Geochim. Cosmochim. Acta 54, 373–386.

Inglis, G.N., Farnsworth, A., Lunt, D.J., Foster, G.L., Hollis, C.J., Pagani, M., Jardine, P.E., Pearson, P.N., Markwick, P.J., Galsworthy, A.M.J., Raynham, L., Taylor, K.W.R., Pancost, R.D., 2015. Descent towards the Icehouse: Eocene sea surface cooling inferred from GDGT distributions. Paleoceanography 30, 1000–1020. doi:10.1002/2014PA002723

IPCC, 2014. Climate Change 2014: Synthesis Report. Contribution of Working Groups I, II and III to the Fifth Assessment Report of the Intergovernmental Panel on Climate Change.

Jacobson, D.M., Anderson, D.M., 1986. Thecate Heterotrophic Dinoflagellates: Feeding Behavior and Mechanisms. J. Phycol. 22, 249–258.

Jamtveit, B., Svensen, H., Podladchikov, Y.Y., Planke, S., 2004. Hydrothermal vent complexes associated with sill intrusions in sedimentary basins. Geol. Soc. Spec. Publ. 234, 233–241.

Jephson, T., Carlsson, P., Fagerberg, T., 2012. Dominant impact of water exchange and disruption of stratification on dinoflagellate vertical distribution. Estuar. Coast. Shelf Sci. 112, 198–206. doi:10.1016/j.ecss.2012.07.020

John, C.M., Banerjee, N.R., Longstaffe, F.J., Sica, C., Law, K.R., Zachos, J.C., 2012. Clay assemblage and oxygen isotopic constraints on the weathering response to the Paleocene-Eocene thermal maximum, East Coast of North America. Geology 40, 591–594. doi:10.1130/G32785.1

John, C.M., Bohaty, S.M., Zachos, J.C., Sluijs, A., Gibbs, S.J., Brinkhuis, H., Bralower, T.J., 2008. North American continental margin records of the Paleocene-Eocene thermal maximum: Implications for global carbon and hydrological cycling. Paleoceanography 23, 1–20. doi:10.1029/2007PA001465

Katz, M.E., Cramer, B.S., Mountain, G.S., Katz, S., Miller, K.G., 2001. Uncorking the bottle: What triggered the Paleocene/Eocene thermal maximum methane release? Paleoceanography 16, 549. doi:10.1029/2000PA000615

Katz, M.E., Pak, D.K., Dickens, G.R., Miller, K.G., 1999. The source and fate of massive carbon input during the latest paleocene thermal maximum. Science (80-.). 286, 1531–1533. doi:10.1126/science.286.5444.1531

Keafer, B.A., Buesseler, K.O., Anderson, D.M., 1992. Burial of living dinoflagellate cysts in estuarine and nearshore sediments. Mar. Micropaleontol. 20, 147–161. doi:10.1016/0377-8398(92)90004-4

Kelly, D.C., 2002. Response of Antarctic (ODP Site 690) planktonic foraminifera to the Paleocene–Eocene thermal maximum: faunal evidence for ocean/climate change. Paleoceanography 17, 13–23. doi:10.1029/2002PA000761

Kelly, D.C., Bralower, T.J., Zachos, J.C., 1998. Evolutionary consequences of the latest Paleocene thermal maximum for tropical planktonic foraminifera. Palaeogeogr. Palaeoclimatol. Palaeoecol. 141, 139–161. doi:10.1016/S0031-0182(98)00017-0

Kelly, D.C., Bralower, T.J., Zachos, J.C., Silva, I.P., Thomas, E., 1996. Rapid diversification of

planktonic foraminifera in the tropical Pacific (ODP Site 865) during the late Paleocene thermal maximum. Geology 24, 423–426.

Kender, S., Stephenson, M.H., Riding, J.B., Leng, M.J., Knox, R.W.O.B., Peck, V.L., Kendrick, C.P., Ellis, M.A., Vane, C.H., Jamieson, R., 2012. Marine and terrestrial environmental changes in NW Europe preceding carbon release at the Paleocene-Eocene transition. Earth Planet. Sci. Lett. 353-354, 108–120. doi:10.1016/j.epsl.2012.08.011

Kennett, J.P., Stott, L.D., 1991. Abrupt deep-sea warming, palaeoceanographic changes and benthic extinctions at the end of the Palaeocene. Nature 353, 225–229.

Kerrick, D.M., 2001. Present and Past Nonanthropogenic CO2. Rev. Geophys. 39, 565–585.

Kim, J.H., Schouten, S., Hopmans, E.C., Donner, B., Sinninghe Damsté, J.S., 2008. Global sediment core-top calibration of the TEX86 paleothermometer in the ocean. Geochim. Cosmochim. Acta 72, 1154–1173. doi:10.1016/j.gca.2007.12.010

Kim, J.H., Schouten, S., Rodrigo-Gámiz, M., Rampen, S., Marino, G., Huguet, C., Helmke, P., Buscail, R., Hopmans, E.C., Pross, J., Sangiorgi, F., Middelburg, J.J., Sinninghe Damsté, J.S., 2015. Influence of deep-water derived isoprenoid tetraether lipids on the paleothermometer in the Mediterranean Sea. Geochim. Cosmochim. Acta 150, 125–141. doi:10.1016/j.gca.2014.11.017

Kim, J.H., van der Meer, J., Schouten, S., Helmke, P., Willmott, V., Sangiorgi, F., Koç, N., Hopmans, E.C., Damsté, J.S.S., Ko??, N., 2010. New indices and calibrations derived from the distribution of crenarchaeal isoprenoid tetraether lipids: Implications for past sea surface temperature reconstructions. Geochim. Cosmochim. Acta 74, 4639–4654. doi:10.1016/j.gca.2010.05.027

Kim, S.-T., O'Neil, J.R., 1997. Equilibrium and nonequilibrium oxygen isotope effects in synthetic carbonates. Geochim. Cosmochim. Acta 61, 3461–3475. doi:10.1016/S0016-7037(97)00169-5

Kodrans-Nsiah, M., De Lange, G.J., Zonneveld, K.A.F., 2008. A natural exposure experiment on short-term species-selective aerobic degradation of dinoflagellate cysts. Rev. Palaeobot. Palynol. 152, 32–39.

Kokinos, J.., Anderson, D.M., 1995. Morphological development of resting cysts in cultures of the marine dinoflagellate Lingulodinium polyedrum (= L. machaerophorum). Palynolgy 19, 143–166. doi:10.1080/01916122.1995.9989457

Kominz, M.A., Browning, J. V., Miller, K.G., Sugarman, P.J., Mizintseva, S., Scotese, C.R., 2008. Late Cretaceous to Miocene sea-level estimates from the New Jersey and Delaware coastal plain coreholes: An error analysis. Basin Res. 20, 211–226.

Kozdon, R., Kelly, D.C., Kita, N.T., Fournelle, J.H., Valley, J.W., 2011. Planktonic foraminiferal oxygen isotope analysis by ion microprobe technique suggests warm tropical sea surface temperatures during the Early Paleogene. Paleoceanography 26, 1–17. doi:10.1029/2010PA002056

Kump, L.R., Arthur, M.A., 1999. Interpreting carbon-isotope excursions: carbonates and organic matter. Chem. Geol. 161, 181–198.

Kurtz, A.C., Kump, L.R., Arthur, M.A., Zachos, J.C., Paytan, A., 2003. Early Cenozoic decoupling of the global carbon and sulfur cycles. Paleoceanography 18.

Kuypers, M.M.M., Blokker, P., Erbacher, J., Kinkel, H., Pancost, R.D., Schouten, S., Sinninghe

Damsté, J.S., 2001. Massive expansion of marine archaea during a mid-Cretaceous oceanic anoxic event. Science (80-.). 293, 92–94.

Kvenvolden, K.A., 2002. Methane hydrate in the global organic carbon cycle. Terra Nov. 14, 302–306.

Kvenvolden, K.A., 1993. Gas hydrates—geological perspective and global change. Rev. Geophys. 31, 173–187.

Lachniet, M.S., 2009. Climatic and environmental controls on speleothem oxygen-isotope values. Quat. Sci. Rev. 28, 412–432. doi:10.1016/j.quascirev.2008.10.021

Langlet, D., Baal, C., Geslin, E., Metzger, E., Zuschin, M., Riedel, B., Risgaard-Petersen, N., Stachowitsch, M., Jorissen, F.J., 2014. Foraminiferal species responses to in situ, experimentally induced anoxia in the Adriatic Sea. Biogeosciences 11, 1775–1797.

Lear, C.H., Rosenthal, Y., Slowey, N., 2002. Benthic foraminiferal Mg/Ca-paleothermometry: A revised core-top calibration. Geochim. Cosmochim. Acta 66, 3375–3387. doi:10.1016/S0016-7037(02)00941-9

Lindzen, R.S., Chou, M.-D., Hou, A.Y., 2001. Does the earth have an adaptive infrared iris? Bull. Am. Meteorol. Soc. 82, 417–432.

Littler, K., Röhl, U., Westerhold, T., Zachos, J.C., 2014. A high-resolution benthic stable-isotope record for the South Atlantic: Implications for orbital-scale changes in Late Paleocene–Early Eocene climate and carbon cycling. Earth Planet. Sci. Lett. 401, 18–30.

Lourens, L.J., Sluijs, A., Kroon, D., Zachos, J.C., Thomas, E., Röhl, U., Bowles, J., Raffi, I., 2005. Astronomical pacing of late Palaeocene to early Eocene global warming events. Nature 435, 1083–1087.

Lowenstein, T.K., 2001. Oscillations in Phanerozoic Seawater Chemistry: Evidence from Fluid Inclusions. Science (80-.). 294, 1086–1088. doi:10.1126/science.1064280

Luciani, V., Giusberti, L., Agnini, C., Backman, J., Fornaciari, E., Rio, D., 2007. The Paleocene–Eocene Thermal Maximum as recorded by Tethyan planktonic foraminifera in the Forada section (northern Italy). Mar. Micropaleontol. 64, 189–214.

Lunt, D.J., Dunkley Jones, T., Heinemann, M., Huber, M., LeGrande, A.N., Winguth, A.M.E., Loptson, C., Marotzke, J., Roberts, C.D., Tindall, J., 2012. A model–data comparison for a multi-model ensemble of early Eocene atmosphere–ocean simulations: EoMIP. Clim. Past 8, 1717–1736.

Lunt, D.J., Haywood, A.M., Schmidt, G. a., Salzmann, U., Valdes, P.J., Dowsett, H.J., 2010a. Earth system sensitivity inferred from Pliocene modelling and data. Nat. Geosci. 3, 1–5. doi:10.1038/ngeo706

Lunt, D.J., Ridgwell, A.J., Sluijs, A., Zachos, J.C., Hunter, S., Haywood, A.M., 2011. A model for orbital pacing of methane hydrate destabilization during the Palaeogene. Nat. Geosci. 4, 775–778. doi:10.1038/ngeo1266

Lunt, D.J., Valdes, P.J., Jones, T.D., Ridgwell, A.J., Haywood, A.M., Schmidt, D.N., Marsh, R., Maslin, M.A., 2010b. CO2-driven ocean circulation changes as an amplifier of Paleocene-Eocene thermal maximum hydrate destabilization. Geology 38, 875–878.

Ma, Z., Gray, E., Thomas, E., Murphy, B., Zachos, J.C., Paytan, A., 2014. Carbon sequestration during the Palaeocene–Eocene Thermal Maximum by an efficient biological pump. Nat.

Geosci. 7, 382–388. doi:10.1038/NGEO2139

MacRae, R.A., Fensome, R.A., Williams, G.L., 1996. Fossil dinoflagellate diversity, originations, and extinctions and their significance. Can. J. Bot. 74, 1687–1694.

Madigan, M.T., Martinko, J.M., Dunlap, P. V, Clark, D.P., 2008. Brock Biology of microorganisms 12th edn. Int. Microbiol. 11, 65–73.

Magioncalda, R., Dupuis, C., Smith, T., Steurbaut, E., Gingerich, P.D., 2004. Paleocene-Eocene carbon isotope excursion in organic carbon and pedogenic carbonate: Direct comparison in a continental stratigraphic section. Geology 32, 553–556.

Mancini, E.A., 1984. Biostratigraphy of Paleocene strata in southwestern Alabama. Micropaleontology 30, 268–291.

Markwick, P.J., 2007. The palaeogeographic and palaeoclimatic significance of climate proxies for data-model comparisons, in: Williams, M., Haywood, A., Gregory, F., Schmidt, D. (Eds.), Deep-Time Perspectives on Climate Change: Marrying the Signal from Computer Models and Biological Proxies. The Micropaleontological Society Special Publication, The Geological Society London, pp. 251–312.

Marret, F., 1994. Distribution of dinoflagellate cysts in recent marine sediments from the east Equatorial Atlantic (Gulf of Guinea). Rev. Palaeobot. Palynol. 84, 1–22. doi:10.1016/0034-6667(94)90038-8

Martínez-Botí, M.A., Foster, G.L., Chalk, T.B., Rohling, E.J., Sexton, P.F., Lunt, D.J., Pancost, R.D., Badger, M.P.S., Schmidt, D.N., 2015. Plio-Pleistocene climate sensitivity evaluated using high-resolution CO2 records. Nature 518, 49–54.

Matthiessen, J., de Vernal, A., Head, M.J., Okolodkov, Y., Zonneveld, K.A.F., Harland, R., 2005. Modern organic-walled dinoflagellate cysts in Arctic marine environments and their (paleo-) environmental significance. Paläontologische Zeitschrift 79, 3–51. doi:10.1007/BF03021752

Mattson, B., 2006. Seismic characteristics and formation of hydrothermal vent complexes . MSc thesis, Univ. Olso. University of Oslo, Oslo.

Mbesse, C.O., 2013. La limite Paléocène-Eocène dans le Bassin de Douala Biostratigraphie et essai de reconstitution des paléoenvironnements.

McInerney, F.A., Wing, S.L., 2011. The Paleocene-Eocene thermal maximum: a perturbation of carbon cycle, climate, and biosphere with implications for the future. Annu. Rev. Earth Planet. Sci. 39, 489–516.

Meissner, K., Bralower, T.J., Alexander, K., Jones, T.D., Sijp, W.P., Ward, M., 2014. The Paleocene-Eocene Thermal Maximum : How much carbon is enough ? 1–18. doi:10.1002/2014PA002650.Received

Mertens, K.N., Ribeiro, S., Bouimetarhan, I., Caner, H., Combourieu Nebout, N., Dale, B., De Vernal, A., Ellegaard, M., Filipova, M., Godhe, A., Goubert, E., Grøsfjeld, K., Holzwarth, U., Kotthoff, U., Leroy, S.A.G., Londeix, L., Marret, F., Matsuoka, K., Mudie, P.J., Naudts, L., Peña-Manjarrez, J.L., Persson, A., Popescu, S.M., Pospelova, V., Sangiorgi, F., van der Meer, M.T.J., Vink, A., Zonneveld, K.A.F., Vercauteren, D., Vlassenbroeck, J., Louwye, S., Nebout, N.C., Dale, B., De Vernal, A., Ellegaard, M., Filipova, M., Godhe, A., 2009. Process length variation in cysts of a dinoflagellate, Lingulodinium machaerophorum, in surface sediments: investigating its potential as salinity proxy. Mar. Micropaleontol. 70,

54–69. doi:10.1016/j.marmicro.2008.10.004

Milkov, A. V., 2005. Molecular and stable isotope compositions of natural gas hydrates: a revised global dataset and basic interpretations in the context of geological settings. Org. Geochem. 36, 681–702.

Moldowan, J.M., Dahl, J., Jacobson, S.R., Huizinga, B.J., Fago, F.J., Shetty, R., Watt, D.S., Peters, K.E., 1996. Chemostratigraphic reconstruction of biofacies: molecular evidence linking cyst-forming dinoflagellates with pre-Triassic ancestors. Geology 24, 159–162. doi:10.1130/0091-7613(1996)024<0159:CROBME>2.3.CO

Morgan, J.P., Reston, T.J., Ranero, C.R., 2004. Contemporaneous mass extinctions, continental flood basalts, and "impact signals": are mantle plume-induced lithospheric gas explosions the causal link? Earth Planet. Sci. Lett. 217, 263–284.

Mudie, P.J., 1996. Pellets of dinoflagellate-eating zooplankton. Palynol. Princ. Appl. Found. 1087–1089.

Muller, R.D., Sdrolias, M., Gaina, C., Steinberger, B., Heine, C., 2008. Long-term sea-level fluctuations driven by ocean basin dynamics. Science 319, 1357–1362. doi:10.1126/science.1151540 [doi]

Murphy, B.H., Farley, K., Zachos, J.C., 2010. An extraterrestrial 3 He-based timescale for the Paleocene–Eocene thermal maximum (PETM) from Walvis Ridge, IODP Site 1266. Geochim. Cosmochim. Acta 74, 5098–5108.

Mutterlose, J., Linnert, C., Norris, R.D., 2007. Calcareous nannofossils from the Paleocene–Eocene Thermal Maximum of the equatorial Atlantic (ODP Site 1260B): evidence for tropical warming. Mar. Micropaleontol. 65, 13–31.

Nagai, S., Matsuyama, Y., Oh, S.-J., Itakura, S., 2004. Effect of nutrients and temperature on encystment of the toxic dinoflagellate Alexandrium tamarense (Dinophyceae). Plankt. Biol.Ecol 51, 103–109.

Naustvoll, L.-J., 2000. Prey size spectra and food preferences in thecate heterotrophic dinoflagellates. Phycologia 39, 187–198.

Nicolo, M.J., Dickens, G.R., Hollis, C.J., Zachos, J.C., 2007. Multiple early Eocene hyperthermals: Their sedimentary expression on the New Zealand continental margin and in the deep sea. Geology 35, 699–702. doi:10.1130/G23648A.1

Nisbet, E.G., Jones, S.M., Maclennan, J., Eagles, G., Moed, J., Warwick, N., Bekki, S., Braesicke, P., Pyle, J. a., Fowler, C.M.R., 2009. Kick-starting ancient warming. Nat. Geosci. 2, 156–159. doi:10.1038/ngeo454

Oboh-Ikuenobe, F.E., Yepes, O., Mascle, J., Lohmann, G.P., Clift, P., Akamaluk, T., Allerton, S., Ask, M., Barrera, E., Barton, E., Basile, C., Bellier, J.P., Benkhelil, J., Brantuoh, E., Edwards, R., Ewert, E., Gon??alves, C., Janik, A.G., Holmes, M.A., Hisada, K.I., Lohmann, K.C., Morita, S., Montera-Gutierrez, C.A., Norris, R.D., Pletsch, T., Pickett, E.A., Ravizza, G., Shafik, S., Shin, I.C., Strand, K.O., Wagner, T., Watkins, D.K., 1997. Palynofacies analysis of sediments from the Cote d'Ivoire-Ghana Transform Margin: Preliminary correlation with some regional events in the Equatorial Atlantic. Palaeogeogr. Palaeoclimatol. Palaeoecol. 129, 291–314. doi:10.1016/S0031-0182(96)00125-3

Okosun, E.A., 1990. A review of the Cretaceous stratigraphy of the Dahomey Embayment, West Africa. Cretac. Res. 11, 17–27. doi:10.1016/S0195-6671(05)80040-0

Paerl, H.W., Hall, N.S., Calandrino, E.S., 2011. Controlling harmful cyanobacterial blooms in a world experiencing anthropogenic and climatic-induced change. Sci. Total Environ. 409, 1739–1745. doi:10.1016/j.scitotenv.2011.02.001

Pagani, M., Caldeira, K., Archer, D., Zachos, J.C., 2006a. An ancient carbon mystery. Science (80-.). 314, 1556–1557.

Pagani, M., Pedentchouk, N., Huber, M., Sluijs, A., Schouten, S., Brinkhuis, H., Damsté, J.S.S., Dickens, G.R., 2006b. Arctic hydrology during global warming at the Palaeocene/Eocene thermal maximum. Nature 442, 671–675. doi:10.1038/nature05043

Pälike, C., Delaney, M.L., Zachos, J.C., 2014. Geochemistry, Geophysics, Geosystems 1038–1053. doi:10.1002/2013GC005074.Received

Pälike, C., Delaney, M.L., Zachos, J.C., 2014. Deep-sea redox across the Paleocene-Eocene thermal maximum. Geochemistry, Geophys. Geosystems 15, 1038–1053. doi:10.1002/2013GC005074

Panchuk, K., Ridgwell, A.J., Kump, L.R., 2008. Sedimentary response to Paleocene-Eocene Thermal Maximum carbon release: A model-data comparison. Geology 36, 315–318. doi:10.1130/G24474A.1

Pandolfi, J.M., Connolly, S.R., Marshall, D.J., Cohen, A.L., 2011. Projecting coral reef futures under global warming and ocean acidification. Science 333, 418–422. doi:10.1126/science.1204794 [doi]

Party, S.S., 1996. Site 959. Mascle, J., Lohmann, GP, Clift, PD, al., Proc. ODP, Init. Repts 159, 65–150.

Paul, V.J., 2008. Global warming and cyanobacterial harmful algal blooms, in: Cyanobacterial Harmful Algal Blooms: State of the Science and Research Needs. Springer, pp. 239–257.

Paytan, A., Averyt, K., Faul, K., Gray, E., Thomas, E., 2007. Barite accumulation, ocean productivity, and Sr/Ba in barite across the Paleocene–Eocene Thermal Maximum. Geology 35, 1139–1142.

Paytan, A., Griffith, E.M., 2007. Marine barite: Recorder of variations in ocean export productivity. Deep. Res. Part II Top. Stud. Oceanogr. 54, 687–705. doi:10.1016/j.dsr2.2007.01.007

Pearson, A., Ingalls, A.E., 2013. Assessing the use of archaeal lipids as marine environmental proxies. Annu. Rev. Earth Planet. Sci. 41, 359–384. doi:10.1146/annurev-earth-050212-123947

Pearson, P.N., van Dongen, B.E., Nicholas, C.J., Pancost, R.D., Schouten, S., Singano, J.M., Wade, B.S., 2007. Stable warm tropical climate through the Eocene Epoch. Geology 35, 211–214.

Peña-Manjarrez, J.L., Helenes, J., Gaxiola-Castro, G., Orellana-Cepeda, E., 2005. Dinoflagellate cysts and bloom events at todos Santos Bay, Baja California, Mexico, 1999–2000. Cont. Shelf Res. 25, 1375–1393. doi:10.1016/j.csr.2005.02.002

Penman, D.E., Hönisch, B., Zeebe, R.E., Thomas, E., Zachos, J.C., 2014. Rapid and sustained surface ocean acidification during the Paleocene-Eocene Thermal Maximum. Paleoceanography 29, 357–369.

Pierrehumbert, R.T., 1995. Thermostats, radiator fins, and the local runaway greenhouse. J. Atmos. Sci. 52, 1784–1806.

Planke, S., Rasmussen, T., Rey, S.S., Myklebust, R., 2005. Seismic characteristics and distribution

of volcanic intrusions and hydrothermal vent complexes in the Vøring and Møre basins. Pet. Geol. Conf. Proc. 6, 833–844. doi:10.1144/0060833

Planke, S., Symonds, P.A., Alvestad, E., Skogseid, J., 2000. Seismic volcanostratigraphy of large-volume basaltic extrusive complexes on rifted margins. J. Geophys. Res. Solid Earth 105, 19335–19351.

Pletsch, T., Erbacher, J., Holbourn, A.E.., Kuhnt, W., Moullade, M., Oboh-Ikuenobe, F., Söding, E., Wagner, T., 2001. Cretaceous separation of Africa and South America: the view from the West African margin (ODP Leg 159). J. South Am. Earth Sci. 14, 147–174. doi:10.1016/S0895-9811(01)00020-7

Powell, A.J., Brinkhuis, H., Bujak, J.P., 1996. Upper Paleocene-Lower Eocene dinoflagellate cyst sequence biostratigraphy of southeast England. Geol. Soc. Spec. Publ.

Pross, J., Brinkhuis, H., 2005. Organic-walled dinoflagellate cysts as paleoenvironmental indicators in the Paleogene ; a synopsis of concepts. Paläontologische Zeitschrift 79, 53–59.

Pross, J., Contreras, L., Bijl, P.K., Greenwood, D.R., Bohaty, S.M., Schouten, S., Bendle, J.A.P., Röhl, U., Tauxe, L., Raine, J.I., Huck, C.E., Van De Flierdt, T., Jamieson, S.S.R., Stickley, C.E., Van De Schootbrugge, B., Escutia, C., Brinkhuis, H., Dotti, C.E., Klaus, A., Fehr, A., Williams, T., Carr, S.A., Dunbar, R.B., Gonzàlez, J.J., Hayden, T.G., Iwai, M., Jimenez-Espejo, F.J., Katsuki, K., Soo Kong, G., Mckay, R.M., Nakai, M., Olney, M.P., Passchier, S., Pekar, S.F., Riesselman, C.R., Sakai, T., Shrivastava, P.K., Sugisaki, S., Tuo, S., Welsh, K., Yamane, M., 2012. Persistent near-tropical warmth on the Antarctic continent during the early Eocene epoch. Nature 487, 73–77. doi:10.1038/nature11300

Radionova, E.P., Beniamovski, V.N., Iakovleva, A.I., Muzylov, N.G., Oreshkina, T. V., Shcherbinina, E.A., Kozlova, G.E., Muzylöv, N.G., Oreshkina, T. V., Shcherbinina, E.A., Kozlova, G.E., 2003. Early Paleogene transgressions: Stratigraphical and sedimentological evidence from the northern Peri-Tethys. Spec. Pap. Soc. Am. 369, 239–262. doi:10.1130/0-8137-2369-8.239

Raffi, I., Backman, J., Pälike, H., 2005. Changes in calcareous nannofossil assemblages across the Paleocene/Eocene transition from the paleo-equatorial Pacific Ocean. Palaeogeogr. Palaeoclimatol. Palaeoecol. 226, 93–126.

Rampino, M.R., 2013. Peraluminous igneous rocks as an indicator of thermogenic methane release from the North Atlantic Volcanic Province at the time of the Paleocene–Eocene Thermal Maximum (PETM). Bull. Volcanol. 75, 1–5. doi:10.1007/s00445-012-0678-x

Reichart, G.-J., Brinkhuis, H., 2003. Late Quaternary< i> Protoperidinium</i> cysts as indicators of paleoproductivity in the northern Arabian Sea. Mar. Micropaleontol. 49, 303–315.

Reichart, G.-J., Brinkhuis, H., Huiskamp, F., Zachariasse, W.J., 2004. Hyperstratification following glacial overturning events in the northern Arabian Sea. Paleoceanography 19, PA2013 1–8.

Reid, P.C., Boalch, G.T., 1987. A new method for the identification of dinoflagellate cysts. J. Plankton Res. 9, 249–253.

Reitz, A., Pfeifer, K., De Lange, G.J., Klump, J., 2004. Biogenic barium and the detrital Ba/Al ratio: a comparison of their direct and indirect determination. Mar. Geol. 204, 289–300.

Röhl, U., Westerhold, T., Bralower, T.J., Zachos, J.C., 2007. On the duration of the Paleocene-

Eocene thermal maximum (PETM). Geochemistry, Geophys. Geosystems 8. doi:10.1029/2007GC001784

Rohling, E.J., Sluijs, A., Dijkstra, H.A., Köhler, P., van de Wal, R.S.W., von der Heydt, A.S., Beerling, D.J., Berger, a., Bijl, P.K., Crucifix, M., DeConto, R.M., Drijfhout, S.S., Fedorov, a., Foster, G.L., Ganopolski, A., Hansen, J., Hönisch, B., Hooghiemstra, H., Huber, M., Huybers, P., Knutti, R., Lea, D.W., Lourens, L.J., Lunt, D.J., Masson-Demotte, V., Medina-Elizalde, M., Otto-Bliesner, B., Pagani, M., Pälike, H., Renssen, H., Royer, D.L., Siddall, M., Valdes, P.J., Zachos, J.C., Zeebe, R.E., Members, P.P., 2012. Making sense of palaeoclimate sensitivity. Nature 491, 683–691. doi:10.1038/nature11574

Rutsch, H.-J.J., Mangini, A., Bonani, G., Dittrich-Hannen, B., Kubik, P.W., Suter, M., Segl, M., 1995. 10Be and Ba concentrations in West African sediments trace productivity in the past. Earth Planet. Sci. Lett. 133, 129–143. doi:10.1016/0012-821X(95)00069-O

Schiøler, P., Brinkhuis, H., Roncaglia, L., Wilson, G.J., 1997. Dinoflagellate biostratigraphy and sequence stratigraphy of the type Maastrichtian (Upper Cretaceous), ENCI Quarry, The Netherlands. Mar. Micropaleontol. Elsevier. doi:10.1016/S0377-8398(96)00058-8

Schmitz, B., Peucker-Ehrenbrink, B., Heilmann-Clausen, C., Aberg, G., Asaro, F., Lee, C.-T.A., 2004. Basaltic explosive volcanism, but no comet impact, at the Paleocene–Eocene boundary: high-resolution chemical and isotopic records from Egypt, Spain and Denmark. Earth Planet. Sci. Lett. 225, 1–17. doi:10.1016/j.epsl.2004.06.017

Schmitz, B., Pujalte, V., 2007. Abrupt increase in seasonal extreme precipitation at the Paleocene-Eocene boundary. Geology 35, 215–218. doi:10.1130/G23261A.1

Schoon, P.L., Heilmann-Clausen, C., Schultz, B.P., Sinninghe Damsté, J.S., Schouten, S., 2015. Warming and environmental changes in the eastern North Sea Basin during the Palaeocene-Eocene Thermal Maximum as revealed by biomarker lipids. Org. Geochem. 78, 79–88. doi:10.1016/j.orggeochem.2014.11.003

Schoon, P.L., Sluijs, A., Sinninghe Damsté, J.S., Schouten, S., 2011. Stable carbon isotope patterns of marine biomarker lipids in the Arctic Ocean during Eocene Thermal Maximum 2. Paleoceanography 26.

Schouten, S., Forster, A., Panoto, F.E., Sinninghe Damsté, J.S., 2007a. Towards calibration of the TEX86 palaeothermometer for tropical sea surface temperatures in ancient greenhouse worlds. Org. Geochem. 38, 1537–1546. doi:http://dx.doi.org/10.1016/j.orggeochem.2007.05.014

Schouten, S., Hopmans, E.C., Schefuß, E., Sinninghe Damsté, J.S., 2002. Distributional variations in marine crenarchaeotal membrane lipids: A new tool for reconstructing ancient sea water temperatures? Earth Planet. Sci. Lett. 204, 265–274. doi:10.1016/S0012-821X(02)00979-2

Schouten, S., Hopmans, E.C., Sinninghe Damsté, J.S., 2013. The organic geochemistry of glycerol dialkyl glycerol tetraether lipids: A review. Org. Geochem. 54, 19–61. doi:http://dx.doi.org/10.1016/j.orggeochem.2012.09.006

Schouten, S., Huguet, C., Hopmans, E.C., Kienhuis, M.V.M., Sinninghe Damsté, J.S., Damsté, J.S.S., 2007b. Analytical methodology for TEX86 paleothermometry by high-performance liquid chromatography/atmospheric pressure chemical ionization-mass spectrometry. Anal. Chem. 79, 2940–2944. doi:10.1029/2004PA001110.This

Schouten, S., Woltering, M., Rijpstra, W.I.C., Sluijs, A., Brinkhuis, H., Sinninghe Damsté, J.S., 2007c. The Paleocene-Eocene carbon isotope excursion in higher plant organic matter:

Differential fractionation of angiosperms and conifers in the Arctic. Earth Planet. Sci. Lett. 258, 581–592. doi:10.1016/j.epsl.2007.04.024

Schrag, D.P., DePaolo, D.J., Richter, F.M., 1995. Reconstructing past sea surface temperatures: Correcting for diagenesis of bulk marine carbonate. Geochim. Cosmochim. Acta 59, 2265–2278.

Schubert, B.A., Hope Jahren, A., 2013. Reconciliation of marine and terrestrial carbon isotope excursions based on changing atmospheric CO2 levels. Nat. Commun. 4, 1653. doi:10.1038/ncomms2659

Secord, R., Gingerich, P.D., Lohmann, K.C., MacLeod, K.G., 2010. Continental warming preceding the Palaeocene-Eocene thermal maximum. Nature 467, 955–958. doi:10.1038/nature09441

Self, S., Widdowson, M., Thordarson, T., Jay, A.E., 2006. Volatile fluxes during flood basalt eruptions and potential effects on the global environment: A Deccan perspective. Earth Planet. Sci. Lett. 248, 518–532.

Seton, M., Müller, R.D., Zahirovic, S., Gaina, C., Torsvik, T.H., Shephard, G., Talsma, A., Gurnis, M., Turner, M., Maus, S., 2012. Global continental and ocean basin reconstructions since 200Ma. Earth-Science Rev. 113, 212–270.

Shafik, S., Watkins, D.K., Shin, I.C., 1998. 32 . Calcareous Nannofossil Paleogene Biostratigraphy , Côte D ' Ivoire-Ghana. Proc. Ocean Drill. Program, Sci. Results 159, 413–431.

Sherr, E.B., Sherr, B.F., 2007. Heterotrophic dinoflagellates: a significant component of microzooplankton biomass and major grazers of diatoms in the sea. Mar. Ecol. Ser. 352, 187.

Sherwood, S.C., Huber, M., 2010. An adaptability limit to climate change due to heat stress. Proc. Natl. Acad. Sci. U. S. A. 107, 9552–9555. doi:10.1073/pnas.0913352107 [doi]

Siever, R., 1991. Silica in the oceans: Biological-geochemical interplay. Sci. gaia 287–295.

Sinninghe Damsté, J.S., Koster, J., Baas, M., Koopmans, M.P., van Kaam-Peters, H.M.E., Geenevasen, J.A.J., Kruk, C., 1995. Cyclisation and aromatisation of carotenoids during sediment diagenesis. J. Chem. Soc. Chem. Commun. 187–188.

Sinninghe Damsté, J.S., Wakeham, S.G., Kohnen, M.E.L., Hayes, J.M., De Leeuw, J.W., 1993. A 6,000-year sedimentary molecular record of chemocline excursions in the Black Sea. Nature 362, 827–829.

Siringan, F.P., Azanza, R. V., Macalalad, N.J.H., Zamora, P.B., Maria, M.Y.Y.S., 2008. Temporal changes in the cyst densities of Pyrodinium bahamense var. compressum and other dinoflagellates in Manila Bay, Philippines. Harmful Algae 7, 523–531.

Sloan, L.C., Huber, M., Crowley, T.J., Sewall, J.O., Baum, S., 2001. Effect of sea surface temperature configuration on model simulations of "equable" climate in the Early Eocene. Palaeogeogr. Palaeoclimatol. Palaeoecol. 167, 321–335.

Slomp, C.P., Thomson, J., De Lange, G.J., 2002. Enhanced regeneration of phosphorus during formation of the most recent eastern Mediterranean sapropel (S1). Geochim. Cosmochim. Acta 66, 1171–1184. doi:http://dx.doi.org/10.1016/S0016-7037(01)00848-1

Sluijs, A., Bijl, P.K., Schouten, S., Röhl, U., Reichart, G.-J., Brinkhuis, H., 2011. Southern ocean warming, sea level and hydrological change during the Paleocene-Eocene thermal

maximum. Clim. Past 7, 47–61. doi:10.5194/cp-7-47-2011

Sluijs, A., Bowen, G.J., Brinkhuis, H., Lourens, L.J., Thomas, E., 2007a. The Palaeocene-Eocene Thermal Maximum super greenhouse: Biotic and geochemical signatures, age models and mechanisms of global change. Geol. Soc. Spec. Publ.

Sluijs, A., Brinkhuis, H., 2009. A dynamic climate and ecosystem state during the Paleocene-Eocene Thermal Maximum – inferences from dinoflagellate cyst assemblages at the New Jersey Shelf. Biogeosciences Discuss. 6, 5163–5215. doi:10.5194/bgd-6-5163-2009

Sluijs, A., Brinkhuis, H., Crouch, E.M., John, C.M., Handley, L., Munsterman, D.K., Bohaty, S.M., Zachos, J.C., Reichart, G.-J., Schouten, S., Pancost, R.D., Damsté, J.S.S., Welters, N., Lotter, A.F., Dickens, G.R., 2008a. Eustatic variations during the Paleocene-Eocene greenhouse world. Paleoceanography 23.

Sluijs, A., Brinkhuis, H., Schouten, S., Bohaty, S.M., John, C.M., Zachos, J.C., Reichart, G.-J., Sinninghe Damsté, J.S., Crouch, E.M., Dickens, G.R., 2007b. Environmental precursors to rapid light carbon injection at the Palaeocene/Eocene boundary. Nature 450, 1218–1221.

Sluijs, A., Brinkhuis, H., Stickley, C.E., Warnaar, J., Williams, G.L., Fuller, M., 2003. Dinoflagellate cysts from the Eocene/Oligocene transition in the Southern Ocean; results from ODP Leg 189, in: Proc. Ocean Drill. Program Sci. Results. pp. 1–42.

Sluijs, A., Dickens, G.R., 2012. Assessing offsets between the δ13C of sedimentary components and the global exogenic carbon pool across early Paleogene carbon cycle perturbations. Global Biogeochem. Cycles 26.

Sluijs, A., Pross, J., Brinkhuis, H., 2005. From greenhouse to icehouse; organic-walled dinoflagellate cysts as paleoenvironmental indicators in the Paleogene. Earth-Science Rev. 68, 281–315. doi:http://dx.doi.org/10.1016/j.earscirev.2004.06.001

Sluijs, A., Röhl, U., Schouten, S., Brumsack, H.J., Sangiorgi, F., Sinninghe Damsté, J.S., Brinkhuis, H., 2008b. Article late Paleocene - Early Eocene paleoenvironments with special emphasis on the Paleocene-Eocene thermal maximum (Lomonosov Ridge, Integrated Ocean Drilling Program Expedition 302). Paleoceanography 23. doi:10.1029/2007PA001495

Sluijs, A., Schouten, S., Donders, T., Schoon, P.L., Röhl, U., Reichart, G.-J., Sangiorgi, F., Kim, J.H., Sinninghe Damsté, J.S., Brinkhuis, H., 2009. Warm and wet conditions in the Arctic region during Eocene Thermal Maximum 2. Nat. Geosci. 2, 777–780.

Sluijs, A., Schouten, S., Pagani, M., Woltering, M., Brinkhuis, H., Sinninghe Damsté, J.S., Dickens, G.R., Huber, M., Reichart, G.-J., Stein, R., Matthiessen, J., Lourens, L.J., Pedentchouk, N., Backman, J., Moran, K., the Expedition, S., 2006. Subtropical Arctic Ocean temperatures during the Palaeocene/Eocene thermal maximum. Nature 441, 610–613. doi:10.1038/nature04668

Sluijs, A., Van Roij, L., Harrington, G.J., Schouten, S., Sessa, J.A., Levay, L.J., Reichart, G.-J., Slomp, C.P., 2014. Warming, euxinia and sea level rise during the paleocene-eocene thermal maximum on the gulf coastal plain: Implications for ocean oxygenation and nutrient cycling. Clim. Past 10, 1421–1439. doi:10.5194/cp-10-1421-2014

Sluijs, A., Zachos, J.C., Zeebe, R.E., 2012. Constraints on hyperthermals. Nat. Geosci. 5, 231.

Soliman, M.F., 2003. Chemostratigraphy of the Paleocene/Eocene (P/E) boundary sediments at Gabal el-Qreiya, Nile Valley, Egypt. Micropaleontology 49, 123–138.

Somero, G.N., 1995. Proteins and temperature. Annu. Rev. Physiol. 57, 43–68.

Speijer, R.P., Morsi, A.-M.M., 2002. Ostracode turnover and sea-level changes associated with the Paleocene-Eocene thermal maximum. Geology 30, 23–26.

Stap, L., Lourens, L.J., Thomas, E., Sluijs, A., Bohaty, S.M., Zachos, J.C., 2010. High-resolution deep-sea carbon and oxygen isotope records of Eocene Thermal Maximum 2 and H2. Geology 38, 607–610. doi:10.1130/G30777.1

Stap, L., Sluijs, A., Thomas, E., Lourens, L.J., 2009. Patterns and magnitude of deep sea carbonate dissolution during Eocene Thermal Maximum 2 and H2, Walvis Ridge, southeastern Atlantic Ocean. Paleoceanography 24, 1–13. doi:10.1029/2008PA001655

Stassen, P., Thomas, E., Speijer, R.P., 2012. Integrated stratigraphy of the Paleocene-Eocene thermal maximum in the New Jersey Coastal Plain: Toward understanding the effects of global warming in a shelf environment. Paleoceanography 27, 1–17. doi:10.1029/2012PA002323

Stockmarr, J., 1971. Tablets with spores used in absolute pollen analysis. Pollen et spores.

Storey, M., Duncan, R.A., Swisher, C.C., 2007. Paleocene-Eocene Thermal Maximum and the Opening of the Northeast Atlantic. Science (80-.). 316, 587–589. doi:10.1126/science.1135274

Stramma, L., Johnson, G.C., Sprintall, J., Mohrholz, V., 2008. Expanding oxygen-minimum zones in the tropical oceans. Science 320, 655–658. doi:10.1126/science.1153847 [doi]

Sunday, J.M., Bates, A.E., Dulvy, N.K., 2011. Global analysis of thermal tolerance and latitude in ectotherms. Proceedings.Biological Sci. / R. Soc. 278, 1823–1830. doi:10.1098/rspb.2010.1295 [doi]

Svensen, H., Jamtveit, B., 2010. Metamorphic fluids and global environmental changes. Elements 6, 179–182. doi:10.2113/gselements.6.3.179

Svensen, H., Planke, S., Corfu, F., 2010. Zircon dating ties NE Atlantic sill emplacement to initial Eocene global warming. J. Geol. Soc. London. 167, 433–436.

Svensen, H., Planke, S., Maithe-Sørensen, A., Jamtveit, B., Myklebust, R., Eidem, T.R., Rey, S.S., 2004. Release of methane from a volcanic basin as a mechanism for initial Eocene global warming. Nature 429, 542–545.

Taylor, K.W.R., Huber, M., Hollis, C.J., Hernandez-Sanchez, M.T., Pancost, R.D., 2013. Re-evaluating modern and Palaeogene GDGT distributions: Implications for SST reconstructions. Glob. Planet. Change 108, 158–174. doi:10.1016/j.gloplacha.2013.06.011

Tewksbury, J.J., Huey, R.B., Deutsch, C. a, 2008. Putting the heat on tropical animals. Science 320, 1296–1297. doi:10.1126/science.1159328

Thomas, D.J., Bralower, T.J., Jones, C.E., 2003. Neodymium isotopic reconstruction of late Paleocene–early Eocene thermohaline circulation. Earth Planet. Sci. Lett. 209, 309–322.

Thomas, D.J., Zachos, J.C., Bralower, T.J., Thomas, E., Bohaty, S.M., 2002. Warming the Fuel for the Fire : Evidence for the Thermal Dissociation of Methane Hydrate During the Paleocene-Eocene Thermal Maximum dissociation of methane hydrate during the Paleocene-Eocene. Geology 30, 1067–1070. doi:10.1130/0091-7613(2002)030<1067:WTFFTF>2.0.CO;2

Thomas, E., 1990. Late Cretaceous–early Eocene mass extinctions in the deep sea. Geol. Soc. Am. Spec. Pap. 247, 481–496.

Thomas, E., Zachos, J.C., 2000. Was the late Paleocene thermal maximum a unique event? Gff

122, 169–170. doi:10.1080/11035890001221169

Tierney, J.E., 2012. GDGT Thermometry: Lipid Tools for Reconstructing Paleotemperatures, in: Ivany, L.C., Huber, B.T. (Eds.), Reconstructing Earth's Deep-Time Climate—The State of the Art in 2012 . The Paleontological Society Papers, pp. 115–131.

Tierney, J.E., Tingley, M.P., 2015. A TEX(8)(6) surface sediment database and extended Bayesian calibration. Sci Data. doi:10.1038/sdata.2015.29

Tierney, J.E., Tingley, M.P., 2014. A Bayesian, spatially-varying calibration model for the TEX86 proxy. Geochim. Cosmochim. Acta 127, 83–106. doi:10.1016/j.gca.2013.11.026

Torricelli, S., Knezaurek, G., Biffi, U., 2006. Sequence biostratigraphy and paleoenvironmental reconstruction in the Early Eocene Figols Group of the Tremp-Graus Basin (south-central Pyrenees, Spain). Palaeogeogr. Palaeoclimatol. Palaeoecol. 232, 1–35. doi:10.1016/j.palaeo.2005.08.009

Tremolada, F., Bralower, T.J., 2004. Nannofossil assemblage fluctuations during the Paleocene–Eocene thermal maximum at Sites 213 (Indian Ocean) and 401 (North Atlantic Ocean): palaeoceanographic implications. Mar. Micropaleontol. 52, 107–116.

Tripati, A.K., 2003. Tropical sea-surface temperature reconstruction for the early Paleogene using Mg/Ca ratios of planktonic foraminifera. Paleoceanography 18, 1101. doi:10.1029/2003PA000937

Trommer, G., Siccha, M., van der Meer, M.T.J., Schouten, S., Sinninghe Damsté, J.S., Schulz, H., Hemleben, C., Kucera, M., 2009. Distribution of Crenarchaeota tetraether membrane lipids in surface sediments from the Red Sea. Org. Geochem. 40, 724–731. doi:10.1016/j.orggeochem.2009.03.001

Turgeon, S.C., Creaser, R.A., 2008. Cretaceous oceanic anoxic event 2 triggered by a massive magmatic episode. Nature 454, 323–326.

Uchikawa, J., Zeebe, R.E., 2010. Examining possible effects of seawater pH decline on foraminiferal stable isotopes during the Paleocene-Eocene Thermal Maximum. Paleoceanography 25, 1–14. doi:10.1029/2009PA001864

Valentine, D.L., Blanton, D.C., Reeburgh, W.S., Kastner, M., 2001. Water column methane oxidation adjacent to an area of active hydrate dissociation, Eel River Basin. Geochim. Cosmochim. Acta 65, 2633–2640.

van Hinsbergen, D.J.J., de Groot, L. V, van Schaik, S.J., Spakman, W., Bijl, P.K., Sluijs, A., Langereis, C.G., Brinkhuis, H., 2015. A Paleolatitude Calculator for Paleoclimate Studies. PLoS One 10, e0126946. doi:10.1371/journal.pone.0126946

Vandenberghe, N., Hilgen, F.J., Speijer, R.P., 2012. The Paleogene Period. Geol. time scale 2012, 855–921.

Verschuren, D., Damsté, J.S.S., Moernaut, J., Kristen, I., Blaauw, M., Fagot, M., Haug, G.H., van Geel, B., De Batist, M., Barker, P., 2009. Half-precessional dynamics of monsoon rainfall near the East African Equator. Nature 462, 637–641.

Villanoy, C.L., Azanza, R. V., Altemerano, A., Casil, A.L., 2006. Attempts to model the bloom dynamics of Pyrodinium, a tropical toxic dinoflagellate. Harmful Algae 5, 156–183.

Villanoy, C.L., Corrales, R.A., Jacinto, G.S., Cuaresma Jr, N.T., Crisostomo, R.P., 1996. Towards the development of a cyst-based model for Pyrodinium red tides in Manila Bay, Philippines.

Harmful toxic algal Bloom. Paris 189–192.

Wade, B.S., Pearson, P.N., Berggren, W.A., P??like, H., Pälike, H., 2011. Review and revision of Cenozoic tropical planktonic foraminiferal biostratigraphy and calibration to the geomagnetic polarity and astronomical time scale. Earth-Science Rev. 104, 111–142. doi:10.1016/j.earscirev.2010.09.003

Wagner, T., 2002. Late Cretaceous to early Quaternary organic sedimentation in the eastern Equatorial Atlantic. Palaeogeogr. Palaeoclimatol. Palaeoecol. 179, 113–147. doi:10.1016/S0031-0182(01)00415-1

Walker, J.C.G., Kasting, J.F., 1992. Effects of fuel and forest conservation on future levels of atmospheric carbon dioxide. Glob. Planet. Change 5, 151–189.

Weijers, J.W.H., Lim, K.L.H., Aquilina, A., Damsté, J.S.S., Pancost, R.D., 2011. Biogeochemical controls on glycerol dialkyl glycerol tetraether lipid distributions in sediments characterized by diffusive methane flux. Geochemistry Geophys. Geosystems 12, Q10010.

Weijers, J.W.H., Schouten, S., Spaargaren, O.C., Sinninghe Damsté, J.S., 2006. Occurrence and distribution of tetraether membrane lipids in soils: Implications for the use of the TEX86 proxy and the BIT index. Org. Geochem. 37, 1680–1693.

Westerhold, T., Röhl, U., Laskar, J., 2012. Time scale controversy: Accurate orbital calibration of the early Paleogene. Geochemistry, Geophys. Geosystems 13, n/a–n/a. doi:10.1029/2012GC004096

Williams, G.L., Brinkhuis, H., Pearce, M.A., Fensome, R.A., Weegink, J.W., 2004. Southern Ocean and global dinoflagellate cyst events compared: index events for the Late Cretaceous–Neogene, in: Proceedings of the Ocean Drilling Program, Scientific Results. pp. 1–98.

Williams, G.L., Damassa, S.P., Fensome, R.A., Guerstein, R., 2015. *Wetzeliella* and its allies – the "hole" story: a taxonomic revision of the Paleogene dinoflagellate subfamily Wetzelielloideae. Palynology 39, 289–344. doi:10.1080/01916122.2014.993888

Williams, I.N., Pierrehumbert, R.T., Huber, M., 2009. Global warming, convective threshold and false thermostats. Geophys. Res. Lett. 36, 2–6. doi:10.1029/2009GL039849

Wilson, K.E., Maslin, M.A., Leng, M.J., Kingston, J.D., Deino, A.L., Edgar, R.K., Mackay, A.W., 2014. East African lake evidence for Pliocene millennial-scale climate variability. Geology 42, 955–958.

Wing, S.L., Harrington, G.J., Smith, F.A., Bloch, J.I., Boyer, D.M., Freeman, K.H., 2005. Transient floral change and rapid global warming at the Paleocene-Eocene boundary. Science 310, 993–996. doi:310/5750/993 [pii]

Woulds, C., Cowie, G.G.L., Levin, L.A., Andersson, J.H., Middelburg, J.J., Vandewiele, S., Lamont, P.A., Larkin, K.E., Gooday, A.J., Schumacher, S., 2007. Oxygen as a control on sea floor biological communities and their roles in sedimentary carbon cycling. Limnol. Oceanogr. 52, 1698–1709. doi:10.2307/4502324

Wu, H., Zhang, S., Feng, Q., Jiang, G., Li, H., Yang, T., 2012. Milankovitch and sub-Milankovitch cycles of the early Triassic Daye Formation, South China and their geochronological and paleoclimatic implications. Gondwana Res. 22, 748–759.

Wuchter, C., Schouten, S., Coolen, M.J.L., Sinninghe Damsté, J.S., 2004. Temperature-dependent variation in the distribution of tetraether membrane lipids of marine Crenarchaeota: Implications for TEX86 paleothermometry. Paleoceanography 19, 1–10.

doi:10.1029/2004PA001041

Yamaguchi, T., Norris, R.D., 2015. No place to retreat: Heavy extinction and delayed recovery on a Pacific guyot during the Paleocene–Eocene Thermal Maximum. Geology 43, 443–446.

Zachos, J.C., 2005. Rapid Acidification of the Ocean During the Paleocene-Eocene Thermal Maximum. Science (80-.). 308, 1611–1615. doi:10.1126/science.1109004

Zachos, J.C., Bohaty, S.M., John, C.M., McCarren, H.K., Kelly, D.C., Nielsen, T.M.J., 2007. The Palaeocene-Eocene carbon isotope excursion: constraints from individual shell planktonic foraminifer records. Philos. Trans. A. Math. Phys. Eng. Sci. 365, 1829–1842. doi:10.1098/rsta.2007.2045

Zachos, J.C., Dickens, G.R., Zeebe, R.E., 2008. An early Cenozoic perspective on greenhouse warming and carbon-cycle dynamics. Nature 451, 279–283. doi:10.1038/nature06588

Zachos, J.C., Röhl, U., Schellenberg, S.A., Sluijs, A., Hodell, D.A., Kelly, D.C., Thomas, E., Nicolo, M.J., Raffi, I., Lourens, L.J., McCarren, H.K., Kroon, D., 2005. Paleoclimate: Rapid acidification of the ocean during the paleocene-eocene thermal maximum. Science (80-.). 308, 1611–1615. doi:10.1126/science.1109004

Zachos, J.C., Schouten, S., Bohaty, S.M., Quattlebaum, T., Sluijs, A., Brinkhuis, H., Gibbs, S.J., Bralower, T.J., 2006. Extreme warming of mid-latitude coastal ocean during the Paleocene-Eocene Thermal Maximum: Inferences from TEX86 and isotope data. Geology 34, 737–740.

Zachos, J.C., Stott, L.D., Lohmann, K.C., 1994. Evolution of early Cenozoic marine temperatures at Equator. Paleoceanography 9, 353–387. doi:10.1029/93PA03266

Zachos, J.C., Wara, M.W., Bohaty, S.M., Delaney, M.L., Petrizzo, M.R., Brill, A., Bralower, T.J., Premoli-Silva, I., 2003. A Transient Rise in Tropical Sea Surface Temperature during the Paleocene-Eocene Thermal Maximum. Science (80-.). 302, 1551–1554.

Zeebe, R.E., 2013. What caused the long duration of the Paleocene-Eocene Thermal Maximum? Paleoceanography 28, 440–452.

Zeebe, R.E., 2012. LOSCAR: Long-term ocean-atmosphere-sediment carbon cycle reservoir model v2. 0.4. Geosci. Model Dev. 5, 149–166.

Zeebe, R.E., 2001. Seawater pH and isotopic paleotemperatures of Cretaceous oceans. Palaeogeogr. Palaeoclimatol. Palaeoecol. 170, 49–57. doi:10.1016/S0031-0182(01)00226-7

Zeebe, R.E., Dickens, G.R., Ridgwell, A.J., Sluijs, A., Thomas, E., 2014. Onset of carbon isotope excursion at the Paleocene-Eocene thermal maximum took millennia, not 13 years. Proc. Natl. Acad. Sci. U. S. A. 111, E1062–3. doi:10.1073/pnas.1321177111

Zeebe, R.E., Zachos, J.C., 2013. Long-term legacy of massive carbon input to the Earth system: Anthropocene versus Eocene. Philos. Trans. A. Math. Phys. Eng. Sci. 371, 20120006. doi:10.1098/rsta.2012.0006

Zeebe, R.E., Zachos, J.C., Dickens, G.R., 2009. Carbon dioxide forcing alone insufficient to explain Palaeocene–Eocene Thermal Maximum warming. Nat. Geosci. 2, 576–580. doi:10.1038/ngeo578

Zhang, Y.G., Zhang, C.L., Liu, X.L., Li, L., Hinrichs, K.U., Noakes, J.E., 2011. Methane Index: A tetraether archaeal lipid biomarker indicator for detecting the instability of marine gas hydrates. Earth Planet. Sci. Lett. 307, 525–534. doi:10.1016/j.epsl.2011.05.031

Zonneveld, K.A.F., Marret, F., Versteegh, G.J.M., Bogus, K., Bonnet, S., Bouimetarhan, I., Crouch, E.M., de Vernal, A., Elshanawany, R., Edwards, L.E., Esper, O., Forke, S., Gr??sfjeld, K., Henry, M., Holzwarth, U., Kielt, J.F.-F.F., Kim, S.-Y.Y., Ladouceur, S., Ledu, D., Chen, L., Limoges, A., Londeix, L., Lu, S.H.-H., Mahmoud, M.S., Marino, G., Matsuoka, K., Matthiessen, J., Mildenhal, D.C., Mudie, P.J., Neil, H.L., Pospelova, V., Qi, Y., Radi, T., Richerol, T., Rochon, A., Sangiorgi, F., Solignac, S., Turon, J.L., Verleye, T., Wang, Y., Wang, Z., Young, M., Grøsfjeld, K., 2013. Atlas of modern dinoflagellate cyst distribution based on 2405 data points. Rev. Palaeobot. Palynol. 191, 1–197. doi:10.1016/j.revpalbo.2012.08.003

Zonneveld, K.A.F., Versteegh, G.J.M., De Lange, G.J., 1997. Preservation of organic-walled dinoflagellate cysts in different oxygen regimes: a 10,000 year natural experiment. Mar. Micropaleontol. 29, 393–405.

Zonneveld, K.A.F., Versteegh, G.J.M., Kodrans-Nsiah, M., 2008. Preservation and organic chemistry of Late Cenozoic organic-walled dinoflagellate cysts: a review. Mar. Micropaleontol. 68, 179–197.

Samenvatting in het Nederlands

CO_2 in het geologisch verleden

Vanaf 1850 tot vandaag de dag is de atmosferische CO_2 concentratie gestegen van 280 partikels per miljoen (ppm) tot 400 ppm. Uit ijskern-onderzoek is gebleken dat de CO_2 concentratie in laatste 800,000 jaar niet hoger geweest is dan 300 ppm. De huidige CO_2 concentratie lijkt sterk op die tijdens het midden Plioceen, ongeveer 4 miljoen jaar (Ma) geleden, gebaseerd op CO_2 proxy data uit sedimenten. Omdat CO_2 een sterk broeikasgas is, zal de temperatuur op aarde stijgen, zoals ook bekend is van het Plioceen. Doordat oceanen nu veel CO_2 opnemen zullen CO_2 in de oceaan en atmosfeer op langere tijdschalen weer met elkaar in evenwicht komen. Dit resulteert echter tegelijkertijd in verzuring van de oceanen omdat CO_2 zeer snel wordt toegevoegd. Het klimaat in het Plioceen warmer was dan vandaag de dag, maar tijdens een groot deel van de laatste 65 miljoen jaar waren CO_2 concentraties in de atmosfeer nog hoger (>1000ppm).

Vooral tijdens het Paleoceen (66-56 Ma) en Eoceen (56-34 Ma) waren CO_2 concentraties zeer hoog en was het klimaat veel warmer. Deze kenmerken maken het Paleoceen en Eoceen geschikt om inzicht te krijgen in hoe het klimaat zich gedraagt bij zeer hoge CO_2 concentraties. Dit kan ook inzicht geven in toekomstige klimaat ontwikkelingen als de CO_2 concentraties de komende eeuwen in de atmosfeer blijven stijgen. Hoewel er duidelijke verschillen zijn in bijvoorbeeld de positie van de continenten, is de periode van 60 tot 50 Ma van belang.

Kenmerken van het klimaat tijdens het Paleoceen en Eoceen

Veel van het Paleoceen en Eoceen wordt gekarakteriseerd door wat extreme broeikasklimaten genoemd worden. Er is geen bewijs voor de aanwezigheid van grote polaire ijskappen op land of in zee. In tegendeel, de midden en hogere breedtegraden werden gekenmerkt door een (sub-) tropisch klimaat. Doordat grote ijskappen afwezig zijn kunnen stabiele zuurstof isotopen ($\delta^{18}O$) van benthische foraminiferen gebruikt worden om de temperatuur van het diepe oceaanwater te reconstrueren. Van 60 tot 50 Ma stijgt de temperatuur van het diepe oceaan water met 8 °C tot 15 °C (heden ~1.5 °C) tijdens het Vroeg Eoceen Klimaat Optimum (EECO). In tegenstelling tot de huidige situatie werd tijdens deze periode wordt het meeste diepe oceaan water in de zuidelijke oceaan gevormd. In deze situatie reflecteertde de temperatuur van de diepe oceaan dus de (winter) temperatuur van de hoge zuidelijke breedtegraden. Doordat er geen grote ijskappen zijn en er veel oceanische korst gevormd wordt is het zeeniveau tijdens het Paleoceen en Eoceen bovendien veel (70 m) hoger dan nu en waren grote delen van continenten overstroomd.

De warmste periode van de laatste 65 Ma, het vroege Eoceen (56 tot 50 Ma) werd gekenmerkt door aanwezigheid van (sub-) tropische flora en fauna, zoals krokodillen, palmbomen en mangrovebossen, op midden en hoge breedtegraden. De aanwezigheid van deze warmte-minnende soorten is bewijs van een belangrijk kenmerk van extreme broeikasklimaten; de midden en hoge breedtegraden warmen veel sterker op dan de tropen. De tropen waren misschien zelfs maar 5 °C hoger dan vandaag terwijl hogere breedtegraden tot 30 °C hoger waren. Dit betekent ook dat de temperatuurverschillen tussen de tropen en de polen veel kleiner waren dan vandaag de dag. Hoewel de meest recente klimaatmodellen de warme temperaturen van de midden breedtegraden redelijk reproduceren, bestaan er nog steeds grote verschillen tussen temperatuur reconstructies van de hoge breedtegraden en modelresultaten.

"***Hyperthermals***"

De periode van 56 tot 50 Ma werd gekenmerkt door verschillende tijdelijke (10 tot 100

duizend jaar, kyr) , snelle, verstoringen van de koolstofcyclus; deze verstoringen lijken op de huidige verstoring van de koolstofcyclus. Deze korte episoden van opwarming worden ook wel "hyperthermals" genoemd en vonden plaats tijdens een langere periode (~6 miljoen jaar, Myr) van langzame opwarming. De hyperthermals delen het kenmerk dat een sterke snelle (~1-10 kyr) wereldwijde opwarming plaatsvindt, dat tegelijkertijd de stabiele koolstofisotopen compositie ($\delta^{13}C$) van de oceaan en atmosfeer negatiever wordt en dat de oceanen verzuren. De combinatie van deze effecten wijst op een toevoeging van koolstof aan de atmosfeer, uit een koolstofreservoir dat normaal niet in open verbinding staat met de korte koolstofcyclus.

Het Paleoceen – Eoceen Thermisch Maximum

Het Paleoceen – Eoceen Thermisch Maximum (PETM; 56 Ma) was het "hyperthermal" met de grootste wereldwijde opwarming (~4 ºC) en de grootste negatieve $\delta^{13}C$ afwijking (>3‰). Het PETM onderscheidt zich van andere hyperthermals door de uitzonderlijke lange duur en de vorm van de $\delta^{13}C$ afwijking. De PETM $\delta^{13}C$ afwijking bestond uit een zeer snel (<10 kyr) begin, een lange (70 kyr) periode van stabiele, maar afwijkende koolstofisotopen, gevolgd door een periode van herstel (100 kyr). Er zijn verstoringen gedocumenteerd in veel verschillende omgevingsfactoren tijdens het PETM. De wereldwijde temperatuurstijging veroorzaakte bijvoorbeeld een extremer karakter in neerslagpatronen en de oceanen bevatten minder zuurstof in zowel het oppervlakte als diepere water. De snelle toevoeging van grote hoeveelheden CO_2 aan de atmosfeer en oceaan veroorzaakte bovendien sterke verzuring en de carbonaat compensatie diepte (CCD) steeg daardoor in de Pacifische Oceaan, maar vooral in de Atlantische Oceaan met wel 2 km. Dit betekent dat veel sediment kernen uit diepere delen van de oceaan te lijden hebben van carbonaat oplossing.

Onbeantwoorde vragen

#1 Koolstofbron(nen)

Sinds de ontdekking van het PETM is er veel dingen gemeten aan sedimenten. Hierdoor zijn onder andere patronen van temperatuur (veranderingen), zuurstofloosheid, stabiele koolstofisotopen, stratificatie in de waterkolom en soortmigraties van flora en fauna bekend. De hoeveelheid publicaties toegespitst op het PETM kan de indruk wekken dat het grootste deel van oorzaak en gevolg bekend is. Integendeel, hoewel er veel bekend is over de gevolgen van de koolstofcyclus verstoring tijdens het PETM is er weinig bekend over de oorzaak. Zo zijn er bijvoorbeeld niet minder dan 6 onafhankelijke hypotheses, maar is het nog steeds onbekend waar de isotopisch lichte koolstof vandaan kwam en is er geen concreet bewijs voor uitstoot van koolstof vanuit een van de hypothetiseerde bronnen tijdens het PETM of een andere hyperthermal.

Op dit moment is er ook geen oplossing die tegelijkertijd de $\delta^{13}C$ afwijking, temperatuur stijging, hoge achtergrond temperaturen en CCD stijging kan verklaren. Hoewel geen van de hypothesen sluitend is, zijn het mogelijk wel oplossingen voor gedeeltes van het probleem. Zo suggereerden Dickens en anderen (1995, 1997) dat de destabilisatie van methaanhydraten uit de zeebodem een grote hoeveelheid isotopisch licht koolstof vrijgemaakt kan hebben. Methaanhydraten zijn methaan moleculen die opgesloten zitten in een water kooi. De vorming en het bestaan van methaanhydraten is sterk temperatuur en druk afhankelijk. Ondanks het warme oceaanwater waren methaanhydraten mogelijk aanwezig vanaf diepten van 1000 m en meer tijdens de Paleoceen – Eoceen overgang. De vorming van de methaanhydraten vindt plaats onder methanogenese, wat zorgt voor een extreem negatieve $\delta^{13}C$ (-60‰) van de methaanhydraten (Milkov, 2005). Dit koolstofreservoir zou dus een CIE kunnen veroorzaken zelfs als er maar een relatief kleine hoeveelheid koolstof

vrijkomt. Echter, doordat de stabiliteit van methaanhydraten afhankelijk is van druk en temperatuur moet er een externe verstoring, bijvoorbeeld in de vorm van een opwarming, hebben plaatsgevonden voor de uitstoot van isotopisch lichte koolstof. Dit benadrukt hoe belangrijk het is om inzicht te krijgen in oorzaak en gevolg tijdens het PETM, ook met betrekking op de nabije toekomst.

Een tweede mogelijke bron zijn permafrost of veenafzettingen op hoge breedtegraden, welke net als methaanhydraten een opwarming nodig hebben om te destabiliseren. Deze opwarming zou bijvoorbeeld veroorzaakt kunnen zijn door toegenomen vulkanische activiteit in het noorden van de Atlantische Oceaan. Een alternatieve verklaring voor opwarming voorafgaand aan destabilisatie van methaanhydraten, permafrost of veenafzettingen zou een specifieke astronomische configuratie zijn, waardoor het klimaat een omslagpunt bereikte.

Een derde mogelijke bron is isotopisch licht koolstof uit hydrothermische bronnen in de Vøring en Møre bekkens, in het noorden van de Atlantische Oceaan. Deze bron, voorgesteld door, komt voort uit intrusie van magma in sedimenten rijk in organisch materiaal, wat onder andere methaan genereert. Dit methaan bereikt samen met vloeistoffen en andere gassen het oceaanwater en atmosfeer door zogenaamde hydrothermale bronnen, waarvan er zeker enkele honderden, maar mogelijk duizenden zijn in de Vøring en Møre bekkens. *Apectodinium augustum*, een dinoflagellaat die alleen voorkomt tijdens het PETM is gevonden in de enige bemonsterde hydrothermale bron en suggereert een direct verband met het PETM.

Het grootste probleem met de aanname van ieder van deze bronnen is dat elke bron de CIE verklaart, maar doorgaans niet de stijging van de CCD, temperatuur stijging, laat staan de absolute temperaturen. Dit heeft geleid tot de hypothese dat koolstof uit meerdere bronnen nodig is om alle verstoringen te kunnen verklaren of een enkele complexe bron die zowel op korte als lange termijn een rol speelde.

#2: Klimaatmodellen versus de data

Naast de onzekerheid over de koolstofbronnen is er sterke twijfel over hoe goed klimaatmodellen kunnen omgaan met de extreem hoge temperaturen die gereconstrueerd zijn voor het PETM. Dit komt deels voort uit de onzekerheid over CO_2 concentraties tijdens het PETM. Een andere onzekerheid is de klimaatgevoeligheid, gedefinieerd als temperatuurstijging per verdubbeling van CO_2 concentratie. De temperatuurverandering daarentegen is uitgebreid gedocumenteerd en dient als een eerste-orde schatting voor klimaatmodellen.

Temperatuur in midden en hoge breedtegraden tijdens het PETM is gereconstrueerd met een aantal verschillende proxies, zoals stabiele zuurstofisotopen en Mg/Ca ratio's van foraminiferen en TEX_{86}, een proxy gebaseerd op membraanlipiden van Thaumarchaea. Tropische temperatuur reconstructies zijn daarentegen zeldzaam en vaak complex of beïnvloed door secundaire carbonaat afzettingen. Hierdoor zijn er op dit moment geen betrouwbare temperatuur reconstructies uit de tropen.

De tropen (30 ^{o}N – 30 ^{o}Z) zijn goed voor 50% van het aardoppervlak en 75% van alle binnenkomende energie. Dit betekent dat een belangrijk punt in het klimaatsysteem dat essentieel is om de globale gemiddelde temperatuur, temperatuurstijging tijdens het PETM en versterkte opwarming van de polen te bepalen, onbekend is. Er is lang gedacht dat de tropen tijdens het PETM net zo warm of zelfs koeler waren dan vandaag de dag; een beeld dat onmogelijk te verklaren is met klimaatmodellen. Het leidde tot de hypothese

van een tropische thermostaat, een mechanisme dat ervoor zorgt dat de temperatuur in de tropen gelijk blijft onder stijgende of dalende CO_2 concentraties. Recent onderzoek heeft echter uitgewezen dat vrijwel alle voorgaande temperatuur reconstructies sterk beinvloed zijn door secundaire afzettingen van carbonaat of herkristallisatie. Verschillende studies hebben geprobeerd deze effecten bewust te omzeilen en reconstrueren inderdaad hogere temperaturen in de tropen, wat dan ook geleid heeft tot een verkleining van het gat tussen klimaatmodellen en de data. Nog steeds blijft er echter grote onzekerheid bestaan over hoe hoog de temperatuur opliep tijdens het PETM in de tropen.

#3: Ecologische gevolgen van de opwarming in de tropen

Hoewel onderzoek naar ecologische veranderingen in de tropen bestaat voor het PETM, is dit onderzoek zonder uitzondering toegespitst op de open oceaan en carbonaat microfossielen. Weinig tot niets is bekend over veranderingen in omgevingsvariabelen en de daarmee samenhangende ecologische gevolgen in kustnabije omgevingen in de tropen. Microfossielen zijn in het algemeen nuttig voor dit soort onderzoek omdat ze gevoelig zijn voor kleine veranderingen in omgevingsvariabelen en bovendien snel reageren door relatief korte levensspanne.

Dinoflagellaten, unicellulaire protisten, zijn onder andere gevoelig voor veranderingen in omgevingsvariabelen zoals temperatuur, zoutgehalte, beschikbaarheid van voedingsstoffen en turbulentie. Een klein gedeelte van de dinoflagellaten maakt, als vast onderdeel van de levencyclus, een organische cyst die bewaard blijft in sedimenten. Deze cysten zijn eerder gebruikt om een gedetailleerd beeld te krijgen van veranderingen in omgevingsvariabelen op midden en hoge breedtegraden. Uit dit onderzoek weten we bijvoorbeeld dat verschillende dinoflagellaten soorten migreren naar hogere breedtegraden tijdens het PETM; het meest bekende voorbeeld hiervan is de bijna globale dominantie van de (sub-) tropische dinoflagellaat *Apectodinium*. Het is echter volledig onbekend wat er gebeurde met dinoflagellaten in de tropen tijdens het PETM.

Synopsis

In dit proefschrift worden de bovenstaande vraagstukken omtrent het PETM aangekaart. Dinoflagellaten cysten worden gebruikt in tandem met organische en inorganische chemische proxies om omgevingsvariabelen te reconstrueren. De observaties worden geplaatst in een raamwerk van lange termijn klimaatverandering, verstoringen tijdens het PETM, dynamiek in de koolstofcyclus en ecologische veranderingen.

In **hoofdstuk 2**, onderzoeken we of de opwarming van 59 tot 52 Ma die gedocumenteerd is in diep oceaan water en oppervlakte van de zuidelijke oceaan ook plaatsvond op het noordelijk halfrond. We gebruiken daarvoor mariene sedimenten afgezet in Siberie, in de buurt van Omsk, Rusland. We reconstrueren oppervlakte temperaturen van het zeewater met behulp van de moleculaire proxy TEX_{86}. De gevonden opwarming is opmerkelijk gelijk aan die van de zuidelijke oceaan en diep oceaan water. Door deze oppervlakte temperatuur reconstructies te combineren met dinoflagellaten cysten, laten we zien dat de minimum temperatuur voor Wetzellioideae, een belangrijke Paleogene dinoflagellaten groep welke ook *Apectodinium* bevat, 20 ^{o}C bedraagt.

In **hoofdstuk 3** worden twee sedimentaire secties uit Nigeria gebruikt om temperatuur te reconstrueren van oppervlakte en bodemwater tijdens het Paleoceen en het PETM. We gebruiken hiervoor zowel stabiele zuurstof isotopen als Mg/Ca ratio's als TEX_{86}. Al deze temperatuur proxies laten oppervlakte temperaturen rond 33 ^{o}C zien in het laatste Paleoceen, 6-7 ^{o}C hoger dan dezelfde regio vandaag de dag. Met TEX_{86} reconstrueren

we een temperatuurstijging van 3 ºC tijdens het PETM. Klimaatmodellen en verzamelde proxy data van andere locaties laat zien dat de opwarming de tropen kleiner was dan elders. Interessant is ook de eensgezindheid van modellen en data, welke zien dat klimaatmodellen zowel absolute temperatuur, temperatuur veranderingen en regio's met versterkte of juist afgezwakte effecten accuraat kunnen voorspellen, wellicht met uitzondering van de uitzonderlijk warme Noord en Zuidpool gebieden.

In **hoofdstuk 4** wordt een temperatuurreconstructie van tweede tropische sectie gepresenteerd, gebaseerd op sedimenten aangeboord tijdens Ocean Drilling Project Leg 159 Site 959D, 150 km ten zuiden van Ivoorkust. Zowel de temperatuurreconstructie van deze sectie als de sectie in Nigeria laat uitzonderlijk hoge temperaturen zien, tot boven 37 ºC tijdens het PETM. In **hoofdstuk 3 en 5** laten we zien dat veel dinoflagellaten cysten niet voorkomen tijdens de periode met de hoogste temperaturen. Met behulp van een diverse proxy dataset laten we zien dat deze tijdelijke afwezigheid van dinoflagellaten gerelateerd is aan temperatuurstress. De dinoflagellaten cysten die er nog wel zijn, zogenaamde Protoperidiniaceae, zijn strikt heterotroof in de moderne oceaan en waarschijnlijk ook in het Paleogeen. Door deze afwijkende strategie migreerden deze dinoflagellaten mogelijk naar dieper, koeler, water. Verschillende studies (Aze et al., 2014; Huber, 2009) hebben voorgesteld dat temperatuurstress een rol zou kunnen spelen tijdens zeer warme perioden zoals het PETM. De secties in Nigeria en ODP Site 959 zijn de eerste waar we kunnen laten zien dat andere, meer voorkomende, stress-factoren geen rol spelen. Intrigerend is ook de afwezigheid van carbonaat en silica microfossielen in Site 959 tijdens het PETM, betekent waarschijnlijk dat alle eukaryote plankton groepen te lijden hadden onder de extreem hoge temperaturen. Een toename in de hoeveelheid benthische foraminiferen op beide locaties suggereert dat productiviteit in het oppervlakte water niet instortte, wat mogelijk duidt op een dominantie van prokaryote primaire producenten.

Veroorzaakte de opwarming een verstoring van de koolstofcyclus of veroorzaakte de koolstofcyclus verstoring alle opwarming? Om deze vraag te beantwoorden heb ik gekeken welke veranderingen eerst plaatsvonden. Hiervoor heb ik bestaande en nieuwe data gebruikt, bestaande uit gekoppelde temperatuur en stabiele koolstof isotopen data. Met behulp van in tijd verschoven correlaties blijkt dat de temperatuur consequent eerder verandert dan de stabiele koolstof isotopen waarde. Dit gebeurt gemiddeld 2-3000 jaar eerder en ongeveer de helft van de opwarming vindt plaats voor de eerste veranderingen in stabiele koolstof isotopen waarden. Dit scenario is consistent met zowel methaan hydraten destabilisatie als het ontdooien van permafrost. Een onderscheidende factor tussen deze twee bronnen is echter dat onder methaan hydraten grote hoeveelheiden Barium opgeslagen zijn, welke kunnen vrijkomen tijdens destabilisatie. Met een compilatie van Ba data, laten we zien dat Ba fluxen sterk toenemen tijdens het PETM; een sterke indicatie voor methaan hydraten.

Voor, tijdens en vlak na het PETM is er verhoogde vulkanische activiteit in het noorden van de Atlantische oceaan. Auteurs hebben geprobeerd dit te koppelen aan het PETM door twee verschillende mechanismen. Storey en anderen (2007) stelden dat vulkanisme mogelijk de bron van CO_2 is die leidt tot de opwarming die nodig is om methaan hydraten te destabiliseren. Svensen en anderen (2004) hypothetiseerde dat vulkanische intrusie in organisch rijke sedimenten mogelijk grote hoeveelheden thermogeen methaan met een lage stabiele koolstof waarden genereerde en het PETM veroorzaakte. De hypothese van Svensen en anderen wordt getest in **hoofdstuk 6**. Met nieuwe stratigrafische data van dinoflagellaten cysten en stabiele koolstof isotopen data laten we zien dat er inderdaad thermogeen methaan vrijkwam uit de hydrothermale bronnen in de Vøring en Møre bekkens tijdens het PETM. Dit is het meest directe bewijs voor een specifieke koolstofbron tijdens het PETM.

Deze koolstofbron was echter actief tijdens het tweede deel van het PETM, wat zou kunnen betekenen dat dit de reden is waarom het PETM langer duurde dan andere hyperthermals. We speculeren dat vulkanisme in het noorden van de Altantische Oceaan een cruciale rol speelt in het veroorzaken van opwarming, welke leidde tot destabilisatie van methaan hydraten en daarna ook de buitengewone lengte van het PETM ten opzichte van andere hyperthermals veroorzaakte door toevoeging van thermogeen methaan.

In **hoofdstuk 7** wordt de data uit **hoofdstukken 2,3 en 5** gebruikt om beter inzicht te krijgen in de ecologische voorkeuren van verschillende dinoflagellaten cysten soorten tijdens het Paleoceen en Eoceen. We combineren dinoflagellaten cysten data met onafhankelijke organische en inorganische chemische proxy data. De toevoeging van meerdere tropische secties kan helpen met begrijpen waarom dinoflagellaten cysten assemblages veranderen in midden en hoge breedtegraden tijdens het PETM. We vinden onder andere dat niet alleen het voorkomen van *Apectodinium* gelimiteerd is door temperatuur (>20 ºC) is zoals gepresenteerd in **hoofdstuk 2**, maar dat hetzelfde geldde voor *Florentinia reichartii* (>30 ºC) en Goniodomideae (>25ºC). We verdelen Peridinioide cysten in verschillende groepen omdat blijkt dat *Senegalinium* voornamelijk lage zoutgehalten tolereerde, terwijl *Cerodinium* en *Deflandrea* beter gedijden onder omstandigheden met lage zuurstofgehalten in het bodemwater. In tegenstelling tot eerdere studies zien we dat *Apectodinium* afwijkt van andere Perinidioide cysten, welke allemaal sterk reageren op proxies die beschouwd kunnen worden als maatstaf voor de hoeveelheid voedingsstoffen in het water. Heterotrofe soorten komen naar verhouding meer voor onder omstandigheden met hogere hoeveelheden voedingsstoffen. We zien dus geen bewijs dat ook *Apectodinium* heterotroof was.

Vooruitblik

De bevindingen die gepresenteerd worden in dit proefschrift roepen nieuwe vragen op over tropische ecosystemen tijdens het PETM en dit resulteert in nieuwe theorieen die getest moeten worden. Zo is bijvoorbeeld de afwezigheid van eukaryoot plankton in de tropen van belang voor het in stand houden van de basis van het voedselketen en zal de gevoeligheid voor snelle temperatuurstijging dus getest moeten worden door middel van experimenten op een brede selectie moderne soorten. Hoewel prokaryoten waarschijnlijk een groot deel van de primaire productie overnemen heeft dit mogelijk verstrekkende gevolgen voor hoe organisch materiaal in de oceaan gerecycled of geexporteerd wordt naar het sediment. Op dit moment is onbekend hoever deze effecten zich geografisch uitstrekken en hoeveel productie prokaryoten overnemen. Deels kan dit mogelijk opgelost worden door een herziening van eerder werk, maar er is vooral kwantificatie van prokaryote versus eukaryote productie nodig.

Verschillende koolstofbronnen die gedeeltes van het PETM kunnen verklaren worden gepresenteerd in dit proefschrift. Het blijft echter onbekend welk deel van de opwarming lokaal veroorzaakt wordt door CO_2 stijging en welk deel gedreven wordt door oceaan circulatie veranderingen. Deze patronen kunnen onderzocht worden door middel van hoge resolutie onderzoek zoals in **hoofdstuk 4**, maar zullen toegespitst moeten worden op regio's die gevoelig zijn voor circulatie veranderingen zoals geidentificeerd door klimaat modellen.

Hoe onwaarschijnlijk het ook lijkt, mensen zeggen mij dat het toch echt af is nu. Wat ze met **het** bedoelen weet ik nog niet.

Wat ik wel weet is dat veel, heel veel, dank verschuldigd ben aan Appy, Gert-Jan en Henk. In de eerste plaats voor het bieden van de kans om te beginnen, maar nog veel meer voor de jaren daarna! De continue positiviteit van Appy gecombineerd met de scepsis van Gert-Jan hebben dit alsnog wel tot een succes(je) gemaakt.

Hoewel Mirja, Mariska,Linda en ik ~5 jaar geleden gestart zijn met het zelfde doel, namelijk het opzetten van een CO2 proxy op basis van dinocysten, bevat mijn thesis toch echt iets heel anders. Ik wil hen dan ook bedanken voor heel leuke en voor mij soms verwarrende discussies.

De bewandelde weg leidde mij o.a. langs organisch geochemici; ik heb door de jaren heen hulp mogen krijgen (en vaak nodig gehad) van Stefan Schouten, Johan Weijers, Francien Peterse, Klaas Nierop en anderen. Behalve organisch geochemisten hebben andere takken van sport ook een rol gespeeld. Ik wil dan ook Jack Middelburg, João Trabucho, Hemmo Abels, Frits Hilgen en anderen bedanken voor alle inzichtvolle discussies.

Als aio spendeer je heel wat tijd in het lab. Ik wil daarom Natasja, Jan, Ton, Helen, Dineke, Dominika, Anita, Coen, Nico en Arnold bedanken voor hun tijd, inzicht, zweet, tranen en alle dingen die ik niet gezien heb maar wel nodig waren.

Uiteraard was /is er ook een leven buiten het lab? Peter, Emmy, Alex, Johan, Timme, Franci, Fabian, Rike, Keechy, Loes, Carolien, Bas, Marjolein, Tjitske en Chloe bedankt voor de grappige, bizarre, leuke en soms verdacht intelligente gesprekken in de koffiehoek en elders.

Meteen toen ik begon werd het plan geopperd en uitgevoerd om het zaalvoetbalteam nieuw leven in te blazen. Helaas was dit niet meteen het winnende team voor de eerste en tweede helft, vooral de wedstrijden waar shirt-sponsor Dan Brinkhuis kwam kijken waren "niet super". Omdat ik niet alle spelers kan bedanken houd ik het hier bij de (harde) kern: Houben, Bijl, Tabor, van Helmond, Grothe, Eijkelenstam, Masselink, Egger, Moji en Lenstra.

Door de jaren heen was het een komen en gaan van studenten (die ik niet allemaal kan noemen omdat ruimtegebrek). Jelmer en Niels waren zo dapper om iets met mijn oorspronkelijke project te proberen. Het staat nog niet helemaal vast wanneer, maar het succes daarvan is nu wel echt gegarandeerd. Hetzelfde geldt voor het grote 959 project waar Ilja en Mike nu hard aan trekken.

As you cannot figure out the world on your own, scientific collaborations are extremely important and I've had the pleasure to work with many interesting people over the years. This includes discussions and collaborations with (and I will undoubtedly forget more than a few), Olabisi Adekeye, Samuel Akande, Luca Giusberti, Ulla Rohl, Matt Huber, Steve Bohaty, Henrik Svensen, Sverre Planke, Jerry Dickens (thanks for the infinite amount of comments on my thesis!), Jorg Pross and Alina Iakovleva.

Ik kan er ook niet omheen om mijn kantoorgenoten te bedanken. Mariska is hier altijd de stabiele factor in geweest. Later kwam daar Julian bij en na de verhuizing ook Tjerk. Ik heb

jullie ondertussen achtergelaten door twee deuren verder bij Arjen, Robin en Margot te gaan zitten, maar in gedachten ben ik nog vaak bij jullie en vooral de Tjerke verhalen ga ik niet snel vergeten!

Niels, Margot, paranimfen; we zien elkaar later in het Pandje.

Rest mij alleen nog om de mensen te bedanken die mij onvoorwaardelijk gesteund hebben en nog steeds steunen. Pap, Mam, zonder jullie was ik er nooit aan begonnen en had ik het zeker nooit af kunnen maken.

Joost Frieling was born in Nijmegen, on the 21st of August 1987. He grew up in the nearby village of Millingen aan de Rijn and attended primary school in the small village of Kekerdom and attended the Stedelijk Gymnasium in Nijmegen high school afterwards. He started his BSc at Utrecht University in 2005, finishing with a focus on Biogeology in 2009 after completing his BSc thesis with Wilma Wessels. He started in 2009 with a MSc in Biogeology at Utrecht University and started a MSc research with Appy Sluijs and Gert-Jan Reichart in 2010 working on the *Paleocene Eocene Thermal Maximum of Nigeria*. His MSc title was obtained in 2011 and he directly afterwards started his PhD as part of the "*From Protist to Proxy*" project, again under supervision of Appy Sluijs and Gert-Jan Reichart.